

Mechanism of Tocopherol Transfer by human α -Tocopherol Transfer Protein (α -hTTP)

Wen Xiao (Wendy) Zhang

A thesis submitted to the Department of Chemistry
Centre for Biotechnology
In partial fulfillment for the requirements for the
degree of the Doctorate of Philosophy

Brock University
St. Catharines, Ontario,
January, 2010

© Wen Xiao (Wendy) Zhang, 2010

ABSTRACT

Vitamin E is a well known fat soluble chain breaking antioxidant. It is a general term used to describe a family of eight stereoisomers of tocopherols. Selective retention of α -tocopherol in the human circulation system is regulated by the α -Tocopherol Transfer Protein (α -TTP).

Using a fluorescently labelled α -tocopherol (NBD- α -Toc) synthesized in our laboratory, a fluorescence resonance energy transfer (FRET) assay was developed to monitor the kinetics of ligand transfer by α -hTTP in lipid vesicles. Preliminary results implied that NBD- α -Toc simply diffused from 6-His- α -hTTP to acceptor membranes since the kinetics of transfer were not responsive to a variety of conditions tested. After a series of trouble shooting experiments, we identified a minor contaminant, *E. coli*. outer membrane porin F (OmpF) that co-purified with 6-His- α -hTTP from the metal affinity column as the source of the problem.

In order to completely avoid OmpF contamination, a GST- α -hTTP fusion protein was purified from a glutathione agarose column followed by an on-column thrombin digestion to remove the GST tag. We then demonstrated that α -hTTP utilizes a collisional mechanism to deliver its ligand. Furthermore, a higher rate of α -tocopherol transfer to small unilamellar vesicles (SUVs) versus large unilamellar vesicles (LUVs) indicated that transfer is sensitive to membrane curvature. These findings suggest that α -hTTP mediated α -Toc transfer is dominated by the hydrophobic nature of α -hTTP and the packing density of phospholipid head groups within acceptor membranes.

Based on the calculated free energy change (ΔG) when a protein is transferred from water to the lipid bilayer, a model was generated to predict the orientation of α -

hTTP when it interacts with lipid membranes. Guided by this model, several hydrophobic residues expected to penetrate deeply into the bilayer hydrophobic core, were mutated to either aspartate or alanine. Utilizing dual polarization interferometry and size exclusion vesicle binding assays, we identified the key residues for membrane binding to be F165, F169 and I202. In addition, the rates of ligand transfer of the α -TTP mutants were directly correlated to their membrane binding capabilities, indicating that membrane binding was likely the rate limiting step in α -TTP mediated transfer of α -Toc. The propensity of α -TTP for highly curved membrane provides a connection to its co-localization with α -Toc in late endosomes.

ACKNOWLEDGEMENTS

I would like to express my deepest gratitude to Dr. Jeffrey Atkinson for giving me an opportunity to study under his guidance. He is a remarkable and inspiring mentor. His devotion to research and teaching is truly admirable.

It has been a blessing to work with and be surrounded by a group of dear friends in IH210. I would like to extend my genuine thanks the A-team (Ryan West, Matilda Baptist, Matt Cecchini, Phil Nava and Grant Frahm) and Dr. Debra Inglis's team (Dr. Ai Lin Beh, Dr. Stephanie Martin, Shiri Sauday, Fei Wang, Eric Humes and Di Qing).

I would like to express my sincere appreciation for Dr. Robert Carlone, Dr. Costa Metallinos, Dr. Douglas Bruce, Dr. Rick Cheel and Dr. Christopher McMaster for their time commitment and evaluation of this work.

I am deeply indebted to the kindred spirit Dr. Candace Panagabko and her critical read of this thesis. Her insightful comments and suggestions are very valuable.

I am also grateful to Mr. Tim Jones at the chemistry department for his assistance with MALDI-TOF peptide sequence analysis, Mr. YuGuo Cui and Dr. Doug Keller (McMaster University) and Dr. Sigrid Kuebler (Wyatt Technology Corporation) for their assistance with the Dynamic Light Scattering vesicle size analysis.

I would also like to thank my parents and brothers for their love and support, especially my dad whom has always encouraged us to achieve the highest education possible.

Finally, this work would not be possible without the constant support and encouragement from my husband and soul mate, who understands the challenges involved in research career. I am fortunate to have him by my side through both good and bad times.

TABLE OF CONTENTS

	Page
1. INTRODUCTION	
1.1. Overview of Vitamin E	1
1.2. Biochemical Properties of Vitamin E	
1.2.1. Vitamin E structures.....	1
1.2.2. Vitamin E as antioxidant.....	3
1.2.3. Bioavailability of Vitamin E isoforms.....	4
1.2.4. α -Tocopherol in lipid membranes.....	5
1.2.5. Vitamin E uptake and metabolism.....	8
1.2.6. Non-antioxidant properties of vitamin E.....	10
1.3. Vitamin E binding proteins.....	11
1.4. α -Tocopherol Transfer Protein (α -TTP)	
1.4.1. α -Tocopherol transfer protein.....	12
1.4.2. Crystal structure of α -TTP.....	13
1.4.3. Role of α -TTP in the intracellular trafficking of α -Toc.....	15
1.4.4. Ataxia with Vitamin E deficiency (AVED).....	16
1.5. CRAL-TRIO protein family.....	20
1.6. Mechanism of hydrophobic ligand transfer.....	21
1.7. Membrane curvature sensing proteins.....	23
1.8. Proposed orientation of α -TTP in the lipid membrane.....	24
2. RESULTS	
2.1. Transfer of NBD- α -Toc to model lipid membranes evaluated with 6-his- α -hTTP isolated from pET28b and pET21b expression vectors	
2.1.1. 6-His- α -hTTP with an extension expressed from α -hTTP/pET28b construct.....	27
2.1.2. Characterization of NBD- α -Toc fluorescent probe.....	28
2.1.3. Development and optimization of Fluorescence Resonance Energy Transfer (FRET) assay.....	33
2.1.4. Kinetics of NBD- α -Toc transfer by 6-His-28TTP.....	35
2.1.5. 6-His- α -hTTP without an extension isolated from α -hTTP/pET21b construct.....	37
2.1.6. Kinetics of NBD- α -Toc transfer by 6-His- α -hTTP.....	39
2.1.7. Troubleshooting experiments	

	Page
2.1.7.1. Removal of NBD- α -Toc from membranes by 6-His α -hTTP....	45
2.1.7.2. Examination of NBD- α -Toc probe.....	47
2.1.7.3. Examination of 6-His- α -hTTP.....	49
2.1.8. Identification of <i>E. coli</i> Outer Membrane Porin F (OmpF).....	51
2.2. NBD- α -Toc transfer by α -hTTP is mediated through a collisional mechanism	
2.2.1 Characterization of α -hTTP purified from α -hTTP/pGEX4T.....	59
2.2.2 Partitioning of NBD- α -Toc between α -hTTP and lipid vesicles.....	62
2.2.3 Kinetics of NBD- α -Toc transfer by α -hTTP.....	63
2.3. Membrane insertion of gating helix A8 and helix A10 are essential for the binding of α -hTTP to the target membranes and the delivery of NBD- α -Toc	
2.3.1. Creation of hydrophobic mutants.....	75
2.3.2. Membrane binding of hydrophobic mutants and their ability to deliver NBD- α -Toc.....	80
2.3.3. Role of three positively charged hinge residue on the membrane binding and subsequent delivery of NBD- α -Toc.....	90
3. DISCUSSIONS AND CONCLUSIONS	
3.1. FRET transfer assay with 6-His- α -hTTP from pET28 and pET21 expression vectors.....	95
3.2. Transfer of NBD- α -Toc by α -hTTP to acceptor membranes utilizes a collisional based mechanism.....	101
3.3. The direct interaction between α -hTTP and lipid membrane is regulated by the anchoring helix A8 and the gating helix A10.....	107
3.4. Proposed recycling of α -Toc facilitated by α -hTTP.....	112
3.5. Conclusions.....	114
4. FUTURE DIRECTIONS.....	116
5. METATERIALS AND METHODS	
5.1. Chemicals and Stock Solutions	
5.1.1. Antibiotics and other chemicals.....	118
5.1.2. Enzymes.....	118
5.1.3. Chemicals used in to generate peptides for MALDI-TOF protein analysis.....	118
5.1.4. Solutions used to process SDS-PAGE gels.....	119
5.1.5. Solutions employed to regenerate glutathione agarose affinity column.....	119
5.2. Phospholipids from Avanti Polar Lipids.....	119

	Page
5.3. Other reagents	
5.3.1. Miscellaneous reagents.....	119
5.3.2. Bacterial Strains.....	120
5.3.3. Bacterial Expression Vectors.....	121
5.4. Molecular methodologies	
5.4.1. Site directed mutagenesis.....	122
5.4.2. Restriction enzyme digestion analysis of α -TTP mutant DNA samples.....	125
5.4.3. DNA concentration analysis.....	125
5.5. Expression of α -hTTP in various expression vectors.....	125
5.6. Purification of α -hTTP (6-His or GST tagged)	
5.6.1. HiTrap IMAC Metal chelating affinity chromatography.....	127
5.6.2. Probond Metal chelating affinity chromatography.....	127
5.6.3. Glutathione agarose affinity chromatography.....	128
5.7. Protein qualification and quantification methods	
5.7.1. Bradford protein concentration determination.....	129
5.7.2. NanoOrange protein quantification method.....	129
5.7.3. Sodium Dodecyl Sulfate-Polyacrylamide Gel Electrophoresis.....	130
5.7.4. Western blot analysis.....	131
5.7.5. Intrinsic tryptophan fluorescence of α -hTTP.....	131
5.7.6. Acrylamide quenching of α -hTTP.....	132
5.7.7. MALDI-TOF protein sequence analysis.....	132
5.7.8. Phospholipid extraction from purified 6-his α -hTTP.....	133
5.7.9. Factor Xa digestion of 6-His tag α -hTTP.....	134
5.7.10. pH stability of α -hTTP.....	134
5.8. Preparation and analysis of phospholipids	
5.8.1. LUVs and SUVs preparation.....	135
5.8.2. Quantification of phospholipid with lipid phosphorous assay.....	136
5.8.3. Dynamic light scattering analysis of the sizes of the SUVs and LUVs..	137
5.9. Characteristics of fluorescent ligand NBD- α -Toc	
5.9.1 Equilibrium titration of α -TTP wild type and mutants with NBD- α -Toc	137
5.9.2 Partitioning of NBD- α -Toc between α -hTTP and PC lipid vesicles.....	138
5.9.3 Spectroscopic measurement of NBD- α -Toc concentration.....	139
5.9.4 Reduction of NBD- α -Toc by Sodium Dithionite.....	139
5.10. Fluorescence resonance energy transfer (FRET assay)	
5.10.1 Spontaneous transfer of NBD- α -Toc from donor vesicles to acceptor vesicles.....	140

	Page
5.10.2 Transfer of NBD- α -Toc from α -hTTP to acceptor vesicles.....	140
5.10.3 Pick up of NBD- α -Toc from membrane vesicles by α -hTTP.....	141
5.11. Assessment of α -hTTP binding to phospholipid membranes	
5.11.1 Size exclusion filtration method.....	142
5.11.2 Dual Polarization Interferometric assessment (DPI).....	143
5.12. Software.....	144
6. REFERENCES.....	146
7. APPENDICES.....	167

LIST OF TABLES

	Page
 2. RESULTS	
Table 1: The hydrodynamic radii of lipid vesicles measured by Dynamic Light Scattering (DLS) at McMaster University.....	71
Table 2: The hydrodynamic radius of extruded and sonicated SUVs determined by Wyatt Technology Inc.....	73
Table 3: Total outer surface area of various sized liposomes and the surface ratio in relative to 100 nm LUVs.....	75
Table 4: Vesicle binding and rate of NBD- α -Toc transfer by wild-type and mutant forms of α -hTTP.....	81
Table 5: Binding of various mutants to the planer PC bilayer measured by DPI.....	85
Table 6: Comparison of calculated change of transfer energy (ΔG) of α -hTTP mutants, rates of NBD- α -Toc transfer (to SUVs) and protein adsorption at 1 μ M protein concentration relative to wildtype α -hTTP.....	87
Table 7: Binding and rate of NBD- α -Toc transfer by α -hTTP wildtype and hinge mutant of α -TTP.....	92
Table 8: Adsorption of α -hTTP wild-type and hinge mutants of α -hTTP to the lipid bilayer measured by DPI.....	93
 5. MATERIALS AND METHODS	
Table 9: Characteristics of the α -hTTP bacterial expression vectors.....	121
Table 10: Oligonucleotides primers used to create hydrophobic mutants of α -hTTP.	123
Table 11: Cycling parameters utilizing turbo pfu polymerase in PCR amplification..	124
Table 12: Cycling parameters utilizing Phusion hot start polymerase in PCR amplification	124

LIST OF FIGURES

Page

1. INTRODUCTIONS

Figure 1: Structure of tocopherols and tocotrienols.....	2
Figure 2: Structures of α -tocopherol (α -Toc) and its oxidative product..... α -tocopheryl quinone (TQ)	4
Figure 3: Three possible locations of α -Toc in POPC membranes.....	6
Figure 4: Chemical structure of Fluorazophore-L.....	7
Figure 5: Uptake and secretion of Vitamin E in circulation system.....	8
Figure 6: Structure of carboxyethyl-hydroxychroman derivatives.....	10
Figure 7: Structure of Trolox and α -Tocopheryl acetate.....	11
Figure 8: Surface comparison of the open and the closed conformation of α -TTP structure.....	14
Figure 9: Location of missense AVED mutations on α -TTP.....	18
Figure 10: Potential mechanisms of cholesterol transfer the NPC2 protein to membranes.....	22
Figure 11: Orientation of α -TTP in a lipid membrane.....	25

2. RESULTS

Figure 12: Nickel chelate affinity column purification of 6-His-28TTP Expressed in <i>E. coli</i> BL21(DE3) cells.....	27
Figure 13: Chemical structure of NBD- α -Toc and the spectra of NBD- α -Toc in absolute ethanol.....	29
Figure 14: Reduction of NBD- α -Toc by sodium dithionite.....	30
Figure 15: Acrylamide quenching of the natural α -Toc or the florescent NBD- α -Toc in PC vesicles.....	32
Figure 16: Chemical structure of lipid quencher TRITC-DHPE.....	34

Figure 17: Cartoon illustration of NBD-Toc delivery by α -TTP detected by Fluorescence Resonance Energy Transfer (FRET) assay.....	35
Figure 18: Time-dependent NBD- α -Toc transfer from 6-His-28TTP to bovine liver PC.....	36
Figure 19: Restriction digestion of α -TTP/pET21b plasmid DNA and the purification of 6-His- α -hTTP from nickel affinity column.....	38
Figure 20: Time-dependent NBD- α -Toc transfer by 6-His- α -hTTP.....	39
Figure 21: Electrostatic potential map of α -Toc bound holo- α -TTP.....	40
Figure 22: Effect of anionic phospholipid on the transfer of NBD- α -Toc.....	41
Figure 23: Effect of vesicle size and curvature on the transfer of NBD- α -Toc....	42
Figure 24: Effect of anionic lipids and vesicle curvature on the transfer of NBD- α -Toc.....	43
Figure 25: Effect of endosomal lipid mixture on the rate of NBD- α -Toc transfer to LUVs.....	44
Figure 26: Effect of vesicle concentration on the rate of NBD- α -Toc transfer.....	45
Figure 27: Reversed transfer of NBD- α -Toc from PC LUVs to α -hTTP.....	46
Figure 28: Effect of anionic lipid on NBD- α -Toc pick up by 6-His- α -hTTP.....	47
Figure 29: Inter-vesicle transfer of NBD- α -Toc from acceptor vesicles to donor vesicles.....	48
Figure 30: Intrinsic tryptophan fluorescence spectrum of 6-His- α -hTTP.....	50
Figure 31: Stern Volmer's plot of α -hTTP quenched with acrylamide.....	51
Figure 32: FPLC separation of 39 kDa unknown protein from 6-His- α -hTTP and the subsequent analysis.....	54
Figure 33: Comparison of the ligand transfer activity of 39 kDa <i>E. coli</i> protein and 6-His- α -hTTP.....	56
Figure 34: Specific binding of NBD- α -Toc to 39 kDa contaminant.....	57

Figure 35: Matrix-assisted laser desorption/ionization MALDI time of flight (TOF) spectrum of trypsin digests of the unknown 39 kDa <i>E. coli</i> porin and α -hTTP.....	58
Figure 36: Structure of <i>E. coli</i> Outer Membrane Porin F (OmpF).....	59
Figure 37: Glutathione affinity purification of GST- α -hTTP expressed from hTTP/pGEX4T and the integrity of α -hTTP during storage.....	61
Figure 38: Titration of α -hTTP with NBD- α -Toc.....	61
Figure 39: Partitioning of NBD- α -Toc between α -hTTP and SUVs or LUVs.....	62
Figure 40: Effect of lipid concentration on the rate of NBD- α -Toc transfer from α -hTTP to PC SUVs and LUVs.....	64
Figure 41: Effect of ionic strength on the rate of NBD- α -Toc transfer to PC or PS SUVs.....	65
Figure 42: NBD- α -Toc transfer from α -hTTP to anionic SUVs or LUVs.....	66
Figure 43: Effect of cationic lipid on the transfer of NBD- α -Toc.....	67
Figure 44: Effect of vesicle size on the rate of NBD- α -Toc transfer from α -hTTP.....	68
Figure 45: Effect of lipid saturation on α -hTTP mediated NBD- α -Toc transfer...	69
Figure 46: Effect of other lipids on α -hTTP mediated NBD- α -Toc transfer.....	70
Figure 47: Dynamic Light Scattering (DLS) analysis of extruded 30 nm SUVs and probe sonicated SUVs.....	72
Figure 48: Schematic representation of a trans-membrane protein in a hydrophobic slab.....	76
Figure 49: Hydrophobic residues predicted to penetrate into lipid bilayer.....	77
Figure 50: Purified protein samples of wild type α -hTTP and the hydrophobic mutants visualized on 15% SDS-PAGE.....	79
Figure 51: Transfer of NBD- α -Toc from α -hTTP wildtype and mutants to SUVs and LUVs of bovine liver PC.....	82

Figure 52: Concentration dependent binding of α -hTTP wild-type and selected aspartate mutants to the immobilized lipid bilayer.....	84
Figure 53: Protein adsorption to the immobilized phospholipid bilayer determined by Dual Polarization Interferometry (DPI).....	86
Figure 54: Binding of wildtype α -hTTP and helix A8 mutants to SUVs as assessed by the size exclusion vesicle binding assay.....	88
Figure 55: Binding of α -hTTP wildtype and helix A8 mutants to LUVs assessed by size exclusion vesicle binding assay.....	90
Figure 56: The positively charged residues on or near the hinge region that may control the movement of the mobile gating helix A10.....	92
Figure 57: Comparison of mutant V217A to α -hTTP wild-type for their binding to SUVs assessed by size exclusion filtration assay.....	93
 3. DISCUSSION	
Figure 58: Dimension of α -Toc estimated from Deepview.....	99
Figure 59: Proposed membrane structure of vesicles prepared from liver PC versus total liver lipid LUV.....	106
Figure 60: Superposition of structures of human α -TTP in “open” and “closed” conformations.....	109
Figure 61: Comparison of protein adsorption to phospholipid bilayers measured by DPI (at 1 μ M TTP) and the rate of NBD- α -Toc to SUVs with the calculated energies of transfer of the “closed” and “open” conformations.....	110
Figure 62: Proposed recycling of α -Toc from endocytic pathway.....	113

ABBREVIATIONS

α -Toc	α -tocopherol
NBD- α -Toc	(<i>R</i>)-2,5,7,8-tetramethylchroman-2-[9-(7-nitrobenz[1,2,5]oxadiazol-4-yl amino) nonyl]-chroman-6-ol
AO- α -Toc	C9-anthroyloxy- α -tocopherol
α -TTP	α -tocopherol transfer protein
α -hTTP	human α -tocopherol transfer protein
6-His-28TTP	N-terminally 6-His-tag α -TTP fusion protein express from pET 28
6-His- α -hTTP	N-terminally 6-His-tag α -TTP fusion protein express from pET 21
GST	glutathione-S-transferase
GST- α -TTP	glutathione-S-transferase α -TTP fusion protein
OmpF	outer membrane porin F
AVED	Ataxia with vitamin E deficiency
CRALB	cellular retinaldehyde binding protein
SPF	supernatant protein factor
TAP	tocopherol associated protein
PITP	phosphatidylinositol transfer protein
FABP	fatty acid binding protein
SR-B1	scavenger receptor B1
CEHC	2,5,7,8-tetramethyl-2(2'-carboxyethyl)-6-hydroxychroman
LUVs	large unilamellar vesicles
SUVs	small unilamellar vesicles
Pfu	DNA polymerase isolated from <i>Pyrococcus furius</i>
DMSO	dimethylsulfoxide
IPTG	isopropyl-D-thiogalactoside
EtOH	ethanol
MeOH	methanol
MALDI-TOF	matrix-assisted laser desorption/ionization-time of flight
TRITC-DHPE	N-(6-tetramethylrhodaminethio-carbamoyl)-1,2-dihexadecanoyl- <i>sn</i> -glycero-3-phosphoethanol-amine, triethylammonium salt
DTT	dithiothreitol
EDTA	ethylenediaminetetraacetic acid
PMSF	phenylmethanesulfonyl fluoride
FPLC	fast-performance liquid chromatography
ACN	acetonitrile
TFA	trifluoroacetic acid
DPI	dual polarization interferometry
FRET	fluorescence resonance energy transfer
ER	endoplasmic reticulum
Golgi	Golgi apparatus
BAR	Bin/Amphiphysin/Rvs-homology
HEPES	(N'-2-Hydroxyethylpiperazine-N'-2 ethanesulphonic
BSA	bovine serum albumin
CL	cardiolipin
LBPA	lysobisphosphatidic acid

PC	phosphatidylcholine
PI	phosphatidylinositol
PS	phosphatidylserine
SM	sphingomyelin
DOPA	1,2-dioleoyl- <i>sn</i> -glycerol-3-phosphate
DOPC	1,2-dioleoyl- <i>sn</i> - glycerol-3-phosphocholine
DOPS	1,2-dioleoyl- <i>sn</i> -glycero-3-phospho-L-serine
DOTAP	1,2-dioleoyl-3-trimethylammonium-propane
DLS	dynamic light scattering
QELS	quasi elastic light scattering
HDL	high density lipoprotein
LDL	low density lipoprotein
VLDL	very low density lipoprotein
kDa	kilo dalton

1. INTRODUCTION

1.1. Overview of Vitamin E

Vitamin E is a well known fat soluble chain breaking antioxidant, it is a general term used to describe a family of eight stereoisomers of tocopherols. Vitamin E is synthesized only in plants. It is abundant in green leafy vegetables and various seed oils [1-3]. Vitamin E was first identified by Evans and Bishop as substance X that was required for reproduction in rats that were being fed rancid fat as an oxidative stress. In the absence of substance X, the animals exhibited normal growth but were sterile due to defective placental development [4]. Two years later, this anti-sterility dietary factor was renamed “vitamin E” in succession to the then recently discovered vitamin D [5]. The chemical structure of vitamin E was not elucidated until 1935, when Evans *et al.* finally crystallized an alcohol from wheat germ oil which contain vitamin E activity [3]. The term “tocopherol” is constructed from the ancient Greek word **tokos**, meaning childbirth and **pherein** to bear or to bring.

The early research effort on the antioxidant properties of vitamin E was pioneered by Mattill and his colleagues [6-8]. Initially, the only significant function of vitamin E was accredited to its antioxidant activity. However, in recent years, increasing evidence suggests that vitamin E may have other important cellular impacts besides its antioxidant properties (reviewed in [9, 10]. Whether or not the alternative cellular functions of vitamin E are directly linked to its antioxidant properties has become a topic for debate in the field of vitamin E research (reviewed in [11, 12]).

1.2. Biochemical Properties of Vitamin E

1.2.1. Vitamin E structures

Vitamin E describes four structurally similar forms (α , β , γ , δ) of tocopherols and tocotrienols (**Fig. 1**) (reviewed in [13]). The structure of vitamin E is composed of a 6-hydroxy-chroman head group with a 16-carbon hydrocarbon side chain linked at the C-2 position, known as a phytyl or isoprenoid tail. As shown in **Fig. 1**, the isomers are differentiated by the degree of methylation at R1 and R2 positions on the 6-chromanol ring, where α -tocopherol features a fully methylated chromanol [13]. Unlike tocopherols with a fully saturated phytyl side chain, tocotrienols contain an isoprenoid chain with three double bonds at the 3', 7' and 11' positions. The naturally occurring α -tocopherol

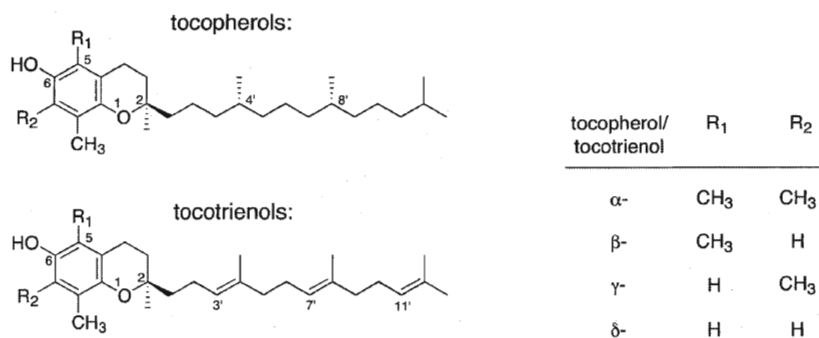
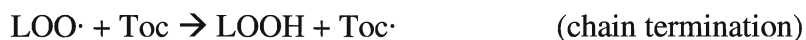
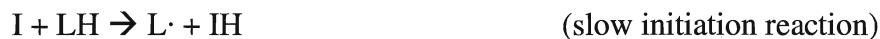


Figure 1: Structure of tocopherols and tocotrienols

has the 2*R*,4'*R*,8'*R* configuration, designated as *RRR* α -tocopherol [2,5,7,8-tetramethyl-2*R*-(4'*R*,8'*R*,12-trimethyltridecyl)-6-chromanol]. Synthetic α -tocopherol, however, consists of an equimolar racemic mixture of eight stereoisomers due to the chiral carbon centers at positions 2', 4', and 8', designated as all-*rac*- α -tocopherol. Therefore, dietary vitamin E supplements contain only 12.5% *RRR*- α -Toc, the most bioactive tocopherol isoform. Despite a similar antioxidant activity, resulting from an identical chromanol ring between racemic and *RRR*- α -Toc, only *RRR*- α -Toc (or α -Toc) is retained in our bodies by a hepatic tocopherol transfer protein (TTP) (reviewed in [14, 15]).

1.2.2. Vitamin E as antioxidant

α -Toc is a well known lipophilic antioxidant. Its primary role is to scavenge chain propagating lipid peroxyradicals, thereby protecting membranes from peroxidative damage. Peroxidation of polyunsaturated fatty acids consists of an initiation, chain propagation and chain termination reaction (reviewed in [16, 17]) outlined below:



where I is the initiator, LH is the fatty acid, $L\cdot$ is the fatty acid alkyl radical, $LOO\cdot$ is the lipid peroxy radical and LOOH is the hydroperoxide of fatty acid, Toc is the tocopherol and $\text{Toc}\cdot$ is the tocopheroxy radical. The initiation reaction is a slow, rate limiting process [6]. The reactive oxidant species (ROS) including superoxide produced by NADPH oxidase are examples of first-chain initiators [18, 19]. The propagation of lipid peroxidation continues until it encounters a tocopherol molecule, which donates a hydrogen atom and converts itself to a relatively stable tocopheroxy radical [20], thereby terminating the chain propagation reaction.

It is well accepted that the antioxidant property resides in the 6-hydroxychroman head group [21] (also reviewed in [22-24]), and that the hydrocarbon chain has no antioxidant function other than keeping the molecule embedded in membrane bilayers or in hydrophobic lipoprotein cores [25, 26]. Burton *et al.* reported that vitamin E is the only major chain breaking antioxidant found in human plasma [26, 27]. Tappel and Zalkin [28, 29] observed that α -Toc inhibited lipid peroxidation in liver mitochondria of

vitamin E deficient rabbits. In the iron-loaded rats, α -Toc was about 2 fold more effective than γ -Toc in reducing pantane produced from lipid peroxidation [30]. The recycling efficiency of the chromanols from their chromanoxyl radicals appeared to impact the antioxidant activity of α -Toc. α -Toc with a shortened hydrocarbon chain [31] or α -tocotrienol with the unsaturated isoprenoid chain [32] have improved recycling efficiency thereby enhancing their antioxidant potency. In both studies, chromanoxyl radicals were produced from enzymatic oxidation involving lipoxygenase and linolenic acid in rat liver microsomes or liposomes. The recycling efficiency of chromanoxyl radical to chromanol in the presence of exogenous reductants such as ascorbate and NADPH was subsequently determined by Electron Spin Resonance (ESR) measurement.

If the tocopheroxyl radical is not recycled, it can also undergo oxidative degradation into α -tocopheryl quinone (TQ) [33] (**Fig. 2**), which can be further reduced

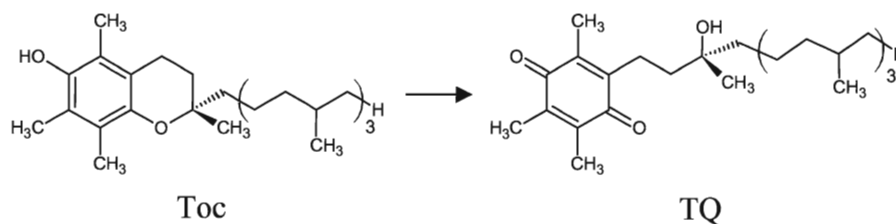


Figure 2: Structures of α -tocopherol (α -Toc) and its oxidative product α -tocopheryl quinone (TQ). These structures were re-drawn with Chems sketch software.

to tocopheryl hydroquinone, also an antioxidant. The TQ/Toc ratio is typically used as a marker for oxidative stress, and has been found in higher concentrations in the inner membrane of rat mitochondria [33]. TQ can bind directly with glutathione-S-transferase (GST) and inhibit its activity [34].

1.2.3. Bioavailability of Vitamin E isoforms

Despite the higher γ -Toc content in the North American diet [2], the circulating α -Toc in human serum is about 10 fold higher than γ -Toc [2, 35]. When vitamin E depleted rats were fed a diet containing α -Toc and γ -Toc at the ratio of 1:3, after 12 hours, their plasma concentration of α -Toc was more than 30 fold higher than γ -Toc [36]. Other animals, such as pigs and monkeys can also discriminate the naturally occurring *RRR*- α -Toc from synthetic homologues such as *all-rac*- α -Toc and *SRR*- α -Toc [37, 38].

The stereospecific retention of *RRR*- α -Toc in circulating plasma was similarly observed in humans [39-43]. Utilizing deuterium-labeled $^3\text{H}_6$ -*RRR*- α -Toc and $^3\text{H}_3$ -*SRR*- α -Toc stereoisomers, the half lives for circulating *RRR*- α -Toc and *SRR*- α -Toc were determined to be 47.5 ± 21.9 hrs and 15.8 ± 5.7 hrs, respectively [39]. However, for patients with familial isolated vitamin E deficiency whom were unable to discriminate between these two stereoisomers, the half-lives measured for both tocopherols were 13 hours. Although absorbed equally in chylomicrons, only *RRR*- α -Toc was enriched and secreted in VLDL (very low density lipoprotein) [40, 42]. Interestingly, the plasma concentration of α -Toc is maintained relatively steady; a maximum two-fold increase was observed when humans were supplemented with large doses of *RRR*- α -tocopheryl acetate [41, 43]. It is now generally accepted that hepatic α -tocopherol transfer protein (α -TTP) is critical to the homeostasis of α -Toc in circulation.

1.2.4. α -Tocopherol in lipid membranes

In order for α -Toc to act efficiently as a powerful antioxidant, it must be in proximity to both the source of peroxyradicals within the lipid bilayer and reductants near the aqueous interface. The location and antioxidant behavior of vitamin E in membranes

has been reviewed in great depth [22, 24, 44]. Fukuzawa [45] initially proposed three possible locations for the chromanol of α -Toc (**Fig. 3**): 1) at the aqueous interface; 2) close to the aqueous phase and forming hydrogen bond(s) with the oxygen of lipid phosphate groups or the acyl-ester of neighboring phospholipids; 3) near the unsaturated double bond of the fatty acid acyl chain that is buried in the membrane.

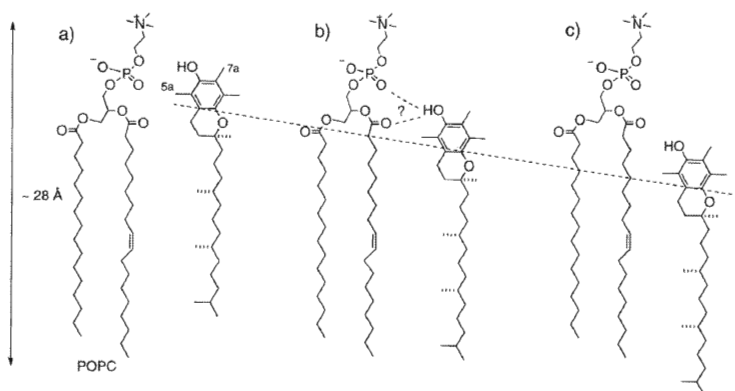
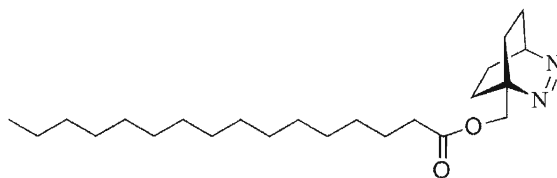


Figure 3: Three possible locations of α -Toc in POPC membranes. This scheme was initially proposed by Fukuzawa,[45] and redrawn by Atkinson *et al.* (reviewed in [22])

Several methods were employed to investigate the location of the chromanol of α -Toc in membranes (reviewed in [22] [24]). Stearic acids labeled with Doxyl (N-oxy-4,4'-dimethyloxazolidine-2-yl) [45] or (9-anthroyloxy) [25] at different positions along the hydrocarbon chain were used as probes. Quenching the intrinsic fluorescence of α -Toc by the above labels indicated that the chromanol moiety of α -Toc is optimally located between the 2' and the 7' position of the acyl chain in the membrane bilayer. The minor quench of α -Toc in DMPC liposomes by water soluble acrylamide was observed [45]. This observation further strengthened the conclusion that α -Toc is indeed close to, but not fully exposed at the membrane surface. For the acyl chains with double bonds buried deep inside the hydrophobic core of the lipid bilayer, the large dipole moment of lipid alkylperoxyl radicals [24] causes the peroxyl radical portion of the lipid acyl chains

to be more hydrophilic. Thus, these peroxy radicals are expected to move toward the aqueous interface and be reduced by α -Toc.

The lateral diffusion of α -Toc in a lipid bilayer was determined to be $1.8 \times 10^{-7} \text{ cm}^2 \text{ s}^{-1}$ as measured by fluorescent quenching of a radical mimick Fluorazophore-L [46], which is much slower than $4.8 \times 10^{-6} \text{ cm}^2 \text{ s}^{-1}$ reported by Fukuzawa *et al.* (reviewed in [24]). Fluorazophore-L is a lipophilic derivative of azoalkane 2,3-diazabicyclo[2.2.2]oct-2-ene (DBO) (**Fig. 4**), that contains a small fluorescent polar headgroup and a palmitoyl chain. The palmitoyl chain anchors the fluorophore to the



Fluorazophore-L

Figure 4: Chemical structure of Fluorazophore-L

lipid bilayer, while its polar reactive headgroup interacts with the phenolic hydroxyl of α -Toc near the lipid:water interface [46, 47]. Quenching rate constants of DBO by tocopherols and tocotrienols are in the order of $\alpha > \beta = \gamma > \delta$, similar to their activity against peroxy radicals [47]. In the presence of 15% or higher cholesterol, the diffusion of α -Toc was greatly reduced. The lateral diffusion of α -Toc also increased linearly with the temperature [47].

NMR spectra of deuterated α -Toc derivatives in organic solution revealed that the heterocyclic phenol ring of α -Toc exists in two half chair conformations in organic solutions [48]. In PC model membranes, the hydrocarbon tail of α -Toc rotates

perpendicularly to the membrane surface with gauche conformations at positions 5' and 9', with the latter been more disordered since it is further along the phytal chain.

1.2.5. Vitamin E uptake and metabolism

Vitamin E is the only major lipid soluble antioxidant found in human plasma [27, 49]. As illustrated in **Fig. 5**, upon dietary intake, vitamin E is first absorbed by enterocytes in the small intestine, then assembled and transported by chylomicrons into the circulatory system. In plasma, lipoprotein lipase (LPL) converts chylomicrons into chylomicron remnants by hydrolyzing triglyceride and some vitamin E and free fatty

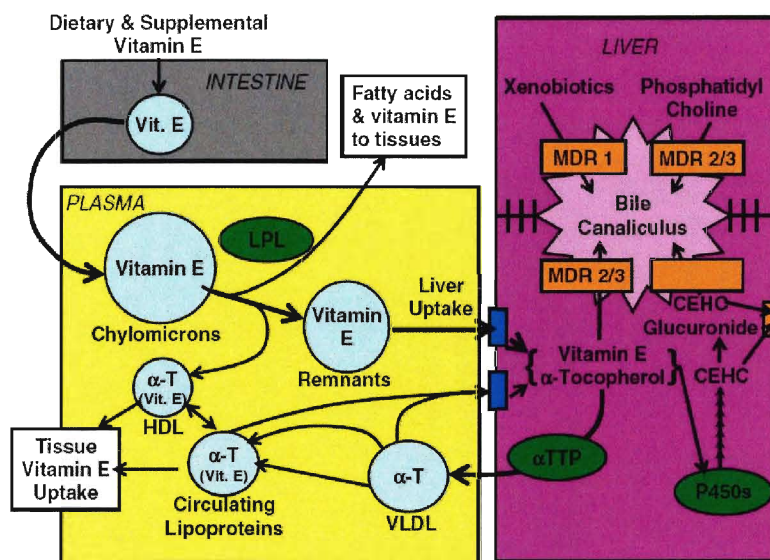


Figure 5: Uptake and secretion of Vitamin E in circulation system. This cartoon was created by Traber *et al.* [50].

acids are transferred non-specifically to various tissues [50]. Lipoprotein lipase mediated tocopherol transfer requires binding of this enzyme to the cell surface [51]. Heparin inhibits the binding of lipase to the cell surface [52], therefore it abolishes the γ -Toc uptake by fibroblast cells when incubated in an artificial lipid emulsion containing only γ -Toc [51]. Bulk of the ingested α -Toc is delivered to liver by circulating low density

lipoprotein (LDL) via receptor mediated uptake [53]. Traber and Kayden stated that the LDL receptor-mediated mechanism was not the only route for vitamin E delivery based on the finding that homozygous familial hypercholesterolemia patients who are incapable of expressing LDL receptors were not deficient in vitamin E [53]. Traber *et al.* also reported that vitamin E is exchanged between high density lipoprotein (HDL) and LDL, with preferred transfer of vitamin E from LDL to HDL [54]. Similar to lipoprotein lipase, transfer of α -Toc by lipoproteins also requires the direct interaction between the protein and macrophage like p388D₁ cells [55]. Scavenger receptor class B, type 1 (SR-BI), a plasma membrane glycoprotein, has been implicated in the uptake of HDL associated α -Toc and facilitates its movement across the blood brain barrier model [56]. Recently, SR-BI has also been shown to mediate vitamin E uptake in enterocytes. Anti-SR-BI antibody treatment of cells greatly inhibited vitamin E uptake [57]. Different tissues demonstrate specific subcellular distribution of α -Toc [58, 59]. For instance, in adipose tissue, α -Toc was found mainly in lipid droplets, not in the plasma membrane or other bilayer membranes [58]. Conversely, Rupar *et al.* found α -Toc to be highly enriched in the membrane of rat liver lysosomes [59].

In the liver, prior to the re-secretion of α -Toc back to the circulation, the excess α -Toc along with other ingested tocopherols are metabolized and degraded. These tocopherols undergo phytol side chain shortening by ω -oxidation followed by β -oxidation to produce the water-soluble metabolites carboxyethyl-hydroxychroman CEHC derivatives (**Fig. 6**), which are excreted in urine [60-67] and bile [68]. The ω -oxidative pathway is likely regulated by cytochrome p450 isoforms CYP3A [60, 61] and CYP 4F2 [64-67]. The

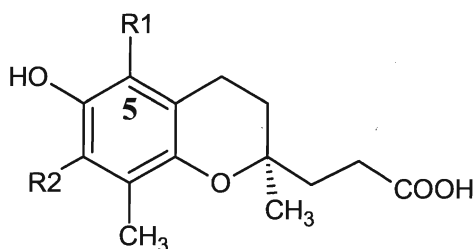


Figure 6: Structure of carboxyethyl-hydroxychroman derivatives. α -Toc: methylation at both R1 and R2; β -Toc: methylation at R1; γ -Toc: methylation at R2; δ -Toc: non-methylated at both R1 and R2.

secretion of α -CEHC was increased 5-fold upon treating the *all-rac*- α -Toc primed human hepatoma HepG2 cells with rifampicin, a CYP3A stimulator [61]. In contrast, CYP3A inhibitor ketoconazole greatly inhibited metabolism of tocopherol isoforms in rat primary hepatocytes and HepG2/C3A cells [60]. More interestingly, tocopherols without methyl group at C-5' position such as γ -Toc and δ -Toc were preferentially metabolized [61, 64-67]. Tocotrienols share the same metabolic oxidative fate as their tocopherol counterparts, consequently produce the same metabolites [62]. The un-metabolized α -Toc is selectively retained and diverted from lysosomal degradation pathway by α -tocopherol transfer protein (α -TTP). The salvaged α -Toc is thought to be incorporated into nascent VLDL and recycled back to the circulation system [69, 70]. Exactly how α -Toc is diverted from lysosomal degradation pathway is still a mystery and remains to be solved.

1.2.6. Non-antioxidant properties of vitamin E

During the last two decades or so, some apparently non-antioxidant related cellular functions of α -Toc have been proposed [71-73]. α -Toc appears to modulate cell proliferation, cell signaling as well as gene expression. The first non-antioxidant function of α -Toc was reported in 1991 by Boscoboinik *et al.*, who found that both protein kinase

C activity [71] and aorta smooth muscle cell proliferation were inhibited by α -Toc, and not by other similar antioxidants (**Fig. 7**) such as Trolox and α -tocopheryl esters including α -tocopheryl acetate [72]. Other enzymes inhibited by α -Toc are

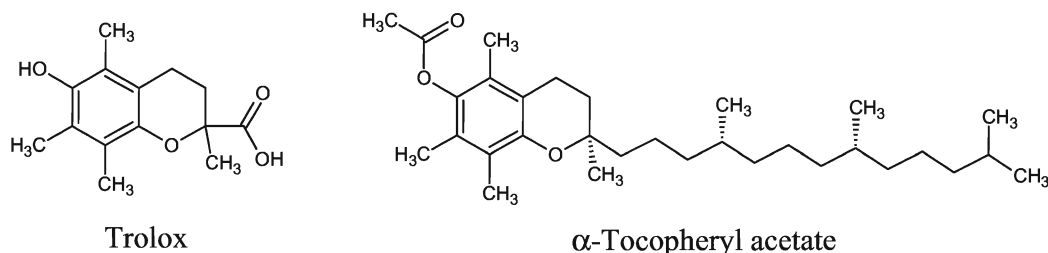


Figure 7: Structure of Trolox and α -tocopheryl acetate

phospholipase A2, cyclooxygenase, diacylglycerol kinase and NADPH oxidase (reviewed in [10]). Aside from the above biological functions, α -Toc also stabilizes membrane integrity by forming complexes with free fatty acids [74] and lysophospholipids [73]. Although similar structure but without a side chain, PMC (2,2,5,7,8-pentamethyl-6-hydroxychromane) was unable to protect membranes from the chaotropic effect introduced by free fatty acids in spite of its equally potent antioxidant activity [73]. α -Toc also prevents the Ca^{2+} induced fusion of PS vesicles and mixing of the aqueous contents, the effect increases with the concentration of α -Toc [75]. α -Toc appears to stabilize the transmembrane potential and increase membrane microviscosity in the phospholipase treated membrane [76].

1.3. Vitamin E binding proteins

Besides the non-specific phospholipid transfer proteins, several unique and not well studied vitamin E binding proteins have been identified. The exact role of these vitamin E binding proteins is not well understood, but they are expected to be involved in the peripheral tissue distribution of vitamin E.

A small 14.2 kDa cytosolic tocopherol binding protein was discovered and studied primarily in Dutta-Roy's laboratory. This protein was first detected in rat liver and heart [77], then also found in rabbit heart, bovine heart and human placenta [78-80]. The function of this protein has not been elucidated.

Afamin, is a 74 kDa glycoprotein from the albumin multi-gene family, found mainly in human plasma and follicular fluid and much less in cerebrospinal fluid. The concentration of afamin is correlated to that of vitamin E in the follicular and cerebrospinal fluids, but not in the plasma [81]. Afamin has a high binding capacity for both α - and γ -tocopherol due to its multiple binding sites (maximum of 18 tocopherol molecule per molecule of afamin), despite the relatively low binding affinity of 18 μ M [82]. Afamin facilitates α -tocopherol crossing the polarized brain capillary endothelial cells to basolaterally cultured astrocytoma cells in the brain [83]. Collectively, these observations imply that afamin might play an important role in vitamin E homeostasis in the central nervous system.

1.4. α -Tocopherol Transfer Protein (α -TTP)

1.4.1. α -Tocopherol transfer protein

α -TTP is a 32 kDa cytosolic protein that was first found in rat liver cytosol [84]. Later, it was also detected in other tissues, such as heart, spleen, lung and placenta [85, 86]. In 1992, Yoshida *et al.* successfully purified α -TTP from rat liver cytosol [87], and shortly after, a homolog of α -TTP was isolated from human liver [88]. α -TTP exhibited high binding affinity for α -Toc that can only be partially displaced by other tocopherol isoforms [89, 90]. The displacement of α -Toc by its homologues was: 38% by β -Toc, 9% by γ -Toc and 2% by δ -Toc, respectively [89]. α -tocopherol acetate and α -tocopherol

quinone also poorly competed for α -Toc with levels similar to γ -Toc. Overall, tocopherol binding affinity and antioxidant activity were directly correlated to the degree of methylation at the chromanol headgroup of α -Toc. Therefore, biological activity of vitamin E appears to be determined by their ability to bind α -TTP.

Although vitamin E deficiency does not seem to alter α -TTP expression, administration of α - or β -Toc to vitamin E deficient rats appeared to up-regulate α -TTP mRNA where both isoforms were equally effective [36]. In normal brain tissues, α -TTP is either absent or below detection level, while in the brains of patients suffering from AVED and other oxidative stress related neurodegenerative diseases, such as Alzheimer's disease and Down's syndrome, Copp *et al.* detected an increase in the expression of α -TTP [91]. Whether oxidative stress truly modulates the α -TTP expression and thereby regulates the tissue redistribution of α -Toc in the brain or not requires more research attention before any firm conclusions can be made.

1.4.2. Crystal structure of α -TTP

The primary structure of α -TTP from rat liver was reported by Sato *et al.* [92] in 1993. This protein contains 278 amino acid residues. In 2003, the crystal structure of α -TTP was published by Meier *et al.* [93] and Min *et al.* [94]. Overall, the α -TTP structures deduced from both studies are very similar. α -TTP is composed of two domains: an N-terminal all-helical domain and a C-terminal lipid binding CRAL-TRIO domain with a $\beta\alpha\beta\alpha\beta\alpha\beta$ fold. The α -Toc binding pocket consists of mainly hydrophobic amino acids, and a few well-defined water molecules that form a tunnel connecting the binding pocket to the bulk solvent. Extensive Van der Waals contacts

form between the methyl groups of the chromanol moiety and the hydrophobic binding pocket of the protein. α -Toc is buried deep in the binding pocket. In order for α -Toc to enter and exit the binding site, α -TTP must undergo a major conformational rearrangement. Furthermore, the isoprenoid side chain of α -Toc bends back on itself around C4' and C8' positions when crystallized inside the binding pocket of α -TTP. **Fig. 8** illustrates the two conformations of α -TTP: the Triton X-100 bound open conformation and the α -Toc bound closed conformation. What differentiates these two structures is the position of the mobile lipid exchange loop or lid (residues 198 – 221, colored in gray). The presence of the detergent molecules appears to induce an “open” conformation and expose the hydrophobic lipid binding pocket. Similar lid and conformational change can be found in other CRAL-TRIO proteins such as supernatant protein factor (SPF) [95], Sec14 and yeast Sfh1 [96, 97].

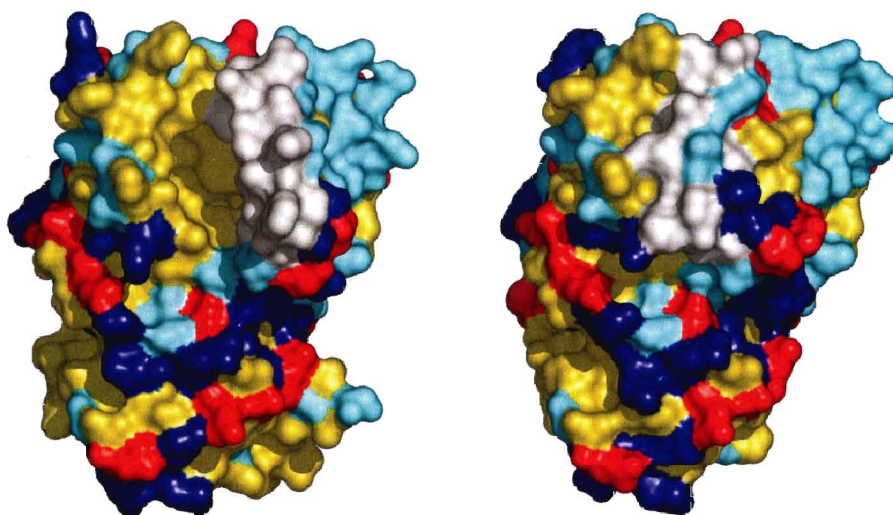


Figure 8: Surface comparison of the open (left) and the closed (right) conformation of α -TTP structure. Hydrophobic residues are colored in yellow, basic residues are colored in blue, acidic residues are red and polar residues are shown in cyan. The mobile lipid exchange loop (residues 198-221) are colored in light gray [93].

The phenolic hydroxyl group of α -Toc forms a hydrogen bond with the carbonyl group of Val 182 and two water molecules [94]. Hence, α -Toc homologues without hydroxyl groups, such α -tocopherol acetate and α -tocopheryl quinone, cannot form hydrogen bonds with Val 182, are poor substrates for α -TTP, with only 10% binding to α -TTP. The methyl groups at C5' and C7' positions of the chromanol are also critical for α -TTP recognition. In comparison to α -Toc, the absence of the C5' or C7' methyl group as in β -Toc and γ -Toc reduce their binding to α -TTP by 62% and 90% respectively. δ -Toc missing both C5' and C7' methyl groups, exhibited only 2% binding to α -TTP [89]. Stereospecific selection occurs primarily at C2' position, which prefers the *RRR*-configuration. Similar preference is also given for the *RRR*-stereochemistry in the phytol tail at 4' and 8' positions. Therefore, *SRR*- α -Toc, α -tocotrienol with unsaturated tail and trolox without phytol chain all exhibited only 10% of binding to α -TTP in comparison to α -Toc.

1.4.3. Role of α -TTP in the intracellular trafficking of α -Toc

Several hepatoma cell lines that stably express α -TTP have been established [98-100]. The intracellular transfer of α -Toc has been studied using radiolabeled and fluorescent tocopherol derivatives. Previous observations indicated that α -Toc is associated with VLDL before its secretion from rat hepatocytes [69, 70]. However, Arita *et al.* [98] concluded that α -TTP mediated transfer of α -Toc is independent of VLDL. Treating McARH7777 hepatoma cells with Brefeldin A, an antibiotic that disrupts the Golgi apparatus and inhibits VLDL secretion, has no effect on α -Toc secretion [98]. In contrast, the anti-malarial drug chloroquine reduced α -TTP mediated α -Toc secretion by

50% or higher [99, 100]. Since chloroquine is a membrane permeable agent that neutralizes the acidic environment of late endosomes/lysosomes, Horiguchi *et al.* concluded that the increase in the late endosomal pH induced the accumulation of α -TTP and also impaired its ability to transfer α -Toc. Furthermore, the N-terminal 21 to 50 amino acid residues of α -TTP (rich in arginine) appeared to be important for its pH-dependent localization [100]. Uptake of α -Toc from HDL was greater than LDL, and treatment with an antibody against scavenger receptor class B type I (SR-BI) inhibited α -Toc uptake by approximately 40% into hepatocytes [99]. Qian *et al.* [99] also found that α -TTP was colocalized with NBD- α -Toc as well as a late endosomal/lysosomal protein LAMP-1 in the endocytic compartment. In the absence of α -TTP expression, most of the imported NBD- α -Toc failed to migrate to the plasma membrane where it would be excreted [99]. Both U18666A (lysosomal lipid trafficking inhibitor) and glyburide (ABC reporter inhibitor) reduced α -Toc secretion. Glyburide completely abolished the α -TTP activity. Interestingly, Brefeldin A only inhibited α -Toc secretion when apolipoprotein A-1 (Apo A1) was absent. Overall, these findings suggest that α -TTP mediated secretion of α -Toc from the liver is likely to associate with Apo-A1, not VLDL. The exact mechanism which α -TTP employs to return α -Toc back to the circulation is currently unknown, and it is still under intensive investigation.

1.4.4. Ataxia with Vitamin E deficiency (AVED)

Mutations in the α -TTP result in the disorder called Ataxia with Vitamin E Deficiency (AVED). It is an autosomal recessive disorder characterized by very low concentration of circulating vitamin E. In normal healthy humans, the serum vitamin E concentration is 9 ± 4 mg/liter (i.e. approximately 20 μ M). Whereas in AVED patients,

serum vitamin E concentration is highly correlated to the severity of the disorder [101-105]. For milder AVED cases, patients retain about 50% or greater of the normal serum vitamin E level [101-103]. However, in the severe form of AVED, patients' serum vitamin E can be as low as 10% or less [102, 104, 105]. Even with plasma α -Toc below the threshold of 30 - 40 $\mu\text{mol/L}$, AVED patients are incapable of retaining α -Toc, which is evident in their increased urinary secretion of the α -Toc metabolite α -CEHC [106].

Patients suffering from AVED exhibited neurological symptoms similar to Friedreich's ataxia and abetalipoproteinemia disorder. Unlike the abetalipoproteinemia disorder, caused by fat mal-absorption in the small intestines, AVED patients experience normal absorption in the small intestines, but due to the mutations in α -TTP, fail to selectively salvage α -Toc and recycle it into the circulation system. Supplementation of α -Toc acetate at 0.8 to 1 g per day during the early stage of the disease, helps to improve the patients' serum vitamin E concentration, thereby ameliorating the symptoms and preventing the disease progression [101, 107].

The AVED locus was first localized to chromosome 8q by homozygosity mapping analysis [104, 108], then refined to 8q13 by Arita *et al.* [109]. The first AVED case was reported in 1981 by Burck *et al.* [110]. Since then, 22 mutations in the α -TTP gene have been identified (reviewed in [15]). Mutations caused by incorrect initiation and termination of α -TTP gene transcription, result in a reduced level of functional α -TTP or defective α -TTP of incorrect sizes. For instance, a single base deletion at position 744 that led to a frame shift in homozygous Moroccan patients, resulted in substitution of the last 30 amino acids with aberrant 14 amino acids [107]. Similarly, one

Japanese female patient with a mutation at an upstream initiation codon in the 5'-untranslated region exhibited a 50% reduction in the level of α -TTP protein.

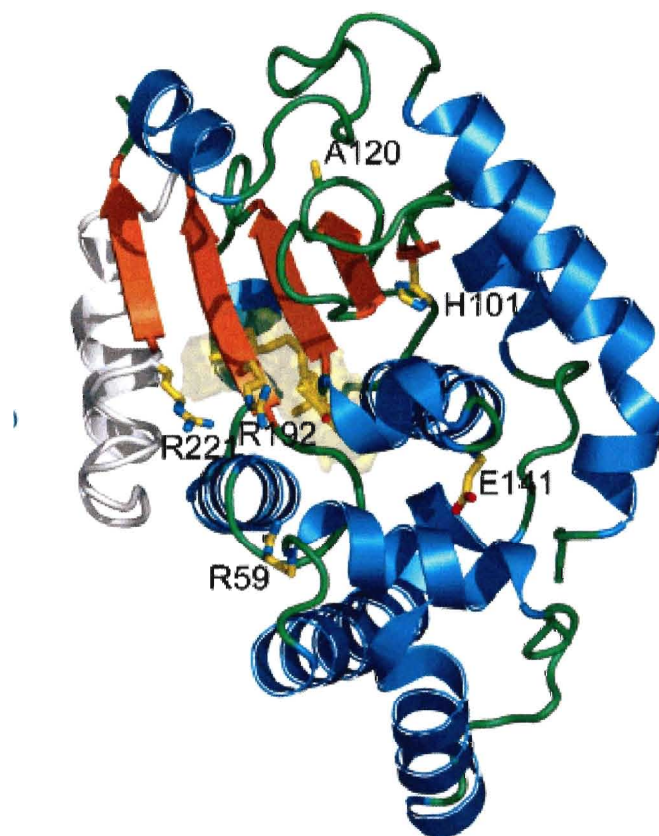


Figure 9: Location of missense AVED mutations on α -TTP. Shown is the three dimensional structure of the protein with mobile lipid exchange loop (residues 198-221) in light gray color and the lipid binding cavity in orange. The original structural image was created by Min *et al.* [94]. Presented here is the redrawn cartoon by Morley *et al.* [111].

Alternatively, a single amino acid residue change in α -TTP due to point mutation in α -TTP gene can also cause AVED of different levels of severity. The locations of the six major mutations of α -TTP are highlighted in **Fig. 9**. As shown, three of these are Arg 59, Arg 192 and Arg 221 located on the protein surface that form a positively charged cleft. His 101 and Glu 141 however are found in the interior of α -TTP. Arg 59, Glu 141 and Arg 221 are highly conserved residues among CRAL-TRIO family proteins.

Mutations at these residues cause the early onset and more severe forms of the disease. Conversely, mutations at the non-conserved His 101, Ala 120 and Arg192 are responsible for the late onset and milder form of the disease. Two additional point mutations have been reported, but are not shown in **Fig. 9** are located at residues Leu 183 and Gly 246 (reviewed in [15]). The only mutation that appears to alter the ligand binding pocket is Leu(183)Pro, this mutation not only reduces the hydrophobicity of the binding pocket, but also introduces a kink into helix 9, and thus disrupts the interaction between α -TTP and α -Toc [94]. Thus, it is not surprising that the Leu(183)Pro mutation leads to a severe form of AVED [112].

The physiological relevance of AVED mutations has been tested in *in vitro* experiments. When six AVED mutants were tested for their abilities to transfer α -tocopherol using purified recombinant α -TTP in a vesicle transfer assay by Morley *et al.* [111], Arg(59)Trp, Glu(141)Lys and Arg(221)Trp mutations introduced a modest 2-3 fold reduction in ligand transfer. Similarly, the milder AVED mutants His(101)Gln, Ala(120)Thr and Arg(192)His behaved almost identical to the wild type α -TTP. These authors concluded that the functional defect in the AVED mutants may not be due to their ligand transfer ability, but rather it is caused by the failure of these variants to interact with other cellular proteins. Further investigation with transfected HepG2/C3A cells indicated that Arg(59)Trp, Arg(221)Trp, and Ala(120)Thr mutants were, similar to wild type, localized to endosomes/lysosomes, but failed to translocate to the plasma membrane, and thus inhibited α -Toc secretion by 33%, 60% and 83%, respectively [113]. Interestingly, Arg(59)Trp, Arg(221)Trp, and Ala(120)Thr were more readily degraded than the wildtype α -TTP. It was recently suggested by Morley *et al.* [114] that the lack

of ability for Arg(221)Trp mutant to extract α -Toc from the lipid bilayer might explain its inability to transfer α -Toc. Therefore, the physiological role of α -TTP depends on its ability to direct the delivery of α -Toc from endosome/lysosomes to the plasma membrane.

Transgenic mice lacking α -TTP gene ($TTP^{-/-}$) were created to explore the physiological significance of α -TTP [115-118]. α -TTP knock-out (KO) mice have less than 10% of normal α -Toc concentrations in their lungs, plasma and brain compared to the wildtype mice [115, 116]. In mice fed a normal diet, both their plasma and brain α -Toc concentration appeared to be regulated by α -TTP expression: with 100% for the wildtype α -TTP^{+/+}, 50% for heterozygous α -TTP^{+/-} and undetected for homozygous α -TTP^{-/-} [117, 118]. Furthermore, male homozygous α -TTP^{-/-} mice were fertile, whereas female homozygous α -TTP^{-/-} mice failed to carry their embryo to full term. Diet supplemented with α -Toc or synthetic antioxidant BO-653 prevented the miscarriage in the homozygous α -TTP^{-/-} pregnant mice [117]. The antioxidant effect of α -Toc was also evaluated in the lungs of both wild type and α -TTP knockout mice. Clusters of immune-inflammatory genes were found to be down regulated upon exposure of this knockout mice to cigarette smoke [115].

1.5 CRAL-TRIO protein family

α -TTP belongs to a lipid binding protein family containing CRAL-TRIO domains (Pfam PF 00650) [119], also known as Sec14 domain (reviewed in [120].) Other members in this family include: cellular retinaldehyde binding protein (CRALBP) which is expressed mainly in retina and binds to 11-*cis*-retinal with high affinity ($K_d = 15$ nM)

[121, 122]; the yeast Sec14 protein which binds and regulates the transfer of phosphatidylinositol (PI) and phosphatidylcholine (PC) between Golgi and plasma membranes [96, 97, 123]; and supernatant factor (SPF) or tocopherol association protein (TAP), which stimulates the epoxidation of squalene to lanosterol during the cholesterol synthesis [124]. In addition to the CRAL-TRIO domain, TAP/SPF also possesses a C-terminal jelly-roll barrel Golgi Dynamics (GOLD) domain [95, 125]. The GOLD domain is speculated to be essential in protein-protein interactions during vesicular trafficking from Golgi. All of these proteins are involved in intracellular transfer of different classes of lipids. Among a few CRAL-TRIO proteins tested, α -TTP exhibited the highest affinity for α -Toc binding [90]. A BLAST search has identified many others non-lipid transfer proteins which also contain the CRAL_TRIO lipid binding domain, such as Rho GTPase-activating protein 1 and MEG2 tyrosine phosphatase.

1.6 Mechanism of hydrophobic ligand transfer

Intracellular compartments are separated by lipid membranes. The transportation of small hydrophobic molecules such as free fatty acids and lipid soluble vitamins across aqueous barrier to its targeted destination is thermodynamically unfavorable. The routes that are known to facilitate the intracellular transportation of hydrophobic molecules are either based on vesicular or protein mediated transfer mechanisms.

Protein mediated transfer of hydrophobic ligand to its acceptor membranes can be either collisional or diffusional. A collisional based transfer mechanism relies on the direct collisional interaction between the protein and the target membranes. Therefore, the rate of ligand transfer is dependent on both the concentration and the lipid composition of the membrane [126-131]. Conversely, the aqueous diffusional transfer is

determined predominantly by the ligand behavior and the aqueous environment, such that the rate limiting step is the dissociation of ligand from the protein [126, 132, 133]. Both diffusional and collisional modes of cholesterol transport have been demonstrated (**Fig. 10**). Based on the study conducted by Cheruku *et al.* [134], lysosomal cholesterol export mediated by Niemann-Pick Type C2 protein (NPC2) is a collisional event. More interestingly, the rate of transfer was greatly enhanced in the presence of lysobisphosphatidic acid (LBPA), a late endosomal specific lipid. In the early studies of cholesterol transport, the aqueous diffusion of cholesterol between serum HDL and LDL [135], or human erythrocytes and plasma [136] were reported. These studies suggested that the mode of cholesterol transportation is determined by its tissue or subcellular localization.

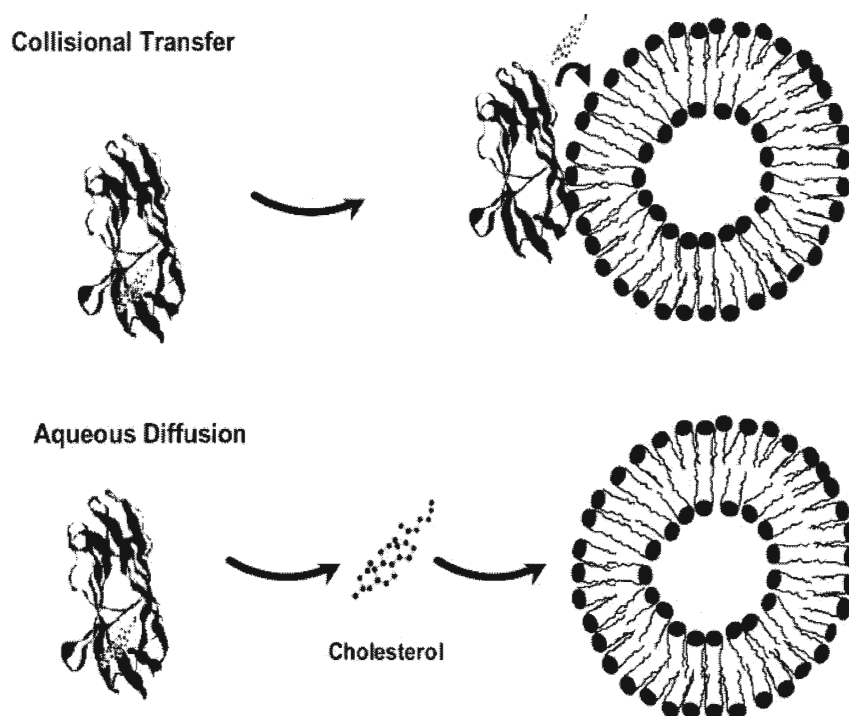


Figure 10: Potential mechanisms of cholesterol transfer by NPC2 protein to membranes. This cartoon was created by Cheruku *et al.* [134], illustrates the collisional mechanism that is mediated by the interaction between NPC2 and membrane; whereas the aqueous diffusion is mediated by the dissociation of cholesterol from NPC2.

Other thoroughly studied lipid transfer proteins are fatty acid binding proteins (FABPs). Nine tissue specific fatty acid binding proteins have been identified so far (reviewed in [127]). All FABPs share similar tertiary structures, composed of a 10-stranded anti-parallel β -barrel and two short α -helices that form a lid on one side of the β -barrel which regulates the entry and exiting of free fatty acids. Unlike other members of its family that transfer one fatty acid per protein by a collisional mechanism, liver FABP with the largest binding cavity, is capable of binding two fatty acids [137] or other larger hydrophobic ligands [137] and delivers its ligand(s) via the aqueous diffusion mechanism [138].

1.7 Membrane curvature sensing proteins

From the above examples, the molecular forces that regulate protein-membrane interactions are electrostatic, hydrophobic and hydrogen bonding. These interactions are therefore essential in the collisional based mechanism of ligand transfer. However, in some scenarios, another type of specific interaction is required, in addition to the electrostatic and the hydrophobic interactions. For example, Saari *et al.* [122] demonstrated that the binding of CRALBP to phosphatidic acid (PA) was critical for the release of its ligand 11-*cis*-retinal. The apparent binding specificity of CRALBP for various phospholipids was: PA > PI (3,4,5)P3 > PS > PI (4,5) P2. Moreover, the efficacy of these phospholipids to facilitate ligand release by CRALBP matched well with their binding affinity leading the authors to speculate that binding was likely mediated by spatial recognition rather than simply electrostatic interaction.

The ability of proteins to sense and induce membrane curvature has become an active research area in recent years. McMahon and Gallop published an excellent review

on membrane remodeling and the formation of membrane curvature [139]. Membrane curvature can be generated by a change in its phospholipid composition, by the introduction of phospholipids with inherently high curvature (reviewed in [22]). Alternatively, membrane curvature can also be formed during protein reorganization, such as the oligomerization of integral membrane proteins, the insertion of an amphipathic helix, or the dimerization of crescent-shaped BAR domains. Proteins with enhanced binding or functional activity toward highly curved membranes are: cytochrome *b*₅ [140], acyl-CoA binding protein (ACBP) [141], Arf GTPase activating protein 1 (ArfGAP1) [142, 143], α -synuclein [144], glycolipid transfer protein [145] and annexin B12 [146]. Membrane curvature also appears to modulate the ability of Magainin 2 (an antimicrobial peptide) to recognize antigens presented by liposomes [147] and to facilitate pore formation within bacterial cell membranes [148].

1.8 Proposed orientation of α -TTP in the lipid membrane

The Orientation of Proteins in Membranes (OPM) database (<http://opm.phar.umich.edu/>) is an excellent tool to explore the impact of hydrophobic forces in protein-membrane interactions. As long as the crystal structure of a particular protein is available, OPM can calculate the changes in free-energy (ΔG) of this protein upon its insertion into the membrane [149, 150]. The transfer energy is minimized based on the flexibility of side chains, not the backbone of the protein [149]. The lipid exchange loop has been hypothesized to interact with lipid membranes from the crystal structures of α -TTP published by Meir *et al.* [93], but the position of the protein on the lipid surface when it interacts with the lipid membrane, is still unknown at the present time. Therefore, the orientation of α -TTP with respect to the lipid membrane was

calculated, and the orientations with the maximum free energy change are presented in **Fig. 11**. According to this model, the gating helices A8 and A10 are submerged into the lipid bilayer, and the hydrophobic residues highlighted in red are predicted to undergo a deep insertion into the hydrophobic core. If this model is correct, then replacing the highlighted hydrophobic residues with charged ones would greatly reduce the binding of α -TTP to the membranes and thereby reduce the transfer of α -Toc. Guided by this model, a mutagenesis study was conducted to investigate the role of helices A8 and A10 on the membrane targeting and the ligand transfer of α -TTP.

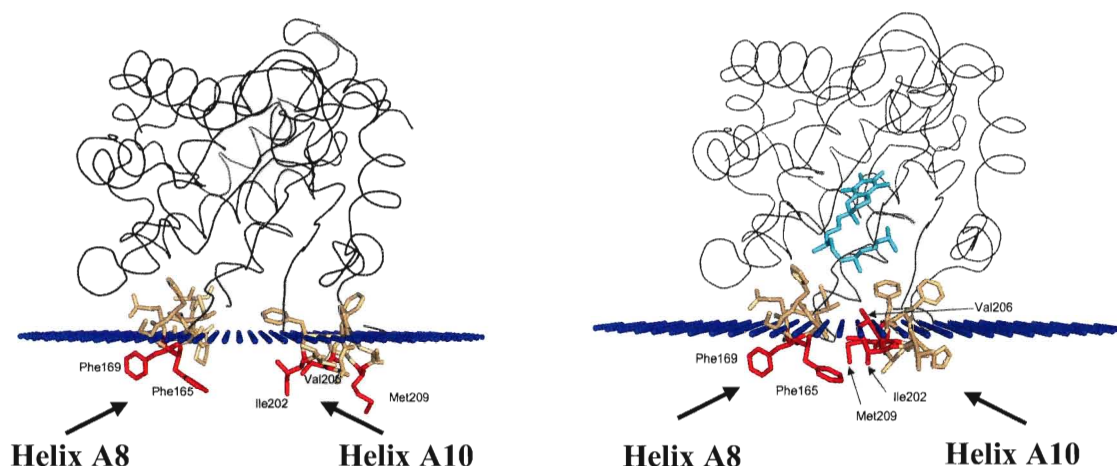


Figure 11: Orientation of α -TTP in a lipid membrane. The blue dots are the calculated hydrophobic membrane boundaries. **A)** Triton-X100 bound apo- α -TTP (pdb:1oiz) and **B)** α -Toc bound halo- α -TTP (pdb:1r51). Highlighted in red are the hydrophobic amino acids which are expected to insert into the membrane, and cyan sticks is α -Toc.

Previous work from our group has demonstrated the preferential binding of α -TTP for α -Toc over other dietary tocopherols. However, the relevance of this protein in the transfer of α -Toc to its target membranes has not been investigated in detail. Since α -TTP is thought to remain in the late endosomal/lysosomal compartment, yet, salvaged α -Toc must be returned to the plasma membranes before re-entering the circulation

system. The exact role of α -TTP in the transfer of α -Toc to plasma membranes is currently unknown. In order to gain more insights into this complicated question, we must first understand the mechanistic basics involved in α -TTP mediated transfer of α -Toc and identify the factors that can impact rate of its ligand transfer. Using a fluorescent probe NBD- α -Toc, a fluorescent resonance energy transfer (FRET) assay was developed and utilized to investigate the mechanism of α -Toc transfer by α -TTP. The data acquired suggest that α -Toc transfer by α -TTP is not only collisional based but also sensitive to membrane curvature. Furthermore, the lipid binding domain(s) as well as the key amino acids that are essential in governing the translocation of α -Toc have been identified from this mutagenesis study.

2. RESULTS

2.1. Transfer of NBD- α -Toc to model lipid membranes evaluated with 6-His- α -hTTP isolated from pET28b and pET21b expression vectors

2.1.1. 6-His- α -hTTP with an extension expressed from hTTP/pET28b construct

Human α -TTP was previously cloned by Panagabko *et al.* [151] (in our lab) into the pET28b vector with SalI and NotI restrictions sites. This construct produced soluble recombinant α -TTP of 35 kDa with an N-terminal 6-histidine tag, denoted here as 6-His-28TTP. Due to the presence of an N-terminal 40 amino acid extension from the pET28b expression vector, this protein was 3 kDa larger than the published size of 31.75 kDa of the native human α -TTP [109]. In spite of the N-terminal extension, 6-His-28TTP bound to tritiated α -Toc with high affinity ($K_D = 25 \pm 2.6$ nM), and with much reduced affinity toward β -, γ - and δ -tocopherol isoforms [90]. Using the nickel affinity purification protocol described in the Methods section, after the removal of several non-specifically

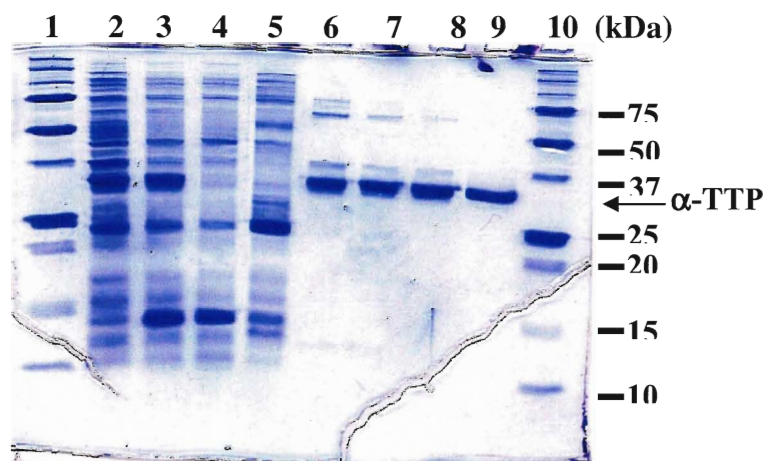


Figure 12: Nickel chelate affinity column purification of 6-His-28TTP expressed in *E. coli* BL21 (DE3) cells. Cell lysate and purified protein samples (~ 5 μ g per lane) were analyzed on 15% SDS-PAGE. Lane 1&10: protein marker (BioRad #161-0363); Lane 2: insoluble cell lysate; Lane 3: soluble cell lysate; Lane 4: nickel column flow through fraction; Lane 5: buffer wash; Lane 6 – 8: 250 mM imidazole wash fraction #1 to 3; Lane 9: 400 mM imidazole elution fraction #2.

bound proteins in 250 mM imidazole (lane #6 to 8), a highly purified 6-His-28TTP was eluted in 400 mM imidazole (lane #9) (**Fig. 12**).

An unknown protein of 37-39 kDa typically co-eluted with 6-His-28TTP in the 400 mM imidazole, as a minor contaminant. A hint of this protein is visible in lane #9 (**Fig. 12**). In order to determine whether this 37-39 kDa protein contained a 6-His tag, western blot analysis was performed with an antibody recognizing the 6-His tag. This antibody detected only the major protein band at 35 kDa, but not the ~39 kDa protein contaminant, suggesting that the 35 kDa protein is indeed 6-His-28TTP and the 39 kDa is an *E. coli* protein with high affinity for nickel ions. Interestingly, the level of 39 kDa unknown protein contamination varied among the preparations. A low level of contamination in a purified recombinant protein is generally accepted and it is not expected to alter the behavior of the recombinant protein. In our case, only one contaminating protein was found and accounted for ~ 5-10 % of the total recovered proteins. The purified 6-His-28TTP was therefore utilized for FRET assay development and optimization.

2.1.2 Characterization of NBD- α -Toc fluorescent probe

[^3H]-RRR- α -Toc was used as early as 1964 by Spencer and Bow [152] to measure the ability of vitamin E to cross the small intestine, and later was employed to identify the α -Toc binding sites on human erythrocytes [153] and its affinity to bind to α -TTP [90]. Utilizing radiolabelled α -Toc to study its inter-membrane transfer is rather indirect and time consuming. Although the end point of transfer can be determined, the real time transfer data is lost during the sample handling and separation. To circumvent these potential complications, a fluorescent analog of α -Toc, (*R*)-2,5,7,8-tetramethyl-chroman-

2-[9-(7-nitro-benzo[1,2,5]oxadiazol-4-ylamino)-nonyl]-chroman-6-ol (NBD- α -Toc) was synthesized in our lab by Nava *et al.* [154]. As shown in **Fig. 13**, an NBD moiety was conjugated at the C9 position of an n-alkyl spacer in place of the α -Toc phytyl side chain. Although three carbons shorter than the natural α -Toc, the total molecular length of NBD- α -Toc (24.5 Å) is almost same as that of α -Toc (22.1 Å). NBD- α -Toc binds to 6-His-28TTP with high affinity, with a dissociation constant (K_D) of 56 ± 15 nM [154], which is slightly reduced compared to [3 H]-*RRR*- α -Toc at 25 ± 2.8 nM [90]. NBD- α -Toc is self-quenched in aqueous solution, fluoresces only in hydrophobic environments such as organic solvents, lipid membranes, or within lipid binding proteins. In absolute ethanol, the maximum excitation and emission determined for NBD- α -Toc were 470 nm and 535 nm, respectively (**Fig. 13**).

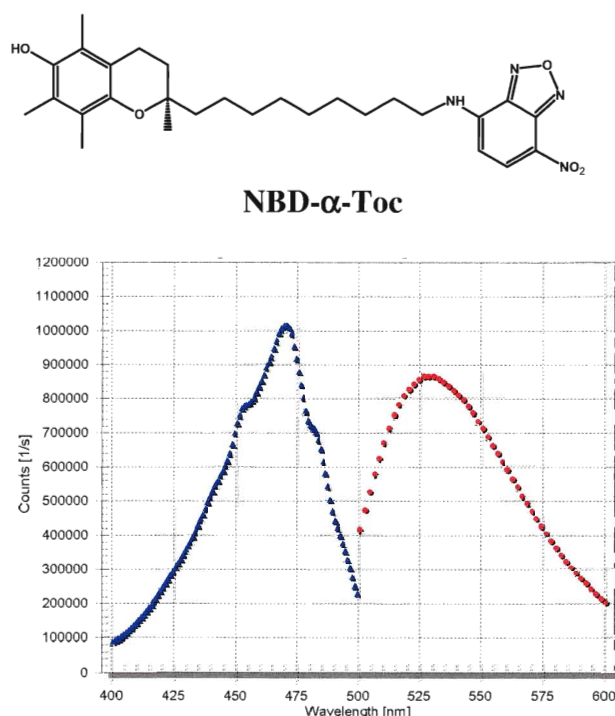


Figure 13: Chemical structure of NBD- α -Toc (top) and the spectra of NBD- α -Toc in absolute ethanol (bottom). The excitation spectrum of NBD- α -Toc (blue) was scanned from 400 to 500 nm with an emission wavelength set at 535 nm. The emission spectrum (red) was monitored from 500 to 600 nm with excitation wavelength at 460 nm.

It has been shown previously that α -Toc is buried in the binding cavity of α -TTP or near the lipid aqueous interface of lipid membranes [45, 93, 94]. In order to test whether NBD- α -Toc behaves similarly when bound to α -TTP or inserted in the lipid bilayer, a dithionite reduction experiment was performed. The dithionite reduction assay has been used frequently to study the kinetics of phospholipid flip-flop (transbilayer movement) and membrane fusion [155-157]. Dithionite, ($\text{Na}_2\text{S}_2\text{O}_4$) is a non-membrane permeable reductant. It reduces the nitro group of NBD to an amine without opening the ring [158], and the quench of NBD fluorescence occurs rapidly in the presence of 25 mM dithionite. According to McIntyre and Sleight [158], more than 95% of NBD-labeled lipid in the outer leaflet of an artificial membrane bilayer was quenched by dithionite.

When NBD- α -Toc was added to 6-His-28TTP (**Fig. 14A**) or extruded PC vesicles (**Fig. 14B**), the fluorescent intensity increased to 125,000 and 300,000, suggesting the

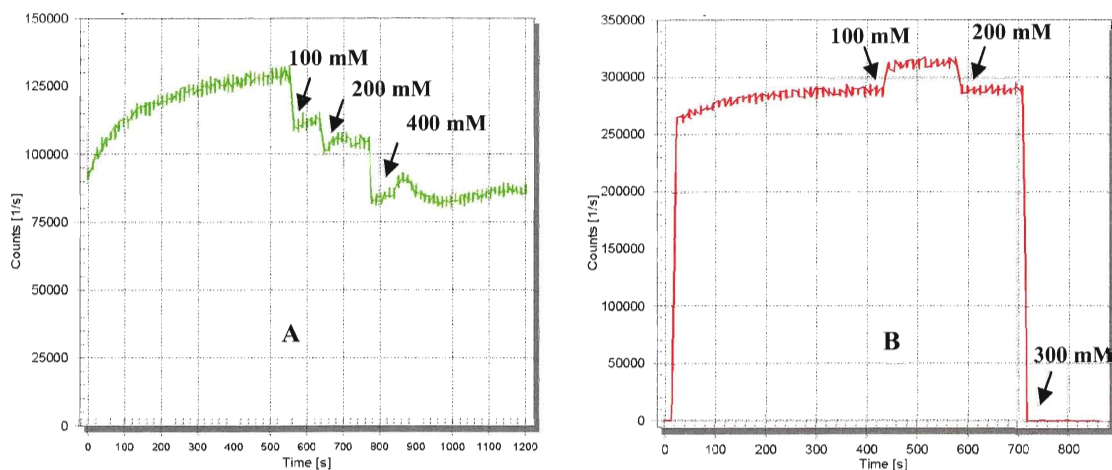


Figure 14: Reduction of NBD- α -Toc by sodium dithionite. 0.5 μM NBD- α -Toc was pre-incubated with 5 μM 6-His-28TTP (**A**) or 1 mM pre-formed PC large unilamellar vesicles (LUVs) (**B**) in a total volume of 400 μl for 15 min. The changes in the fluorescent signal were monitored before and after a stepwise addition of 50 μl $\text{Na}_2\text{S}_2\text{O}_4$ at 1M stock concentration. Final $\text{Na}_2\text{S}_2\text{O}_4$ concentrations are denoted with arrows.

insertion of NBD- α -Toc into 6-His-28TTP and PC vesicles, respectively. Increasing the concentration of Na₂S₂O₄ up to 400 mM did not reduce 6-His-28TTP bound NBD- α -Toc. The stepwise reduction in the fluorescent signal was due to the dilution effect caused by the added volume of sodium dithionite, as the same level of reduction was observed when sodium dithionite was replaced with mQH₂O (data not shown). Therefore, NBD- α -Toc was protected from sodium dithionite reduction (**Fig. 14A**) and is likely buried deep inside 6-His-28TTP. In contrast, 300 mM Na₂S₂O₄ completely ruptured PC vesicles, indicated by the sudden termination of fluorescent signal detection (**Fig. 14B**). In the latter case, no reduction of NBD- α -Toc fluorescence was observed up to 200 mM Na₂S₂O₄. Unlike in 6-His-28TTP, the first addition of Na₂S₂O₄ to PC vesicles appeared to enhance the fluorescence intensity by about 10%. It is unclear why the addition of Na₂S₂O₄ would enhance the fluorescence intensity. We speculate that some of the self-quenching was relieved by dithionite reducing some of the NBD at the surface of the bilayer before it accessed all of the NBD in the bilayer. Since the Na₂S₂O₄ concentrations applied in this experiment far exceeded the effective concentrations reported in other studies, we concluded that the NBD- α -Toc was probably incorporated into 6-His-28TTP or lipid membranes in a similar manner as its natural analog, and the NBD moiety did not drastically alter its interaction with α -TTP or the membrane bilayer.

The water soluble quencher, acrylamide, has been used previously to probe the location of the chromanol headgroup of α -Toc in lipid membranes [45]. It is not known whether the attachment of NBD to the tail of α -Toc would affect the location of chromanol in the membrane. Therefore, the acrylamide quenching of the intrinsic fluorescence of the chromanol headgroup of NBD- α -Toc and α -Toc in the PC vesicles

was compared. As shown in **Fig. 15A & B**, acrylamide gradually quenched NBD- α -Toc and α -Toc in the lipid vesicles, with 79% and 87% of total fluorescence being quenched in the presence of 1.5 M acrylamide. Acrylamide quenching was also used in an attempt to characterize the location of NBD within the lipid membranes. The change in NBD fluorescence was monitored with an excitation wavelength of 466 nm. As depicted in **Fig. 15C**, only 15% of the total fluorescence signal was quenched in the presence of 1 M acrylamide. All three sets of acrylamide quenching data are presented in **Fig. 15D** as a plot of F_0/F versus quencher concentration. The quenching constant k_{SV} can be calculated

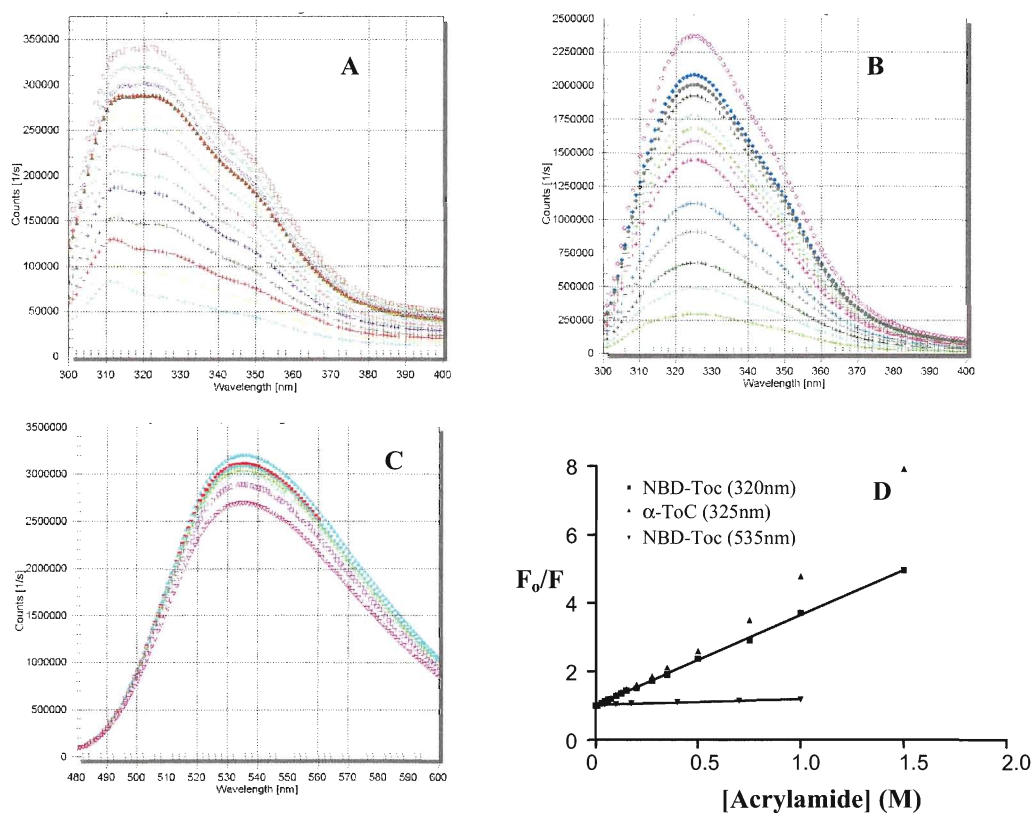


Figure 15: Acrylamide quenching of the natural α -Toc or the florescent NBD- α -Toc in PC vesicles. Bovine PC LUVs (1 mM) containing 3% NBD- α -Toc (**A**) or 0.5 μ M α -Toc (**B**) were quenched with 7.5, 30, 45, 60, 75, 100, 125, 150, 200, 275, 350, 500, 750, 1000 and 1500 mM acrylamide, excitation wavelength was set at 295 nm. **C**) PC LUVs (40 μ M) containing 3% NBD- α -Toc were quenched with 15, 30, 45, 100, 175, 400, 700, 1000 mM acrylamide with excitation wavelength of 466 nm. **D**) Stern Volmer's plot analysis from the maximum fluorescence at each condition tested.

as the slope from the Stern-Volmer's plot, according to the Stern-Volmer's equation [159]:

$$F_0/F = 1 + k_{sv} [Q] \quad \text{Eqn 1}$$

where F_0 and F are the observed fluorescence in the absence and presence of quencher, k_{sv} is the Stern-Volmer constant, $[Q]$ is the quencher concentration. The quenching constants calculated for NBD- α -Toc were 2.63 M^{-1} and 0.17 M^{-1} for the chromanol and NBD moiety, respectively. The fluorescence quenching of α -Toc was linear up to 0.75 M acrylamide, which (with the two highest quenching concentrations removed) resulted in a quenching constant of 3.30 M^{-1} , indicative of a slightly more aqueous exposed chromanol moiety compared to NBD- α -Toc. The negligible quench of NBD fluorescence by acrylamide reconfirmed that this moiety is inserted inside the bilayer and at a location that is away from the aqueous phase.

2.1.3. Development and optimization of Fluorescence Resonance Energy Transfer (FRET) assay

An efficient FRET assay requires the energy donor and the energy acceptor to be in close proximity - between 1 to 10 nm. Moreover, the emission band of the donor must overlap with the excitation band of the acceptor. Therefore, in this study, NBD- α -Toc ($\lambda_{\text{ex}}^{\text{max}} 470 \text{ nm}$, $\lambda_{\text{em}}^{\text{max}} 535 \text{ nm}$) and TRITC-DHPE ($\lambda_{\text{ex}}^{\text{max}} 555 \text{ nm}$, $\lambda_{\text{em}}^{\text{max}} 580 \text{ nm}$) were chosen as energy donor and acceptor, respectively. The energy acceptor tetramethylrhodamine TRITC was linked to the free amine on the head group of dihexadecanoyl phosphatidylethanolamine, DHPE (**Fig. 16**). Thus, TRITC is expected to protrude from lipid membranes and to be exposed to the aqueous phase. The rates of inter-vesicular transfer as well as the transmembrane movement of various NBD labeled

phospholipids have been reported previously [160-162]. These studies concluded that the fluorescently labeled phospholipids were transferred only to the outer leaflet of the bilayer, and the transbilayer migration of phospholipids was unlikely or occurred at extremely slow rates that lasted ($T_{1/2} = 11$ days) for days [162]. It is, therefore, reasonable to expect that NBD- α -Toc transferred from α -TTP is inserted only into the outer leaflet. The Förster distance between NBD- α -Toc and TRITC-DHPE is 37.3 Å when incorporated into the same membrane [163] and the membrane thickness was determined to be 61 ± 10 Å by Huang and Thompson [164]. Since TRITC-DHPE is uniformly distributed in both leaflets of model PC membranes, it will be able to quench NBD- α -Toc in the membrane bilayers regardless of the leaflet in which it is located.

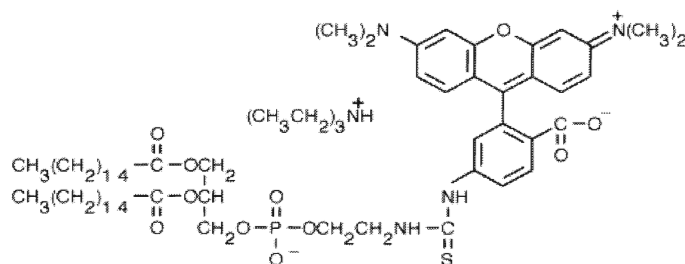


Figure 16: Chemical structure of lipid quencher TRITC-DHPE. N-(tetramethylrhodamine-6-thiocarbamoyl)-1,2-dihexadecanoyl-*sn*-glycero-3-phosphoethanolamine. It was purchased from Invitrogen.

α -TTP mediated NBD- α -Toc transfer is likely bidirectional, as illustrated in **Fig. 17**. Ligand bound α -TTP delivers and inserts NBD- α -Toc into the target membranes containing quencher TRITC-DHPE, thereby reducing the fluorescence signal of NBD- α -Toc. In the reverse direction, the unbound α -TTP binds to and picks up NBD- α -Toc, relieving quenching of the fluorescence signal as NBD- α -Toc leaves the quencher/TRITC-PE containing membrane.

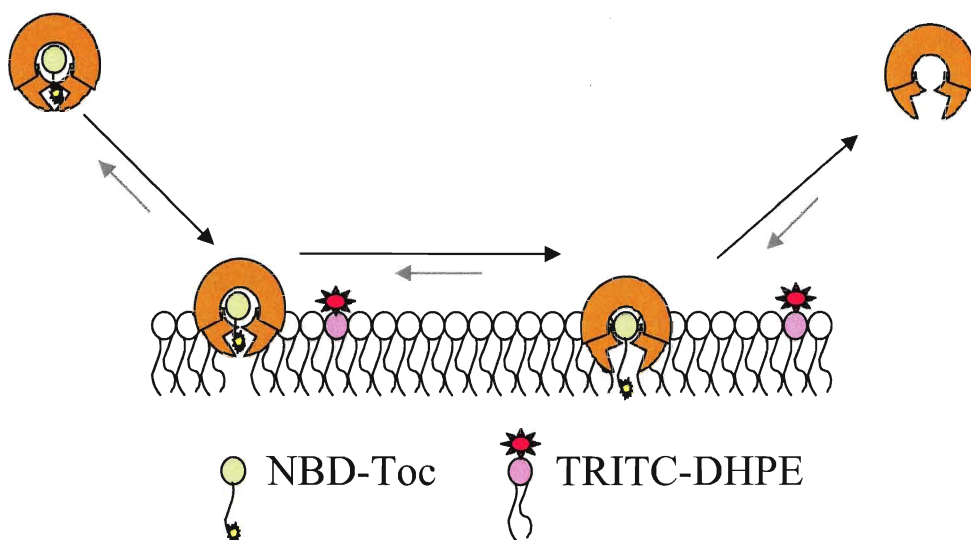


Figure 17: Cartoon illustration of NBD-Toc delivery by α -TTP detected by Fluorescence Resonance Energy Transfer (FRET) assay. The forward insertion and the reversed pick up of NBD- α -Toc (green) by α -TTP (orange) are indicated by black and grey arrows respectively. NBD- α -Toc is quenched by TRITC-DHPE (pink), when it is within the Förster distance of 37.3 Å.

In this study, the rate of α -hTTP mediated transfer of NBD- α -Toc to membranes was determined by following the fluorescence decay as NBD- α -Toc bound to α -hTTP was transferred to TRITC-PE containing PC vesicles. A stopped-flow device was employed to monitor the fluorescence change when NBD- α -Toc bound α -hTTP was mixed with the extruded PC vesicles containing TRITC-DHPE. During assay development and optimization, 3% TRITC-DHPE was chosen. To ensure that all of NBD- α -Toc was bound to α -hTTP, the ratio of NBD- α -Toc to α -hTTP was kept at 1:10. Thus, the fluorescence decay reflected the transfer of NBD- α -Toc from α -hTTP to the modeled membranes. Similarly, the molar ratio of α -hTTP to bovine PC vesicles was 1:50 or greater to guarantee a unidirectional transfer from α -TTP to lipid vesicles.

2.1.4. Kinetics of NBD- α -Toc transfer by 6-His-28TTP

Initially, the FRET assay was performed with the final concentrations of 0.5 μM NBD- α -Toc, 5 μM 6-His-28TTP and 250 μM liver PC (ratio = 1:10:500). Under these assay conditions, 30-35 % of the initial fluorescence signal was lost. The mixing time for the SPF-17 stopped-flow device is ~ 20 ms. Therefore, it is possible that the NBD- α -Toc transfer was too fast to be monitored by our instrument. If this was so, then we expected that diluting the reagents to slow down transfer would solve the problem. To test our hypothesis, the ratios of NBD- α -Toc/ α -hTTP/liver PC were kept at 1:10:500, while their concentrations were diluted two- to four-fold. Thus, the transfer rates were expected to reduce by 8 fold and 64 fold, respectively. To our surprise, in response to the 64 fold dilution in reagents, the rates of transfer were only slightly reduced ($0.064 \pm 0.0004 \text{ s}^{-1}$ to $0.054 \pm 0.0001 \text{ s}^{-1}$). Even at the lowest assay concentration, the initial 20% of total fluorescence was still missing, as shown in **Fig. 18A**. The top green line denotes 100% of fluorescence when NBD- α -Toc was bound to 6-His-28TTP. Transfer of NBD- α -Toc to

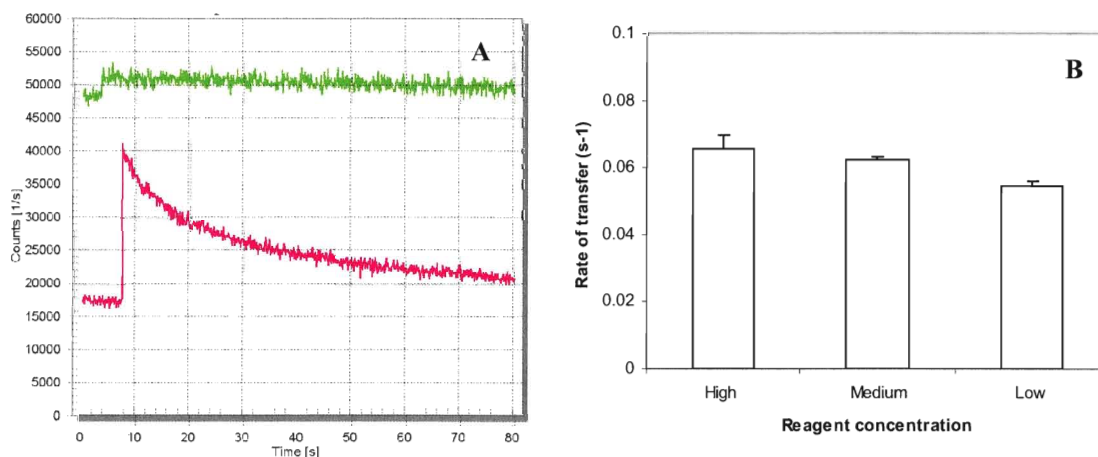


Figure 18: Time-dependent NBD- α -Toc transfer from 6-His-28TTP to bovine liver PC. **A)** 0.125 μM NBD- α -Toc was pre-incubated with 1.25 μM α -hTTP for 15 min, the transfer of NBD- α -Toc was monitored for 80 seconds after mixing with either SET buffer (green) or 62.5 μM bovine liver PC (pink). **B)** 0.5 μM NBD- α -Toc / 5 μM 6-His-28TTP / 250 μM PC (High), 0.25 μM NBD- α -Toc / 2.5 μM 6-His-28TTP / 125 μM PC (Medium) and 0.125 μM NBD- α -Toc / 1.25 μM 6-His-28TTP / 62.5 μM PC (Low).

TRITC-DHPE containing vesicles resulted in an exponential decay of fluorescence (pink curve). The system's lack of response to the change in both donor and acceptor concentrations, as shown in **Fig. 18B**, can only be explained by the spontaneous transfer of NBD- α -Toc from 6-His-28TTP to PC vesicles. However, the missing initial transfer cannot be explained by these results. As mentioned previously, 6-His-28TTP has an N-terminal extension, including the 6-His tag. This extension was predicted to contain only 12.5% extended sheet and 87.5% loops [151]. Thus, it was not expected to introduce significant secondary structure which may cause protein aggregation or misfolding [151]. Whether or not this extension interfered with the binding of α -hTTP to PC vesicles had not been resolved conclusively. With this concern in mind, we decided to switch our research effort to using the 6-His tagged α -hTTP expressed without the 40 amino acid extension from α -hTTP/pET21b construct. The α -hTTP/pET21b construct was a gift from Dr. Stephen Hyland at DSM Nutritional Products.

2.1.5. 6-His- α -hTTP without an extension isolated from α -hTTP/pET21b construct

The 837 bp human α -TTP gene was engineered with a 3'-NdeI and a 5'-XhoI restriction sites, before being inserted into the 5.44 kb pET21b expression vector to create the α -hTTP/pET21 construct of ~ 6.28 kb. In order to verify the integrity of the construct, the plasmid DNA of α -hTTP/pET21 was digested with two pairs of restriction enzymes: NdeI and EcoRI or NdeI and XhoI. Two small fragments of approximately 700 bps and 900 bps respectively were obtained from the above double digestions (**Fig. 19**, left panel, lane #3 & 4) that were close to the calculated size of 762 bp and 890 bp expected. Interestingly, the majority of the uncut plasmid (lane #2) migrated between

molecular size of 4 kb to 5 kb, instead of its true size of 6.3 kb, where two faint bands with retarded speed were also visible in the same lane. The irregular migration pattern was likely due to the formation of supercoil (major lower band) and partially nicked strands (upper two bands). The sequence of this plasmid was later confirmed by sequencing (Robarts Research Institute, London, ON).

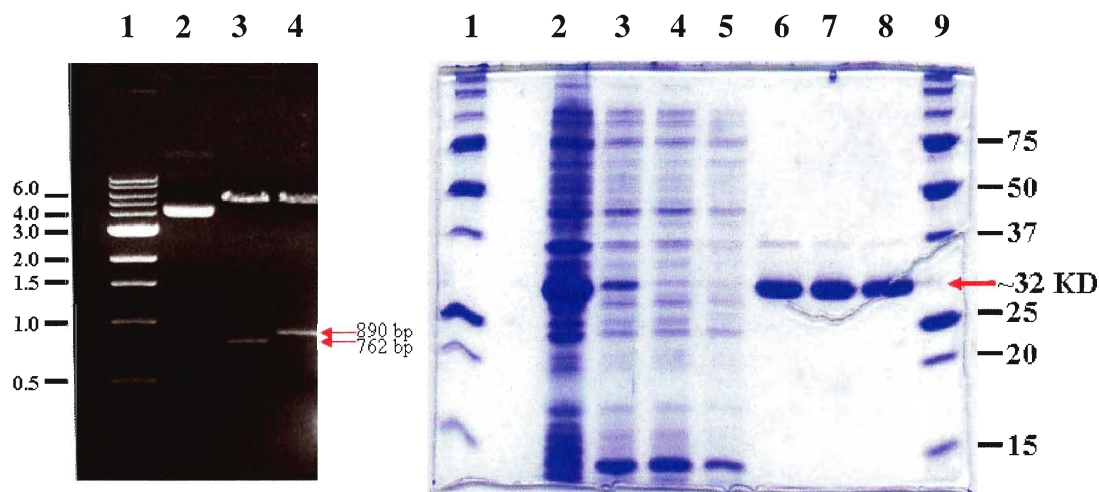


Figure 19: Restriction digestion of α -hTTP/pET21b plasmid DNA (left) and the purification of 6-His- α -hTTP from nickel affinity column (right). Left panel: α -hTTP/pET21b plasmid digested with NdeI and EcoRI or NdeI and XhoI. Lane 1: 1 kb DNA ladder; Lane 2: uncut plasmid; Lane 3: NdeI and EcoRI digestion; Lane 4: NdeI and XhoI digestion. Right panel: Analysis of 6-His- α -hTTP on 15% SDS-PAGE. Lane 1 & 9, marker; Lane 2, insoluble cell fraction; Lane 3, soluble cell fraction; Lane 4, flow through; Lane 5, buffer wash; Lane 6 - 8, purified 6-His- α -hTTP eluted in 400 mM imidazole, fraction #2 - #4.

Expression of hTTP/pET21b construct resulted in the over-production of a ~ 32 kDa protein, lane #2 in the right panel of **Fig. 19** as would be expected for the fusion protein with a calculated size of 32.4 kDa. Although the majority of this 32 kDa protein remained in the insoluble fraction (lane #2), a small level was found in the soluble fraction (lane #3). After subjecting the soluble cell lysate to a nickel affinity column purification, the protein eluted in 400 mM imidazole was very pure, with less than 5% contamination of a ~ 37-39 kDa unknown protein, shown in lane #6 to #8 in the right

panel of **Fig. 19**. α -hTTP expressed from pET21b contains an N-terminal 6-His tag, denoted as 6-His- α -hTTP. Purified 6-His- α -hTTP was subsequently tested for its ability to bind and transfer NBD- α -Toc. The binding affinity was determined to be 83 ± 7 nM, slightly higher than that of 6-His-28TTP (56 ± 15 nM). However, unlike 6-His-28TTP, 6-His- α -hTTP enabled us to monitor the complete transfer of NBD- α -Toc as illustrated in **Fig. 20**. In the absence of bovine liver PC vesicles, 6-His- α -hTTP bound NBD- α -Toc fluoresced steadily with insignificant photobleaching (blue line). Upon mixing of

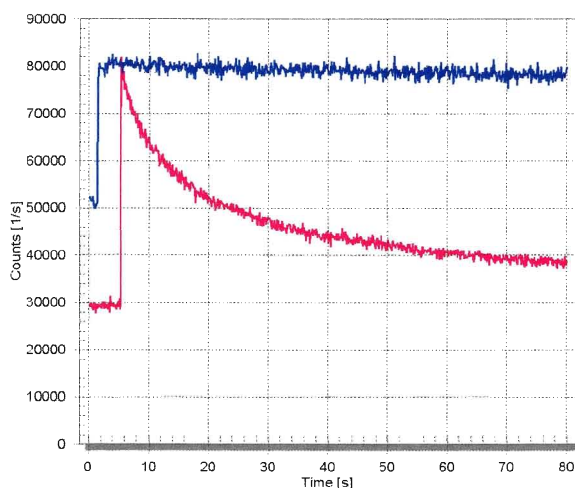


Figure 20: Time-dependent NBD- α -Toc transfer by 6-His- α -hTTP. 0.25 μ M NBD- α -Toc was pre-incubated with 2.5 μ M 6-His- α -hTTP for 15 min, the transfer of NBD- α -Toc was monitored for 80 second after mixing with either SET buffer (blue line) or 125 μ M bovine liver PC (pink curve).

the preloaded 6-His- α -hTTP with bovine PC LUVs, NBD- α -Toc fluorescence underwent a time dependent exponential decay. The half life calculated from the single exponential decay equation was 11.86 ± 1.02 s, reflecting a transfer rate at 0.059 ± 0.004 s⁻¹ (n=3), similar to the pET28/TTP of 0.064 ± 0.004 s⁻¹.

2.1.6. Kinetics of NBD- α -Toc transfer by 6-His- α -hTTP

The interaction between protein and lipid membranes is regulated primarily by electrostatic and hydrophobic forces. α -TTP possesses a large number of charged surface exposed residues, which divide the protein into two distinctive regions of electrostatic potential as depicted in **Fig. 21**, with the positive patch formed by mainly arginine and lysine residues. The membrane exchange loop (a.a. 198 to 221) is composed of mainly hydrophobic residues, three acidic residues and five basic residues, with His 204 and Lys 211 situated right on the membrane interacting mobile helix A10. We initially proposed that both His 204 and Lys 211 could potentially mediate the electrostatic interaction between α -TTP and the negatively charged phospholipid headgroups in the membranes.

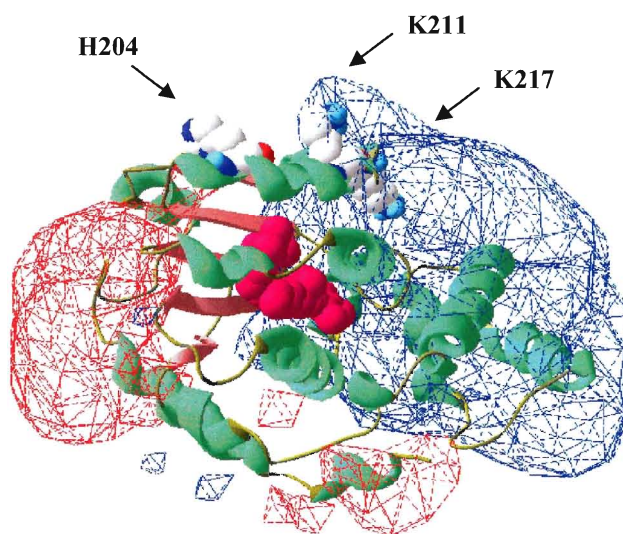


Figure 21: Electrostatic potential map of α -Toc bound holo- α -TTP (pdb:loip) calculated and presented by Deepview. Areas of positive electrostatic potential are highlighted in blue, and negative in red. α -Toc is shown in pink. Basic residues on the lipid exchange loop (residues 198-221) are shown as space filled molecules and indicated by arrows.

To test our hypothesis that electrostatic interactions are important to α -hTTP binding to membranes, bovine liver PC LUVs were prepared containing 15% of anionic phospholipid, such as phosphatidylinositol (PI), phosphatidylserine (PS) or cardiolipin (CL), then the transfer rates of NBD- α -Toc to these vesicles were compared. A minor

enhancement was observed for PS containing vesicles versus pure PC vesicles, such that the rates increased from $0.062 \pm 0.005 \text{ s}^{-1}$ to $0.072 \pm 0.008 \text{ s}^{-1}$, while PI and CL had no impact on the transfer (**Fig. 22**). If electrostatic interaction were truly involved, CL should have had a much greater impact than both PI and PS, because CL possesses two

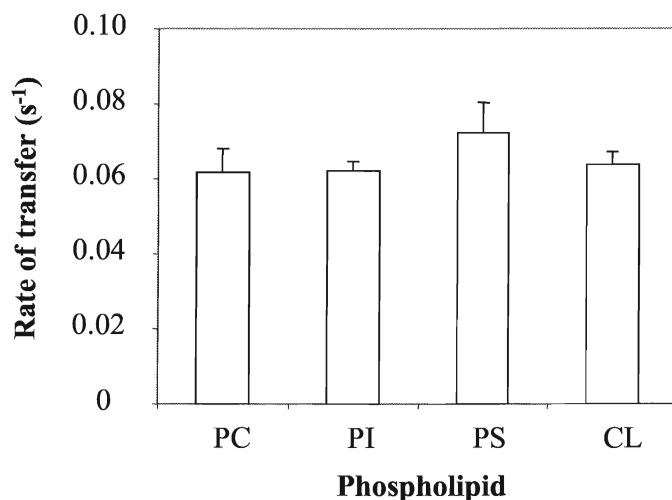


Figure 22: Effect of anionic phospholipid on the transfer of NBD- α -Toc. NBD- α -Toc was pre-incubated with 6-His- α -hTTP for 15 minutes prior to mixing with 100% liver PC or in the presence of 15% of phosphatidyl inositol (PI), phosphatidyl serine (PS) and cardiolipin (CL). Presented are the averages \pm the standard deviation. $n=8$ for PC and PI, $n=9$ for PS and $n=6$ for CL.

negatively charged phosphate groups, rather than one. Therefore, we chose to examine other characteristics of the membrane that may influence its recognition by α -hTTP. Until then, we had used only 100 nm extruded large unilamellar vesicles (LUVs) in all experiments. Knowing that membrane curvature could impact the membrane binding ability of some proteins including ArfGAP1 [142, 143], and that membrane curvature or lipid packing density could be also influenced by the acyl chain composition of phospholipids, we investigated the effect of membrane curvature and acyl chain composition on the rates of NBD- α -Toc transfer. Soy PC has a much greater (ratio of S/U = 0.30) percentage of unsaturated fatty acids than the routinely used bovine liver PC

(ratio of S/U = 0.91). The transfer rates for both soy and liver PC were similar for 25 nm sonicated vesicles, 50 nm and 100 nm extruded vesicles (shown in **Fig. 23**). These

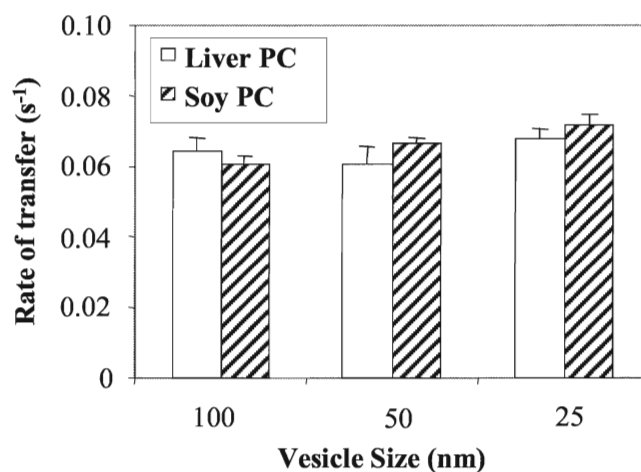


Figure 23: Effect of vesicle size and curvature on the transfer of NBD- α -Toc. Lipid vesicles of different sizes were prepared by extrusion or sonication method as described in the Methods section. The average of three determinations are shown \pm the standard deviation.

results were not completely unexpected, considering that only a very few curvature sensing proteins have been reported. It was possible that curvature alone was not sufficient to introduce major impact on the binding of α -hTTP to the acceptor membranes. Thus, electrostatic interaction was also tested in SUVs by including 15 % of various anionic phospholipid in SUVs and LUVs preparations (**Fig. 24**). To our surprise, in the presence of PS, PI or CL, the average transfer rates to the anionic SUVs were decreased. Due to the large variation in the PC SUV controls, the difference observed for CL SUVs may not be as significant. In contrast, the transfer rates to LUVs were similar whether in the presence or the absence of anionic lipids. These data suggested that 6-His- α -hTTP mediated transfer of NBD- α -Toc was independent of membrane curvature and electrostatic interaction between protein and membranes.

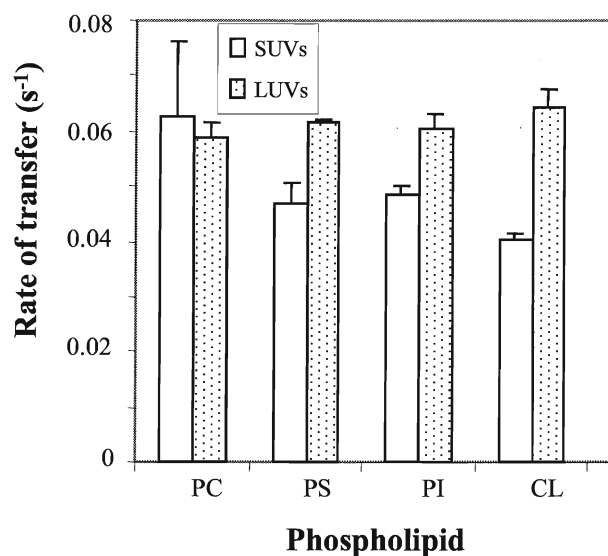


Figure 24: Effect of anionic lipids and vesicle curvature on the transfer of NBD- α -Toc. NBD- α -Toc was pre-incubated with 6-His- α -hTTP for 15 minutes prior to mixing with liver PC containing 15% of various anionic phospholipid.

In the liver, α -TTP is localized to late endosomes and lysosomes [99, 100]. The internal membranes of late endosomes contains a very unique lipid called bis(mono-acylglycero) phosphate or LBPA [165]. This lipid accounts for 15% of the total late endosome lipid extracts. LBPA promotes the formation of multilamellar vesicles (MLVs) at acidic pH but not at neutral pH [166]. LBPA has been implicated in the endosomal sorting of lipids and proteins [165]. Recently, LBPA has been also shown to mediate the lysosomal cholesterol export by NPC2 [134, 167]. Hence, it would be interesting to know whether LBPA or an endosomal lipid mixture also assists α -hTTP mediated ligand transfer. Thus, transfer experiments were conducted using LUVs simulating the membrane composition of late endosomes [168] (65% DOPC, 20% DOPE, 5% sphingomyelin (SM), 5% liver PI and 5% PS) in the presence and the absence of 15% LBPA. These lipid compositions were compared directly to the PC containing 20% PE or 15% LBPA. As shown in **Fig. 25**, in the absence and the presence of 15%

LBPA (En-LBPA vs En+LBPA), the transfer rates to endosomal lipid mixture were $0.051 \pm 0.002 \text{ s}^{-1}$ and $0.054 \pm 0.001 \text{ s}^{-1}$ respectively. These rates were similar to both the

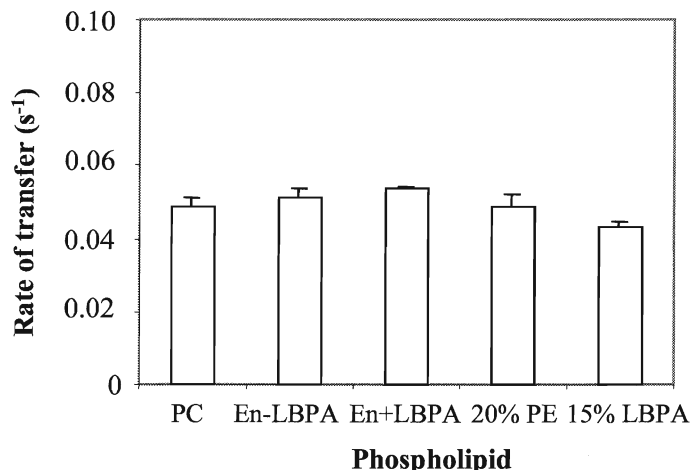


Figure 25: Effect of endosomal lipid mixture on the rate of NBD-Toc transfer to LUVs. LUV's were prepared from pure endosomal mixture (En-LBPA) consisting of 65% DOPC, 20% DOPE, 5% sphingomyelin (SM), 5% liver PI, 5% PS as indicated or from bovine liver PC with the addition of PE or LBPA.

PC control ($0.049 \pm 0.002 \text{ s}^{-1}$) and PC with 20% DOPE ($0.049 \pm 0.004 \text{ s}^{-1}$). Interestingly, the inclusion of 15% LBPA in PC LUVs displayed the lowest transfer rate, $0.043 \pm 0.002 \text{ s}^{-1}$. Clearly, these results indicated that the endosomal lipid mixture and LBPA did not significantly influence α -hTTP mediate transfer of NBD- α -Toc.

So far, the rate of NBD- α -Toc transfer appeared to be independent of acceptor lipid composition, which was indicative of a diffusional mediated transfer mechanism. A true testimony for the diffusional transfer in our FRET system would be the lack of response to the change in the acceptor vesicle concentrations. Therefore, the transfer rate of NBD- α -Toc to PC LUVs from $5 \mu\text{M}$ to $1250 \mu\text{M}$ was compared. As illustrated in **Fig. 26**, the rates calculated for the $5 \mu\text{M}$ and $1250 \mu\text{M}$ LUVs were $0.033 \pm 0.0002 \text{ s}^{-1}$ and $0.053 \pm 0.0005 \text{ s}^{-1}$ respectively. When the acceptor concentration was increased by 250-

fold, the transfer rate was only increased by 60%. This result clearly suggested that the forward transfer and insertion of NBD- α -Toc into membranes was mediated by aqueous

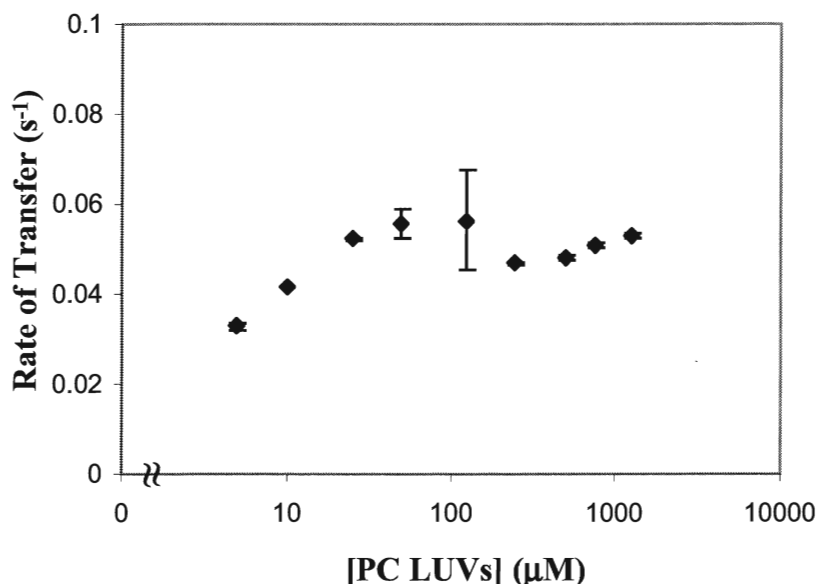


Figure 26: Effect of vesicle concentration on the rate of NBD- α -Toc transfer. 0.25 μ M NBD- α -Toc pre-incubated with 2.5 μ M 6-His- α -hTTP for 15 min., then mixed with PC LUVs at indicated concentrations.

diffusion. It was tempting for us to draw the conclusion that α -hTTP mediated ligand transfer is diffusional, since all of the parameters tested so far had failed to introduce any changes to the rate of ligand transfer. However, the collisional based transfer of α -Toc by lipoproteins and α -TTP has been suggested [55, 89]. Therefore, we decided to conduct a series of troubleshooting experiments to ensure that we were investigating the correct rate limiting step for changes, and our FRET transfer assay was free from any systematic errors.

2.1.7. Troubleshooting experiments

2.1.7.1 Removal of NBD- α -Toc from membranes by 6-His- α -hTTP

Perhaps the rate limiting step of α -Toc transfer is not its insertion into the membrane, but rather its removal from the membrane. If so, we expected that the rate of

ligand pickup would be altered in response to the change in the protein concentration and lipid composition. To test this hypothesis, a “pick-up” assay was developed and optimized. In this assay, donor vesicles contained both NBD- α -Toc and the quencher TRITC-DHPE. Thus, the fluorescence of NBD- α -Toc increased as it was extracted from the quencher containing lipid vesicles by α -hTTP. The optimal lipid concentration was composed of 50 μ M PC, 2% NBD- α -Toc and 6% TRIC-DHPC. The rate of α -Toc pickup by 6-His- α -hTTP was measured at the increasing concentrations of 6-His- α -hTTP. **Fig. 27A** shows the time dependent increase in the fluorescence signal when α -hTTP was added to the NBD- α -Toc containing LUVs. Moreover, the absolute signal enhancement was proportional to 6-His- α -hTTP concentration. The raw data fit better to a two-phase exponential association model consisting of a fast and slow phase. The pick up rates (fast) were calculated and are displayed in **Fig. 27B**. The R^2 values generated

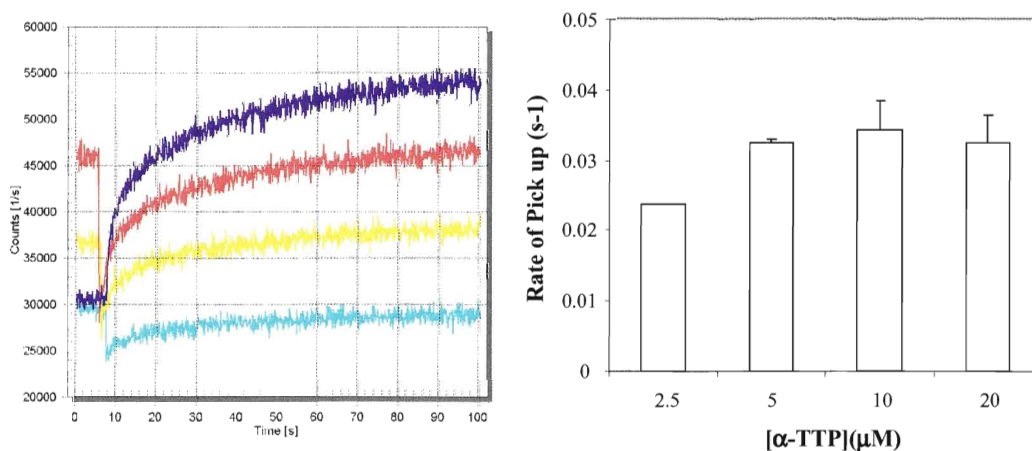


Figure 27: Reversed transfer of NBD- α -Toc from PC LUVs to α -hTTP. 50 μ M PC LUVs contained 2% NBD-Toc and 6% TRITC-DHPE were prepared by extrusion. The change in fluorescence intensity was monitored after mixing with the indicated concentration of 6-His- α -hTTP. The data shown are the average \pm the standard deviation, $n=2$ for 2.5 μ M TTP and $n=3$ for other concentrations.

were greater than 0.95 for all concentrations, except for 2.5 μM ($R^2 = 0.71$). The pick up by 2.5 μM 6-His- α -hTTP was 0.023 s^{-1} , and the rates for other concentrations determined ranged from $0.032 \pm 0.004 \text{ s}^{-1}$ to $0.034 \pm 0.004 \text{ s}^{-1}$.

Subsequently, the effect of electrostatic interactions on ligand pickup was examined with 5%, 10% and 15% PS or CL in bovine PC LUVs. As shown in **Fig. 28**,

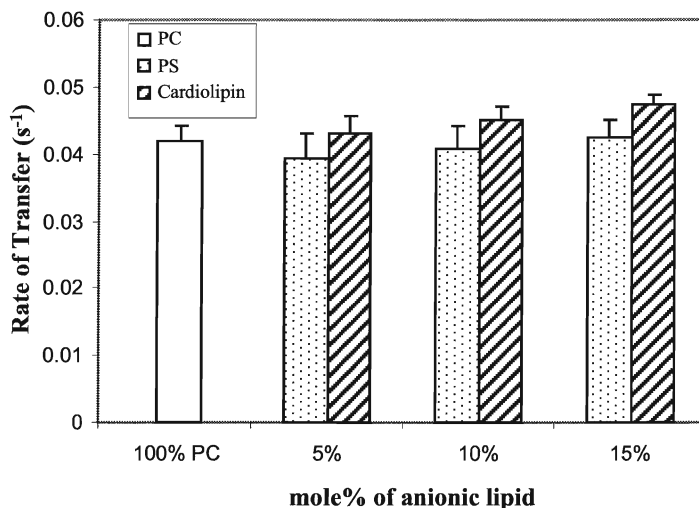


Figure 28: Effect of anionic lipid on NBD- α -Toc pickup by 6-His- α -hTTP. 50 μM PC LUVs contained 0.25 μM NBD- α -Toc and 3% TRITC-DHPE and anionic lipid as indicated. Shown are the average \pm standard deviation, $n=9$ for 100% PC, $n=5$ and $n=8$ for 10% CL and 5% PS, respectively, $n=6$ for all other conditions tested.

no significant difference in the pick up rates was observed for the PC vesicles with or without PS or CL. The pick up data collectively also supported the spontaneous diffusional transfer of NBD- α -Toc to or from lipid membranes.

2.1.7.2. Examination of NBD- α -Toc probe

We then directed our attention to NBD- α -Toc, which was expected to be less hydrophobic and more water soluble than α -Toc. Based on the calculated lipophilicity index, the logP values calculated were 7.34 and 9.60 for NBD- α -Toc and α -Toc, respectively. We hypothesized that, perhaps, the increased aqueous solubility of NBD- α -

Toc was to blame for its apparent spontaneous diffusion from α -hTTP to the membranes. To test our hypothesis, the spontaneous transfer of NBD- α -Toc between donor and acceptor vesicles of different sizes was investigated. Illustrated in **Fig. 29**, in the absence of α -hTTP, the spontaneous rate of transfer was greater with SUVs as donor vesicles. Vesicle fusion was unlikely during the monitored assay time as both SUVs and LUVs were expected to be stable for more than 20 hours at 37°C [169]. The highest rate was observed for the movement of NBD- α -Toc from donor SUVs to acceptor SUVs, which was $0.041 \pm 0.002 \text{ s}^{-1}$, and the rate was lowered to about 50%, when LUVs were the donor vesicles. When both the donor and the acceptor were LUVs, the rate of NBD- α -Toc transfer was greatly reduced to $0.012 \pm 0.0003 \text{ s}^{-1}$, which was equivalent to 30% of the transfer rate from SUVs to SUVs. Therefore, the enhanced transfer to SUVs was due likely to their reduced phospholipid headgroup packing density, rather than to the solubility of NBD- α -Toc.

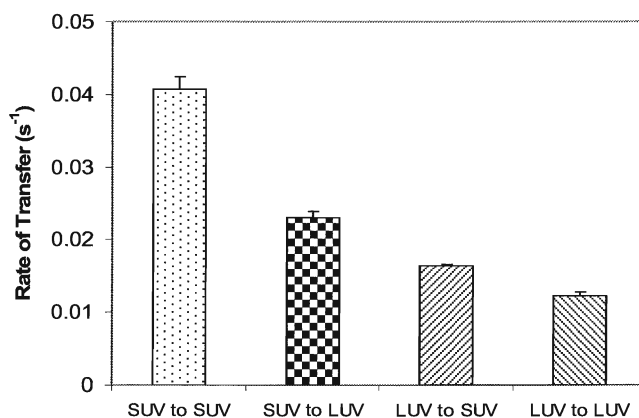


Figure 29: Intervesicle transfer of NBD- α -Toc from acceptor vesicles to donor vesicles. 1 μ M NBD- α -Toc incorporated in 100 μ M donor PC SUVs or LUVs was transferred to 100 μ M acceptor bovine liver PC SUVs or LUVs containing 3% TRITC-PE. The data shown represents an average of six determinations \pm the standard deviation.

The concern about the enhanced water solubility of NBD- α -Toc was partially resolved when the transfer of NBD- α -Toc was tested with human SPF, another member from the CRAL-TRIO family, capable of binding to α -Toc. Interestingly, the fluorescence signal of NBD- α -Toc bound SPF was not quenched, when mixed with TRITC-PE containing PC vesicle (data not shown). This data implied that NBD- α -Toc bound to SPF, but failed to transfer to the lipid vesicles. In spite of its improved water solubility, the transfer of NBD- α -toc by protein was strictly regulated. Thus, NBD- α -Toc is unlikely to undergo a simple diffusion from protein to vesicles.

2.1.7.3 Examination of 6-His- α -hTTP

The binding of natural ligand α -Toc was predicted to induce a conformational change in α -TTP. A conformational change in a protein can be detected simply by following the intrinsic tryptophan fluorescent change, resulting from the change in the environment and solvent accessibility of the residues in ligand_bound and free states. α -hTTP has five tryptophans that are located at residues 67, 76, 122, 163 and 259. In the absence of α -Toc, the maximum fluorescence of 6-His- α -hTTP peaked at 332 nm, while in the presence of α -Toc, the maximum fluorescent peak shifted to 326 nm (**Fig. 30**). A similar wavelength shift upon α -Toc binding to 6-His-28TTP (TTP with the N-terminal 40 amino acid extension) was detected previously by others in the lab. A blue shift of 6 nm to the left suggested that the tryptophan residues became less exposed to the solvent upon α -Toc binding, indicative of a conformational change. This change is likely introduced by tryptophan residues 122 and 163, because they are located near α -Toc binding site. The fluorescence of α -Toc is negligible in aqueous buffer. However, in the

organic environment, the fluorescence characteristics of α -Toc ($\lambda_{\text{ex}} = 295\text{nm}$, $\lambda_{\text{em}} = 325\text{nm}$) [170] overlap with tryptophan. Therefore, we expected the total fluorescence intensity would increase in the presence of α -Toc. Instead, when α -Toc was bound to α -TTP, we observed an approximately 10% reduction. Such reduction in the absolute fluorescence was likely caused by a small amount of ethanol (less than 1%) when α -Toc in ethanol solution was added to α -TTP in SET buffer.

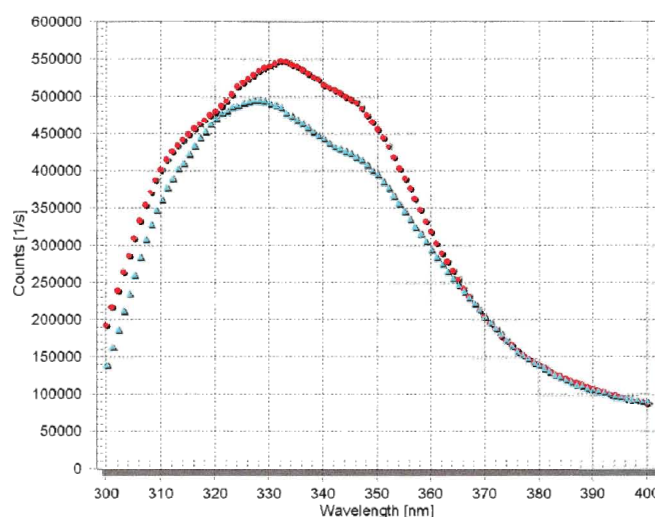


Figure 30: Intrinsic tryptophan fluorescence spectrum of 6-His- α -hTTP. The fluorescence of 1 μM 6-His- α -hTTP alone (red) or in the presence of 10 μM α -Toc (blue). The excitation wavelength was set at 295 nm.

To compare the solvent accessibility of protein bound to either α -Toc or NBD- α -Toc, an acrylamide quenching experiment was performed and the quenching constant k_{sv} was determined from the Stern Volmer's plot. As shown in **Fig. 31**, the quenching plots for both ligand bound 6-His- α -hTTP were super-imposable, with an identical quenching constant of 7.8 M^{-1} . The ligand free α -TTP was slightly more solvent exposed, with a quenching constant of 8.9 M^{-1} . All of the above evidence implied that NBD- α -Toc was a suitable probe to be used for the FRET assay. We next decided to inspect the source of the protein more critically.

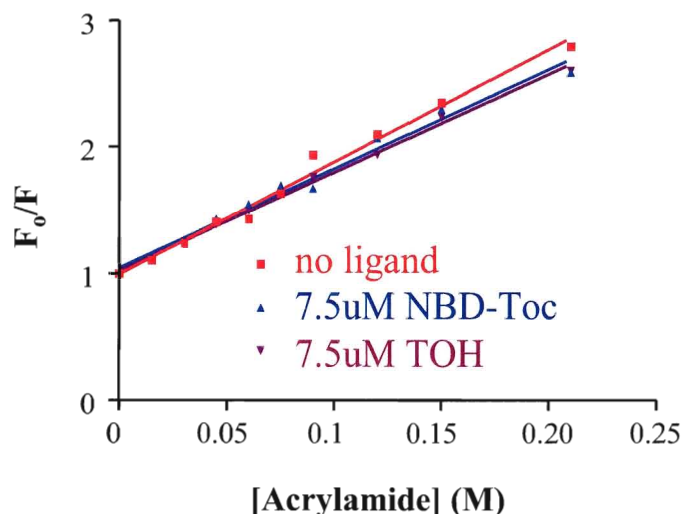


Figure 31: Stern Volmer's plot of α -hTTP quenched with acrylamide. 6-His- α -hTTP (2.5 μ M) in the presence or the absence of 7.5 μ M NBD- α -Toc or α -Toc was quenched with the indicated acrylamide concentrations.

2.1.8 Identification of *E. coli* Outer Membrane Porin F (*OmpF*)

We had always noticed a 37-39 kDa *E. coli* protein co-purified with 6-His tagged α -hTTP expressed from both pET28b and pET21b expression vectors (**Fig. 12 & 19 & 32A**). This 39 kDa unknown protein typically accounted for 5% to 10% of the total purified protein. Ideally, only 6-His tagged α -hTTP can be absorbed to the metal affinity column. It was possible that protein degradation occurred during purification, and thus, the 39 kDa and 32 kDa protein bands represented the full length 6-His- α -hTTP and its degradation product. Although the calculated molecular weights of both versions of Histidine tagged α -hTTP (from pET21b and pET28b bacterial vectors) were less than 39 kDa, the elevated molecular weights of these purified proteins were perhaps due to their retarded migration on the SDS-PAGE or normalized to the non-precise protein marker. To prevent protein degradation, a protease inhibitor cocktail was included in the lysis

buffer during purification of 6-His- α -hTTP. Unfortunately, this modification did not help to increase the yield of the full length protein of 37-39 kDa. Subsequently, western blot analysis of the 6-His- α -hTTP was performed, utilizing a primary antibody recognizing 6-His tag. Only the 32 kDa protein band was recognized by the 6-His antibody, suggesting that this protein contained the engineered 6-His tag and it was most likely 6-His- α -hTTP, whereas the 39 kDa protein was an *E. coli* protein with high affinity for nickel ions. Therefore, it co-eluted with 6-His- α -hTTP in 400 mM imidazole. At the time, we were not particularly alarmed by this protein contaminant, due to its insignificant presence in the total purified protein.

We continued our troubleshooting with 6-His- α -hTTP. According to Meier *et al.* [93], in the absence of α -Toc, two monomers of α -TTP form a dimer through the contact of their lipid exchange loops during crystallization. Based on the structure of α -TTP dimer, the membrane binding lids were locked in an open position. This conformation may have allowed α -Toc to move freely in and out of α -TTP. Thus, α -TTP dimers were presumably less active than the monomers in regulating the exchange of α -Toc. Although no evidence suggested α -TTP forms a dimer in the cell, but we did not want to rule the possibility that dimers form during purification in a similar way as observed during crystallization. Our next attempt was to separate the active α -TTP monomers from the inactive dimers. To do so, 6-His- α -hTTP, obtained from the nickel affinity purification was subjected to a further purification on a sephacryl S-300 gel filtration column by FPLC. Three peaks were resolved, as shown in **Fig. 32A**, the first narrow peak indicated a homogenous protein population. When normalized to the calibrated protein standards, this protein was determined to be ~130 kDa. The second peak was

slightly broader, indicating a more heterogeneous protein population, with average predicted size of ~35 kDa. Imidazole was eluted in the last peak. The fractions # 18 to 22 from the first peak, and fractions #89 to 95 from the second peak, were each pooled. Sample of these two peaks were subjected to SDS-PAGE and western blot analysis. Shown in **Fig. 32B**, lane #1 contains the mixture of 32 kDa 6-His- α -hTTP and 39 kDa contaminant prior to the size exclusion FPLC separation. FPLC purification appeared to produce pure 6-His- α -hTTP (lane #4) corresponding to peak #2. However, a small level of 6-His- α -hTTP co-purified with the 39 kDa contaminant (lane #3). It was uncertain whether a complex formed between 6-His- α -hTTP and the 39 kDa contaminant. The western blot analysis with the 6-His antibody detected only 6-His- α -hTTP, not the 39 kDa contaminant (**Fig. 32C**). Based on these results, fractions 18 to 22 were composed mainly of trimers of 39 kDa, and fractions 89 to 95 contained only pure 6-His- α -hTTP. When both proteins were tested in FRET transfer assay (**Fig. 32D**), to our surprise, the fluorescence intensity of NBD- α -Toc bound to the 39 kDa contaminant was ~250,000 (top purple & blue lines), which was 5 times of α -hTTP bound (bottom yellow line). More interestingly, the transfer of NBD- α -Toc was observed from the 39 kDa contaminant to PC LUVs (**Fig. 32D**, Fr #18-22), with an observed rate of 0.05 s^{-1} . The rate was increased to $0.073 \pm 0.005 \text{ s}^{-1}$ when the acceptor vesicles were 15% PS SUVs (data not shown). These rates were fairly similar to the rates we had observed for the unfractionated 6-His- α -hTTP (e.g. 0.059 s^{-1} , **Fig. 20**). In the same experiment, the transfer mediated by pure 6-His- α -hTTP (pink line) was insignificant, due to the overwhelmingly high fluorescence signal from 39 kDa contaminant. It is also possible

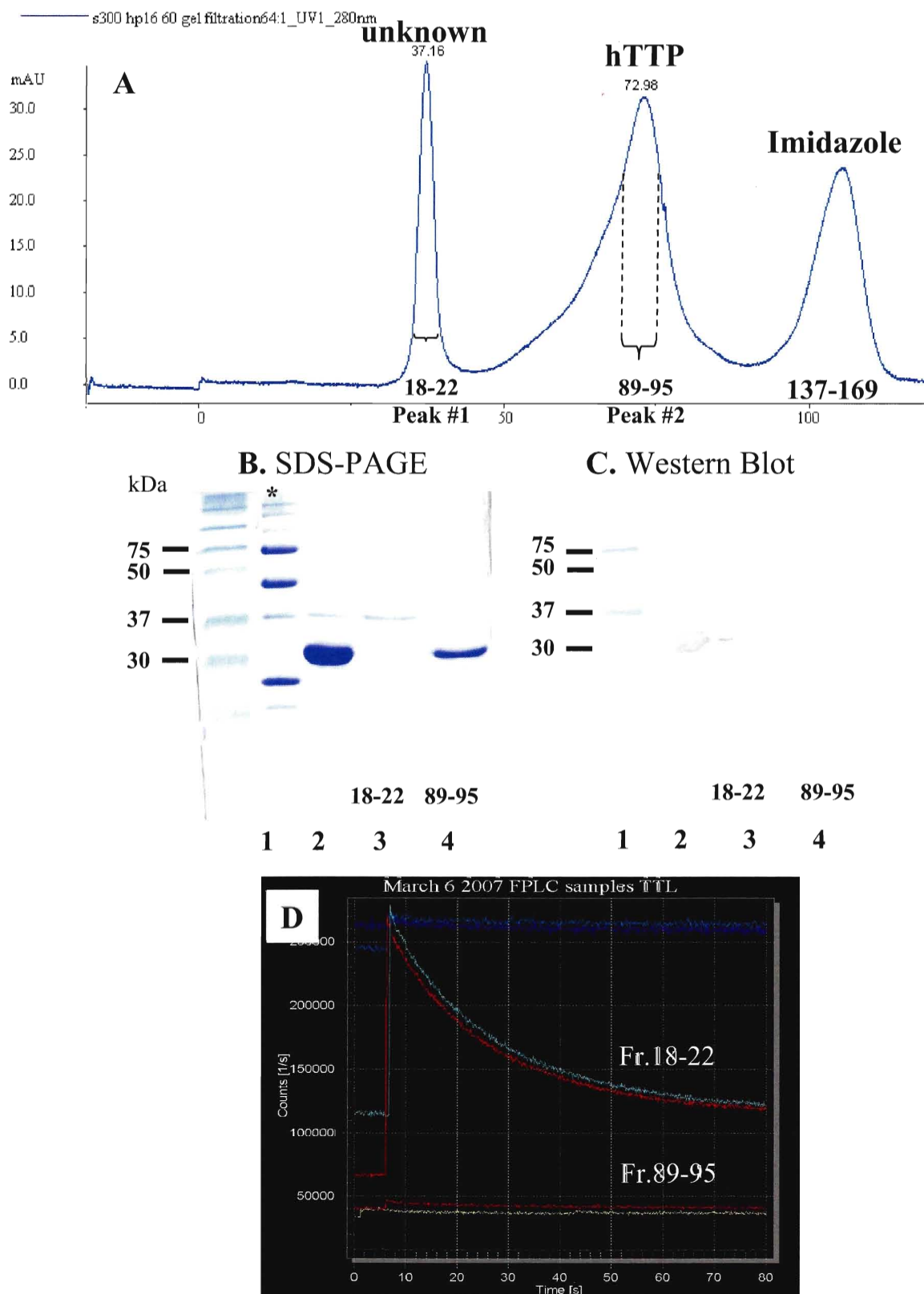


Figure 32: FPLC separation of 39 kDa unknown protein from 6-His- α -hTTP and the subsequent analysis. A) Approximately 3 mg of 6-His- α -hTTP eluted from the

nickel affinity column were further separated on a sephacryl S-300 high resolution gel filtration column. The chromatogram of protein elution was recorded at 280 nm. Running buffer contained 25mM PO₄, 0.5M NaCl, pH 7.5. The peaks for 39 kDa unknown protein and 6-His- α -hTTP were observed at retention volumes of 37.16 ml and 72.96 ml respectively. The pooled fractions #18-22 and fractions #89-95 were subjected to analysis by SDS-PAGE (**B**) and western blot with anti 6-His antibody (**C**), Lane #1: marker; Lane #2 6-His- α -hTTP (5 μ g per lane) prior to FPLC separation; Lane #3: pooled fraction #18-22 (~ 0.5 μ g per lane); Lane #4: pooled fraction #89-95 (~1 μ g per lane); star denotes a different molecular weight marker BioRad 161-0363. **D**) FRET transfer activity of pooled fractions 18-22 and 89-95 respectively. Top straight lines are the duplicates of NBD- α -Toc bound to Fr. 18-22, the bottom yellow straight line is NBD- α -Toc bound to Fr. 89-95.

that the purified 6-His- α -hTTP became less active during the lengthy FPLC purification at room temperature.

To confirm that 39 kDa *E. coli* contaminant is capable of binding and transferring NBD- α -Toc, hTTP/pET21b transformed BL21(DE3) *E. coli* were induced in the absence and the presence of 400 μ M IPTG. Only IPTG induced *E. coli* would produce 6-His- α -hTTP. Both cultures of *E. coli* were lysed, and the fractionated supernatant samples were subjected to the nickel affinity purification. Probond metal affinity purification protocol (Invitrogen) was followed in an attempt to cleanly separate the 39 kDa *E. coli* protein from 6-His- α -hTTP. **Fig. 33A** shows the expression of the 39 kDa contaminant (red dashed boxes) in both *E. coli* cultures. Unfortunately, the Probond protocol did not improve the purity of 6-His- α -hTTP. The semi-purified 39 kDa contaminant (-IPTG), eluted in 200 mM imidazole, was able to transfer NBD- α -Toc (**Fig. 33B**), with transfer rates increasing from 0.029 ± 0.005 to 0.058 ± 0.002 s⁻¹ in response to a 5 fold increase in protein from 80 μ g to 400 μ g. In the IPTG induced *E. coli* sample, 200 mM imidazole elution resulted in a semi-purified sample containing both 39 kDa contaminant and 6-His- α -hTTP (**Fig. 33A**). As illustrated in **Fig. 33C**, 2.5 μ M (~18 μ g) of highly purified 6-

His- α -hTTP eluted in 300 mM imidazole (pink curve), transferred NBD- α -Toc at a slower rate than that of 80 μ g (green grey curve) and 160 μ g (yellow curve) of the protein mixture eluted in 200 mM imidazole.

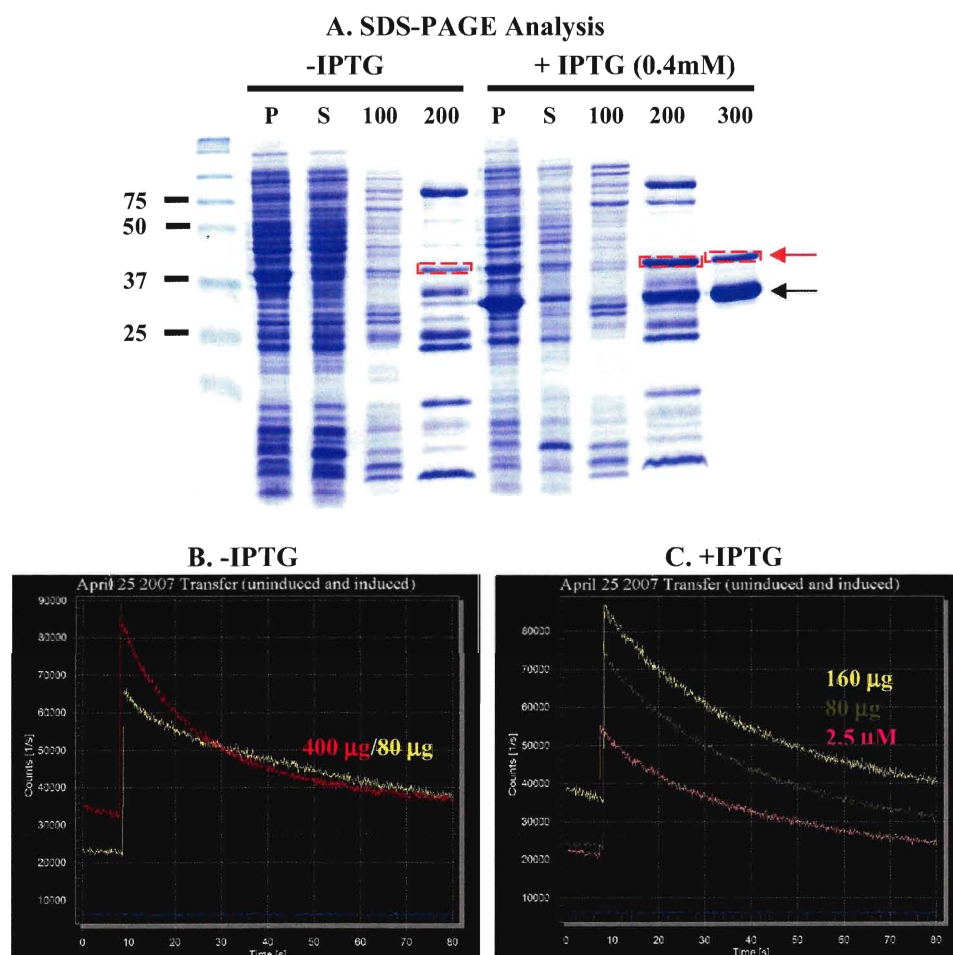


Figure 33: Comparison of the ligand transfer activity of 39 kDa *E. coli* protein and 6-His- α -hTTP. A) SDS-PAGE analysis of protein fractionations from the Nickel affinity purification of 39 kDa *E. coli* protein in the absence and the presence of 6-His- α -hTTP. B) FRET activity of semi purified 39 kDa *E. coli* protein and C) FRET activity of the mixture of 39 kDa protein and 6-His- α -hTTP.

More strikingly, binding assays with the 39 kDa protein using NBD- α -toc indicated the 39 kDa *E. coli* contaminant not only bound to NBD- α -Toc with high affinity ($K_D = 89$ nM vs 48 nM for α -hTTP) (Fig. 34A), but the binding also appeared to be specific, as it could only be replaced by natural α -Toc, not cholesterol (Fig. 34B).

This evidence further strengthened our hypothesis that the 39 kDa *E. coli* protein was not simply a minor contaminant. Its presence overpowered the fluorescence assay's sensitivity to α -hTTP. In order to properly study α -hTTP and its ligand transfer ability, the 39 kDa contaminant had to be completely removed. Yet, the number of methods employed to separate these two proteins proved unsuccessful.

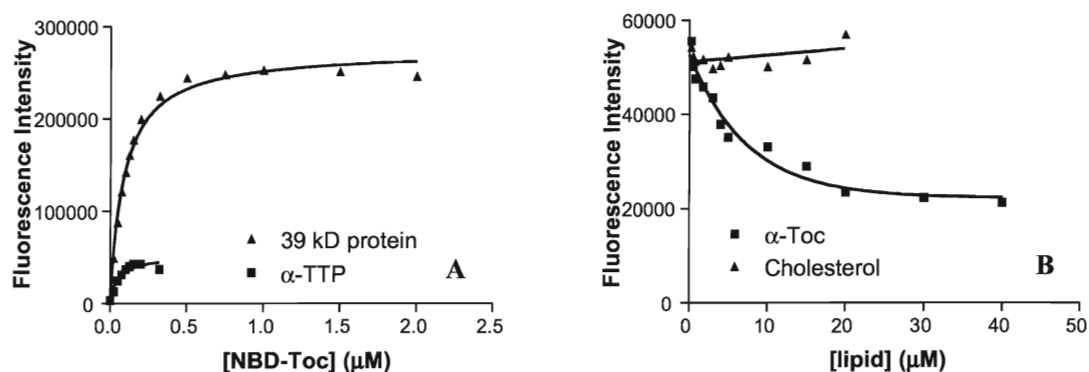


Figure 34: Specific binding of NBD- α -Toc to 39 kDa contaminant. A) Stepwise titration of 200 nM 39 kDa protein or α -TTP with NBD- α -Toc. B) Displacement of NBD- α -Toc bound to 39 kDa protein by the increasing concentration of α -Toc or cholesterol.

Due to the limited knowledge we had about this contaminating protein, we had to perform a literature search for a 39 kDa *E. coli* protein with propensity for metal ions and a tendency for trimer formation. We quickly identified our suspect as one of the *E. coli* outer membrane porins, OmpC or OmpF [171-173]. OmpC binds to divalent Mg^{2+} and it shares 74% sequence homology with OmpF [171]. These proteins are integral membrane porins that regulate the osmotic pressure between cells. They facilitate the passive diffusion of small, polar molecules of 600-700 Da through the outer membrane of *E. coli*. In 1989, Veeraragavan *et al.* [172] identified OmpF as one of the two major contaminating proteins in *E. coli* inclusion bodies. However, during the high cell density

cultivation, OmpF was also found to secret into the culture medium [173]. We generally allowed 18-hour IPTG induction, so as to increase the expression of α -hTTP. The cell

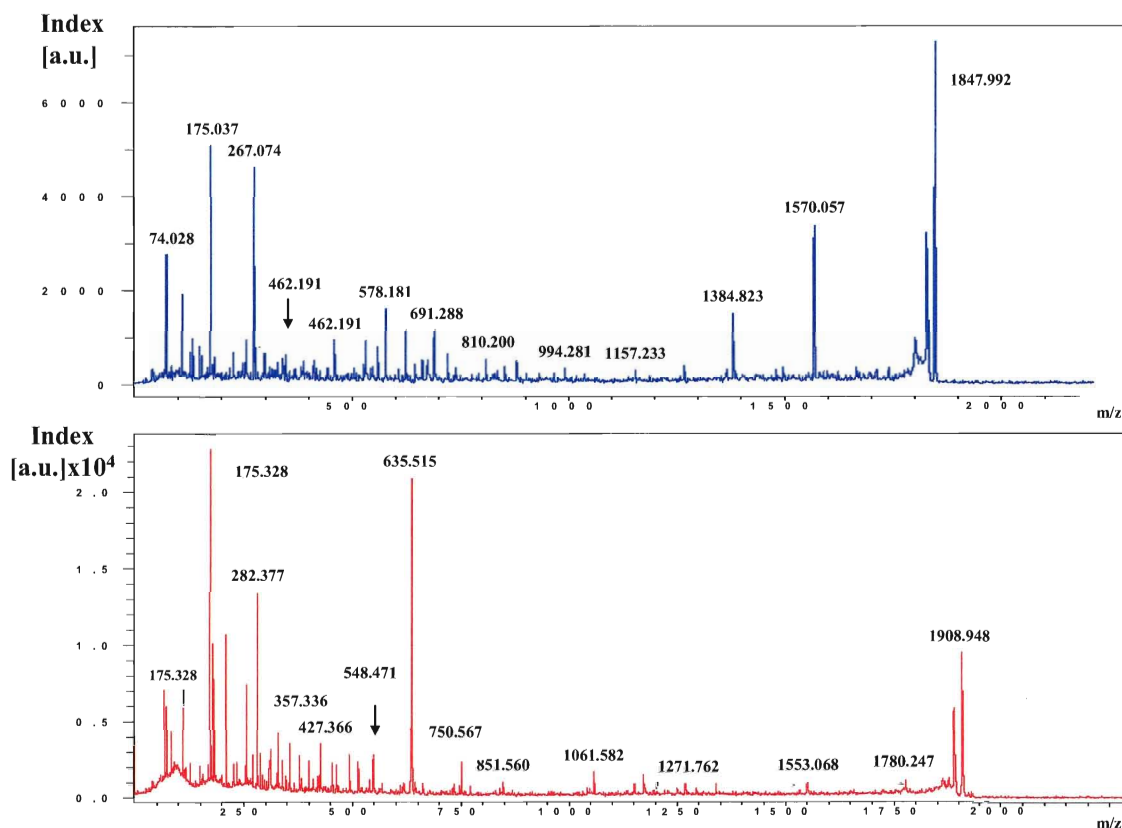


Figure 35: Matrix-assisted laser desorption/ionization MALDI time of flight (TOF) spectrum of trypsin digests of the unknown 39 kDa *E. coli* porin (top) and α -hTTP (bottom). Peptides are indicated as peaks with monoisotopic masses. Shown are representative spectra from several trials. The peak lists are reported in the **Appendix I**.

density before harvest was usually very high, and therefore, it was not unexpected to find soluble OmpF in the culture medium. Since OmpF is capable of binding to both monovalent and divalent ions [174, 175], it was therefore bound to the nickel affinity column during fusion protein purification.

To identify the 39 kDa *E. coli* contaminant experimentally, MALDI-TOF mass spectroscopy analysis of the trypsin digested 39 kDa protein with α -hTTP as a control, were performed. Shown in **Fig. 35** are representatives of the spectra from several trials.

The trypsin digested peptides YDANNIYLAANYGETR (m.w. 1847.992) (top panel) and EAGVPLAPLPLTDSFLLR (m.w.1908.948) (bottom panel) were used to search for their prospective proteins in mass spectrometry protein database (MSDB). The unknown contaminant was subsequently identified as OmpF, with a molecular weight of 39,309 Dalton, based on a high match score of 89% to the trypsin digested peptide. Similarly, the control protein was identified as human α -TTP of 31,844 Dalton with a match score between 65-72%. The detailed peak lists of ions can be found in **Appendix I**.

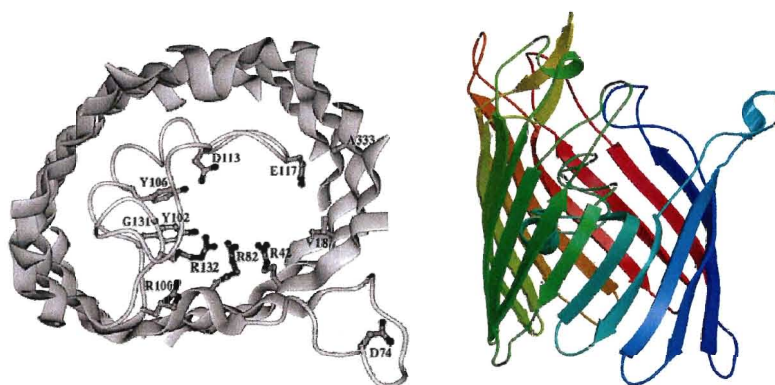


Figure 36: Structure of *E. coli* Outer Membrane Porin F (OmpF). Left panel is the top view and right panel is the side view of the protein.

Two different views of OmpF are depicted in **Fig. 36**. As shown in this figure, OmpF is barrel shaped. It is structurally similar to but larger than the fatty acid binding proteins. OmpF consists of 3 α -helix strands, 16 antiparallel β -helix strands, and looping strands that connect the β -helices to each other. The large cavity allows its ligand to diffuse out of the *E. coli* outer membrane. This explains the apparent diffusional transfer of NBD- α -Toc in the presence of the OmpF contaminant.

2.2. NBD- α -Toc transfer by α -hTTP is mediated through a collisional mechanism

2.2.1. Characterization of α -hTTP purified from α -hTTP/pGEX4T

In order to completely avoid OmpF contamination, it was necessary to seek another mean of expressing α -hTTP without a His-tag. Our collaborators provided a GST- α -TTP fusion construct, hTTP/pGEX4T, which consisted of the human α -TTP gene fused to the gene for glutathione-S-transferase in the pGEX-4T-3 vector. This construct would produce GST (26 kDa) followed by a linker region containing a thrombin cleavage site (LVPR↓GS), four amino acids before hTTP due to the presence of the multiple cloning sites. Thrombin recognizes the linker sequences LVPRG or LVPRGS [176], and cleaves after arginine, leaving α -hTTP with an extra GS plus four amino acids (PNSR) at the N-terminus after thrombin digestion [111]. A non-metal containing glutathione agarose purification method was employed to purify the GST- α -hTTP fusion protein following expression of the α -hTTP-GST fusion protein from the α -hTTP/pGEX4T construct. As shown in **Fig. 37A**, after buffer washes to remove non-specifically bound proteins, only two major proteins plus 4 to 5 minor ones remained on the glutathione column (lane #5). The top band represented the ~56 kDa GST- α -hTTP, and the bottom ~26 kDa band was likely the GST fusion tag. The two hours on-column thrombin digestion produced a 32 kDa α -hTTP (lane #6 & 7) and a 26 kDa GST (lane #8 & 9). In addition, an *E. coli* protein of ~65 kDa (< 2%) was found to co-purify with α -hTTP. Although thrombin cleavage is fairly specific, it can also digest proteins at other sequences [176]. To prevent secondary protein degradation during storage, the protease inhibitor, phenylmethylsulphonyl fluoride (PMSF), was always added to the purified α -hTTP fractions. After three days of storage at 4°C, no change in α -hTTP was observed (**Fig. 37B**, lane 7 & 8) compared to the freshly cleaved α -hTTP (**Fig. 37B**, lane 5 & 6). α -hTTP was typically used within the first few days of purification.

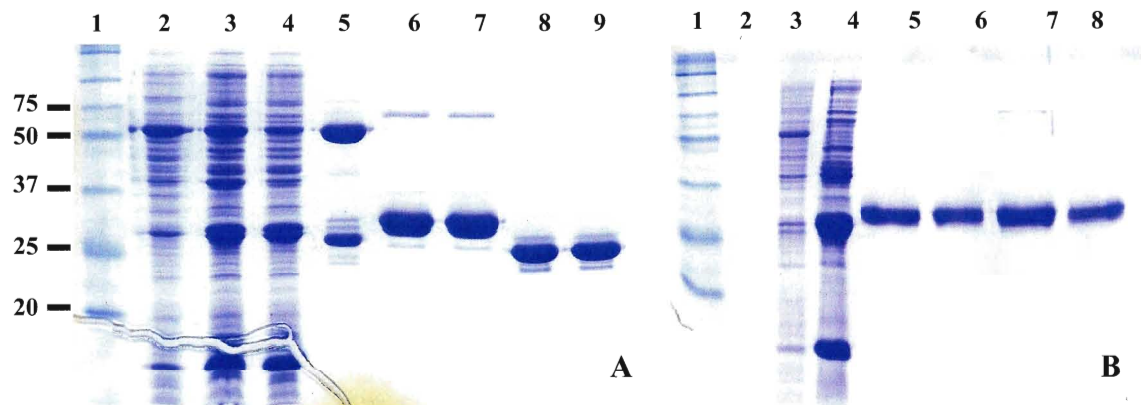


Figure 37: Glutathione affinity purification of GST- α -hTTP expressed from hTTP/pGEX4T (A) and the integrity of α -hTTP during storage (B). Crude lysate fractions and purified protein samples ($\sim 5 \mu\text{g}$ per lane) were analyzed on 15% SDS-PAGE. Protein markers are shown in Lane 1 for both gels. **A)** Lane 2: insoluble cell lysate; Lane 3: soluble cell lysate; Lane 4: flow through fraction; Lane 5: full length GST-hTTP; Lane 6 & 7: cleaved hTTP fractions #1 and 2; Lane 8 & 9: GST fraction #1 and 2. **B)** Lane 3: total cell lysate; Lane 4: insoluble fraction; Lane 5 & 6: hTTP day 1; Lane 7 & 8, hTTP 3 days after purification.

The same experiments previously performed with 6-His- α -hTTP were repeated with the thrombin cleaved α -hTTP. This version of α -hTTP had high affinity for NBD- α -Toc (**Fig. 38**), with a dissociation constant (K_D) at $18.9 \pm 0.4 \text{ nM}$ ($n=3$), improved from 6-His- α -hTTP ($K_D = \sim 48 \text{ nM}$) or 6-His-28TTP ($K_D = 56 \pm 15 \text{ nM}$).

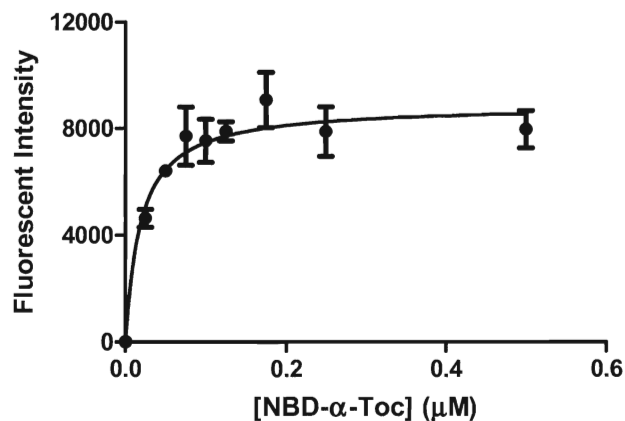


Figure 38: Titration of α -hTTP with NBD- α -Toc. Thrombin cleaved α -hTTP (200 nM) was titrated with 1 μ L additions of NBD- α -Toc (in EtOH) of various stock concentrations until saturation was achieved. Shown is the fluorescence recorded at 535 nm with excitation at 466 nm.

2.2.2 Partitioning of NBD- α -Toc between α -hTTP and lipid vesicles

Next, the transfer of NBD- α -Toc by this α -hTTP was assessed by determining the partition of NBD- α -toc between α -hTTP and vesicles for vesicles of two different sizes as illustrated in **Fig. 39**. The slopes of the lines for both LUVs and SUVs over the indicated lipid concentration range are very similar and shallow. From these assays, the average values of the determined partition coefficient, K_p , of NBD- α -Toc between α -hTTP and bovine liver PC vesicles were 0.064 ± 0.026 for LUVs and 0.098 ± 0.035 for SUVs, respectively. These values are not significantly different from each other. As the

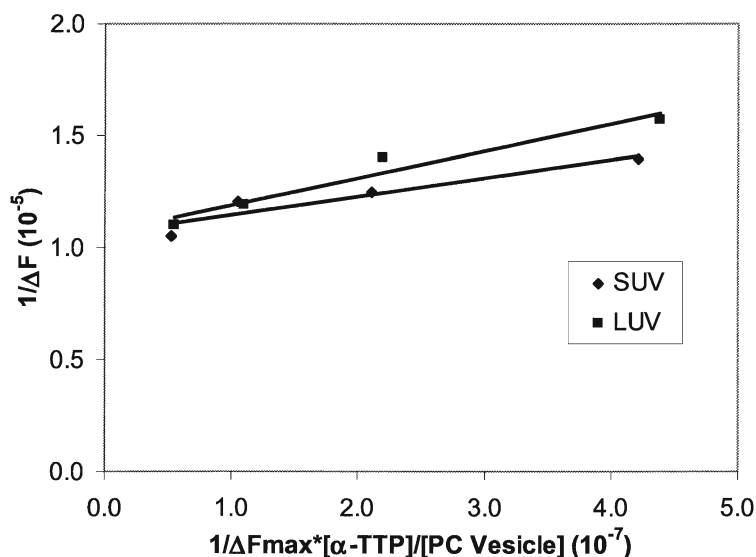


Figure 39: Partitioning of NBD- α -Toc between α -hTTP and SUVs or LUVs. Titration of NBD- α -Toc (0.225 μ M) bound to α -hTTP (2 μ M) with PC SUVs (\blacklozenge) or LUVs (\blacksquare) at the concentration of 50 μ M, 100 μ M, 200 μ M and 400 μ M. The change in fluorescence intensity between NBD- α -Toc bound to α -hTTP and at each lipid concentration is expressed as ΔF . The partition coefficients determined for this particular experiment are 0.122 and 0.082 for SUVs and LUVs respectively.

units of K_p are (mol lipid-bound NBD- α -Toc/mol phospholipid)/(mol protein-bound NBD- α -Toc/mol protein), the magnitude of K_p shows that NBD- α -Toc binds to α -hTTP with ~ 10 - 15 times greater affinity than to lipid vesicles. Thus, for our transfer assay conditions to reflect unidirectional movement from protein to vesicle, an excess of phospholipids must be provided. Our assays used a 50-fold molar excess of phospholipids over α -hTTP to ensure unidirectional transfer, and also maintained the rate of transfer within the kinetic window of our stopped-flow device (mixing dead time ~ 20 ms). At equilibrium, the assays showed a $\sim 50\%$ loss of the original fluorescence from protein-bound NBD- α -Toc.

2.2.3. Kinetics of NBD- α -Toc transfer by α -hTTP

We then determined whether α -hTTP utilizes a collisional mechanism, which requires the binding of the protein to the membranes. To do so, the concentration of acceptor vesicles was increased, while the protein and ligand concentration was kept constant. If protein-membrane collision is required, then the rate of transfer should increase with the increasing concentration of phospholipid. As shown in **Fig. 40**, the rate of transfer of NBD- α -Toc from α -hTTP is quite insensitive to LUV concentration. However, the rates did increase about 50% ($0.011 \pm 0.0017 \text{ s}^{-1}$ to $0.017 \pm 0.005 \text{ s}^{-1}$), when the LUV concentration was increased from 50 μM to 750 μM . When SUVs were the ligand acceptor, the enhancement of transfer was much more dramatic. The transfer rate increased ~ 4.5 -fold from 25 μM to 625 μM phospholipids. We also noted a 4 nm red-shift of the intrinsic tryptophan fluorescence of α -hTTP, when bound to PC SUVs [114], suggesting that α -hTTP binding to these vesicles was accompanied by a significant environmental change around tryptophan residues.

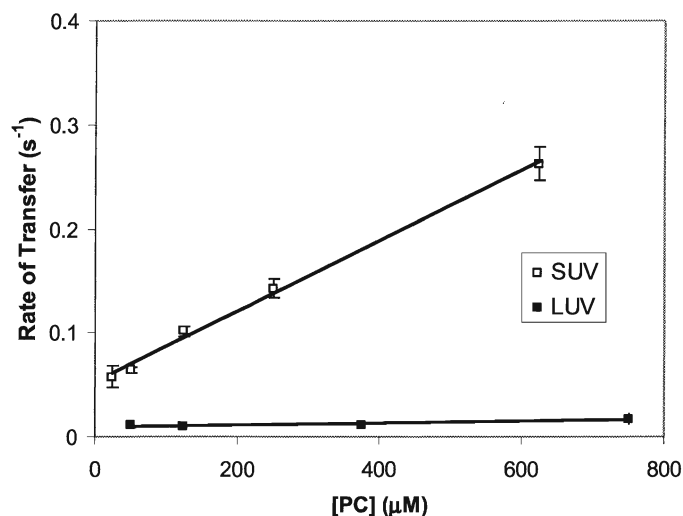


Figure 40: Effect of lipid concentration on the rate of NBD- α -Toc transfer from α -hTTP to PC SUVs and LUVs. Transfer of 0.125 μ M NBD- α -Toc from 1.25 μ M α -hTTP to SUVs (□) or LUVs (■) at the indicated concentration was monitored at room temperature (20°C). Results are the average of 3 determinations \pm the standard deviation.

Supporting evidence for a collisional versus diffusional mechanism can be obtained if the rate of transfer is affected by an increase in ionic strength of the medium. If the ligand must first leave the protein and diffuse to a nearby membrane, high ionic strength slows the rate of transfer. Hydrophobic compounds such as α -Toc and NBD- α -Toc, which already have very low aqueous solubility, should be even less likely to exist freely in buffer due to the increased solvent polarity of the high salt buffer. This has been demonstrated for the liver FABP [128]. **Fig. 41** shows that there is no reduction in the rate NBD- α -Toc transfer from α -hTTP to SUVs (100% PC or 15mol% PS in PC) in up to 1.0 M salt.

We hypothesized that α -hTTP would show enhanced rates of ligand transfer to membranes that contained anionic lipids, since this has been noted for other lipid transfer proteins such as the FABPs [131, 177-180], and cellular retinol binding protein I [181]. Thus, the effect of anionic lipids on the transfer of NBD- α -toc by α -hTTP to SUVs and

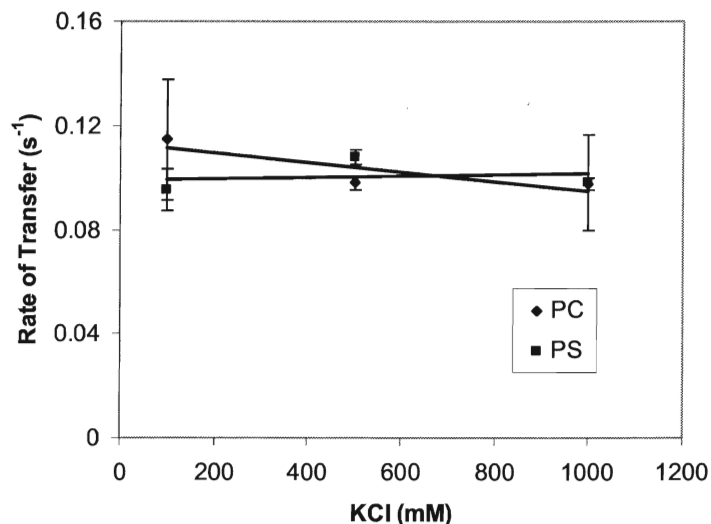


Figure 41: Effect of ionic strength on the rate of NBD- α -Toc transfer to PC or PS SUVs. 0.225 μ M NBD- α -Toc transferred from 2 μ M α -hTTP to 100 μ M PC SUVs (●) or PC SUVs containing 15% PS (■) in the presence of increasing concentration of KCl. Data shown represents an average \pm the standard deviation, $n=12$ for PC at 100 mM KCl, $n=3$ for other conditions tested. The data shown are compiled from separate experiments with different protein and lipid preparations.

LUVs was investigated. However, when SUVs were prepared, containing 15% of anionic phospholipids, such as bovine liver phosphatidylinositol (PI), dioleoylphosphatidylserine (DOPS), lysobisphosphatidic acid (LBPA), or dioleoylphosphatic acid (DOPA), the transfer rates of NBD- α -Toc by α -hTTP showed only minor rate variations (**Fig. 42**, open bars). Transfer rates from α -hTTP to LUVs were on average 4-10 times slower than for SUVs. An increase in the concentration of PS from 15 to 25% did not significantly increase the observed rate (data not shown). In contrast to SUVs, the transfer of NBD- α -Toc was enhanced to the anionic phospholipid containing LUVs (hatched bars). The rates increased 1.2 to 8-fold above transfer to PC LUVs, but most notably in the presence of CL, which was almost equivalent to the rate obtained for SUVs. Transfer to CL containing SUVs was also investigated (data not shown). To our surprise, upon mixing of α -hTTP and the acceptor SUVs, instead of the

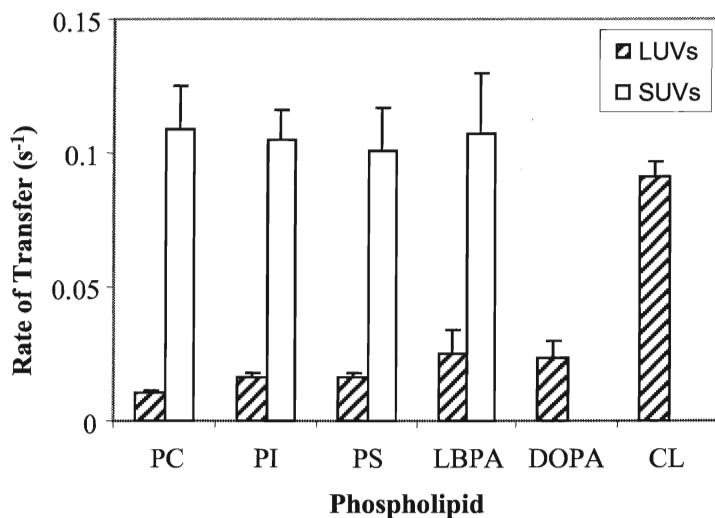


Figure 42: NBD- α -Toc transfer from α -hTTP to anionic SUVs or LUVs. Transfer of 0.225 μ M from 2 μ M α -hTTP to 100 μ M bovine liver PC LUVs (**hatched bars**) or SUVs (**open bars**) containing 15 mol% of PI, PS, LBPA and DOPA. Results are the average of average \pm the standard deviation, $n=3$ for PI, PS, LBPA, DOPA and CL and $n=12$ for PC only controls. P values for SUVs were calculated with unpaired t-tests, there is no significant difference between the SUVs tested.

usual fluorescence decay, the fluorescence signal was actually increased. It was not clear why TRITC-PE when present in CL SUVs failed to quench NBD- α -Toc.

Electrostatic interactions clearly played an important role in the transfer of NBD- α -Toc to the anionic LUVs, but not to the SUVs. It is possible that the planar lipid surface of LUVs has higher packing density, the orientation of α -hTTP is thus influenced by the headgroup environment of lipid bilayer. As the electrostatic potential map indicated in **Fig. 21**, α -hTTP is divided into regions of positive and negative potential. We speculated that the anionic surface could also interact with the positively charged lipids. For this reason, cationic 1,2-dioleoyl-3-trimethylammonium propane, DOTAP was tested. Transfer of NBD- α -Toc to LUVs was enhanced by up to ~79% (0.019 ± 0.003 s⁻¹ to 0.034 ± 0.005 s⁻¹) in the presence of 10% DOTAP, but it was not significantly altered by DOTAP containing SUVs (**Fig. 43**).

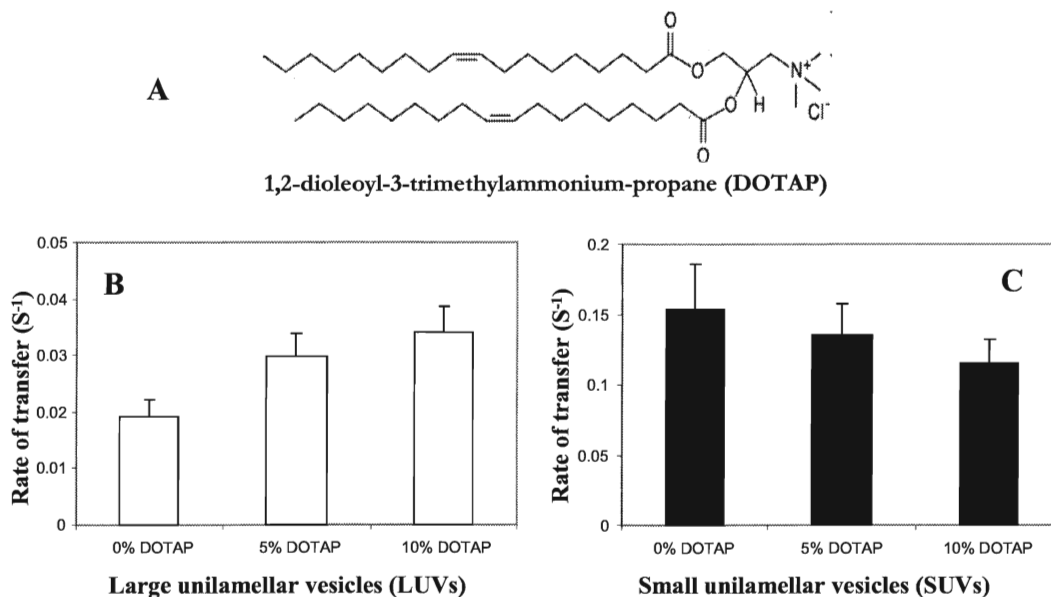


Figure 43: Effect of cationic lipid on the transfer of NBD- α -Toc. A) Chemical structure of DOTAP. Acceptor liver PC LUVs (B) and SUVs (C) contained the indicated amount of DOTAP were tested for their effect on the rate of NBD- α -Toc transfer. P values calculated with t-tests using the two-tailed distribution are: 2.81×10^{-6} for 5% LUVs; 5.23×10^{-7} for 10% LUVs; 0.28 for 5% SUVs and 0.025 for 10% SUVs.

To explore the effect of membrane surface curvature further, vesicles of differing size were prepared by liposome extrusion through specific pore size filters and by sonication. The rates of α -hTTP mediated NBD- α -Toc transfer to PC vesicles of 50, 100, or 200 nm diameters were similar ($k = \sim 0.017 \pm 0.0009 \text{ s}^{-1}$), as shown in **Fig. 44**. For the probe-sonicated vesicles, the rate was $0.114 \text{ s}^{-1} \pm 0.023 \text{ s}^{-1}$, and for bath sonicated it was $0.098 \pm 0.005 \text{ s}^{-1}$. Sonicated vesicles, using either an immersion probe or bath sonicator, are generally expected to yield SUVs of about $\sim 25 \text{ nm}$ in diameter [182, 183]. α -hTTP mediated ligand transfer to 25 nm vesicles consistently showed 8-10 fold faster than to 100 nm LUVs, whereas transfer to 30 nm vesicles was 2.2 fold greater than transfer to 50 nm vesicles yet only 50-60% of the transfer rate to 25 nm SUVs.

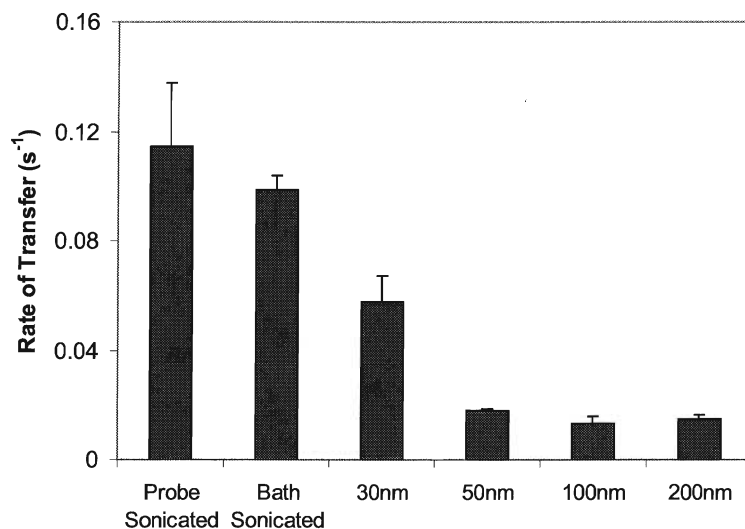


Figure 44: Effect of vesicle size on the rate of NBD- α -Toc transfer from α -hTTP. PC vesicles were prepared by probe sonication, bath sonication or extrusion. 0.225 μ M NBD- α -Toc transferred from 2 μ M α -hTTP to 100 μ M vesicle of various sizes was monitored. The data shown represent the average \pm the standard deviation, $n=12$ for the probe sonicated PC SUV, $n=18$ for 100nm PC LUV, $n=3$ for other conditions tested. The data shown are compiled from separate experiments with different protein and lipid preparations.

To assess the influence of lipid packing (bilayer fluidity) on the transfer process, the rate of NBD- α -Toc transfer to acceptor phospholipid vesicles of differing degrees of unsaturation is shown in **Fig. 45**. Three different sources of phosphatidylcholine were tested: soy PC with a saturated to unsaturated lipid ratio (S/U) of 0.30 and consisting predominately of 18:2 acyl chains; synthetic dioleoylphosphatidylcholine (DOPC); and bovine liver PC with a S/U ratio of 0.91 and a higher proportion of 18:0 acyl chains. Regardless of the lipid composition, the rates of α -hTTP mediated ligand transfer were faster to SUV than LUV acceptors, and soy PC lipids that contained the larger fraction of unsaturated acyl chains supported a transfer rate twice as fast as either DOPC or bovine liver PC.

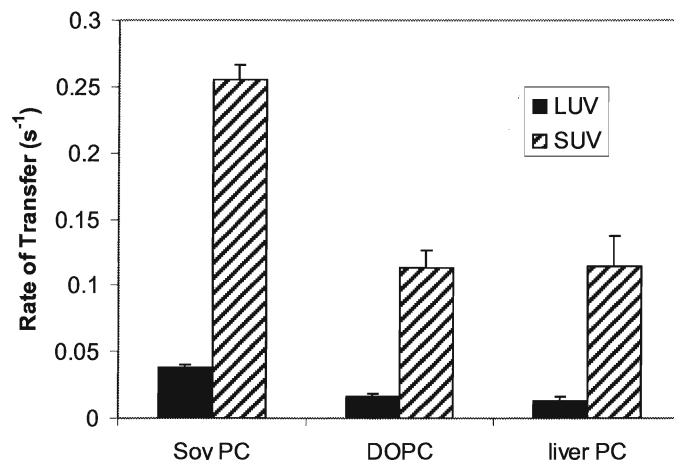


Figure 45: Effect of lipid saturation on α -hTTP mediated NBD- α -Toc transfer. Transfer of 0.225 μ M NBD- α -Toc from 2 μ M α -hTTP to 100 μ M PC LUVs (closed bars) and SUVs (hatched bars) of soy PC, DOPC and liver PC was monitored. Data shown represents an average \pm the standard deviation, n=3 for soy PC and DOPC, n=12 for PC SUVs and n=18 for PC LUVs. The data shown are compiled from separate experiments performed with different protein and lipid preparations.

Cholesterol is known to regulate the fluidity of lipid membranes; it fills in the void space between the fatty acyl chains in the membrane, thereby making the disordered conformations of unsaturated acyl chains more rigid, while increasing membrane fluidity in the more ordered environment. We speculated that cholesterol would reduce the membrane fluidity of bovine liver PC and thus hinder NBD- α -Toc transfer to the membrane. In order to assess the effect of cholesterol on α -hTTP-mediated transfer, vesicles were prepared from the heterogenous bovine liver PC that contains of ~9% each of the highly unsaturated fatty acids 20:3 and 20:4, and a few percent of 20:6. For comparison, addition of cholesterol to bovine liver PC was compared to an even more heterogenous lipid mixture of the total liver lipid extract. The liver total lipid extract was composed of 42% PC, 7% cholesterol, 22% PE, 8% PI, 1% lysoPI and 21% others, including neutral lipids. As shown in **Fig. 46**, the inclusion of 15 % cholesterol in bovine

liver PC LUVs but not SUVs modestly enhanced the rate of transfer when compared to vesicles without cholesterol. The most striking result was observed in the vesicles

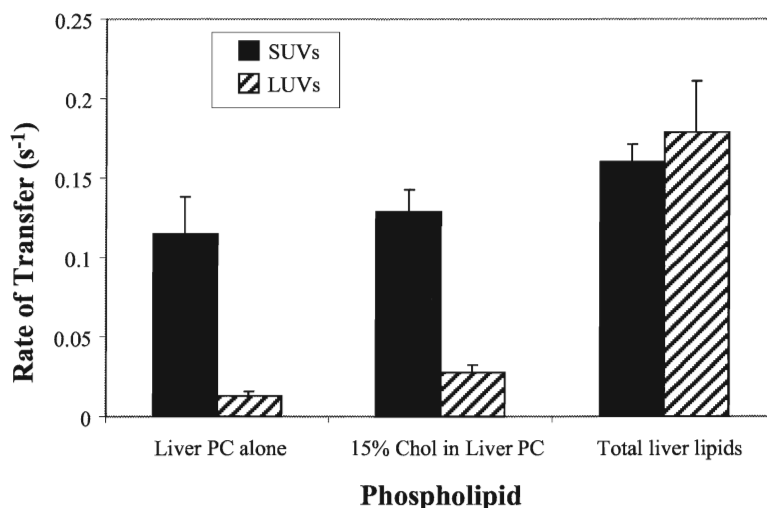


Figure 46: Effect of other lipids on α -hTTP mediated NBD- α -Toc transfer. Transfer of 0.225 μ M NBD- α -Toc from 2 μ M α -hTTP to 100 μ M PC SUVs (closed bar) and LUVs (hatched bar). Lipids tested are indicated in the graph. Data shown represents an average \pm the standard deviation, n=3 for 15% Chol and total liver lipids, n=12 for PC SUVs and n=18 for PC LUVs.

prepared from the total liver lipid extract, where α -hTTP could no longer discriminate between SUVs and LUVs, as the transfer rate to SUVs and LUVs were determined to be $0.160 \pm 0.011\text{s}^{-1}$ and $0.179 \pm 0.033\text{s}^{-1}$, respectively. We have tested cholesterol, PE and PI, individually, and they were found to have minimal impact on the transfer of NBD- α -Toc to both SUVs and LUVs. Whether a particular unique lipid component in the 21% unspecified lipids, or the unique combination of this total lipid exact creates a similar membrane packing effect for LUVs and SUVs is unknown, and demands further investigation.

The above data suggested the importance of the membrane curvature in regulating the ligand transfer. However, our knowledge regarding the vesicle size was based on the assumption that sonication and extrusion with a filter of certain pore size would produce

the vesicles of desired size. To ascertain that the vesicles tested were true to their predicted sizes, vesicles were subjected to Quasi Elastic Light Scattering (QELS) analysis. Light scattering detects the Brownian motion of small particles. The hydrodynamic radii measured are presented in **Table 1**. The LUVs of 100 nm in Tris and SET buffer were determined to be 113.8 nm and 158 nm, respectively. The sizes determined for vesicles of 80 nm or less were higher than expected, with the SET buffer alone produced a high background value. Therefore, the higher vesicle size estimates were possibly due to the viscosity of the SET buffer that contained 8.6% sucrose. The viscosity of this buffer was determined to be 1.28. The average diameter for SUVs prepared in HEPES buffer containing 9% sucrose was reported to be approximately 72 nm determined by electron microscopy [184]. The dynamic radius R_h is related to the

Table 1: The hydrodynamic radii of lipid vesicles measured by Dynamic Light Scattering (DLS) at McMaster University

PC vesicle sample	ACR (kcps)	Polydispersity index	Eff. Diameter (nm)
SET background	13.7	0.452	78.1
30nm	153.5	0.122	91.4
50nm	227.9	0.119	106.7
100nm	120.4	0.116	158
200nm	210.1	0.103	219.5
Probe sonicated SUV	184	0.273	107
Bath sonicated SUV	150	0.266	134
Tris background	6.2	undefined	undefined
100nm LUV Tris	221.4	0.085	113.8

translational diffusion coefficient D_T (of the particle to be measured) through the Stokes-Einstein equation [185], and therefore, it is also related to the solution viscosity:

$$D_T = K_B T / (6\eta R_h) \quad \text{Eqn 2}$$

where K_B is the Boltzmann's constant, T is the temperature, η is the viscosity of the medium. The parameters used for hydrodynamic radius analysis were: a 90° scattering angle θ , a 628.3 nm wavelength, and 0.89 buffer viscosity. Because the viscosity was not corrected to 1.28, the vesicles' radii determined were therefore not as precise as expected.

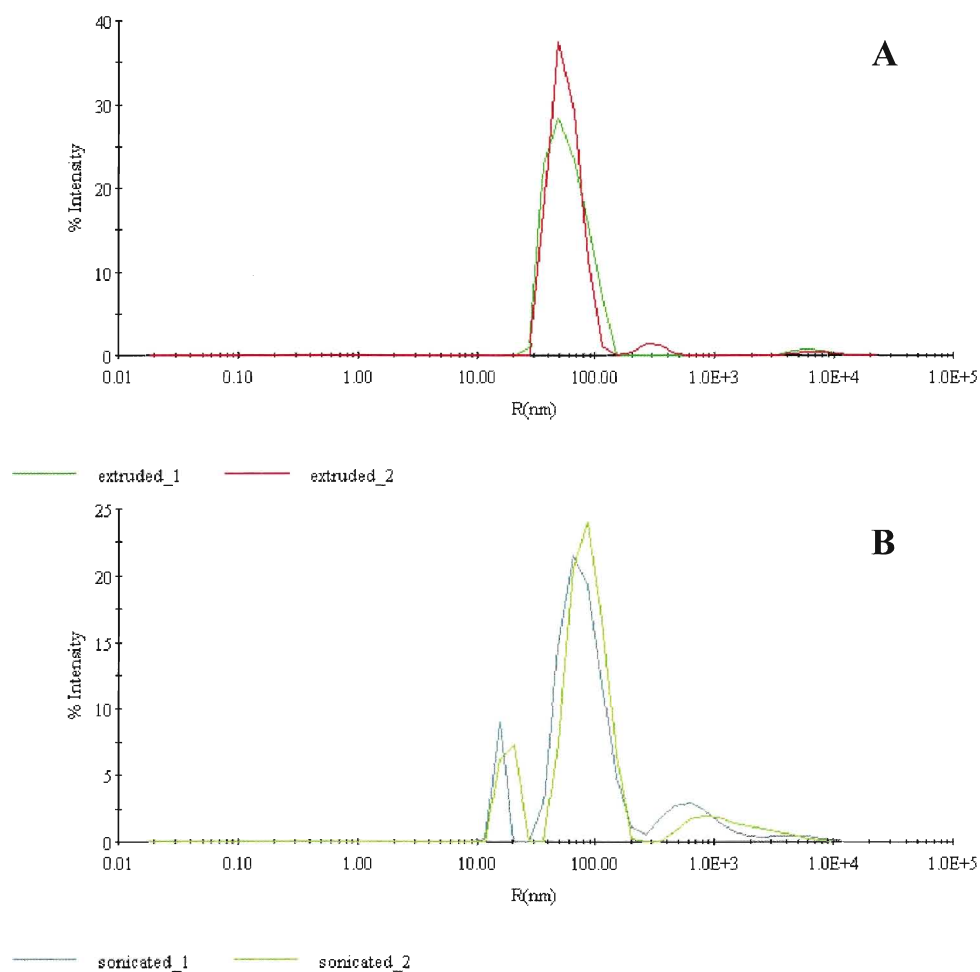


Figure 47: Dynamic Light Scattering (DLS) analysis of extruded 30 nm SUVs (A) and probe sonicated SUVs (B). Samples were measured at 25°C at 660 nm in a Dynapro NanoStar Instrument. Presented are the duplicate runs of SUV samples.

Since NBD- α -Toc transfer was greatly enhanced to the sonicated SUVs and 30 nm extruded SUVs, we were particularly interested in learning the accurate size of these

vesicles. Due to the small size of these vesicles, any particles of equal size or greater would introduce error in the measurement. Thus, SET buffer was first vacuum filtered through a 30 nm filter to remove potentially larger aggregated sucrose prior to vesicle preparation. Both sonicated and extruded SUV samples were then shipped to be analyzed by Wyatt Technology Inc. (Santa Barbara, CA). As illustrated in **Fig. 47**, the duplicate runs of both extruded and sonicated samples were fairly reproducible, and the results are summarized in **Table 2**. Extrusion through 30 nm membranes produced uniform SUVs, with a polydispersity index between 0.031 and 0.037, and a cumulative radius of ~ 55nm. Greater than 96% of the population were vesicles smaller than 60.1 nm, and the rest were large aggregates of ~ 6 μ m. Sonication, on the other hand, produced a rather heterogeneous population of vesicles indicated by the high polydispersity index of 0.326. Three populations of vesicles were detected: 9.2 to 13.5% vesicles of 20 nm and smaller, ~75% median size vesicles of 80 nm, and ~12% large aggregates. Due to the

Table 2: The hydrodynamic radius of extruded and sonicated SUVs determined by Wyatt Technology Inc.

Sample	Cumulants Analysis		Regularization Analysis			
	Radius (nm)	Polydispersity Index	Peak #	Peak R (nm)	Peak % Pd	Peak % Int
Extruded_1	55.4	0.037	1	60.1	36.9	98.2
			2	6329.0	25.1	1.8
Extruded_2	55.5	0.031	1	56.5	27.9	96.0
			2	296.5	20.4	2.9
			3	7820.2	33.4	1.0
Sonicated_1	67.5	0.326	1	15.7	4.1	9.2
			2	82.3	43.4	76.5
			3	785.0	58.2	12.8
			4	5422.1	35.9	1.5
Sonicated_2	67.5	0.326	1	18.5	13.8	13.5
			2	88.5	32.5	75.3
			3	1614.9	79.3	11.3

heterogeneity in vesicle preparation, the actual average size was determined to be 67.5 nm, not 25 nm or less, as expected. The effective diameter determined from QELS in general tends to be higher than values obtained by freeze fracture electron microscopy [169, 186]. Although the actual sizes measured were higher than expected, the size relationship was consistent among the extruded vesicles (Table 1), 200 nm > 100 nm > 50 nm > 30 nm. Due to the high polydispersity index, sonicated SUVs should not be directly compared to the extruded vesicles.

To ensure that the enhanced transfer of NBD- α -Toc to SUVs was introduced by the increase in membrane curvature and not by the increase in the total lipid surface available, we calculated the total number of liposomes and outer surface area that could be produced from a particular lipid sample using the equations (3-5) listed below. The estimated surface area for a molecule of POPC is approximately 70 Å² [187].

$$\# \text{ lipids per liposome} = [4\pi(\frac{1}{2}d)^2 + 4\pi(\frac{1}{2}d-h)^2]/a \quad \text{Eqn 3}$$

$$\# \text{ of liposomes} = (M_{\text{lipid}} * N_A)/N_{\text{total}} * \text{Vol.} \quad \text{Eqn 4}$$

$$\text{Total outer surface area} = \# \text{ of liposomes} * 4\pi(\frac{1}{2}d)^2 \quad \text{Eqn 5}$$

where **h** is the thickness of bilayer (8 nm), **a** is the headgroup area of PC (0.7 nm²), **N_A** is Avogadro's number (6.02 x 10²³), **d** is the diameter of vesicles, **M_{lipid}** is the molar concentration of lipid sample, and **N_{total}** is the total number of lipids per liposome. The total number of liposomes increased by approximately 14 fold when the vesicle size was decreased from 100 nm to 30 nm (Table 3), yet the total outer surface area increased by only 40%. According to the calculated surface values using the theoretical sizes of LUVs (100 nm) and SUVs (30 nm), the 8 to 10 fold enhancement in NBD- α -Toc transfer to

SUVs versus LUVs could not have been caused by such a minor increase in the total outer surface area of the smaller vesicles.

Table 3: Total outer surface area of various sized liposomes and the surface ratio in relative to 100 nm LUVs. Please note the above equations used in calculation were obtained from web site: www.liposomes.org/2009/01/number-of-lipid-molecules-per-liposome.html.

Vesicle diameter (nm)	Total # of lipids per liposome	# of liposome (1mL @ 200 uM)	Outer surface area (nm ²)	Surface Ratio
200	33146	1.82E+12	2.28E+17	0.92
100	7655	7.86E+12	2.47E+17	1.00
50	1641	3.67E+13	2.88E+17	1.17
30	492	1.22E+14	3.46E+17	1.40
20	187	3.22E+14	4.05E+17	1.64

2.3. Membrane insertion of gating helix A8 and helix A10 are essential for the binding of α -hTTP to the target membranes and the delivery of NBD- α -Toc

2.3.1. Creation of hydrophobic mutants

The orientation of α -TTP with respect to the lipid membrane can be calculated by estimating the free energy change (ΔG) when a portion of the protein surface is transferred from water to the lipid bilayer. The calculation was performed by our collaborator Dr. Andrei Lomize (University of Michigan) using a program called PPM (Positioning of Proteins in Membranes). The details of the calculations have been published [149]. Briefly, the transfer energy (ΔG) was calculated as a function of four variables d , z_0 , τ , and ϕ (**Fig. 48**) in a coordinate system with Z-axis coincides with the membrane normal:

$$\Delta G(d, z_0, \tau, \phi) = \sum_i \text{ASA}_i \sigma_i^{\text{W-M}} f(z_i) \quad \text{Eqn 6}$$

where ASA_i is accessible surface area of atom i , $\sigma_i^{\text{W-M}}$ is the salvation parameter of atom i and $f(z_i)$ is interfacial water concentration profile. The optimal spatial arrangement of a

protein in membrane is determined by minimizing its transfer energy from water to the hydrophobic solvent such as decadiene [149].

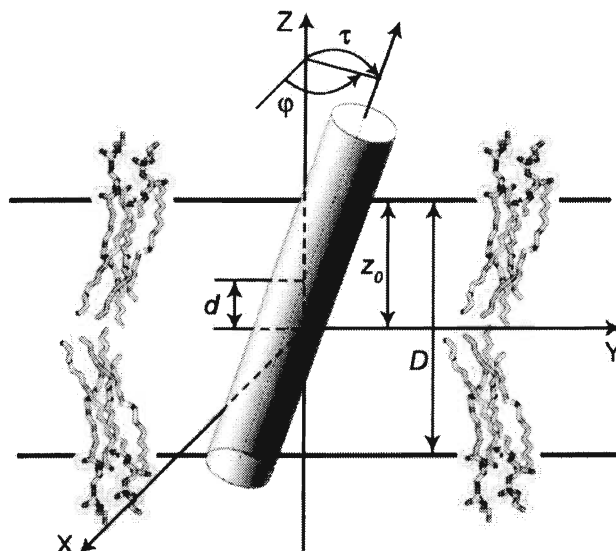


Figure 48: Schematic representation of a transmembrane protein in a hydrophobic slab. Parameters that defined the arrangement of a TM protein in the membrane hydrocarbon core: d , shift along the bilayer normal; τ , tilt angle; ϕ , rotational angle, and $D = z_0$, hydrophobic thickness of the protein. This image was created by Lomize *et al.* [149].

Fig. 49A illustrates the proposed orientation of α -TTP (ligand bound, closed) in relation to the lipid bilayer and the immersion of the two gating helices: helix A8 and helix A10 into the membrane. Helix A8 is spatially fixed, while the helix A10 is mobile, which allows ligand to enter and exit the protein. The hydrophobic residues of helix A8 (F165 and F169) and helix A10 (I202, V206 and M209), shown in **Fig. 49B**, are predicted to penetrate deep into the lipid membrane. In the open conformation, helix 8 and helix 10 are further apart. Calculations of change in transfer energy show that when the open, ligand-free form of α -TTP binds to the membrane, the initial penetration into the membrane is estimated to be 8.4 ± 0.9 Å deep, with a change in free energy (ΔG) of -

20.7 kcal/mol. The binding of α -hTTP to the bilayer stabilizes the “closed” conformation of the protein, which reduces the depth of penetration to 4.0 ± 0.5 Å and the free energy change of binding to -10.6 kcal/mol.

Guided by this model, the hydrophobic residues highlighted in **Fig 49** were mutated to either the acidic aspartate or hydrophobic alanine. The acidic aspartate residues were expected to produce the greatest effect on the free energy of transfer (making ΔG more positive) due to the cost of insertion of these charged residues into the hydrophobic membranes. Residue M264 located on the opposite side of the protein away from helices A8 and A10 was chosen as a control. The substitution of M264 with an aspartate should have minimal impact on the membrane binding of α -hTTP if the above

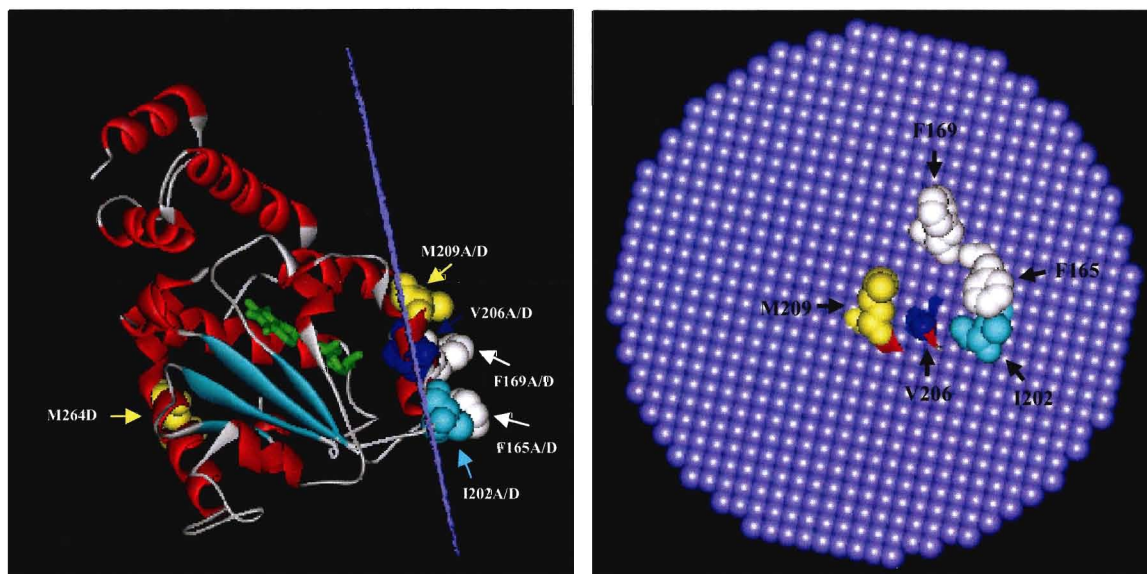


Figure 49: Hydrophobic residues predicted to penetrate into lipid bilayer. The left panel is the side view of α -hTTP (α -Toc bound, pdb:1R51) highlighted with the membrane penetrating hydrophobic residues to be mutated and the control residue M264. The right panel is the view of these amino acids from the hydrophobic core of the membrane bilayer. The space filled molecules shown are: M209 and M264 in yellow, V206 in deep blue, F165 and F169 in white and I202 in cyan. α -Toc is the molecule shown in green sticks. These images were created with ViewerLite.

model has correctly located the face of α -hTTP that directly touches the membrane. The mutant proteins created were assessed for their ability to transfer ligand to lipid vesicles and to adsorb to both immobilized planar lipid bilayers and highly curved unilamellar vesicles.

All hydrophobic mutants were created successfully using Turbo Pfu polymerase and the Quikchange mutagenesis protocol, as described in the Methods. The sequences determined by Robarts Research Institute (London, ON) were aligned with the α -hTTP nucleotide sequence obtained from the Pubmed database to verify the presence of the desired mutations. The alignments produced by BioEdit are included in **Appendix II**. All mutants were expressed in BL21 (DE3) and purified to homogeneity using glutathione affinity chromatography of the soluble cell fractions. Both I202A and V206D were over-expressed in the same vector, but based on SDS-PAGE of total cell lysates. V206D was expressed almost exclusively in inclusion bodies, and I202A resulted in a soluble but apparently mis-folded protein that failed to bind to the glutathione affinity column. Extremely low levels of purified protein were recovered for I202A and V206D, and they were, therefore, not included in most of the testing. All purified proteins were analyzed on SDS-PAGE. As shown in **Fig. 50**, in addition to the major α -hTTP band migrating at the correct size of 32 kDa, two minor contaminants were also detected at ~25 kDa and ~ 65 kDa respectively.

Initially, glutathione agarose (pre-swelled) from Invitrogen was employed for affinity purification of α -hTTP wild-type and the mutants. The protein recovery rate was fairly low – less than 0.5 mg α -hTTP was obtained from each gram of *E. coli* cells. We then tested glutathione agarose provided by Sigma, and the protein recovery was

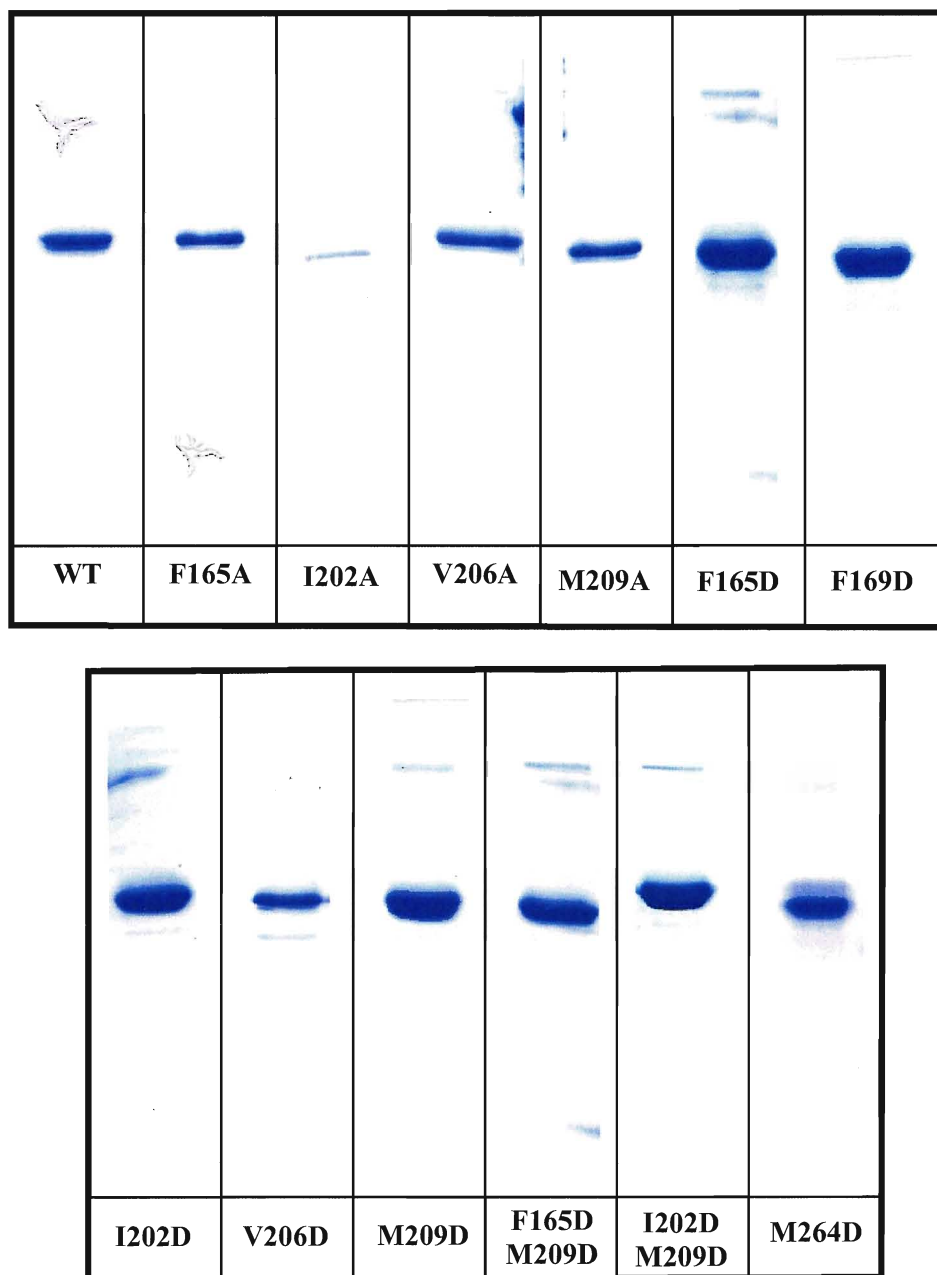


Figure 50: Purified protein samples of wild type α -hTTP and the hydrophobic mutants visualized on 15% SDS-PAGE. Typically, 5 to 10 μ g per lane (except I202A and V206D) were analyzed on SDS-PAGE gel. Note: protein samples shown are for qualitative purpose only, amount of protein visible varied due to sample preparation and handling.

improved by several fold to 1.59 ± 0.19 mg of wild-type α -hTTP per gram of *E. coli* cells. The amount of protein recovered for most of the hydrophobic mutants was fairly similar to the wild-type α -hTTP, except for I202A and V206D, with the recovery rate at 0.06 and 0.08 mg per gram of *E. coli* cells, respectively. The purification recovery data is summarized in **Appendix III**.

2.3.2. Membrane binding of hydrophobic mutants and their ability to deliver NBD- α -Toc

The ability of the hydrophobic mutant proteins to bind and transfer NBD- α -Toc to acceptor membranes was determined and compared to the wild-type (**Table 4**). Most of the mutants exhibited similar abilities to bind NBD- α -Toc as the wild-type protein, except for F169D and M209A, which demonstrated a 3 to 4 fold reduction in their binding affinities. Nevertheless, the dissociation constants (K_D) determined for F169D and M209A were very low, at 79 nM and 89 nM, respectively. These data indicated that the mutated residues did not introduce major changes to the ligand binding pocket of α -hTTP.

We subsequently determined the ability of these hydrophobic mutants to deliver NBD- α -Toc to both SUVs and LUVs of bovine liver PC. As shown in **Table 4** and **Fig. 51**, all aspartate mutants except M264D (control) had greatly reduced abilities to transfer NBD- α -Toc (**Fig. 51A**, open bars). Substitution of a single phenylalanine by aspartate at either residue 165 or 169 decreased ligand transfer by 90%, which was equivalent to that of the double mutant I202D/M209D. The I202D/M209D mutant was designed to completely disrupt the binding of mobile helix A10 to the lipid bilayer. However, replacing V206 or M209 with conservative alanine residue had virtually no impact on the

Table 4: Vesicle binding and rate of NBD- α -Toc transfer by wild-type and mutant forms of α -hTTP. K_D values shown are averages of duplicate measurements, with expected error within 20% of the reported values.

TTP	NBD- α -Toc K_D (nM)	Transfer to SUVs (s^{-1})	% WT Rate	Transfer to LUVs (s^{-1})	% WT Rate
WT	19	0.127 ± 0.012	100	0.016 ± 0.002	100
F165D	17.23	0.013 ± 0.001	10	0.009 ± 0.005	56
F169D	79.38	0.015 ± 0.002	12	0.000	0
I202D	26.06	0.028 ± 0.002	22	0.005 ± 0.005	31
M209D	12	0.047 ± 0.004	37	0.013 ± 0.001	81
F165D/M209D	28.84	0.034 ± 0.003	27	0.010 ± 0.001	63
I202D/M209D	24.75	0.014 ± 0.001	11	0.008 ± 0.003	50
M264D	29.22	0.116 ± 0.013	91	0.008 ± 0.001	50
F165A	51.75	0.037 ± 0.002	29	0.005 ± 0.002	31
V206A	23.37	0.154 ± 0.012	121	0.016 ± 0.002	100
M209A	89.35	0.140 ± 0.012	110	0.025 ± 0.005	167

ligand delivery of these mutants (**Fig. 51A**, hatched bars). In contrast, substitution of F165 with alanine reduced the transfer rate by 71% compared to the wild-type protein. These findings clearly indicated the significance of the hydrophobic interaction between helices A8 and A10 and acceptor lipid membranes. In addition, the deep insertion and anchoring of helix A8 appears to be essential for α -hTTP membrane binding since the replacement of the bulky phenylalanine (F165) with a much smaller hydrophobic alanine compromised the ability of α -hTTP to bind to membranes and consequently, to transfer its ligand.

The rates of NBD- α -Toc transfer from aspartate mutants to LUVs were also reduced, but to a much lesser extent, as compared to that of SUVs. Interestingly, F169D completely lost its ability to transfer NBD- α -Toc (**Fig. 51B**). Two other mutants with significantly decreased transfer rates were F165A and I202D. The conservative mutation F165A exhibited ~70% reduction in its transfer rate. Moreover, the control mutant M264D also exhibited ~50% reduction in the rate of transfer of ligand to LUVs compared to the wild-type protein. Due to the very low rate of ligand transfer mediated by the wild-

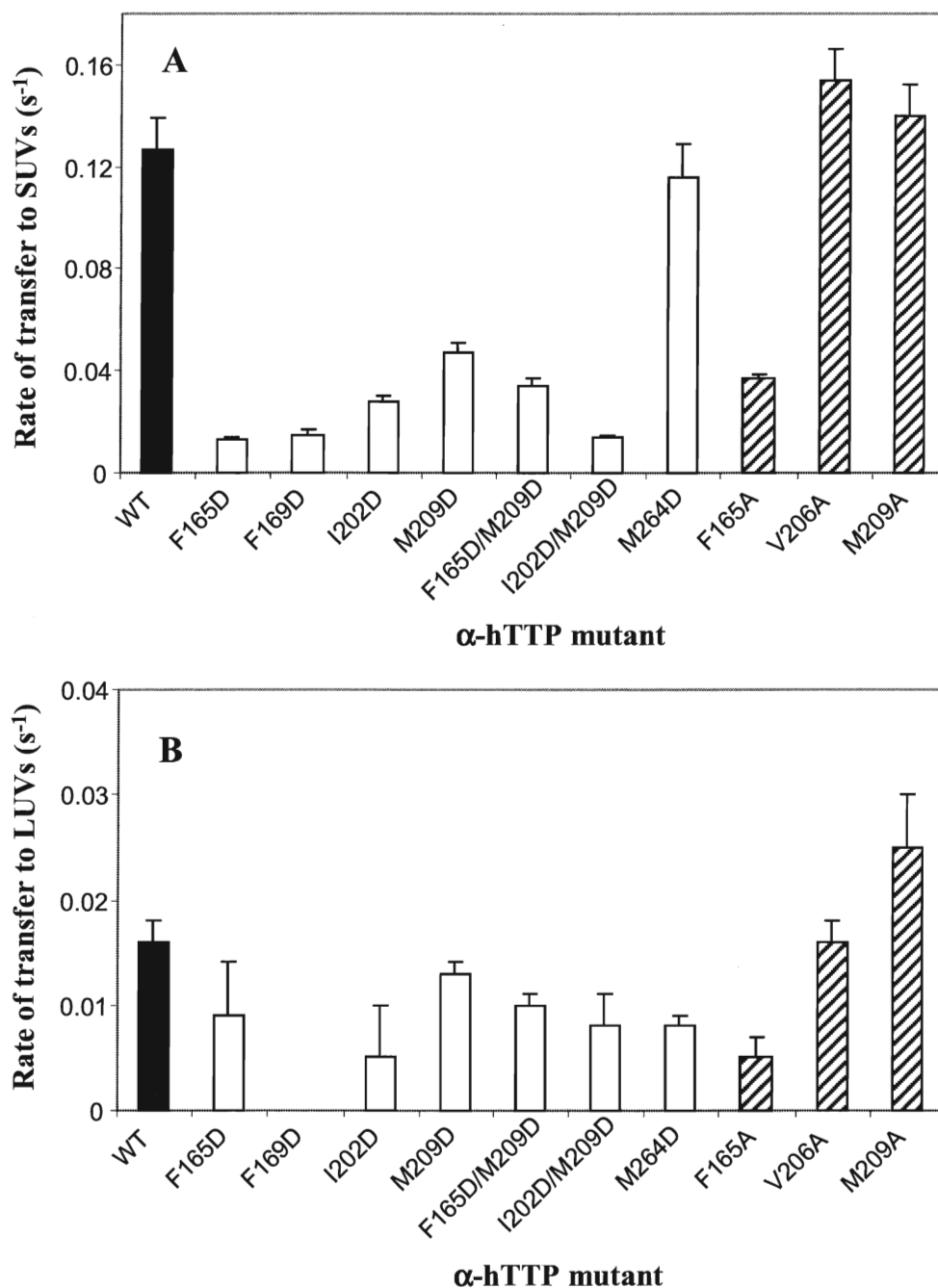


Figure 51: Transfer of NBD- α -Toc from α -hTTP wildtype and mutants to SUVs (A) and LUVs (B) of bovine liver PC. Shown are averages of six to nine determinants \pm the standard deviation. The data for the wild-type protein is presented in closed bar, the aspartate mutants in open bars, and alanine mutants in hatched bars.

type α -hTTP to LUVs ($k = \sim 0.017 \pm 0.0009 \text{ s}^{-1}$), it is possible that the rate differences observed for measurements involving LUVs were simply data fluctuation – essentially small changes in small numbers. The low rate of ligand transfer to LUVs could be caused by the weak association between the wild-type α -hTTP and the tightly packed lipid bilayer of LUVs. α -hTTP is expected to rotate randomly on the planar lipid bilayer until it is able to insert hydrophobic residues F165 and F169 into the membrane.

The collisional mechanism of ligand transfer predicts that the ability of α -hTTP to transfer ligand is directly correlated with the ability of the protein to bind to lipid membranes. Specifically, this would only be true if membrane binding (rather than ligand delivery) was the rate limiting step. To test this, an optical biosensor technique, called Dual Polarization Interferometry (DPI) was utilized. This method has been used and characterized previously by other researchers [188, 189]. As described in the Methods, a lipid bilayer was created after vesicles were absorbed onto a sensor chip and ruptured to form a stable bilayer. Subsequently, protein samples at various concentrations were introduced over the immobilized lipid surface and the real time protein adsorption was monitored and recorded, enabling determination of the binding affinity of α -hTTP for the bilayer. The binding curves of mutated proteins containing aspartate residues in the mobile gating helix A10 were obtained and are illustrated in **Fig. 52**. The maximum protein adsorption detected was $\sim 0.6 \text{ ng/nm}^2$ for wild-type α -hTTP as well as the V206D mutant. Wild-type α -hTTP bound to the immobilized lipid bilayer with an apparent binding affinity K_D calculated to be $0.342 \pm 0.055 \text{ }\mu\text{M}$. V206D had slightly decreased binding affinity, compared to the wild-type. However, V206D total adsorption continued to increase in response to further increases in protein concentration,

suggesting that V206D had not yet reached saturation at these protein concentrations, whereas the wild-type exhibited saturable binding. At 5 μM concentration, the total amounts of protein bound to the lipid bilayer were almost the same for V206D and the wild-type. On the other hand, both the I202D and I202D/M209D proteins showed minimal binding to the lipid bilayer, even at 10 μM protein concentration. Similar to

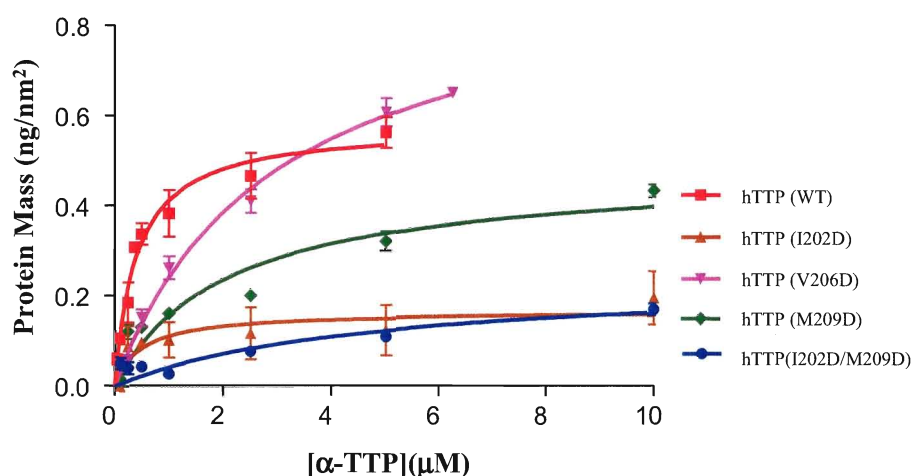


Figure 52: Concentration dependent binding of α -hTTP wild-type and selected aspartate mutants to the immobilized lipid bilayer. The protein adsorption was analyzed by Dual Polarization Interferometry (DPI). Presented are averages of quadruplicate analyses \pm the standard deviation.

I202D and I202D/M209D, the apparent K_D calculated for F165 A/D and F169D mutants appeared to be 5- to 10-fold lower, as compared to the wild-type protein (data not shown). Many of the mutants demonstrated reduced binding to the bilayer evident from the lower adsorbed masses. Since the mutated proteins did not reach the same total mass adsorbed as the wild-type, the dissociation constants reported by the curves were not meaningful for comparing their lipid binding affinities.

The absolute binding of wild-type α -hTTP and the mutants were therefore compared at 0.5 μM and 1 μM protein concentrations. At these concentrations,

adsorption of α -hTTP was approaching saturation (**Fig. 52**). The data are summarized in **Table 5** and plotted in **Fig. 53**. As shown, the binding patterns observed for these proteins were remarkably similar to their transfer of NBD- α -Toc to SUVs (**Table 4 & Fig. 51A**) measured in the FRET transfer assays. Also, aside from M209D and M264D (control), the aspartate mutations had much reduced lipid binding. At 0.5 μ M protein concentration, less than 20% of wild-type binding was observed for these mutants.

Table 5: Binding of various mutants to the planer PC bilayer measured by DPI

TTP	0.5 μ M TTP ng/nm ²	% of WT	1.0 μ M TTP ng/nm ²	% of WT
WT	0.338 \pm 0.058	100	0.383 \pm 0.089	100
F165D	0.038 \pm 0.02	11	0.071 \pm 0.004	19
F169D	0.062 \pm 0.032	18	0.086 \pm 0.047	22
I202D	0.097	18	0.103	27
M209D	0.132	39	0.162	42
F165D/M209D	0.002 \pm 0.003	1	0.069 \pm 0.035	18
I202D/M209D	0.044 \pm 0.02	13	0.028 \pm 0.009	7
M264D	0.224 \pm 0.015	66	0.31 \pm 0.083	81
F165A	0.126 \pm 0.069	37	0.172 \pm 0.018	45
V206A	0.314 \pm 0.031	93	0.436 \pm 0.057	114
M209A	0.34 \pm 0.039	101	0.43 \pm 0.049	112

Increasing protein to 1.0 μ M did not drastically improve the level of binding relative to wild-type. The conserved alanine mutations, such as V206A and M209A, fully retained their binding capability, whereas the conserved mutation F165A once again had less than 50% binding at both protein concentrations.

Overall, the calculated change in the transfer energy ($\Delta\Delta G$) of protein that have had key hydrophobic residues mutated correlated well with the experimentally determined rates of ligand transfer to SUVs and the levels of protein binding to planar lipid

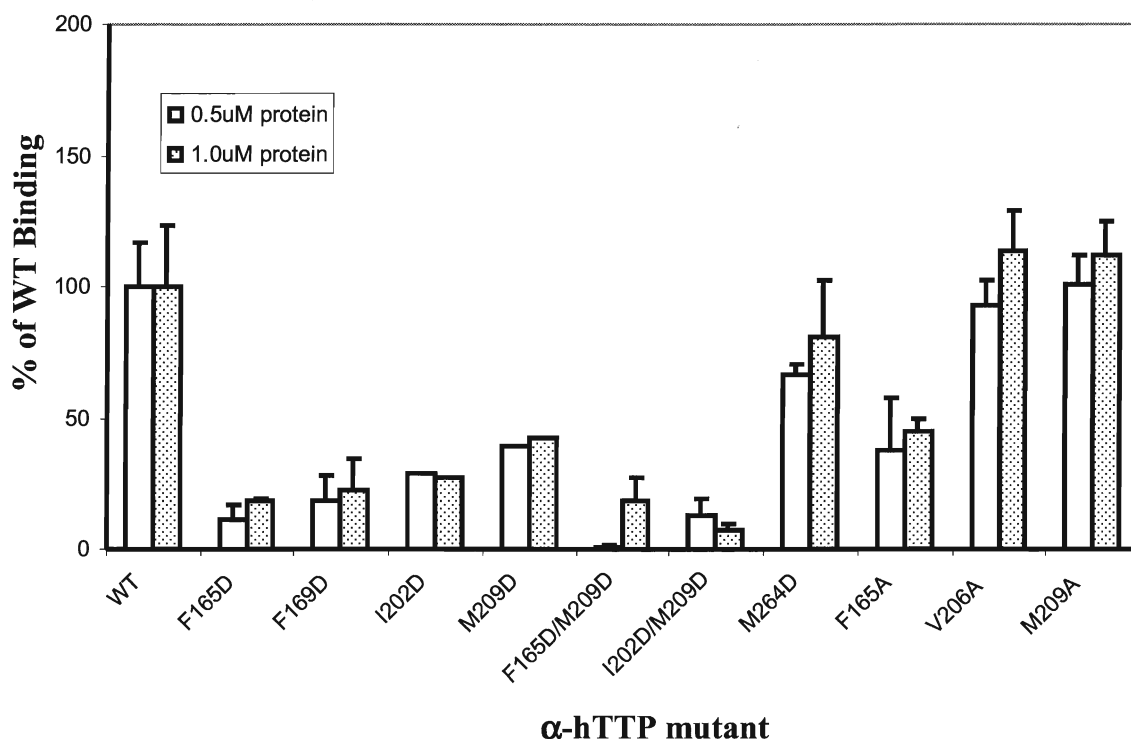


Figure 53: Protein adsorption to the immobilized phospholipid bilayer determined by Dual Polarization Interferometry (DPI). Wildtype and mutant α -hTTPs at 0.5 μ M (open bars) and 1.0 μ M (dotted bars) were tested for their binding to phospholipid bilayers consisting of 10% DOPS and 90% DOPC. Data presented are averages of quadruplicate \pm the standard deviations.

membrane (**Table 6**). The mutant proteins with the greater change in their transfer energy such as F165D ($\Delta\Delta G = 11.1$ kcal/mol), I202D/M209D ($\Delta\Delta G = 13.2$ kcal/mol) and F165D/M209D ($\Delta\Delta G = 15.4$ kcal/mol), exhibited much reduced rate of ligand transfer (10 to 27%) and protein binding (7 to 19%) compared to the wildtype. In general, the binding of α -hTTP to the membrane appears to stabilize the closed conformation of this protein, reflected in the lower change in transfer energy ($\Delta\Delta G$) compared to its open conformation. The only mutant that exhibited inconsistent changes in the free energy of transfer and lipid binding and ligand transfer capability is the conserved F165A mutant, which had a calculated ΔG of 0.8 kcal/mol and 1.2 kcal/mol for the closed and open conformation, respectively. Yet, the ligand transfer rate to SUVs and lipid binding were

Table 6: Comparison of calculated change of transfer energy (ΔG) of α -hTTP mutants, rates of NBD- α -Toc transfer (to SUVs) and protein adsorption at 1 μ M protein concentration relative to wildtype α -hTTP. The change in transfer energy values were calculated by Dr. Andrei Lomize (University of Michigan).

mutant	1r5l: ΔG kcal/mol (closed)	1oiz: ΔG kcal/mol (open)	1r5l: $\Delta\Delta G$ kcal/mol (closed)	1oiz: $\Delta\Delta G$ kcal/mol (open)	Rate ^{mut} / Rate ^{wt}	Ads ^{mut} / Ads ^{wt}
WT	-10.6	-20.7	0	0	1	1
F165D	-7.0	-9.6	3.6	11.1	0.10	0.19
F169D	-7.1	-13.5	3.5	7.2	0.12	0.23
I202D	-7.9	-11.2	2.7	9.5	0.22	0.42
M209D	-7.0	-10.8	3.6	9.9	0.37	0.27
I202D/M209D	-3.9	-7.5	6.7	13.2	0.11	0.07
F165D/M209D	-3.6	-5.3	7	15.4	0.27	0.18
V206D	-10.6	-12.7	0	8.0	n/a	0.69
F165A	-9.8	-19.5	0.8	1.2	0.29	0.45
V206A	-10.6	-20.5	0	0.2	1.21	1.14
M209A	-9.6	-19.6	1	1.1	1.10	1.12

reduced by 71% and 55%, respectively. This discrepancy may be caused by the simplification of the current computational model (PPM 1.0) that does not account for the increased flexibility when a bulky membrane anchoring residue is replaced by a much smaller one.

Ideally, it would have been more logical to compare the lipid binding data generated from DPI experiments directly to the rates of ligand transfer to LUVs, given that both assays utilized the planar lipid membranes. However, due to the very small rates of transfer measured for LUVs accompanied by large errors, the correlation between these two sets of data is not well defined. Therefore, the transfer rates to SUVs were chosen for direct comparison.

Since α -hTTP mediated transfer of NBD- α -Toc was much more efficient to the highly curved smaller vesicles, and the DPI technique in our case was designed to evaluate the binding of α -hTTP to a planar lipid surface, we decided to perform size

exclusion vesicle binding assays, to compare the lipid binding affinity to both sonicated SUVs and extruded 100 nm vesicles, the two vesicle sizes investigated in the FRET transfer assay. In the vesicles binding assay, 31.5 μg (or ~ 1 nmole) of α -hTTP samples were incubated with increasing concentrations of SUVs or LUVs for 30 minutes. At the end of incubation, the lipid-bound α -hTTP was separated from the free α -TTP using YM-100 Microcon filters (with the molecular weight cutoff at 100 kDa). Vesicle bound protein was retained by the filter and free protein passed through it. Both bound and free α -hTTP fractions were visualized by SDS-PAGE electrophoresis and the intensity of the stained protein bands were analyzed using Scion Image software (Scion Corp.). The two

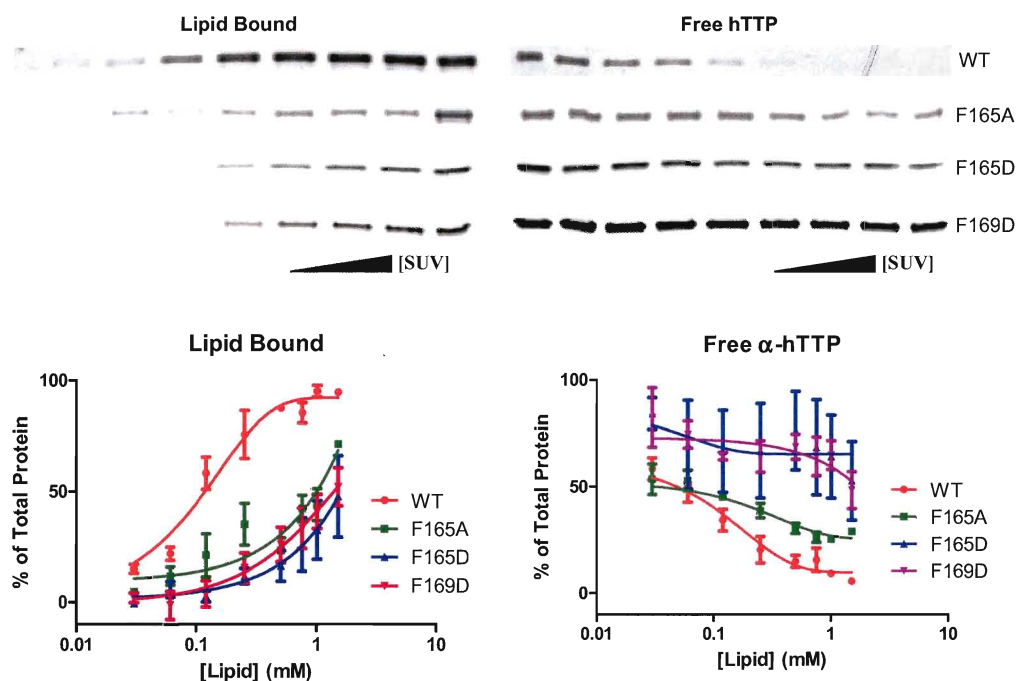


Figure 54: Binding of wildtype α -hTTP and helix A8 mutants to SUVs as assessed by the size exclusion vesicle binding assay. α -hTTP (31.5 μg) bound to small unilamellar vesicles of DOPC were separated from the free proteins. The samples were visualized on SDS-PAGE (top panels), stained, and the protein bands subsequently analyzed by densitometry (bottom panels). Data was normalized to the total protein, the combined lipid bound and free protein at the highest lipid concentration. Shown are averages of measurements \pm the standard deviation, $n=4$ for WT, $n=3$ for mutants.

mutants with the most compromised ligand transfer and lipid binding capabilities (F165D and F169D) were tested in this assay, along with the conservative F165A mutant and wild-type α -hTTP. As illustrated in the top panel of **Fig. 54**, the binding of wild-type α -hTTP increased in response to the increased concentration of PC SUVs, until saturation occurred at 0.75 mM phospholipid in the form of SUVs. Interestingly, at saturation, all α -hTTP was bound to SUVs, and protein was no longer detected in the unbound fractions. Although the binding of the mutant proteins was also sensitive to phospholipid concentration, protein saturation was never achieved, and the majority of these mutant proteins remained in the unbound fractions, even at the highest lipid concentration. The densitometric analyses of protein bands were normalized and compared to the total protein available for binding (bottom panels). Compared to the wild-type (with an apparent K_D at $0.12 \pm 0.06 \mu\text{M}$, $R^2 = 0.92$, which represented the lipid concentration at the half maximal protein bound), binding affinity of F165A was reduced by ~45 fold ($K_D \sim 5.04 \mu\text{M}$, $R^2 = 0.76$), and more than 75 and 7 fold, for F165D ($K_D \sim 8.29 \mu\text{M}$, $R^2 = 0.58$) and F169D ($K_D \sim 0.84 \mu\text{M}$, $R^2 = 0.77$), respectively.

When the same vesicle binding assay was employed to assess the binding of α -hTTP wild-type to PC LUVs, no saturation was observed (**Fig. 55**). At the highest LUV concentration tested, only 60% of wild-type or 20% of mutant proteins were lipid-bound. These results illustrated that α -hTTP bound to the highly curved SUVs more avidly than to LUVs, and the preferential binding is thus responsible for the enhanced transfer of NBD- α -Toc to SUVs.

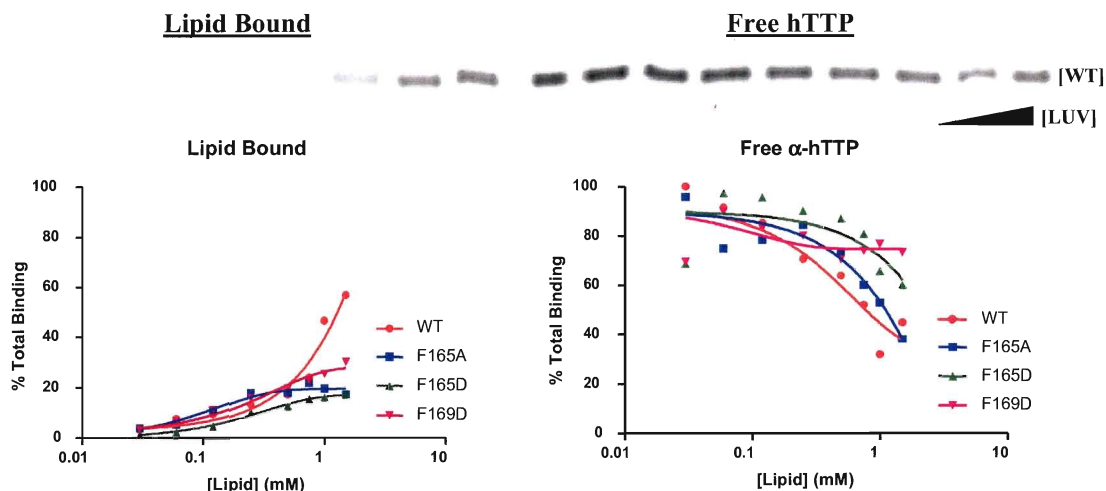


Figure 55: Binding of α -hTTP wildtype and helix A8 mutants to LUVs assessed by size exclusion vesicle binding assay. All values were normalized to the total protein, the combined lipid bound and free protein at the highest lipid concentration. Shown are the averages of three determinations \pm the standard deviation, except the WT, which was tested in duplicates.

Comparing to the DPI method, size exclusion vesicle binding assay certainly was much less sensitive and unable to resolve the fine difference between F165A/D and F169D, for their ability to bind to LUVs. According to DPI analysis, at 1 μ M protein concentration, conserved mutant F165A bound to the planer lipid membrane (45% of WT binding) better than both F165D (19%) and F169D (22%). In the vesicle binding assay, at the highest LUV concentration, F169D exhibited 50% of the wild type α -hTTP binding, which was greater than both F165A (30%) and F165D (30%). The weak correlation between DPI and LUV vesicle binding results are mainly due to the weak interaction between α -hTTP and LUVs. In contrary, the binding of these mutants to SUVs correlated much better with DPI results, in which F165A exhibited greater binding affinity (66%) than both F165D (25%) and F169D (29%).

2.3.3. Role of three positively charged hinge residues on the membrane binding and subsequent delivery of NBD- α Toc

According to Dr. Lomize's computed orientation of α -hTTP in relation to the lipid membrane, several positively charged lysine residues were found near the membrane boundary, which may interact with the charged head groups of phospholipids, thereby regulating the movement of the mobile gating helix A10 (a.a 198-221). The functional significance of residues near the membrane within the positively charged surface of α -hTTP was investigated with mutants R192H, K211A and K217A shown in left panel of **Fig. 56**. These mutants were made available to us by our collaborators Dr. Danny Manor and Dr. Samantha Morley (Case Western Reserve University). K217 was of particular interest to us as it was located on the critical "hinge" that controlled the movement of the mobile helix A10. K217 may form ionic interactions with the negatively charged residues on helix A9, thereby stabilizes the "open" conformation of the protein. The mutation of K217 to alanine would disrupt this electrostatic interaction and promote the protein to switch between the "open" and the "closed" conformations, thereby increase its rate of ligand exchange. It is worth noting that the interactions between α -TTP and highly curved membrane of SUVs appeared to be dominated by a few hydrophobic residues on Helix A8 (F165 & F169) and A10 (I202) as shown in the previous section. R192 is located slightly further away from the membrane boundary. Since the effect of electrostatic interaction is only apparent with LUVs, the positively charged R192 may come in contact with membrane surface only when α -hTTP is rotating randomly on the surface of LUV.

All three mutants (R192H, K211A and K217A) were purified to a high degree (**Fig. 56**, right panel). Two minor contaminating proteins at 65 to 70 kDa were visible. Compared to the wild-type α -hTTP, K211A and K217A had slightly reduced (but likely

insignificant) ligand binding affinities (**Table 7**) and the rates of NBD- α -Toc transfer to LUVs. The transfer to SUVs was not affected by these mutations (**Table 7**).

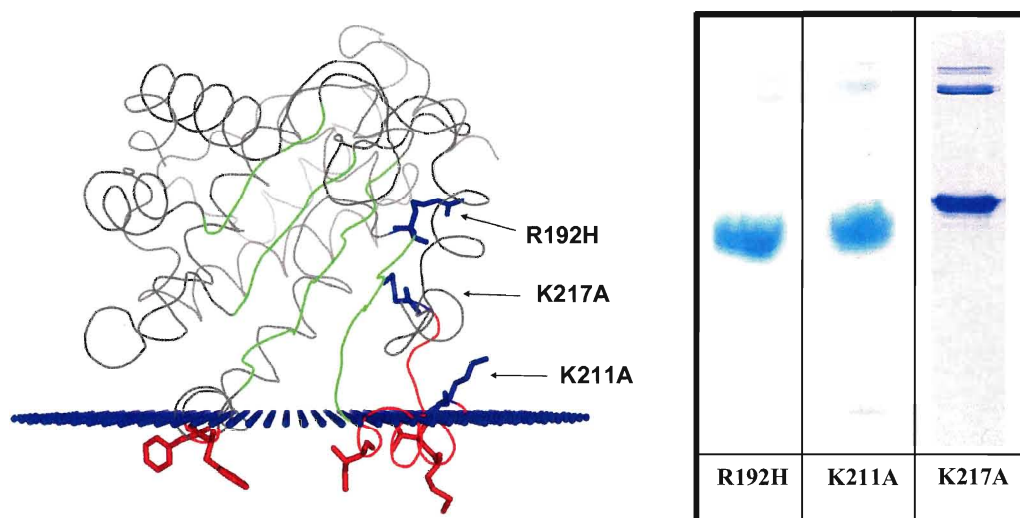


Figure 56: The positively charged residues on or near the hinge region that may control the movement of the mobile gating helix A10. Left panel: Cartoon representation of α -hTTP (pdb:1oiz) with the binding cavity $\alpha\beta\alpha\beta$ sheet colored in green. Membrane penetrating hydrophobic residues are colored in red. Basic residues that may form electrostatic interaction with lipid bilayer are colored in blue. The first methylene of the acyl chains in the membrane are shown in blue dots. Right panel: SDS-PAGE analysis of the purified hinge mutants. R192H and K211A were analyzed on the pre-cast 10% Tris-HCl mini gel, followed by ProtoBlue Safe Colloidal Coomassie G-250 staining. K217 was analyzed on 15% Tris-HCl, followed by Coomassie Brilliant blue staining.

Table 7: Binding and rate of NBD- α -Toc transfer by α -hTTP wildtype and hinge mutant of α -TTP. K_D values shown are averages of duplicate measurements, with an expected error of 20% within the reported values.

TTP	NBD- α -Toc K_D (nM)	Transfer to SUVs (s^{-1})	% WT Rate	Transfer to LUVs (s^{-1})	% WT Rate
WT	19	0.127 ± 0.012	100	0.016 ± 0.002	100
R192H	21.98	0.106 ± 0.008	83	0.012 ± 0.003	75
K211A	36.37	0.105 ± 0.008	83	0.011 ± 0.001	69
K217A	32.08	0.130 ± 0.011	102	0.010 ± 0.004	63

Interestingly, when these mutants were assessed for their ability to bind to lipid membranes by DPI, both R192H and K217A (at 0.5 μ M) experienced 58 and 71%

Table 8: Adsorption of α -hTTP wild-type and hinge mutants of α -hTTP to the lipid bilayer measured by DPI. Values for the adsorbed protein mass (ng/nm²) at the indicated protein concentration injected are shown.

α -hTTP	0.5 μ M TTP ng/nm ²	% WT binding	1.0 μ M TTP ng/nm ²	% WT binding
WT	0.534	100	0.762	100
R192H	0.843 \pm 0.103	158	1.141 \pm 0.149	150
K211A	0.655 \pm 0.215	123	0.721 \pm 0.162	95
K217A	0.912 \pm 0.149	171	1.368 \pm 0.213	180

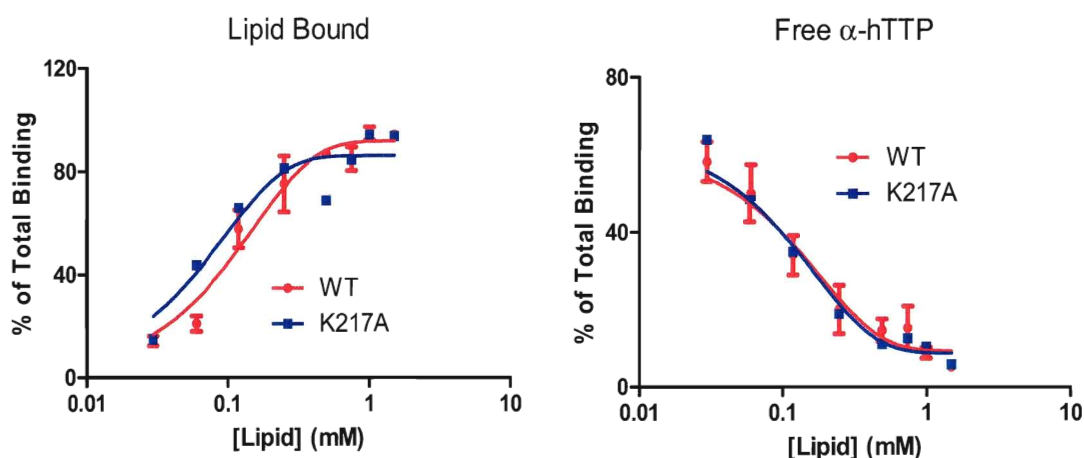


Figure 57: Comparison of mutant V217A to α -hTTP wild-type for their binding to SUVs assessed by size exclusion filtration assay. Shown are the averages of four determinations \pm the standard deviation for wild-type and average of two measurements for K217A.

increased binding to the planar lipid bilayer (Table 8), respectively. Doubling of protein to 1.0 μ M did not further increase the level of protein binding to the lipid membrane. In comparison, the binding of K217A to SUVs by the size-exclusion assay was essentially same as the wild-type (Fig. 57). It is hard to reconcile the discrepancies between the increased binding of the hinge mutants to the planar bilayers with the reduced rate of transfer to the LUVs unless the differences observed were due to the data variation, and these hinge residues are not directly involved in modulating the movement of the mobile helix A10. Alternatively, the increased binding of these hinge mutants to the lipid

bilayer may reduce the dynamic of the mobile helix, thereby compromise their ability to transfer ligand.

3. DISCUSSION AND CONCLUSIONS

α -TTP plays a critical role in vitamin E homeostasis. Mutations in the *ttpA* gene render α -TTP less active, and as a consequence, patients with the inherited Ataxia with Vitamin E deficiency (AVED) disorder have significantly reduced circulating vitamin E. α -TTP binds specifically to α -Toc [89, 90]. In hepatocytes, α -Toc co-localizes with α -TTP in late endosomes prior to its secretion at the plasma membrane [190]. The exact mechanism utilized by α -TTP to transport α -Toc has not been fully elucidated. In the current study, which utilizes a fluorescence resonance energy transfer (FRET) assay, we sought to characterize the mechanism of α -TTP mediated transfer of α -Toc and identify the factors that may influence the rate of α -Toc transfer.

Protein mediated transportation of small hydrophobic ligands typically utilizes one of the two well-characterized mechanisms: free aqueous diffusion of ligand from protein to lipid membranes or collisional interaction between protein and phospholipid bilayer. These two mechanisms can easily be distinguished based on the kinetics of the rate limiting step. For instance, liver FABP transfers free fatty acids facilitating aqueous diffusion, and the rate-limiting step occurs when ligand dissociates from the protein. Thus, the rate of transfer is greatly dependent on the properties of both the ligand and the aqueous phase [126, 128, 133]. In contrast, all other members of FABP family utilize a collisional mechanism of transfer, which requires the direct interaction between protein and acceptor lipid membrane. In this case, the rate of transfer is dependent on the concentration and the composition of the phospholipid bilayer [127-130, 179]. In general, collisional transfer is believed to target the ligand to a specific subcellular

location [134, 191], rather than merely equilibrating the ligand concentration in the same cellular compartment.

3.1. FRET transfer assay with 6-His- α -hTTP from pET28 and pET21 expression vectors

Initially, 6-His- α -hTTP with an N-terminal extension of 40 amino acids from the expression vector pET28b was tested in a FRET assay. With this protein, 35% of total fluorescence was missing in the early times when α -hTTP bound NBD- α -Toc was transferred to the quencher containing lipid vesicles. The initial ~25% of total fluorescence signal was still missing after diluting the overall reagent concentration by 64 fold (**Fig. 18A**). It was unclear whether the N-terminal extension was responsible for missing of the initial fluorescence detection. It was nevertheless cumbersome to have an extension with an undefined function that might potentially complicate the data interpretation. Fortunately, the hTTP/pET21b construct was made available to us, and this construct produced an N-terminally 6-His tagged protein without the extra 40 amino acids. A transfer curve without the initial lost of fluorescence signal was attained with this version of 6-His- α -hTTP (**Fig. 20**). Interestingly, the rate of NBD- α -Toc transfer by this protein appeared to be independent of the composition, concentration and curvature of the acceptor vesicles. These observations supported the aqueous diffusion of NBD- α -Toc from α -hTTP to the acceptor membranes. However, according to the crystal structure of α -TTP [93, 94], α -Toc is buried deep in the hydrophobic binding pocket and a major conformational change is required for the ligand to enter and exit the protein. It is therefore highly unlikely for α -Toc to simply diffuse from the protein to lipid membranes. The collisional based transfer of α -Toc by lipoproteins was previously

reported by Asmis [55]. Similarly, α -Toc transfer from liposomes to crude liver membrane fraction appeared to be correlated directly to α -TTP concentration [89]. Recently, Morley *et al.* reported the increased rate of α -Toc extraction from lipid bilayers in response to increased α -TTP concentrations [114]. The discrepancy between our data and the findings reported in the literature implied a systematic error(s) in our FRET assay, which might have been responsible for the deceptive observations. We decided to closely examine the potential suspects: fluorescent ligand NBD- α -Toc and α -hTTP.

NBD fluorescent probes have been used widely to determine the rates of spontaneous transfer of various lipids to and from membranes [158, 161, 162, 192]. The off-rate of NBD-labeled phospholipids from lipid vesicles is significantly influenced by the acyl chain length. Thus the half-time for C₁₂-NBD-PA increased by ~226 fold compared to C₆-NBD-PA [161]. Phospholipids with shorter hydrocarbon chains are typically chosen to allow the timely investigation of the lipid diffusion between artificial lipid vesicles or biological membranes [158, 161, 192]. The NBD group is substantially more water soluble than boron-dipyrromethene (BODIPY) analogs [193]. When NBD was attached to the *sn*-2 position of the acyl chain of POPC, it was found to loop back to near the lipid-water interface [194]. In this case, NBD induced lipid chain disorder by adding ~2.0 Å² to POPC molecule, which accounted for a ~3% increase in the surface area of the lipid molecule. Moreover, the calculated lipophilicity index logP for NBD- α -Toc was calculated to be 9.60, which was more hydrophilic than that of α -Toc (7.34). Therefore, we were concerned that NBD- α -Toc might have increased solubility and bulkiness compared to α -Toc. The enhanced solubility and bulkiness may have prevented NBD- α -Toc from entering deep into the hydrophobic binding pocket of α -

hTTP, thus allowing it to diffuse freely from protein to its lipid acceptor. At the time, we considered replacing NBD- α -Toc with C9-AO- α -Toc for the FRET studies. The anthroyloxy probe is expected to be more hydrophobic than NBD, and it has been used extensively in the fatty acid transfer studies [126, 127, 138]. However, in our research, C9-AO- α -Toc underwent significant (~30%) photobleaching during a relatively short interval of 60 seconds (data not shown). Thus, it was not a suitable probe to be used in our FRET assay. As expected, NBD- α -Toc underwent spontaneous transfer between donor and acceptor vesicles. The rate of transfer was dependent on the size of both donor and acceptor vesicles and thus the curvature of the lipid membrane (**Fig. 29**).

After critically examining the protein source purity, we identified a minor contaminant of the 39 kDa *E. coli* outer membrane porin F (OmpF) as the source of the problem. OmpF had been previously identified as one of two major contaminants during the purification of a LacZ-papain fusion protein from inclusion bodies [172]. OmpF normally remains in the insoluble pellet fraction. However, during high cell density cultivation, OmpF was found to excreted into the culture medium [173]. We typically allowed 18-hours of IPTG induction to increase soluble α -hTTP production, and the cell density at the time of harvesting was usually very high. Thus, it was not surprising to have some OmpF remained with the cell pellets after centrifugation, which then contaminate the cell lysate prior to purification. More importantly, nickel-affinity chromatography was utilized to purify 6-His tagged α -hTTP. At neutral pH, OmpF is cation selective; it binds to both monovalent and divalent metal ions including nickel and magnesium [174, 175].

Although OmpF accounted for only about 5-10% of total recovered protein, the high fluorescence signal observed when NBD- α -Toc bound to OmpF overwhelmed the lower fluorescence produced by the majority of the protein, α -hTTP (**Fig. 32D**). The approximately four-fold greater fluorescence signal observed for OmpF was likely due to the ability of each OmpF monomer to bind multiple molecules of NBD- α -Toc. OmpF is a barrel protein elliptical in cross section. The pore dimensions of OmpF determined from the crystal structure are 11 x 19 Å at the mouth, 11x7 Å in a central constriction zone formed by the internal L3 loop, and 22 x 15 Å at the smooth end [195]. The height for the inner wall of the barrel is 30 Å. As shown in **Fig. 58**, the length of α -Toc is estimated to be 13.43 Å, and due to the tendency of NBD moiety of NBD probes to loop back to align with the chromanol moiety when present in membranes, conjugation of NBD to the tail of α -Toc is unlikely to increase the length of the molecule. The bent hydrocarbon chain has a width of 7.9 Å, which is about 2 Å larger than the chromanol head group. Based on the height of OmpF, it can accommodate 2 molecules of

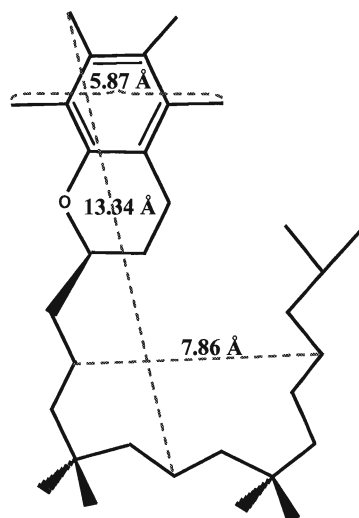


Figure 58: Dimension of α -Toc estimated from Deepview.

NBD- α -Toc stacked head to tail vertically. Horizontally, OmpF should be able to accommodate 2 or more NBD- α -Toc. Thus, the high stoichiometry may explain the apparent high affinity of OmpF for NBD- α -Toc and the subsequent high fluorescence signal observed when NBD- α -Toc bound to OmpF.

Several methods were employed to remove OmpF contamination (data not shown). One attempt was to cleave 6-His- α -hTTP with factor Xa, then elute α -hTTP in a buffer without imidazole. OmpF was expected to stay on the nickel column until elution with imidazole solution. To our surprise, a small level of OmpF still co-eluted with the cleaved α -hTTP, indicating a weak association between OmpF and immobilized nickel ions. Alternatively, 6-His- α -hTTP purified from nickel affinity column was subjected to further purification with DEAE anion exchange column. Again, no clean separation of OmpF from 6-His- α -hTTP was achieved. It is possible that the resolution would have been improved if a larger column had been used. However, utilizing a 120 ml (16 x 600 mm) Sephacryl S-300 high resolution gel filtration column and FPLC, we were able to completely separate α -hTTP from OmpF, though OmpF still contained tiny traces of α -hTTP (**Fig. 32 B&C**). Unfortunately, due to the lengthy purification procedure at room temperature, the pure α -hTTP obtained seemed to have lost most of its activity. These results suggest that OmpF is not only able to bind nickel ions, but it also is likely to form a complex with 6-His- α -hTTP, perhaps through its association with the positively charged histidine tag. The only way to eliminate OmpF contamination was to avoid a hexahistidine tagged α -hTTP. Therefore, the hTTP/pGEX-4T construct producing GST- α -hTTP was tested. A full length α -hTTP without the GST tag was obtained after a 2-hour on-column digestion of GST- α -hTTP with thrombin protease, and OmpF was no

longer found in the purified α -hTTP (**Fig. 37**). This version of α -hTTP had slightly improved affinity for NBD- α -Toc ($K_D = 18.9 \pm 0.4$ nM), compared to both 6-His- α -hTTP ($K_D = \sim 46$ nM) and 6-His-28TTP (56 ± 15 nM).

3.2 Transfer of NBD- α -Toc by α -hTTP to acceptor membranes utilizes a collisional based mechanism

The results from FRET transfer assays demonstrated that α -hTTP mediated α -Toc transfer requires a collisional interaction between the protein and the lipid bilayer. Thus, the rate of transfer was increased in response to an increase in the concentration of lipid vesicles (**Fig. 40**). The transfer of NBD- α -Toc to SUVs was much more sensitive to the change in lipid concentration compared to LUVs. Furthermore, the transfer rate increased as vesicle size decreased (**Fig. 44**). Compared to the extruded 100 nm LUVs, the rate increased by ~ 4 fold when 30 nm extruded SUVs were used and ~ 8 -10 fold for probe sonicated SUVs. To make sure that the observed rate difference was not due to the difference in the methods of vesicle preparation, bath sonicated SUVs were also included in the comparison. Bath ultrasonication usually produces SUVs of 20 to 50 nm diameter [196, 197] similar to the size generated by probe sonication. Comparable rates of ligand transfer were observed for SUVs prepared from both sonication methods. For vesicles of 50 nm and larger, ligand transfer was no longer sensitive to the change in the vesicle size.

The enhanced ligand transfer of anthroxyloxy-labeled fatty acid to SUVs has also been reported for adipocyte and heart fatty acid binding proteins [129]. The authors suggested that the 10-fold increase in the transfer rate observed was likely due to the greater number of SUVs available for protein binding. However, they did not rule out the possibility that the reduced transfer to LUVs was due to the increase in the packing of the

phospholipid acyl chain caused by the flatter bilayer structure. This hypothesis was supported by the reduced rate of fatty acid transfer to the lipid bilayer containing the fully saturated dimyristoyl-PC (DMPC) as compared to the unsaturated 1-palmitoyl-2-oleoyl-PC (POPC). Furthermore, the transfer rate was also reduced when cholesterol and sphingomyelin (SM) was present [129].

According to the lipid surface area calculation (data summarized in **Table 3**), for the same amount of lipid, about ~14 fold greater number of 30 nm SUVs can be produced, compared to 100 nm LUVs. At the same time, the total outer lipid surface is increased only by 40%. Thus, the 10 fold increase in transfer rate to smaller vesicles cannot be explained by an increase in lipid surface area. Instead, this suggests that the enhanced transfer results from the reduction in the phospholipid acyl chain packing density in response to the increase in the membrane curvature. This is consistent with our previous observation that LUVs were both poor acceptors and donors during the spontaneous transfer of NBD- α -Toc (**Fig. 29**). Furthermore, we have shown that α -TTP binds better to SUVs than to LUVs (**Fig. 54** & **Fig. 55**). All evidences suggest that the enhanced NBD- α -Toc transfer to SUV by α -hTTP was due to the ease of protein and ligand insertion into the membrane with high curvature [198].

The interactions between soluble cytosolic proteins and lipid membranes are typically regulated by both electrostatic interactions and hydrophobic forces. Proteins which rely predominantly on the electrostatic interaction with anionic lipids are fairly common. For instance, the binding of cellular retinaldehyde-binding protein to membranes containing phosphatidic acid PA is responsible for the release of bound ligand 11-cis retinal [122]. A number of signaling proteins including myristoylated

alanine rich C-kinase substrate protein, MARCKS rely on a basic motif for targeting to the plasma membrane [199-201]. Fatty acid binding proteins also contain a cluster of basic residues on the portal lid that are key for their recognition of anionic membranes [138, 178]. On the other hand, soluble proteins that depend solely on the hydrophobic force to interact with the membrane are rare, unless they also contain membrane recognition domains, such as the FYVE, zinc finger, Pleckstrin-homology (PH) or Phox (PX) domain [202-205]. These domains interact with the anionic phosphoinositides in the membranes. The sensitivity of membrane binding proteins to the curvature of membranes has also been identified. As previously mentioned, increased ligand transfer from protein to SUVs has been observed for fatty acid binding protein [132, 206]. Sterol carrier protein 2 [207] and glycolipid transfer protein [208] also preferentially bind to the highly curved membranes. ArfGAP1 (Arf GTPase activating protein 1) consists of two disordered ArfGAP1 lipid-packing sensors (ALPS) that form amphipathic helices when docking onto membranes of high curvature and subsequently increases the activity of Arf-GTP [142, 143]. The soluble monomer of Annexin B12 undergoes a membrane curvature induced “inside-out” conformational change, exposing internal hydrophobic residues at the surface upon binding to a highly curved phospholipid membranes [146].

NBD- α -Toc transfer by α -hTTP appears to be regulated by the size of the acceptor vesicles. Electrostatic interaction clearly plays an important role in ligand transfer to LUVs with flatter lipid surface (**Fig. 42**) since the rate of transfer increased (58% for PI & PS; 145% and 124% for LBPA & DOPA) in the presence of 15% anionic lipid. The most drastic increase in the rate of transfer was introduced by cardiolipin (CL), which caused ~8 fold increase in the rate of ligand transfer. Similar or even greater

effects of CL for the fatty acid transfer by intestinal and adipocyte FABP have been reported [126, 209, 210] in studies which employed PC SUVs containing 25% CL. In our hands, the transfer of NBD- α -Toc to CL SUVs could not be determined. Unexpectedly, the fluorescence of NBD- α -Toc was not quenched when the ligand bound α -hTTP was mixed with quencher containing SUVs. CL is known to undergo a lamellar to inverted hexagonal phase transition in the presence of high concentration of divalent ion such as Ca^{2+} or Mg^{2+} [211, 212]. The lamellar to hexagonal phase transition occurs when the binding ratio of Ca^{2+} to CL increases from 0.35:1 to 1:1 [212]. The SET buffer used in our FRET transfer assay did not contain any divalent ions. Moreover, only 15% CL was incorporated in the SUV preparation, hence a phase transition was highly unlikely. However, we can't rule out the possibility of α -hTTP induced aggregation in CL SUVs.

Unlike anionic lipids, the cationic DOTAP (**Fig. 43**) only increased the transfer rate to LUVs by ~80%. These observations suggested that acidic residues of α -hTTP were less effective than the basic protein surface in forming electrostatic interactions with the charged head groups of the phospholipid bilayer. The slower ligand transfer to the zwitterionic PC LUVs implied that α -hTTP forms transient contacts with the densely packed flatter lipid bilayer. The binding to the lipid bilayer was greater when α -hTTP encountered anionic lipids such as PA and CL. On the other hand, the ligand transfer to SUVs appeared to be dominated by the combination of hydrophobic interactions and the preference of α -hTTP for membranes of higher curvature, suggesting that a specific region or domain of the protein might be critical for such an interaction. The incorporation of 15% anionic phospholipid in the acceptor SUVs had no effect on the rate

of transfer. The lipid acyl chain packing also influenced the ligand transfer to SUVs and LUVs, as α -hTTP transferred NBD- α -Toc to soy PC with much greater (S/U ratio = 0.30) percentage of unsaturated lipids exhibited a greater rate of transfer, compared to both bovine liver PC (S/U ratio = 0.91) and synthetic DOPC (**Fig. 45**).

In the current study, we relied solely on dynamic light scattering (DSL) to determine the hydrodynamic radius of vesicles, with the assumption that membrane curvature stress is inversely proportional to the radius of the vesicle. Although the average size measured for the sonicated SUVs was ~12 nm larger than the extruded 30 nm SUVs, the rate of ligand transfer to these vesicles nevertheless was higher. It is worth noting that the probe sonication produced two populations of SUVs, ~75% of 80 nm and ~11% of tiny vesicles of 20 nm or less (**Table 2 and Fig. 47**). The extrusion through 30 nm filter produced a homogenous population of SUVs, ~98% of 60 nm vesicles. The increased ligand transfer to the sonicated SUVs versus 30 nm extrude SUVs was likely due to the presence of the small population of 20 nm SUVs. In order to accurately determine the rate of ligand transfer to these 20 nm vesicles, they must be separated from the larger SUVs by Sephacryl S-500 to S-1000 size exclusion chromatography [213].

Throughout the study, we consistently observed ~10 fold enhanced transfer to SUVs versus LUVs. However, when the total liver lipid extract was used to prepare LUVs and SUVs, α -hTTP was no longer able to discriminate LUVs from SUVs (**Fig. 46**). Besides 42% PC, the total lipid extract also contains 7% cholesterol, 22% PE, 8% PI, 1% lysoPI, and 21% others unspecified lipids. When tested individually, cholesterol, PE or PI had minimal impact on the transfer of NBD- α -Toc to both SUVs and LUVs. The similar ligand transfer to SUVs and LUVs can probably be explained by the

localized membrane defects and curvature introduced by the unique lipid composition of the total lipid extract, or the existence of lipid(s) with high binding affinity toward α -hTTP. As illustrated in **Fig. 59**, when the membrane consists of only homogenous cylindrical PC, its phospholipid head group packing density can be altered only by the change in membrane curvature. However, in a heterogeneous lipid mixture such as the total liver lipid extract, the phospholipid head group packing density depends on both the

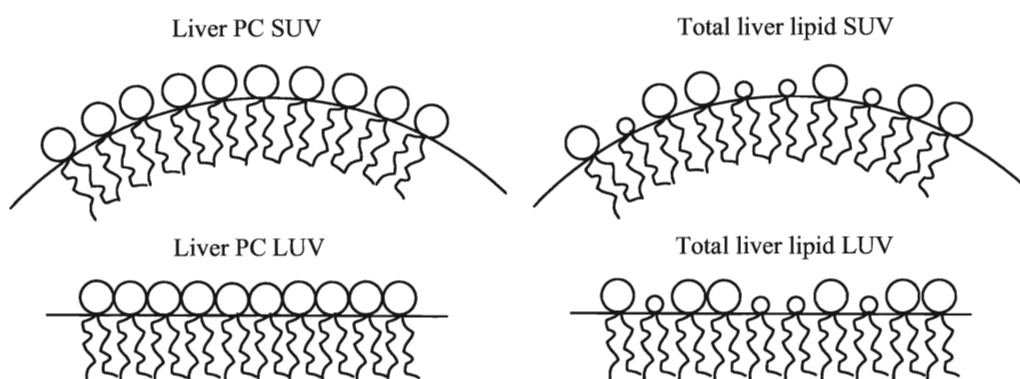


Figure 59: Proposed membrane structure of vesicles prepared from liver PC versus total liver lipid extract.

curvature and the lipid composition of the membrane. Due to the similar local membrane environment such as head group and acyl chain packing in both SUVs and LUVs, α -hTTP was expected to interact similarly to these vesicles and therefore similar transfer rates were observed. To test this hypothesis, the size difference between these SUVs and LUVs needs to be confirmed by dynamic light scattering (DLS). These vesicles will then be subjected to differential scanning calorimetry measurement to determine whether the vesicle size difference can cause any changes in phase transition temperature of the lipid mixture. The impact of membrane curvature on membrane properties, such as the phase transition temperature, has been reported previously [214]. Differential scanning

calorimetry detected a 3°C reduction in T_m (gel to liquid transition) for SUVs that contained pure dimyristoyl-PC (DMPC) or distearoyl-PC (DSPC) compared to much larger multilamellar vesicles (MLV). In the mixture of DMPC and DSPC (1:1), the phase separation for these two lipids increased as the membrane curvature increased from 640 nm to 60 nm.

3.3 The direct interaction between α -hTTP and lipid membrane is regulated by the anchoring helix A8 and the mobile helix A10

α -TTP and Sec14p share similar tertiary structures. However, the distance between the two corresponding helices that cover the ligand binding pocket are different [94]. In Sec14p, helices A10 and A11 are 25 Å apart, which makes the binding pocket more exposed. A “bulldozer” model has been hypothesized for Sec14 mediated exchange of phospholipid [96]. Sec14p was proposed to insert its helix A10/T4 (lipid binding lid) deep into the outer leaflet of the lipid bilayer, and it then exchanges its cargo lipid with the membrane lipid. However, in α -TTP, the corresponding helices A9 and A10 are much closer in distance, only 10 Å apart [94]. Thus, the ligand is shielded away from the solvent. Based on the free energy change (ΔG), calculated when a protein is transferred from water to the lipid bilayer, a model was generated to predict the most stable orientation of α -hTTP with respect to the lipid membrane. From this model, α -hTTP is expected to have both helices A8 and A10 submerged into the lipid bilayer (**Fig. 49**). It is possible that α -hTTP also utilizes a “bulldozer” like mechanism to deliver α -Toc, which requires the insertion of the mobile helix A10 into the membrane, followed by the opening of this lid to deposit or extract α -Toc from the lipid membrane.

The results of our measurements of the ligand transfer rate of mutant forms of α -hTTP support the hypothesis that ligand delivery by α -hTTP requires a direct interaction between the protein and lipid bilayer. The collisional interaction appears to be regulated by the lipid binding helices A8 and A10 since substitution of residues within these helices diminished the ability of α -hTTP to interact with lipid membrane. When the hydrophobic residues F165 and F169 of the docking helix A8, that are proposed to deeply penetrate the membrane, were substituted with acidic aspartate, the binding of these mutants (1.0 μ M) to the flatter lipid on the DPI chip surface was reduced by approximately 80%, compared to the wild type protein (**Table 5 & Fig. 53**). Interestingly, alanine mutation of the conserved F165 also reduced its lipid binding by ~55%. Clearly, preserving the hydrophobicity of F165 alone was not adequate to retain its lipid binding capability. This suggests the depth of lipid penetration is diminished in the F165A mutant when the bulky phenylalanine was replaced with a much smaller alanine. When these mutants were assessed for their binding to SUVs, the binding affinity of F169A was reduced by ~8 fold and more than 20 fold for F165D and F169D, compared to that of the wild type protein. As a consequence, the rates of transfer by F165D and F169D were reduced by ~90% to SUVs, and F169D completely lost its ability to transfer to LUVs. Similarly, the rate of transfer by F165A was reduced by 70% to both LUVs and SUVs (**Table 4 & Fig. 51**).

The lipid insertion of the mobile helix A10 appears to be more superficial, compared to the docking helix A8, as the conserved alanine mutation of V206 or M209 still faithfully retained their full capacity to bind to membranes and to transfer NBD- α -Toc. **Fig. 60** illustrates how the mobile helix A10 opens and closes the entrance to

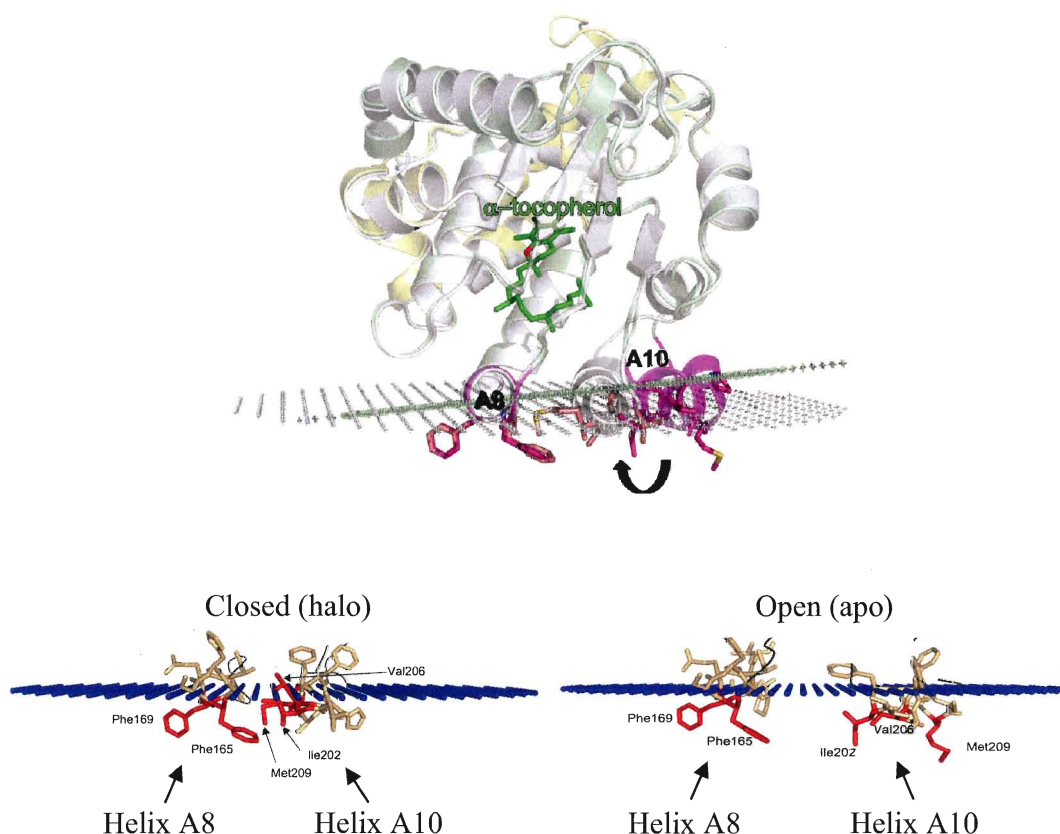


Figure 60: Superposition of structures of human α -TTP in “open” and “closed” conformations. **Top panel:** Protein backbone is shown in a cartoon representation with helices from N-terminal domain colored in yellow, from C-terminal lipid-binding domain colored in green and from “gating” helices A8 and A10 colored in purple; residues that penetrate into lipid acyl chain region are shown by sticks colored in purple and pink for “open” and “closed” conformation, respectively. α -Toc bound to the closed conformation is shown by sticks colored in green. Calculated boundaries between lipid head groups and acyl chain region are shown by dots colored green for 1oiz (open) and grey for 1r5l (closed). **Bottom Panels:** Close up of the membrane penetrating residues. Pictures were drawn using PyMol.

the ligand binding pocket and thus allows the ligand exchange between the protein and the lipid membrane. Based on the model, this movement leads to the deeper penetration of residues V206 and M209 into the hydrocarbon core of the lipid bilayer, thereby slightly altering the orientation of the protein with respect to the lipid membrane. According to this model (**Fig. 60, bottom panels**), both I202 and M209 appeared to have similar depths of lipid penetration in both open and closed conformations. However,

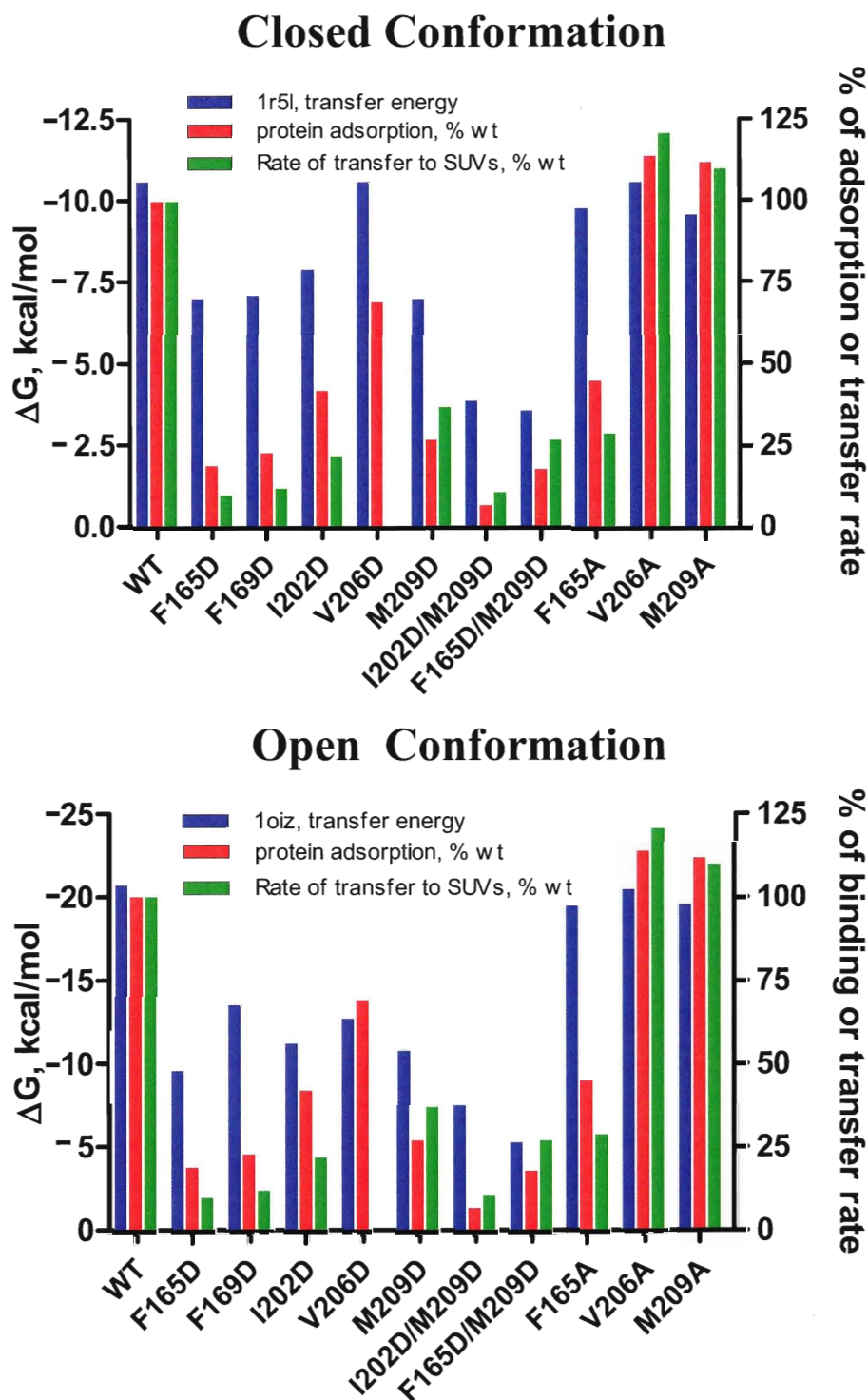


Figure 61: Comparison of protein adsorption to phospholipid bilayers measured by DPI (at 1 μ M TTP) and the rate of NBD- α -Toc to SUVs with the calculated energies of transfer (A) Closed conformation and (B) open conformations.

aspartate mutation of I202 (I202D) caused a greater perturbation in the ability of protein to bind and transfer its ligand. This is perhaps due to the fact that during the membrane anchoring of the helix A8, I202 is required for the stable insertion of other residues on the mobile helix A10. Unfortunately, due to difficulties in purification, the I202A mutant protein was not available for testing. Overall, the experimental data correlated slightly better with the calculated transfer energy change for the “closed” conformation of the protein (**Table 6 & Fig. 61**). Thus the closed conformation is likely preferred upon α -hTTP binding to the phospholipid bilayer and subsequently delivers its ligand. The observed correlation between the rates of NBD- α -Toc transfer and the membrane binding of α -hTTP also clearly suggests that the membrane binding is the rate limiting step.

The role of the three charged hinge residues (R192H, K211A and K217A) remained inconclusive. These mutants had improved binding (23% to 71%) to membranes as measured by DPI, yet their rates of transfer to LUVs were slightly reduced (by 25 to 37%). The ligand transfer from these mutants to SUVs was not significantly different from the wildtype protein. These contradicting observations are difficult to explain, unless the data inconsistency was due to the experimental variation, or K211 and K217, though located close to the lipid bilayer, were not actively participating in the phospholipid binding. These preliminary data implied that these hinge residues probably had no functional impact on the movement of the mobile helix A10.

Based on our data, we propose the following steps for the interaction of α -TTP with lipid membranes: 1) ligand bound α -hTTP rolls randomly on the membrane until it inserts helix A8 onto the lipid bilayer; 2) membrane contact of the mobile lid helix A10 leads to the opening of the hydrophobic ligand binding cavity; 3) deep insertion of the lid

helix A10 into the hydrocarbon core of the membrane; 4) deposition of ligand into the membrane; 5) ligand free protein is stabilized in the “open” conformation; 6) desorption of α -TTP from membrane.

3.4 Proposed recycling of α -Toc facilitated by α -hTTP

Vitamin E is packaged in chylomicron remnants or lipoproteins when circulating in serum plasma prior to its arrival at liver [50]. In liver, α -Toc was found to localize to the late endosomes along with α -hTTP [99, 113]. The membrane structure of late endosome is highly dynamic, cocomposed of tubular, cisternal and multivesicular structures, with an average diameter of 500 nm [215]. Late endosomes serve as the last sorting station in the endocytic pathway, which determines whether internalized molecules are to be recycled back to the plasma membrane or to be degraded in lysosomes. In late endosomes, the internalized lipoproteins and chylomicron remnants are hydrolyzed in the acidic environment (pH 5.0 – 5.5), which likely results in the release of the bound vitamin E. α -hTTP in the cytoplasm binds to α -Toc and is retained in the late endosome, while other isoforms continue their journey to lysosomes for degradation. **Fig. 62** illustrates the proposed transfer of α -Toc by α -hTTP in late endosomes. Due to its high affinity for the highly curved small vesicles, α -hTTP delivers its bound ligand α -Toc to the highly curved intraluminal vesicles that are enriched in LBPA, a late endosome specific phospholipid [165, 191]. LBPA is known to promote the formation of multivesicular bodies (MVB) in the acidic environment [166, 216]. These intraluminal vesicles are typically about 20 to 25 nm in diameter [215]. The co-localization of α -hTTP with LBPA is presumably due to the curvature effect in these small vesicles and not due to the direct interaction between α -hTTP and LBPA. Other

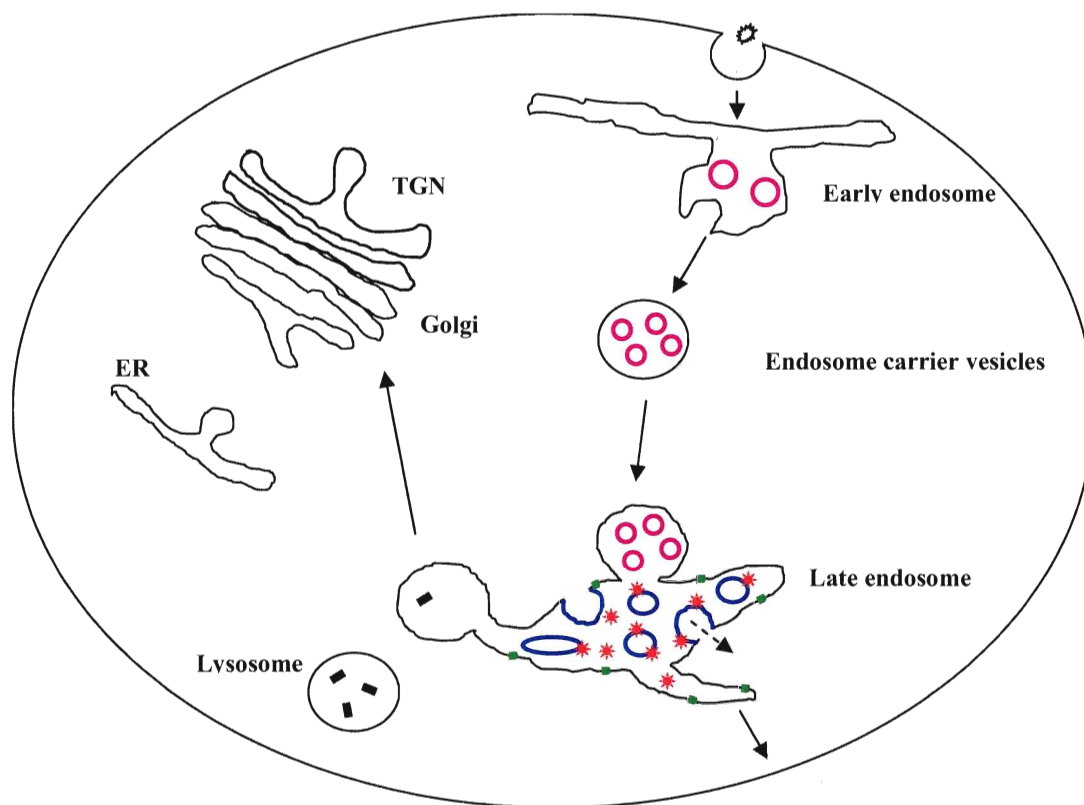


Figure 62: Proposed recycling of α -Toc from endocytic pathway. This drawing is modified from the cartoon created by Van der Goot and Gruenberg [217]. The α -Toc bound lipoprotein or chylomicron remnant undergoes receptor mediated endocytosis. Early endosome contains intraluminal vesicles rich in PI3P and cholesterol (purple). In late endosome, α -TTP (red stars) selectively binds and delivers α -Toc to LBPA enriched intraluminal vesicles (blue). These LBPA rich vesicles undergo back fusion via ABCA1 transporter (green bars) containing limiting membrane (the outer membrane of late endosomes). ABCA1 presumably delivers α -Toc to the plasma membrane during the fission/fusion events.

small non-LBPA containing intraluminal vesicles are also found in the late endosomes to which α -TTP can presumably also bind. However, only intraluminal membranes enriched in LBPA are capable of back fusion with the limiting membrane (outer membrane) of the late endosomes. Several lines of evidence suggested that ATP-binding cassette protein-A1 (ABCA1) transporter is involved in α -TTP dependent secretion of α -Toc [99, 218], moreover, α -Toc efflux mediated by apoA-1 lipoprotein is dependent on the expression of ABCA1 [219]. ABCA1 shuttles between the plasma membrane and

endocytic compartments [220, 221] and is known to regulate the cholesterol efflux to apoA-1 to form high density lipoproteins (HDL). Therefore, ABCA1 in the limiting membrane of the late endosomes may facilitate the secretion of α -Toc from late endosomes to the plasma membrane during the ABCA1 mediated fusion/fission events. This may help to explain why the treatment with ABCA1 inhibitors glyburide and probucol reduced α -hTTP mediated α -Toc secretion [99, 218].

3.5 Conclusions

The data from this study demonstrated the preference of α -TTP for the highly curved small unilamellar vesicles (SUVs) of ~25 nm, as shown by the ten-fold increase in the rate of NBD- α -Toc transfer compared to the flatter large unilamellar vesicles (LUVs). Although binding of α -TTP to SUVs and LUVs are both collisional, the mechanisms of interaction appeared to be different. Binding of α -TTP to LUVs is influenced by the electrostatic interaction between the basic residues of the protein and the anionic phospholipids in the membrane. In contrast, α -TTP binding to SUVs appeared to be dominated by the hydrophobic interaction and a greater ease of membrane penetration when curvature is high. The mutagenesis study guided by the calculated transfer energy model allowed us to identify two membrane interacting helices, A8 and A10, which are critical in the binding of α -TTP to phospholipid membranes. Mutation of the hydrophobic residues F165, F169 (helix A8) and I202 (helix A10) to negatively charged aspartates nearly completely abolished the ability of α -TTP to interact with the phospholipid bilayer and subsequently to transfer its ligand. The propensity of α -TTP for the highly curved membrane provides a connection to its colocalization with α -Toc to the small intraluminal vesicles in the late endosome. The back fusion of LBPA enriched

intraluminal vesicles containing α -Toc via ABCA1 containing limiting membrane may be the key to the secretion of α -Toc from late endosome to plasma membrane.

4. FUTURE DIRECTIONS

In the current study, we have demonstrated that the propensity of α -hTTP to bind to small and highly curved lipid membrane requires the deep insertion of the membrane binding helices A8 and A10. The data we have obtained so far have relied exclusively on artificial lipid vesicles. We speculated that α -hTTP targets α -Toc to the LBPA enriched small intraluminal vesicles of the late endosomes prior to its secretion by ABCA1 transporter to the plasma membrane. To test our hypothesis, it would be necessary to isolate these intraluminal vesicles from HepG2 cells and measure the binding affinity of α -TTP (wildtype and hydrophobic mutant proteins) for these small vesicles. Furthermore, two unresolved phenomena observed during the membrane curvature study remain to be addressed in future studies: the unexpected lack of fluorescence decay when NBD- α -Toc loaded TTP was mixed with vesicles containing a quencher and CL and the inability of α -hTTP to distinguish LUVs from SUVs prepared from total liver lipid extract. The probe sonicated vesicles yielded two populations of SUVs, ~75% of 80 nm and ~11% of tiny vesicles of 20 nm or less. The rates of transfer to SUVs reported in this study was the average from both sizes, yet the transfer to the 20 nm vesicles is likely to be much faster than the reported value for the mixture of sizes. Since 20 nm SUVs are comparable in size to the intraluminal vesicles, it is therefore important to separate 20 nm SUVs from the ~80 nm SUVs in order to accurately determine the rate of ligand transfer to these tiny vesicles.

In vitro, the mutations in the anchoring helix A8 exhibited the most compromised lipid binding and consequently the most impaired ability of α -TTP to transfer NBD- α -Toc. To validate the physiological relevance of the catastrophic mutations such as

F165D and F169D, the DNA construct of these mutants and the conserved mutation F165A will be created and stably expressed in the human hepatoblastoma HepG2 cell line. The expression level of these mutants as well as their ability to facilitate α -Toc secretion will be examined. The intracellular localization of these mutants will be also be followed by an immuno-fluorescence microscopy study. If the preference of α -hTTP to bind to the small and highly curved lipid vesicles is indeed due to the ease of the deep membrane insertion of helix A8, F165D and F169D are predicted to have much reduced binding to the small LBPA enriched intraluminal vesicles in the late endosomes and consequently less α -Toc will be secreted to the cell surface. The colocalization of NBD- α -Toc and ABCA1 transporter will also be assessed using a GFP (green fluorescence probe) tagged ABCA1.

These studies will hopefully advance our understanding on the membrane binding behavior of α -hTTP both *in vitro* and *in vivo*. They will also help to determine whether LBPA and ABCA1 transporter are directly involved in α -TTP dependent secretion of α -Toc.

5. MATERIALS AND METHODS

5.1. Chemicals and Stock Solutions

5.1.1. Antibiotics and other chemicals (stored at -30°C)

Ampicillin – 100 mg/mL in milliQ purified sterile H₂O (mQH₂O) (BioShops)

Chloramphenicol – 20 mg/mL in EtOH

Kanamycin – 30 mg/mL in mQH₂O (BioShops, Mississauga)

Ethidium Bromide (EtBr) – 10 mg/mL in mQH₂O (Sigma, Oakville)

Ethylenediaminetetraacetic acid (EDTA) – 500 mM in mQH₂O

Phenylmethylsulphonyl fluoride (PMSF) – 100 mM in EtOH (stored at -30°C)

Triton X-100 (Sigma, Oakville)

5.1.2. Enzymes (Stocks solutions were stored at -30°C in single use aliquots)

Lysozyme – 100 mg/mL in mQH₂O

RNase (Ribonuclease) – 50 mg/mL in mQH₂O

DNase I (Deoxyribonuclease I) 375 U/μL (Invitrogen, Burlington, ON).

Pfu Turbo DNA polymerase – 2.5 U/μL (Stratagene, Cedar Creek, TX)

Fusion hot start polymerase – 2 units/μL (New England Biolabs, Pickering, ON)

Thrombin – 50 units in PBS (GE Healthcare, Baie D'Urfe, PQ)

Trypsin Gold, Mass Spectrometry Grade – 1 μg/μL in 50 mM acetic acid (Promega)

5.1.3. Chemicals used in to generate peptides for MALDI-TOF protein analysis

Acetonitrile (ACN) (Fisher, stored at room temperature in the fume hood)

Ammonium bicarbonate (NH₄HCO₃) – 250 mM in mQH₂O freshly prepared (Sigma)

Acetic acid – 50 mM in mQH₂O

α-cyano-4-hydroxycinnamic acid (Sigma, stored at 4°C)

Iodoacetimide – 55 mM in 25 mM NH_4HCO_3 (Sigma, stored at 4°C)

Sinapinic acid (Sigma, stored at 4°C)

Trifluoroacetic acid (TFA) (Sigma, stored at 4°C)

5.1.4. Solutions used to process SDS-PAGE gels

Fixing solution: 40% EtOH and 10% acetic acid in mQH_2O

Staining solution: 0.1% Coomassie R-250, 25% MeOH and 10% acetic acid in mQH_2O

Destain solution: 5% MeOH and 7% acetic acid in mQH_2O

Gel drying solution: 40% MeOH, 10% glycerol and 7.5% acetic acid in mQH_2O

5.1.5. Solutions employed to regenerate glutathione agarose affinity column (Sigma)

Cleansing solution 1: 0.1 M borate acid, 0.5 M NaCl, adjust to pH 8.5 with 1 M NaOH

Cleansing solution 2: 0.1 M sodium acetate, 0.5 M NaCl, adjust to pH 4.5 with acetic acid

5.2. Phospholipids from Avanti Polar Lipids (Alabaster, AL)

These phospholipids in chloroform were stored in -30°C until use: 1,2-dioleoyl-*sn*-glycerol-3-phosphocholine (DOPC), 1,2-dioleoyl-*sn*-glycerol-3-phosphate (DOPA), 1,2-dioleoyl-*sn*-glycero-3-phospho-L-serine (DOPS), 1,2-dioleoyl-3-trimethylammonium-propane (DOTAP), bovine liver L- α -phosphatidylcholine (liver PC), bovine liver phosphatidylinositol (PI), soy L- α -phosphatidylcholine (soy PC), porcine brain L- α -phosphatidylserine (PS), oleoyl lysobisphosphatidic acid (LBPA) and bovine heart cardiolipin (CL) and sphingomyelin (SM).

5.3. Other reagents

5.3.1. Miscellaneous reagents

Fluorescent lipid quencher s(N-teramethylrhodamine-6-thiocarbamoyl)-1-2-dihexadecanoyl-*sn*-glycero-3-phosphoethanolamine, triethylammonium salt (TRITC-DHPE) – lyophilized powder or 810 μ M in chloroform stored at -30°C (Molecular Probes, Eugene, Oregon)

Glutathione agarose linked through sulfur, provided in 20% EtOH, stored at 4°C (Invitrogen, Burlington, ON)

Lyophilized glutathione agarose – swelled to 1 g/ mL in mQH₂O prior to use, after the initial usage, it was stored in 2M NaCl at 4°C (Sigma, Oakville, ON)

Microcon YM-100 filters (Millipore, Billerica, MA)

Polycarbonate membranes (>=50 nm) (Avestin, Ottawa, ON)

Polycarbonate membranes (30 nm) (Avanti Polar Lipids, Alabaster, AL)

Precast 10% Tris·HCl mini gels (BioRad Laboratories, Mississauga, ON)

Prestained broad range protein marker (New England Biolabs, Pickering, ON)

ProtoBlue Safe Colloidal Coomassie G-250 Stain (National Diagnostics, Atlanta, GA)

Qiaprep Spin Miniprep kit was from Qiagen (Mississauga, ON)

mouse anti 6-His antibody and horse anti-mouse secondary antibody conjugated to alkaline phosphatase were purchased from Cell Signaling Technology (Pickering, ON)

Unmodified sensor DPI chips (Farfield Sensors Ltd (Manchester, England)

All other reagents were from BioShop Canada Inc. (Burlington, ON).

5.3.2. Bacterial Strains

The bacterial strains utilized in the study were: NovaBlue was purchased from Novagen (Madison, WI), and XL1-Blue and BL21 (DE3) were from Stratagene (Cedar Creek, TX). Both NovaBlue and XL1-Blue strains were employed for routine cloning

due to their high transformation efficiency and the blue/white screening capability. The deficient in endonuclease (*endA*) and recombination protein (*recA*) enable these host strains to produce high quality plasmid DNA. BL21 (DE3) strain promotes the production of more stable recombinant protein due to its lack of λ (a heat shock protein) and OmpT proteases, it also carries a copy of the T7 RNA polymerase under control of the IPTG inducible lacUV5 promoter, therefore, this host strain was utilized for the controlled expression of 6-His α -hTTP and GST- α -hTTP recombinant proteins.

5.3.3. Bacterial Expression Vectors

The three bacterial expression vectors containing the α -hTTP gene investigated in this project were: pET28b produced α -hTTP with an N-terminal 6-His-tag followed by an extension of 40 amino acids, pET21b produced α -hTTP with an N-terminal 6-His-tag followed by a factor Xa cleavage site and pGEX-4T-3 produced α -hTTP with an N-terminal GST tag plus six extra amino acids. A few characteristics of these vectors are listed in **Table 7**. The expression vectors pET-28b and pET-21b were used during the

Table 9: Characteristics of the α -hTTP bacterial expression vectors

Vector	Backbone Size (bp)	insertion sites	Selection marker	Source
pET-28b	5369	Sall/NotI	Kanamycin	Donated
pET-21b	5443	NdeI/XhoI	Ampicillin	DSM
pGex-4T-3	4968	NotI/Sall	Ampicillin	Collaborator (Dr. Manor)

early stage of this research project to produce 6-His tagged α -hTTP with and without an N-terminal linker between the gene and the tag respectively. The α -hTTP/pET-21b construct was created by Stephen Hyland (DSM Nutritional Products), whom amplified

the human α -hTTP gene by PCR with 5'-primer starting with an NdeI restriction site (comprising the start codon), followed by an N-terminal 6-His tag and a factor Xa cleavage site and 3'-primer containing a XhoI-site and the stop codon. Thus, the pET-21b construct generated α -hTTP with an N-terminal 6-His tag.

5.4. Molecular methodologies

5.4.1. Site directed mutagenesis

The human α -TTP gene flanked by SalI (5') and Not I (3') restriction sites from pET28b and subcloned into pGEX-4T-3 vector was created by Morley *et al.* [111]. With this fusion construct, only six additional amino acids were attached to the purified protein after the removal of GST tag by thrombin. This pGEX fusion construct was used as a template to create the following mutant constructs: F165A/D, F169A, I202A/D, V206A/D, M209A/D, F165D/M209D, I202/M209 and M264D. The double mutant constructs such as F165D/M209D and I202D/M209D were created by using primers encoding the F165D or I202D mutations for PCR with the α -hTTP M209D mutant DNA as a template. Turbo Pfu DNA polymerase was utilized to generate these mutations following the QuickChange Site-Directed mutagenesis protocol (Stratagene) with 10% DMSO in the reaction mixture. All primers (**Table 9**) were designed according to the guidelines suggested by the QuickChange protocol and were acquired from Sigma-Genosys (Oakville, Ontario).

The cycling parameters used for DNA amplification with turbo Pfu polymerase are listed in **Table 10**. The PCR products were then digested with DpnI endonuclease for 1 hour at 37 °C prior to their transformation into XL1-Blue super competent cells. The transformed XL1-Blue cells were selected on agar plates containing 100 μ g/mL

ampicillin and the cells were grown overnight at 37°C. Several ampicillin resistant colonies of each mutant construct were selected and amplified in 10 mL LB media.

Table 10: Oligonucleotides primers used to create hydrophobic mutants of α -hTTP

Primer	Sequence	T _m (°C)
F165AF	5' CTTTGATCTGGAAGGTTGGCAG <u>GCTT</u> CTCATGCTTTTCAAATC 3'	82.4
F165AR	5' GTGATTTGAAAAGCATGAGAA <u>AGCCT</u> GCCAACCTTCCAGATCA 3'	83.4
F165DF	5' CTTTGATCTGGAAGGTTGGCAG <u>GATT</u> CTCATGCTTTTCAAATCA 3'	82.4
F165DR	5' AGTGATTTGAAAAGCATGAGAA <u>ATCCT</u> GCCAACCTTCCAGATCAA 3'	82.4
F169DF	5' CAGTTTTTCTCATGCT <u>GAT</u> CAAATCACTCCATCC 3'	75.3
F169DR	5' GGATGGAGTGATTG <u>ATC</u> AGCATGAGAAACTG 3'	75.3
I202AF	5' GATAAATGAACCAGTAG <u>GCTT</u> TCCATGCTGTCTTTTCC 3'	74.9
I202AR	5' GAAAAGACAGCATGGAAAG <u>GCT</u> ACTGGTTCATTTATC 3'	73.3
I202DF	5' GATAAATGAACCAGTAG <u>GATT</u> TCCATGCTGTCTTTTCC 3'	73.6
I202DR	5' GGAAAAGACAGCATGGAA <u>ATCT</u> ACTGGTTCATTTATC 3'	73.6
V206AF	5' CAGTAATTTTCCATGCT <u>GCCT</u> TTTCCATGATCAAACC 3'	78.2
V206AR	5' GGTTCATCATGGAAAAG <u>GGC</u> CAGCATGGAAAATTACTG 3'	78.2
V206DF	5' CAGTAATTTTCCATGCT <u>GACT</u> TTTCCATGATCAAACC 3'	76.0
V206DR	5' GGTTCATCATGGAAAAG <u>GTC</u> CAGCATGGAAAATTACTG 3'	76.0
M209AF	5' CCATGCTGTCTTTTCC <u>GCG</u> ATCAAACCATTCCTGAC 3'	82.8
M209AR	5' CAGGAATGGTTTGAT <u>CGC</u> GGAAAAGACAGCATGG 3'	82.1
M209DF	5' CCAGTAATTTTCCATGCTGTCTTTTCC <u>GAT</u> ATCAAACCATTCCT 3'	79.5
M209DR	5' AATTTTTCAGTCAGGAATGGTTTGAT <u>ATC</u> GGAAAAGACAGCATG 3'	79.5
M264DF	5' GGAATGGACAAATTTTATAG <u>GAT</u> AAGTCTGAAGATTATCTC 3'	68.8
M264DR	5' CTGAGATAATCTTCAGACTT <u>ATC</u> TATAAAATTTGTCCATTCTGA 3'	72.6

The Qiaprep Spin Miniprep kit was subsequently employed to purify plasmid DNA from each of the mutant TTP cultures. This kit utilizes an alkaline lysis based extraction method with improved DNA binding to the silica membrane. The targeted mutations were confirmed by sequencing by the Robarts Research Institute (London, ON) with a custom designed forward sense primer 5'-ATGGCAGAGGCGCGATCCCAGC-3'

Table 11: Cycling parameters utilizing turbo pfu polymerase in PCR amplification

Segment	Cycles	Temp.	Time	Function
1	1	95°C	30 s	Denaturation
2	18	95°C	30 s	Denaturation
		55 °C	1 min.	Annealing
		68 °C	6 min.	Extension
3	1	4°C	24 hrs	End

During the initial stage of the mutagenesis study, the phusion hot start polymerase was used for DNA amplification of α -hTTP/pGEX-4T-3. With this polymerase, a greater number of amplification cycles were implemented as recommended by the supplier (**Table 11**). The reaction mixture contained: 10 μ L Phusion buffer (actual composition unknown), 1 μ L dNTP (200 μ M), 5 μ L each of forward and reverse primers (0.5 μ M), 10 ng DNA template, 2.5 μ L DMSO, 1.5 μ L Phusion polymerase and mQH₂O.

Table 12: Cycling parameters utilizing Phusion hot start polymerase

Segment	Cycles	Temp.	Time	Function
1	1	98°C	30 s	Denaturation
2	30	98°C	10 s	Denaturation
		55 °C	0.5 min.	Annealing
		72 °C	3.5 min.	Extension
3	1	72°C	10 min	Final extension
	hold	4°C	hold	

Besides the greater number of amplification cycles might introduce some undesired off site mutations, hot start Pushion polymerase also requires phosphorylated primers and produces blunt end elongated DNA products which requires T4 DNA ligation. Due to the potential complication during T4 DNA ligation step, and the author's familiarity toward turbo Pfu polymerase based mutagenesis method, turbo Pfu polymerase facilitated PCR reaction was utilized to generate the targeted mutations listed in **Table 9**.

5.4.2. Restriction enzyme digestion analysis of α -TTP mutant DNA samples

Endonuclease digestion with NdeI/XhoI or NdeI/EcoRI was conducted at 37°C for 1 hr followed by enzyme inactivation at 65°C for 20 minutes. The reaction condition typically consisted of 10 μ L plasmid DNA (~ 1 to 1.5 μ g) , 1 μ L NdeI (20 U/ μ l), 1 μ L XhoI (20 U/ μ l), 0.5 μ L BSA (100x) and 5 μ L NE buffer 4 (10X) (final concentration consisted 50 mM potassium acetate, 20 mM Tris-acetate, 10 mM magnesium acetate and 1 mM dithiothreitol, pH 7.9 at 25°C).

5.4.3. DNA concentration analysis

In order to determine the DNA concentration of plasmid preparations and PCR products, purified samples were diluted in mQH₂O and measured at 260 nm in a quartz cuvette. Since the absorbance of 1 unit at 260 nm corresponds to 50 μ g plasmid DNA, the concentration of the plasmid DNA can be easily calculated using the following equation (Quantification of DNA, Qiagen):

$$[\text{DNA}] = \text{Abs}_{260} * 50 \mu\text{g/ml} \quad \text{Eqn 7}$$

5.5. Expression of α -hTTP in various expression vectors

The amount and identity of antibiotic added to the 10 mL pre-cultures varied depending on the expression vector. For α -hTTP/pET28b, the pre-culture was prepared to contain 30 μ g/mL kanamycin and 50 μ g/mL chloramphenicol, whereas 50 μ g/mL ampicillin was used to select for α -hTTP/pET21b and α -hTTP/pGEX-4T-3 transformed *E. coli* cells. Wild-type α -hTTP and the mutant constructs were transformed into *E. coli* BL21 (DE3) competent cells for protein expression. The pre-cultures were grown overnight at 37°C. Five milliliters of overnight pre-culture was used to inoculate 500 mL LB media in 1 L baffled flasks for protein expression experiments.

Typically, *E. coli* cultures were grown in baffled flasks at 37°C until reaching an OD at 600 nm between 0.4 and 0.6. Then the bacterial culture was cooled to room temperature before induction with 400 μ M IPTG. To improve the yield of soluble protein, the culture was grown at room temperature for 16 hours, except for I202A and V206D. Most of V206D remained in inclusion bodies when grown under these conditions, therefore the induction was carried out at 10°C and 100 μ M IPTG in an attempt to improve soluble protein production. I202A on the other hand, appeared to be soluble, yet could not be purified. Various expression and purification conditions were evaluated to overcome the purification issues for I202A and V206D, but all were futile, hence, these two mutants (especially I202A) were not included in most of tests. Following expression, the cells were harvested by centrifugation at 8000 rpm for 15 minutes. Cell pellets were frozen, thawed twice and stored at -80°C until use.

5.6. Purification of α -hTTP (6-His or GST tagged)

Regardless of the purification methods, the purified protein was stored at 4°C and used within a few days after the purification. The purified protein was visualized on an

SDS-PAGE gel prior to use in assays. In general, α -hTTP ligand transfer activity remained intact within five days of purification. Purified protein samples were discarded if not used within the first five days.

5.6.1. HiTrap IMAC Metal chelating affinity chromatography

The thawed *E. coli* pellets were re-suspended in 10 ml lysis buffer (25 mM phosphate, 0.5 M NaCl, 40 mM imidazole, pH 7.4) containing 4 mg lysozyme and incubated at room temperature for 45 minutes. The viscous cell lysate was clarified after 3 x 15 seconds sonication with 15 seconds pulse on ice between the sonication. The sonicated lysate was centrifuged at 40,000xg for 30 minutes at 4°C. Purification of 6-His-tag proteins was conducted using a pre-packed 1 mL HiTrap IMAC affinity column (GE Healthcare, Uppsala, Sweden) that had been rinsed with 5 mL of mQH₂O to remove ethanol or storage buffer. A volume of 0.5 mL of NiSO₄·6H₂O at 0.1 M was passed through the column, followed by a wash with 5 mL of mQH₂O to remove excess unbound NiSO₄. The column was then equilibrated with 5 mL start buffer (25mM phosphate, 40 mM imidazole, 0.5M NaCl, pH 7.4). The lysate supernatant was applied to the column at a flow rate of about 1 mL/min. The column was washed with 5 ml of start buffer followed by wash with 100 mM imidazole in the start buffer. The non-specifically bound proteins were removed after a wash with 200 mM imidazole in the start buffer. Pure α -hTTP was eluted with elution buffer consisting of 25 mM phosphate, 0.5 M NaCl and 400 mM imidazole. The recovery of the pure α -hTTP was typically about 3 % of total protein from the cell lysate.

5.6.2. Probond Metal chelating affinity chromatography

Alternatively, the Probond purification method was used in an attempt to resolve 6-His α -hTTP from a 39 kDa unknown protein contaminant. In this case, *E. coli* pellets were resuspended in 10 ml purification buffer (50 mM NaH₂PO₄, 0.5 M NaCl, pH 8.0), lysozyme was added and the cell lysate was incubated on ice for 30 minutes. The lysate mixture was sonicated with 6 x 10 second bursts, with 10-second cooling on ice between bursts. The viscosity of the sonicated lysate was reduced by passing the lysate through an 18-gauge syringe needle 5 to 6 times. The lysate was centrifuged at 40,000xg at 4°C for 30 minutes. The supernatant was then applied to the prewashed Probond column and allowed to bind to the column matrix for 30 minutes. The non-specific binding was removed by washing the column with 30 column volumes of 20 mM imidazole in purification buffer. Pure histidine tagged α -hTTP was eluted with purification buffer containing 250 mM imidazole. Unfortunately, this purity of α -hTTP was not improved by this purification method.

5.6.3. Glutathione agarose affinity chromatography

E. coli pellets were re-suspended in 10 mL buffer A (150mM Tris pH 8.0, 150 mM NaCl, 1 mM EDTA, 10% glycerol, 0.1 mM DTT and 0.1 mM PMSF). Lysozyme (4 mg/ml) was added to the cell suspension, followed by 30 min incubation on ice. Nucleic acids were digested with the addition of 10 mM MgCl₂, DNase I (500 units) and RNase (50 μ g/mL), followed by an additional 30 min incubation on ice. The cells were then sonicated for 3 x 15 seconds (with 15 seconds cooling on ice between the bursts) and centrifuged at 40,000xg for 30 min at 4°C. The supernatant was applied to a 1mL glutathione affinity column prepared in buffer A. Nonspecific binding proteins were removed by 15 column volumes wash each of buffer B (Buffer A plus 0.5 % Triton X

and 10 mM MgCl₂) and buffer C (50 mM Tris, pH 8, 150 mM NaCl, 10 mM MgCl₂ and 0.1 mM DTT), respectively. On-column thrombin cleavage of GST- α -hTTP was completed after 2 hours of incubation at RT with 50 units of thrombin in phosphate buffered saline (20 mM NaH₂PO₄/Na₂HPO₄ and 150 mM NaCl, pH 7.4) for every 1 to 1.5 mL glutathione agarose. The α -hTTP was eluted in buffer C and a final concentration of 0.5 mM PMSF was added to prevent further secondary thrombin degradation. GST bound on the column was eluted with PBS containing 20 mM glutathione, and the column was regenerated with five column volumes each of cleaning buffer #1 (0.1 M H₃BO₃, 0.5 M NaCl, pH 8.5) and cleaning buffer #2 (0.1 M CH₃COONa, 0.5 M NaCl, pH 4.5), with mQH₂O washes between the cleaning buffer washes. The regenerated column was stored in 2 M NaCl at 4°C for re-use about 15 times.

5.7. Protein qualification and quantification methods

5.7.1. Bradford protein concentration determination

Protein concentrations were usually determined by the Bradford assay [222]. Briefly, ten microliters of purified protein diluted in 40 μ l PBS was mixed with 1 mL Bradford reagent, the absorbance of the protein samples at 595 nm was recorded. The protein concentration was extrapolated from a standard curve of BSA based on the Beer Lambert Law [223].

$$A = \log_{10} (I_0/I) = \epsilon l c \quad \text{Eqn 8}$$

Where A = absorbance at 595 nm, I₀ = intensity of the incident light, I = intensity of the transmitted beam, ϵ = extinction coefficient, c = concentration of protein sample, l = light path of 1 cm.

5.7.2. NanoOrange protein quantification method

The NanoOrange quantification method was intended to improve the detection of the extremely diluted 6-his α -hTTP fractions obtained from fast performance liquid chromatography (FPLC) that were below the detection limit of the Bradford method. The kit was purchased from Molecular Probes and features increased sensitivity down to 10 ng/mL due to fluorescent detection of the NanoOrange dye:protein complexes (Eugene, Oregon). Ten microliter protein samples were diluted with 240 μ L of NanoOrange working solution as suggested by the manufacture's protocol in a 96-well microtiter plate. The plate was covered in aluminum foil. The mixture was incubated at 95°C for 10 minutes and cooled to RT for 20 minutes before fluorescent measurement in a fluorescence-based microplate reader. The protein bound NanoOrange reagent illustrates strong emission fluorescence at 570 nm with excitation wavelength at 470 nm. Sample concentrations were determined using a standard curve of BSA.

5.7.3. Sodium Dodecyl Sulfate-Polyacrylamine Gel Electrophoresis (SDS-PAGE)

The homogeneity of α -hTTP was determined by SDS-PAGE performed according to Laemmli [224] using 3% and 12.5% polyacrylamide for stacking and resolving gels, respectively. Gels were subsequently incubated in fixing buffer (40% EtOH and 10% acetic acid) for 30 minutes, washed in dH₂O for 5 minutes before subjecting the gels to overnight staining with 0.025% Coomassie staining solution (0.1% Coomassie R-250, 25% MeOH and 10% acetic acid). The background staining was removed with destain solution (10% MeOH and 10% acetic acid) for approximately three hours or until the complete removal of the background staining. For vesicle binding samples, the staining solution was freshly prepared by combining 1 part of ProtoBlue Safe Colloidal Coomassie G-250 Stain with 9 parts of absolute EtOH. Distilled water

was used to destain these gels. To preserve these gels for record keeping, films and gels were soaked in gel drying solution (40% MeOH, 10% glycerol, 7.5% acetic acid) for about 10 minutes, and then the gel - sandwiched with 2 preserving films - was assembled on the top of a clean glass. This assembly was allowed to air dry for at least 48 hours. For record keep, the dried gels were trimmed and taped to a notebook.

5.7.4. Western blot analysis

Following purification, protein samples were first separated by 15% SDS-PAGE, then transferred to PVDF membranes using a 200 mA current for 2 hours. It is important to prevent gels from melting by keeping the transfer buffer cool with an ice block. The PVDF membrane was subsequently blocked with 3% BSA in Tris buffered saline (TBS), then incubated with a mouse antibody that recognizes the 6-His tag (Cell Signaling Technology, 1:2500 dilution in TBS) for 1.5 hrs, then washed using 6 x 5 min washes in TBS. Then the membrane was incubated with horse anti-mouse secondary antibody conjugated to alkaline phosphatase (Cell Signaling Technology, 1:2000 in TBS) for 1 hr. The blot was washed again with 6 x 5 min in TBS, and subsequently incubated with the ready to use 5-bromo-4-chloro-3-indoyl phosphate/nitroblue tetrazolium (BCIP/NBT) liquid substrate system (Sigma) for a few minutes or until the appearance of any purple bands. The alkaline phosphatase reaction was terminated by the replacement of BCIP/NBT with mQH₂O.

5.7.5. Intrinsic tryptophan fluorescence of α -hTTP

Fluorescence measurements were performed on QuantaMaster-QM-2001-4 fluorometer at RT. Spectra were recorded at a range of 300 – 400 nm with a fixed excitation wavelength set at 280 nm for tyrosine and 295 nm for tryptophan. The

fluorescence spectra of α -hTTP (10 μ M) in a 3 ml cuvette in the presence of either α -Toc or NBD- α -Toc in SET buffer were monitored. The effect of 2M NaCl on the protein conformation was also investigated.

5.7.6. Acrylamide quenching of α -hTTP

The intrinsic fluorescence of α -hTTP (2.5 μ M) was recorded before and after the addition of the soluble quencher acrylamide at concentrations ranging from 0.1 to 0.5 M. The quenching data was fitted to the Stern-Volmer equation:

$$I_0/I = 1 + K_{SV} [Q] \quad \text{Eqn 9}$$

where I_0 is the initial fluorescence, I is the fluorescence after addition of quencher, $[Q]$ is the concentration of quencher and K_{SV} is the Stern-Volmer constant for dynamic quenching [225].

5.7.7. MALDI-TOF protein sequence analysis

The detailed method was kindly provided by Amanda Rochon. The method is fairly similar to the protocol cited in *Methods in Molecular Biology* [226]. Purified 6-His α -hTTP with a contaminating 39 kDa protein was separated on a small 15% SDS-PAGE and the gel was fixed for 1 hour in fixing solution (7% glacial acetic acid and 40% (v/v) MeOH). The gel was stained in a staining solution (4 parts of 1x Colloidal Brilliant Blue G working solution and 1 part of MeOH) for 4 hours. Destaining the gel was achieved with 10% acetic acid in 25% (v/v) MeOH for 30 minutes on a shaker. The gel was rinsed with 25% MeOH, and destained in 25% MeOH for overnight. The gel was scanned and stored in 25% (v/v) ammonium sulfate at RT until further processing. The microcentrifuge tubes (1.5 mL) to be used were rinsed twice with 50% acetonitrile (ACN) and 0.1% trifluoroacetic acid solution. A clean razor blade was used to cut out

the 39 kDa and α -TTP bands along with a blank area as a negative control. These gel pieces were destained twice with 200 μ L of 100 mM NH_4HCO_3 /50% ACN for 45 minutes each at 37°C. The gel slices were dehydrated in 100 μ L ACN for 5 to 10 minutes at RT. ACN was subsequently removed in a high speed vacuum concentrator for 5 to 10 minutes at RT. Trypsin used for digestion was first reconstituted in 50 mM acetic acid and then diluted to 20 μ g/mL in 40 mM NH_4HCO_3 /10% ACN. The ACN dried gel slices were rehydrated in 20 μ L trypsin at 20 μ g/mL for 1 hour at RT. At the end of incubation, excess trypsin solution was removed. Gel slices were covered in digestion buffer (40 mM NH_4HCO_3 /10% ACN) and incubated overnight at 37°C. One hundred fifty microliters of MQH₂O was added and incubate for 10 minutes with frequent vortexing. The supernatant was transferred to a pre-rinsed microcentrifuge tube. The gel slices were mixed and extracted two more times with 50 μ L 50% ACN/5% TFA (v/v) for 60 minutes at RT. The extracts were combined and dried in a speed vac concentrator for 2 hrs at RT. The dried sample was resuspended in 10 μ L 2.5% TFA in MQH₂O. The peptides were subsequently purified and concentrated using a C18 ZipTip (Millipore) following the manufacturer's protocols. Samples eluted in 50% MeOH/0.1% TFA were submitted to Mr. Tim Jones in the Chemistry department for MALDI-TOF mass spectroscopy analysis.

5.7.8. Phospholipid extraction from purified 6-his α -TTP

The Bligh and Dyer phospholipid extraction procedure [227] was used to extract any *E. coli* phospholipids that might have bound to α -hTTP during expression and purification. To each milliliter of purified protein sample, 3.75 mL of CHCl_3 : MeOH solvent mixture (1:2, v/v) was added and the sample vortexed. Then 1.25 mL CHCl_3 was

added with vigorous vortex mixing. Another 1.25 mL mQH₂O was added and the sample was vortexed. The resulting mixture was centrifuged at 1000 rpm in an IEC table top centrifuge for 5 minutes at room temperature to generate both organic and aqueous phases. The bottom organic phase was recovered with a Pasteur pipette, and dried under N₂. A few drops of CHCl₃: MeOH solvent mixture was added to dissolve the dried lipid. The extracted lipids were separated on a silica plate in an organic solvent mixture (CHCl₃: MeOH: NH₄OH/60:35:8).

5.7.9. Factor Xa digestion of 6-His tag α -hTTP

Purified 6-His tag α -hTTP was diluted in and dialyzed against reaction buffer (20 mM Tris·HCl, 100 mM NaCl, pH 8.2) for 45 minutes at 4°C. At the end of dialysis, the protein solution was centrifuged at 5000 rpm for 5 min. Dialyzed 6-His α -hTTP at 0.5 mg/ mL concentration was digested by 6 μ L Factor Xa (1 mg/mL) in the presence of 1 mM CaCl₂ at room temperature for a time course of 0, 1 hr, 2 hrs, 3 hrs and 4 hrs. Alternatively, on-column digestion was performed following the routine metal affinity purification procedure with the exception that, following the wash with 200 mM imidazole, the matrix was washed with 5 column volumes of the above reaction buffer to remove imidazole. Pure α -hTTP that was bound to the column was digested with 20 μ g of Factor Xa added to the column in reaction buffer for 2 hours with gentle rocking. The cleaved α -hTTP was first eluted with reaction buffer, then 400 mM imidazole was applied to remove the undigested α -hTTP and the 39 kDa protein contaminant that were still bound to the column.

5.7.10. pH stability of α -hTTP

The stability of 6-His α -hTTP at 10 μ M was tested in two buffer systems at neutral and acidic pH. Both Buffer 1 (20 mM sodium citrate, and 150 mM NaCl, pH 7.08) and Buffer 2 (250 mM sucrose, 150 mM KCl, 50 mM sodium citrate, 1 mM EDTA, pH 7.40) tested were at neutral pH. SEA buffer (250 mM sucrose, 50 mM sodium acetate and 150 mM KCl, pH 5.0) was the acidic buffer tested. Ligand binding and transfer were also tested at low pH with SEA buffer.

5.8. Preparation and analysis of phospholipids

5.8.1. LUVs and SUVs preparation

Acceptor lipid vesicles for ligand transfer assays contained 97 mol% PC and 3 mol% quencher TRITC-DHPE, unless otherwise specified. For anionic lipid vesicles, 15 mol% of the indicated anionic phospholipids was incorporated in vesicle preparations. For DPI and vesicle filtration methods, 90% DOPC and 10% DOPS phospholipid vesicles were utilized.

Lipids dissolved in chloroform were evaporated under a stream of N₂ and the residual solvent removed by continued evaporation under vacuum at 0.5 mmHg. Lipid mixtures were rehydrated in SET buffer (250 mM sucrose, 100 mM KCl, 50 mM Tris, 1 mM EDTA, pH 7.4). The lipid suspensions were vortexed and incubated for 30 min at room temperature before liposome preparation. Large unilamellar vesicles (LUVs) were prepared with a Liposofast mini-extruder (Avestin, Inc). Briefly, lipid suspension was extruded through a polycarbonate membrane (100 nm membrane was used for standard LUV preparation) using 15 passages to produce uniformly sized LUVs. Small unilamellar vesicles (SUVs) were prepared, following the procedure described by Schroeder and Thompson [228] with minor modifications. Briefly, lipid suspensions

were sonicated using a titanium microprobe and a W-375 cell disruptor (Heat Systems-Ultrasonic, Inc.). Lipid samples were sonicated on ice for 45 min with an output setting level of 2.5 and 35% duty cycle. The resulting liposomes were centrifuged at 110,000 x g for 2 hours at 4°C with a 40Ti rotor to remove large vesicles and titanium particles. Following centrifugation, the supernatant was collected and stored at 4°C until use. To compare the difference between probe and bath sonicated SUVs, SUVs were also prepared by sonication for 45 min with a Branson bath sonicator Model 2510 (Branson, USA). SUVs produced from both methods appeared to behave similarly for α -TTP mediated tocopherol transfer. Ideally, the phosphorous assay should be performed to determine the phospholipid concentration after each vesicle preparation, and this was attempted. However, due to the presence of high sucrose content in the SET buffer, lipid samples turned black during acidic digestion at 190°C, therefore phosphorus assays can not be used regularly to assess phospholipid concentration.

To confirm there was no loss of phospholipid due to extrusion or sonication, the phosphorous assay was performed initially with SET buffer without sucrose. The result showed that the lipid concentration remains the same before and after the preparation. For the experiments that directly compared vesicles of different sizes, the same rehydrated lipid mixture (multilamellar vesicles or MLVs) was used to generate SUVs or LUVs of the same stock concentration. A rough estimation of vesicle concentration could be determined based on the emission spectrum of the quencher TRITC-DHPE at approximately 575nm. Lipid samples were prepared freshly for each experiment.

5.8.2. Quantification of phospholipid with lipid phosphorous assay

The concentration of phospholipids was determined according to the method published by Rouser *et al.* [229]. Typically, lipid samples were oxidized in 150 μL of 70% perchloric acid (HClO_4) at 180 to 190°C in test tubes covered in foil paper. The samples were allowed to cool to RT. The sides of the tubes were rinsed with 900 mL mQH_2O , and the contents were mixed by gentle vortexing. An equal volume of 167 μL of 2.5% (v/v) ammonium molybdate and 10% ascorbic acid were added to the sample tubes followed by vortex mixing. All samples were incubated for 15 minutes at 50°C and then cooled to RT before measuring the optical density (O.D.) at 820 nm. The sample should appear from grey-green to blue. Duplicate measurements of 0-50 nmoles Na_2HPO_4 standards were run at the same time as other phospholipid samples.

5.8.3. Dynamic light scattering analysis of the sizes of the SUVs and LUVs

The sizes of vesicles were determined at two institutions. Wyatt Technology Corporation (Sant Barbara, CA) analyzed SUVs samples with a Dynamic Titan dynamic light scattering instrument called DynaPro Nanostar with a detection radius ranging from 0.5 to 10000 nm at a laser wavelength of 660 nm. Similarly, the measurement of various sizes of vesicles at McMaster University was performed using a fixed angle quasi-elastic light-scattering instrument (QELS) with kind assistance from Mr. Yuguo Cui.

5.9. Characteristics of fluorescent ligand NBD- α -Toc

5.9.1. Equilibrium titration of α -hTTP wild type and mutants with NBD- α -Toc

200 nM of wild type α -hTTP or the mutants was titrated in a 3 mL cuvette with serial additions of 2 μL aliquots of NBD- α -Toc from concentrated stocks in EtOH. The final EtOH was kept below 2% (v/v) of the total volume. The mixture was allowed to equilibrate for 10 min with end-over-end rotation after each addition of NBD- α -Toc.

The fluorescence emission between 525 nm and 535 nm was recorded until the maximum fluorescence was achieved. The excitation wavelength was set at 466 nm. For competition experiments, α -hTTP (200 nM) was pre-incubated with NBD- α -Toc (1 μ M) for 15 minutes. 100 μ M Triton X-100 was included in the SET buffer for competition experiments to provide a more thermodynamically favorable aqueous environment for such competition [163] to occur. Competitor such as cholesterol or natural tocopherol was added in incremental concentrations up to 40 μ M.

5.9.2. Partitioning of NBD- α -Toc between α -hTTP and PC lipid vesicles

The partition coefficient of NBD- α -Toc was measured following literature procedures for fluorescent fatty acid transfer from albumins and FABPs to lipid vesicles [138, 177]. The method enables determination of the partition coefficient of α -hTTP for lipid vesicles by incubating the protein with a range of mole ratios of lipids. Briefly, several solutions were prepared containing a 10:1 ratio of α -hTTP:NBD- α -Toc that assured the absence of appreciable amounts of free NBD- α -Toc. The samples were incubated for 15 min with gentle rotation at RT. To each of these solutions amounts of LUVs or SUVs containing TRITC-DHPE (measured as μ M total phospholipid) were added so that the final lipid concentration ranged from 50 to 400 μ M. The final protein and ligand concentrations were 1.0 μ M α -hTTP and 0.1 μ M NBD- α -Toc in SET buffer at pH 7.4. The resulting mixture was incubated for 15 min to allow NBD- α -Toc to equilibrate between α -hTTP and acceptor SUVs or LUVs. The fluorescence spectrum of NBD- α -Toc from 475nm to 600nm was recorded, and the changes in the fluorescence at 520 nm were applied to the following equation [177, 230] to calculate the partition coefficients:

$$1/\Delta F = 1/K_p(1/\Delta F_{\max})(\text{mol } \alpha\text{-hTTP/mol PC}) + 1/\Delta F_{\max} \quad \text{Eqn 10}$$

where ΔF is the difference between the initial fluorescence of NBD- α -Toc bound to α -hTTP and the fluorescence at a given protein/PC ratio, and ΔF_{\max} is the maximum fluorescence change [128]. A plot of $1/\Delta F$ versus $(1/\Delta F_{\max})(\text{mol } \alpha\text{-hTTP/mol PC})$ gave a straight line whose slope was equal to $1/K_p$.

5.9.3. Spectroscopic measurement of NBD- α -Toc concentration

The absorbance of the diluted NBD- α -Toc in 1 ml EtOH was measured at 469 nm in a UV spectrometer (Spectronic Genesys 2). The concentration was calculated using Beer-Lambert's law with an extinction coefficient of $17,602 \text{ cm}^{-1} \cdot \text{M}^{-1}$.

5.9.4. Reduction of NBD- α -Toc by Sodium Dithionite ($\text{Na}_2\text{S}_2\text{O}_4$)

NBD- α -Toc was reduced in a 500 μL quartz cuvette, by first incubating 2 μM α -hTTP with 0.2 μM NBD- α -Toc for 15 minutes or until the fluorescent curve reached its plateau. Several additions of 50 μL of 1M sodium dithionite were added to the mixture as the change in fluorescence after each addition was monitored at 526 nm with an excitation wavelength of 466 nm. Alternatively, sodium dithionite reduction of NBD- α -Toc was also tested in the presence of 800 μM bovine liver PC alone or in combination with 2 μM α -hTTP.

5.10. Fluorescence resonance energy transfer (FRET assay)

Experiments were performed using a Photon Technologies, Inc. QuantaMaster-QM-2001-4 fluorometer (Photon Technologies International, Inc.) equipped with a SPF-17 stopped flow device in order to determine the kinetics of NBD- α -Toc transfer. The excitation and emission wavelengths used were 466 nm and 526 nm respectively. The emission spectrum of NBD- α -Toc overlaps with the excitation spectrum of TRITC-

DHPE, thus, upon mixing of NBD- α -Toc containing donor and TRITC-DHPE containing acceptor vesicles, the fluorescence intensity decreases with time. Alternatively, for the reversed transfer of NBD- α -Toc, the extraction of NBD- α -Toc from the quencher containing vesicles exhibited a time dependent increase in the fluorescence intensity. All samples were prepared in SET buffer, and mixing of an equal volume of the donor and the acceptor samples was achieved by the SPF-17 stopped-flow device. All experiments were performed at RT.

5.10.1. Spontaneous transfer of NBD- α -Toc from donor vesicles to acceptor vesicles.

To study the inter-vesicular transfer of NBD- α -Toc, 1 mol% of NBD- α -Toc was incorporated into PC LUVs, and the transfer of NBD- α -Toc from PC LUVs to PC LUVs or SUVs was monitored. In one occasion, C9-anthroyloxy- α -tocopherol (AO- α -Toc) was tested in the place of NBD- α -Toc to determine the kinetics of α -Toc transfer when it is conjugate to a more hydrophobic anthroylxy label.

5.10.2. Transfer of NBD- α -Toc from α -hTTP to acceptor vesicles.

Standard transfer experiments were performed by incubating 0.45 μ M NBD- α -Toc with 4 μ M α -hTTP for 15 minutes at RT prior to mixing the sample with 200 μ M acceptor vesicles using the SPF-17 stopped-flow device. The final concentrations after mixing were 0.225 μ M NBD- α -Toc, 2 μ M α -hTTP and 100 μ M vesicles. The ratio of α -hTTP to NBD- α -Toc was kept at 9:1 to ensure that there was no free ligand and that the fluorescence signal was solely contributed by protein-bound NBD- α -Toc. A 50-fold molar excess of acceptor vesicle to α -hTTP was used based on the partition coefficient of NBD- α -Toc between α -hTTP and vesicles. The fluorescence quenching was monitored over time and the fluorescence values were normalized to the starting fluorescent

intensity of NBD- α -Toc bound to α -hTTP as 100%. Under our assay conditions, the rate of NBD- α -Toc transfer was best fitted with a single exponential decay equation (**Eqn 11**) provided by Prism software (version 5, GraphPad Software, Inc., El Camino Real, San Diego, CA) as:

$$y = (y_0 - y_{inf}) * \exp(-k * x) + y_{inf} \quad \text{Eqn 11}$$

where y_0 is the initial fluorescence when NBD- α -Toc bound to α -hTTP, k is the rate constant, x is the half time for transfer, and y_{inf} is the remaining fluorescence signal after NBD- α -Toc has been transferred to the acceptor vesicle which in our case is approximately 55% of the original fluorescence signal.

5.10.3. Pick up of NBD- α -Toc from membrane vesicles by α -hTTP

The donor vesicles in the optimized pick-up assay consisted of 0.25 μ M NBD- α -Toc in 50 μ M bovine liver PC plus 1.5 μ M quencher TRITC-DHPE. In some experiments, other lipids such as PS, LBPA and CL were also included in the donor vesicles to be tested at 5%, 10% and 15% of the total 50 μ M respectively. The baseline fluorescence at 526 nm was obtained by recording the initial fluorescence of the donor vesicles. Subsequently, NBD- α -Toc in the donor vesicles was extracted by mixing the donor vesicles with 2.5 μ M α -hTTP. The rate of NBD- α -Toc transfer to α -hTTP was best fitted with a single exponential association equation (**Eqn 12**) provided by Prism software

$$Y = Y_{max} * (1 - \exp(-k * X)) \quad \text{Eqn 12}$$

where Y_{max} is the final fluorescence when the maximum amount of NBD- α -Toc is bound to α -hTTP, k is the rate constant for ligand binding, X is the time when half of the maximum NBD- α -toc is bound to α -hTTP.

5.11. Assessment of α -hTTP binding to phospholipid membranes

Binding of α -hTTP to lipid membranes was investigated using two different methods. A size exclusion filtration method was utilized to study the effect of membrane curvature on the binding of the protein to lipid membranes by testing protein binding to both SUVs and LUVs. In contrast, a Dual Polarization Interferometric (DPI) method was used primarily to measure the interaction between α -hTTP and a more planar lipid bilayer on the surface of the DPI sensor chip rather than vesicles.

5.11.1. Size exclusion filtration method

The binding of α -hTTP to lipid vesicles was performed similar to the previously published method by Huang *et al.* [207]. Wild type or mutant α -hTTP (31.5 μ g) was incubated with increasing concentrations of SUVs or LUVs in a total of 200 μ L SET buffer with gentle rocking for 30 minutes at room temperature. The samples were subsequently loaded onto pre-wet YM-100 microcon filters with the molecular weight cutoff at 100 kDa. These samples were then centrifuged at 10,000 x g in a bench top microcentrifuge for 20 minutes. The filters were washed once with 100 μ L SET buffer, where the flow-through represents the free protein fraction that failed to bind to lipid vesicles. The microcon filters were inverted and washed three times with 100 μ L SET buffer containing 150 μ M Triton X-100 to collect the vesicle bound α -hTTP fractions. Each wash was completed by centrifugation at 3000 x g for 5 minutes. The samples were then separated on precast 10% SDS-PAGE mini gels and visualized after staining with Colloidal Coomassie G-250 overnight. After the gel destaining, the intensity of each protein band was quantified with Scion Image software (developed by Scion Corp.). The data analysis was completed with Prism software by plotting band intensities of each α -

hTTP sample versus its concentration. A blank lane of the gel was taken as background control.

5.11.2. Dual Polarization Interferometric assessment (DPI)

The Analight Bio 200 dual polarization interferometer (Farfield Sensors Ltd, Manchester, UK) was used to study the association of α -hTTP to planar lipid bilayer containing 10% DOPS and 90% DOPC assembled on the DPI chip surface. DPI has been characterized in depth as a valuable quantitative tool to study protein conformation or protein and lipid interaction *in vitro* since DPI measures the changes in the mass, thickness and refractive index of the layer adsorbed on the chip's surface. Thus, when a protein is adsorbed on the surface of the sensor chip, the protein's behavior or interactions can be followed under different conditions [231, 232]. Due to the hypersensitive detection in the changes on the sensor surface, all solutions were degassed for at least 30 minutes to remove any fine bubbles prior to use. Running buffer (10 mM potassium phosphate, 137 mM NaCl, pH 7.4) was used to dilute α -hTTP samples and prepare LUVs. All experiments were performed at 20°C. The instrument was first loaded with an unmodified silicon oxynitride sensor chip, then calibrated with 80% (v/v) ethanol and 20% (v/v) mQH₂O. Once a stable baseline was established, 100 nm DOPS/DOPC (1:9) vesicles were passed over the sensor chip at a flow rate of 25 μ L per minutes for 8 minutes. The vesicles ruptured and a stable bilayer was attained approximately 5 minutes after each injection. At the end of lipid injection, buffer was passed over the lipid bilayer for approximately 4 minutes at the rate of 50 μ L per minute to remove any extra lipid that was deposited on the top of lipid bilayer. α -hTTP at the desired concentration was then injected over the lipid bilayer at a rate of 25 μ L per

minute for 8 minutes. At the end of the injection, the protein layer was washed with buffer for a few minutes at 50 μ L per minute to remove nonspecifically bound protein until a stable reading was obtained. To regenerate the sensor chip for another run of testing, existing lipid and protein layers were stripped with 150 μ L each of 2% SDS followed by 50% isopropyl alcohol. The procedure was repeated until the entire set of the data was collected. The data collected from the first 450 seconds of α -hTTP injection was resolved and fitted to a one site binding equation to calculate the maximum mass of protein (B_{max}) deposited onto the lipid bilayer from a plot of the layer's mass versus time. Occasionally, the maximum binding data (B_{max}) were plotted against protein concentrations to determine the binding affinity of the α -hTTP mutants to the lipid bilayer according to the one phase association equation.

5.12. Software

DeepView & PyMol

Both software programs were used to visualize and create the crystal structure presentations of human α -hTTP. The coordinates for the crystal structures used in this study are: triton-X100 bound α -hTTP (pdb: IOIP, IOIZ) and α -tocopherol bound holo- α -hTTP (pdb:1R5L).

Scion Image software

This program was exploited to quantify the intensity of protein bands obtained from the size exclusion filtration vesicle binding experiments.

Bioedit

Bioedit was used mainly to analyze the presence of the targeted mutations by generating a sequence alignment of the mutants and wild type α -hTTP. It was also used

to generate the restriction map and to translate nucleotide sequences into protein sequences.

Graphpad Prism version 5

Prism software was utilized to characterize the kinetics of lipid binding and ligand transfer by α -hTTP using non-linear regression analysis (for a one site binding model). It was also occasionally used to perform T-tests to determine whether there was significant difference between two or more data sets.

6. REFERENCES

- 1 Bieri, J. G. and Evarts, R. P. (1974) Gamma tocopherol: metabolism, biological activity and significance in human vitamin E nutrition. *Am J Clin Nutr* **27**, 980-986
- 2 Chow, C. K. (1975) Distribution of tocopherols in human plasma and red blood cells. *Am J Clin Nutr* **28**, 756-760
- 3 Evans, H. M., Emerson, O. H. and Emerson, G. A. (1936) The isolation from wheat germ oil of an alcohol, α -tocopherol, having the properties of vitamin E. *J. Biol. Chem.* **113**, 319-332
- 4 Evans, H. M. and Bishop, K. S. (1922) On the Existence of a Hitherto Unrecognized Dietary Factor Essential for Reproduction. *Science* **56**, 650-651
- 5 Sure, B. (1924) Dietary requirement for reproduction. II. The existence of a specific vitamin for reproduction. *J. Biol. Chem.* **58**, 693-709
- 6 Cummings, M. J. and Mattill, H. A. (1931) The auto-oxidation of fats with reference to their destructive effect on vitamin E. *J. Nutri.* **3**, 421-432
- 7 Olcott, H. S. and Mattill, H. A. (1934) Vitamin E. I. Some chemical and physiological properties. *J. Biol. Chem.* **104**, 423-435
- 8 Olcott, H. S. and Mattill, H. A. (1936) Antioxidants and the auto-oxidation of fats. VI. Inhibitors. *J. Am. Chem. Soc.* **58**, 1627-1630
- 9 Azzi, A., Gysin, R., Kempna, P., Munteanu, A., Negis, Y., Villacorta, L., Visarius, T. and Zingg, J. M. (2004) Vitamin E mediates cell signaling and regulation of gene expression. *Ann N Y Acad Sci* **1031**, 86-95
- 10 Zingg, J. M. and Azzi, A. (2004) Non-antioxidant activities of vitamin E. *Curr Med Chem* **11**, 1113-1133
- 11 Traber, M. G. and Atkinson, J. (2007) Vitamin E, antioxidant and nothing more. *Free Radic Biol Med* **43**, 4-15
- 12 Brigelius-Flohe, R. and Davies, K. J. (2007) Is vitamin E an antioxidant, a regulator of signal transduction and gene expression, or a 'junk' food? Comments on the two accompanying papers: "Molecular mechanism of alpha-tocopherol action" by A. Azzi and "Vitamin E, antioxidant and nothing more" by M. Traber and J. Atkinson. *Free Radic Biol Med* **43**, 2-3
- 13 Schneider, C. (2005) Chemistry and biology of vitamin E. *Mol Nutr Food Res* **49**, 7-30

- 14 Blatt, D. H., Leonard, S. W. and Traber, M. G. (2001) Vitamin E kinetics and the function of tocopherol regulatory proteins. *Nutrition* **17**, 799-805
- 15 Manor, D. and Morley, S. (2007) The alpha-tocopherol transfer protein. *Vitam Horm* **76**, 45-65
- 16 Wolf, G. (2005) The discovery of the antioxidant function of vitamin E: the contribution of Henry A. Mattill. *J Nutr* **135**, 363-366
- 17 Kamal-Eldin, A. and Appelqvist, L. A. (1996) The chemistry and antioxidant properties of tocopherols and tocotrienols. *Lipids* **31**, 671-701
- 18 Dix, T. A. and Aikens, J. (1993) Mechanisms and biological relevance of lipid peroxidation initiation. *Chem Res Toxicol* **6**, 2-18
- 19 Winterbourn, C. C. (2008) Reconciling the chemistry and biology of reactive oxygen species. *Nat Chem Biol* **4**, 278-286
- 20 Ingold, K. U. and Howard, J. A. (1962) Reaction of Phenols with Peroxy Radicals. *Nature* **195**, 280-281
- 21 Burton, G. W. and Ingold, K. U. (1981) Autooxidation of Biological Molecules. 1. The Antioxidant Activity of Vitamin E and Related Chain-Breaking Phenolic Antioxidants *in vitro*. *J. Am. Chem. Soc.* **103**, 6472-6477
- 22 Atkinson, J., Epand, R. F. and Epand, R. M. (2008) Tocopherols and tocotrienols in membranes: a critical review. *Free Radic Biol Med* **44**, 739-764
- 23 McCay, P. B. (1985) Vitamin E: interactions with free radicals and ascorbate. *Annu Rev Nutr* **5**, 323-340
- 24 Fukuzawa, K. (2008) Dynamics of lipid peroxidation and antioxidation of alpha-tocopherol in membranes. *J Nutr Sci Vitaminol (Tokyo)* **54**, 273-285
- 25 Kagan, V. E. and Quinn, P. J. (1988) The interaction of alpha-tocopherol and homologues with shorter hydrocarbon chains with phospholipid bilayer dispersions. A fluorescence probe study. *Eur J Biochem* **171**, 661-667
- 26 Burton, G. W. and Ingold, K. U. (1986) Vitamin E: Application of the Principles of Physical Organic Chemistry to the Exploration of Its Structure and Function. *Acc. Chem. Res* **19**, 194-201
- 27 Burton, G. W., Joyce, A. and Ingold, K. U. (1982) First proof that vitamin E is major lipid-soluble, chain-breaking antioxidant in human blood plasma. *Lancet* **2**, 327

- 28 Tappel, A. and Zalkin, H. (1959) Inhibition of Lipide Peroxidation in Mitochondria by Vitamin E. *Arch Biochem Biophys*. **80**, 333-336
- 29 Tappel, A. and Zalkin, H. (1960) Inhibition of lipid peroxidation in microsomes by vitamin E. *Nature* **185**, 35
- 30 Dillard, C. J., Gavino, V. C. and Tappel, A. L. (1983) Relative antioxidant effectiveness of alpha-tocopherol and gamma-tocopherol in iron-loaded rats. *J Nutr* **113**, 2266-2273
- 31 Kagan, V. E., Serbinova, E. A. and Packer, L. (1990) Recycling and antioxidant activity of tocopherol homologs of differing hydrocarbon chain lengths in liver microsomes. *Arch Biochem Biophys* **282**, 221-225
- 32 Serbinova, E., Kagan, V., Han, D. and Packer, L. (1991) Free radical recycling and intramembrane mobility in the antioxidant properties of alpha-tocopherol and alpha-tocotrienol. *Free Radic Biol Med* **10**, 263-275
- 33 Gregor, W., Staniek, K., Nohl, H. and Gille, L. (2006) Distribution of tocopheryl quinone in mitochondrial membranes and interference with ubiquinone-mediated electron transfer. *Biochem Pharmacol* **71**, 1589-1601
- 34 Arita, M., Sato, Y., Arai, H. and Inoue, K. (1998) Binding of alpha-tocopherylquinone, an oxidized form of alpha-tocopherol, to glutathione-S-transferase in the liver cytosol. *FEBS Lett* **436**, 424-426
- 35 Behrens, W. A. and Madere, R. (1986) Alpha- and gamma tocopherol concentrations in human serum. *J Am Coll Nutr* **5**, 91-96
- 36 Fechner, H., Schlame, M., Guthmann, F., Stevens, P. A. and Rustow, B. (1998) alpha- and delta-tocopherol induce expression of hepatic alpha-tocopherol-transfer-protein mRNA. *Biochem J* **331** (Pt 2), 577-581
- 37 Lauridsen, C., Engel, H., Craig, A. M. and Traber, M. G. (2002) Relative bioactivity of dietary RRR- and all-rac-alpha-tocopheryl acetates in swine assessed with deuterium-labeled vitamin E. *J Anim Sci* **80**, 702-707
- 38 Traber, M. G., Rudel, L. L., Burton, G. W., Hughes, L., Ingold, K. U. and Kayden, H. J. (1990) Nascent VLDL from liver perfusions of cynomolgus monkeys are preferentially enriched in RRR- compared with SRR-alpha-tocopherol: studies using deuterated tocopherols. *J Lipid Res* **31**, 687-694
- 39 Traber, M. G., Ramakrishnan, R. and Kayden, H. J. (1994) Human plasma vitamin E kinetics demonstrate rapid recycling of plasma RRR-alpha-tocopherol. *Proc Natl Acad Sci U S A* **91**, 10005-10008

- 40 Traber, M. G., Burton, G. W., Ingold, K. U. and Kayden, H. J. (1990) RRR- and SRR-alpha-tocopherols are secreted without discrimination in human chylomicrons, but RRR-alpha-tocopherol is preferentially secreted in very low density lipoproteins. *J Lipid Res* **31**, 675-685
- 41 Traber, M. G., Rader, D., Acuff, R. V., Ramakrishnan, R., Brewer, H. B. and Kayden, H. J. (1998) Vitamin E dose-response studies in humans with use of deuterated RRR-alpha-tocopherol. *Am J Clin Nutr* **68**, 847-853
- 42 Traber, M. G. and Kayden, H. J. (1989) Preferential incorporation of alpha-tocopherol vs gamma-tocopherol in human lipoproteins. *Am J Clin Nutr* **49**, 517-526
- 43 Burton, G. W., Traber, M. G., Acuff, R. V., Walters, D. N., Kayden, H., Hughes, L. and Ingold, K. U. (1998) Human plasma and tissue alpha-tocopherol concentrations in response to supplementation with deuterated natural and synthetic vitamin E. *Am J Clin Nutr* **67**, 669-684
- 44 Wang, X. and Quinn, P. J. (2000) The location and function of vitamin E in membranes (review). *Mol Membr Biol* **17**, 143-156
- 45 Fukuzawa, K., Ikebata, W., Shibata, A., Kumadaki, I., Sakanaka, T. and Urano, S. (1992) Location and dynamics of alpha-tocopherol in model phospholipid membranes with different charges. *Chem Phys Lipids* **63**, 69-75
- 46 Gramlich, G., Zhang, J. and Nau, W. M. (2004) Diffusion of alpha-tocopherol in membrane models: probing the kinetics of vitamin E antioxidant action by fluorescence in real time. *J Am Chem Soc* **126**, 5482-5492
- 47 Sonnen, A. F., Bakirci, H., Netscher, T. and Nau, W. M. (2005) Effect of temperature, cholesterol content, and antioxidant structure on the mobility of vitamin E constituents in biomembrane models studied by laterally diffusion-controlled fluorescence quenching. *J Am Chem Soc* **127**, 15575-15584
- 48 Ekiel, I. H., Hughes, L., Burton, G. W., Jovall, P. A., Ingold, K. U. and Smith, I. C. (1988) Structure and dynamics of alpha-tocopherol in model membranes and in solution: a broad-line and high-resolution NMR study. *Biochemistry* **27**, 1432-1440
- 49 Burton, G. W., Joyce, A. and Ingold, K. U. (1983) Is vitamin E the only lipid-soluble, chain-breaking antioxidant in human blood plasma and erythrocyte membranes? *Arch Biochem Biophys* **221**, 281-290
- 50 Traber, M. G. (2007) Vitamin E regulatory mechanisms. *Annu Rev Nutr* **27**, 347-362

- 51 Traber, M. G., Olivecrona, T. and Kayden, H. J. (1985) Bovine milk lipoprotein lipase transfers tocopherol to human fibroblasts during triglyceride hydrolysis in vitro. *J Clin Invest* **75**, 1729-1734
- 52 Chajek-Shaul, T., Friedman, G., Stein, O., Olivecrona, T. and Stein, Y. (1982) Binding of lipoprotein lipase to the cell surface is essential for the transmembrane transport of chylomicron cholesteryl ester. *Biochim Biophys Acta* **712**, 200-210
- 53 Traber, M. G. and Kayden, H. J. (1984) Vitamin E is delivered to cells via the high affinity receptor for low-density lipoprotein. *Am J Clin Nutr* **40**, 747-751
- 54 Traber, M. G., Lane, J. C., Lagmay, N. R. and Kayden, H. J. (1992) Studies on the transfer of tocopherol between lipoproteins. *Lipids* **27**, 657-663
- 55 Asmis, R. (1997) Physical partitioning is the main mechanism of alpha-tocopherol and cholesterol transfer between lipoproteins and P388D1 macrophage-like cells. *Eur J Biochem* **250**, 600-607
- 56 Balazs, Z., Panzenboeck, U., Hammer, A., Sovic, A., Quehenberger, O., Malle, E. and Sattler, W. (2004) Uptake and transport of high-density lipoprotein (HDL) and HDL-associated alpha-tocopherol by an in vitro blood-brain barrier model. *J Neurochem* **89**, 939-950
- 57 Reboul, E., Klein, A., Bietrix, F., Gleize, B., Malezet-Desmoulins, C., Schneider, M., Margotat, A., Lagrost, L., Collet, X. and Borel, P. (2006) Scavenger receptor class B type I (SR-BI) is involved in vitamin E transport across the enterocyte. *J Biol Chem* **281**, 4739-4745
- 58 Traber, M. G. and Kayden, H. J. (1987) Tocopherol distribution and intracellular localization in human adipose tissue. *Am J Clin Nutr* **46**, 488-495
- 59 Rupar, C. A., Albo, S. and Whitehall, J. D. (1992) Rat liver lysosome membranes are enriched in alpha-tocopherol. *Biochem Cell Biol* **70**, 486-488
- 60 Parker, R. S., Sontag, T. J. and Swanson, J. E. (2000) Cytochrome P4503A-dependent metabolism of tocopherols and inhibition by sesamin. *Biochem Biophys Res Commun* **277**, 531-534
- 61 Birringer, M., Drohan, D. and Brigelius-Flohe, R. (2001) Tocopherols are metabolized in HepG2 cells by side chain omega-oxidation and consecutive beta-oxidation. *Free Radic Biol Med* **31**, 226-232
- 62 Lodge, J. K., Ridlington, J., Leonard, S., Vaule, H. and Traber, M. G. (2001) Alpha- and gamma-tocotrienols are metabolized to carboxyethyl-hydroxychroman derivatives and excreted in human urine. *Lipids* **36**, 43-48

- 63 Chiku, S., Hamamura, K. and Nakamura, T. (1984) Novel urinary metabolite of d-delta-tocopherol in rats. *J Lipid Res* **25**, 40-48
- 64 Sontag, T. J. and Parker, R. S. (2002) Cytochrome P450 omega-hydroxylase pathway of tocopherol catabolism. Novel mechanism of regulation of vitamin E status. *J Biol Chem* **277**, 25290-25296
- 65 Parker, R. S., Sontag, T. J., Swanson, J. E. and McCormick, C. C. (2004) Discovery, characterization, and significance of the cytochrome P450 omega-hydroxylase pathway of vitamin E catabolism. *Ann N Y Acad Sci* **1031**, 13-21
- 66 Parker, R. S. and McCormick, C. C. (2005) Selective accumulation of alpha-tocopherol in *Drosophila* is associated with cytochrome P450 tocopherol-omega-hydroxylase activity but not alpha-tocopherol transfer protein. *Biochem Biophys Res Commun* **338**, 1537-1541
- 67 Sontag, T. J. and Parker, R. S. (2007) Influence of major structural features of tocopherols and tocotrienols on their omega-oxidation by tocopherol-omega-hydroxylase. *J Lipid Res* **48**, 1090-1098
- 68 Kiyose, C., Saito, H., Kaneko, K., Hamamura, K., Tomioka, M., Ueda, T. and Igarashi, O. (2001) Alpha-tocopherol affects the urinary and biliary excretion of 2,7,8-trimethyl-2 (2'-carboxyethyl)-6-hydroxychroman, gamma-tocopherol metabolite, in rats. *Lipids* **36**, 467-472
- 69 Cohn, W., Loechleiter, F. and Weber, F. (1988) Alpha-tocopherol is secreted from rat liver in very low density lipoproteins. *J Lipid Res* **29**, 1359-1366
- 70 Bjorneboe, A., Bjorneboe, G. E., Hagen, B. F., Nossen, J. O. and Drevon, C. A. (1987) Secretion of alpha-tocopherol from cultured rat hepatocytes. *Biochim Biophys Acta* **922**, 199-205
- 71 Boscoboinik, D., Szewczyk, A., Hensey, C. and Azzi, A. (1991) Inhibition of cell proliferation by alpha-tocopherol. Role of protein kinase C. *J Biol Chem* **266**, 6188-6194
- 72 Boscoboinik, D., Szewczyk, A. and Azzi, A. (1991) Alpha-tocopherol (vitamin E) regulates vascular smooth muscle cell proliferation and protein kinase C activity. *Arch Biochem Biophys* **286**, 264-269
- 73 Kagan, V. E. (1989) Tocopherol stabilizes membrane against phospholipase A, free fatty acids, and lysophospholipids. *Ann N Y Acad Sci* **570**, 121-135
- 74 Erin, A. N., Spirin, M. M., Tabidze, L. V. and Kagan, V. E. (1984) Formation of alpha-tocopherol complexes with fatty acids. A hypothetical mechanism of stabilization of biomembranes by vitamin E. *Biochim Biophys Acta* **774**, 96-102

- 75 Aranda, F. J., Sanchez-Migallon, M. P. and Gomez-Fernandez, J. C. (1996) Influence of alpha-tocopherol incorporation on Ca(2+)-induced fusion of phosphatidylserine vesicles. *Arch Biochem Biophys* **333**, 394-400
- 76 Erin, A. N., Gorbunov, N. V., Brusovanik, V. I., Tyurin, V. A. and Prilipko, L. L. (1986) Stabilization of synaptic membranes by alpha-tocopherol against the damaging action of phospholipases. Possible mechanism of biological action of vitamin E. *Brain Res* **398**, 85-90
- 77 Dutta-Roy, A. K., Leishman, D. J., Gordon, M. J., Campbell, F. M. and Duthie, G. G. (1993) Identification of a low molecular mass (14.2 kDa) alpha-tocopherol-binding protein in the cytosol of rat liver and heart. *Biochem Biophys Res Commun* **196**, 1108-1112
- 78 Dutta-Roy, A. K., Gordon, M. J., Leishman, D. J., Paterson, B. J., Duthie, G. G. and James, W. P. (1993) Purification and partial characterisation of an alpha-tocopherol-binding protein from rabbit heart cytosol. *Mol Cell Biochem* **123**, 139-144
- 79 Gordon, M. J., Campbell, F. M., Duthie, G. G. and Dutta-Roy, A. K. (1995) Characterization of a novel alpha-tocopherol-binding protein from bovine heart cytosol. *Arch Biochem Biophys* **318**, 140-146
- 80 Gordon, M. J., Campbell, F. M. and Dutta-Roy, A. K. (1996) alpha-Tocopherol-binding protein in the cytosol of the human placenta. *Biochem Soc Trans* **24**, 202S
- 81 Jerkovic, L., Voegelé, A. F., Chwatal, S., Kronenberg, F., Radcliffe, C. M., Wormald, M. R., Lobentanz, E. M., Ezech, B., Eller, P., Dejori, N., Dieplinger, B., Lottspeich, F., Sattler, W., Uhr, M., Mechtler, K., Dwek, R. A., Rudd, P. M., Baier, G. and Dieplinger, H. (2005) Afamin is a novel human vitamin E-binding glycoprotein characterization and in vitro expression. *J Proteome Res* **4**, 889-899
- 82 Voegelé, A. F., Jerkovic, L., Wellenzohn, B., Eller, P., Kronenberg, F., Liedl, K. R. and Dieplinger, H. (2002) Characterization of the vitamin E-binding properties of human plasma afamin. *Biochemistry* **41**, 14532-14538
- 83 Kratzer, I., Bernhart, E., Wintersperger, A., Hammer, A., Walzl, S., Malle, E., Sperk, G., Wietzorrek, G., Dieplinger, H. and Sattler, W. (2009) Afamin is synthesized by cerebrovascular endothelial cells and mediates alpha-tocopherol transport across an in vitro model of the blood-brain barrier. *J Neurochem* **108**, 707-718
- 84 Catignani, G. L. (1975) An alpha-tocopherol binding protein in rat liver cytoplasm. *Biochem Biophys Res Commun* **67**, 66-72

- 85 Mowri, H., Nakagawa, Y., Inoue, K. and Nojima, S. (1981) Enhancement of the transfer of alpha-tocopherol between liposomes and mitochondria by rat-liver protein(s). *Eur J Biochem* **117**, 537-542
- 86 Kaempf-Rotzoll, D. E., Horiguchi, M., Hashiguchi, K., Aoki, J., Tamai, H., Linderkamp, O. and Arai, H. (2003) Human placental trophoblast cells express alpha-tocopherol transfer protein. *Placenta* **24**, 439-444
- 87 Yoshida, H., Yusin, M., Ren, I., Kuhlenkamp, J., Hirano, T., Stolz, A. and Kaplowitz, N. (1992) Identification, purification, and immunochemical characterization of a tocopherol-binding protein in rat liver cytosol. *J Lipid Res* **33**, 343-350
- 88 Kuhlenkamp, J., Ronk, M., Yusin, M., Stolz, A. and Kaplowitz, N. (1993) Identification and purification of a human liver cytosolic tocopherol binding protein. *Protein Expr Purif* **4**, 382-389
- 89 Hosomi, A., Arita, M., Sato, Y., Kiyose, C., Ueda, T., Igarashi, O., Arai, H. and Inoue, K. (1997) Affinity for alpha-tocopherol transfer protein as a determinant of the biological activities of vitamin E analogs. *FEBS Lett* **409**, 105-108
- 90 Panagabko, C., Morley, S., Hernandez, M., Cassolato, P., Gordon, H., Parsons, R., Manor, D. and Atkinson, J. (2003) Ligand specificity in the CRAL-TRIO protein family. *Biochemistry* **42**, 6467-6474
- 91 Copp, R. P., Wisniewski, T., Hentati, F., Larnaout, A., Ben Hamida, M. and Kayden, H. J. (1999) Localization of alpha-tocopherol transfer protein in the brains of patients with ataxia with vitamin E deficiency and other oxidative stress related neurodegenerative disorders. *Brain Res* **822**, 80-87
- 92 Sato, Y., Arai, H., Miyata, A., Tokita, S., Yamamoto, K., Tanabe, T. and Inoue, K. (1993) Primary structure of alpha-tocopherol transfer protein from rat liver. Homology with cellular retinaldehyde-binding protein. *J Biol Chem* **268**, 17705-17710
- 93 Meier, R., Tomizaki, T., Schulze-Briesse, C., Baumann, U. and Stocker, A. (2003) The molecular basis of vitamin E retention: structure of human alpha-tocopherol transfer protein. *J Mol Biol* **331**, 725-734
- 94 Min, K. C., Kovall, R. A. and Hendrickson, W. A. (2003) Crystal structure of human alpha-tocopherol transfer protein bound to its ligand: implications for ataxia with vitamin E deficiency. *Proc Natl Acad Sci U S A* **100**, 14713-14718
- 95 Stocker, A., Tomizaki, T., Schulze-Briesse, C. and Baumann, U. (2002) Crystal structure of the human supernatant protein factor. *Structure* **10**, 1533-1540

- 96 Sha, B., Phillips, S. E., Bankaitis, V. A. and Luo, M. (1998) Crystal structure of the *Saccharomyces cerevisiae* phosphatidylinositol-transfer protein. *Nature* **391**, 506-510
- 97 Schaaf, G., Ortlund, E. A., Tyeryar, K. R., Mousley, C. J., Ile, K. E., Garrett, T. A., Ren, J., Woolls, M. J., Raetz, C. R., Redinbo, M. R. and Bankaitis, V. A. (2008) Functional anatomy of phospholipid binding and regulation of phosphoinositide homeostasis by proteins of the sec14 superfamily. *Mol Cell* **29**, 191-206
- 98 Arita, M., Nomura, K., Arai, H. and Inoue, K. (1997) alpha-tocopherol transfer protein stimulates the secretion of alpha-tocopherol from a cultured liver cell line through a brefeldin A-insensitive pathway. *Proc Natl Acad Sci U S A* **94**, 12437-12441
- 99 Qian, J., Morley, S., Wilson, K., Nava, P., Atkinson, J. and Manor, D. (2005) Intracellular trafficking of vitamin E in hepatocytes: the role of tocopherol transfer protein. *J Lipid Res* **46**, 2072-2082
- 100 Horiguchi, M., Arita, M., Kaempf-Rotzoll, D. E., Tsujimoto, M., Inoue, K. and Arai, H. (2003) pH-dependent translocation of alpha-tocopherol transfer protein (alpha-TTP) between hepatic cytosol and late endosomes. *Genes Cells* **8**, 789-800
- 101 Usuki, F. and Maruyama, K. (2000) Ataxia caused by mutations in the alpha-tocopherol transfer protein gene. *J Neurol Neurosurg Psychiatry* **69**, 254-256
- 102 Gotoda, T., Arita, M., Arai, H., Inoue, K., Yokota, T., Fukuo, Y., Yazaki, Y. and Yamada, N. (1995) Adult-onset spinocerebellar dysfunction caused by a mutation in the gene for the alpha-tocopherol-transfer protein. *N Engl J Med* **333**, 1313-1318
- 103 Kono, S., Otsuji, A., Hattori, H., Shirakawa, K., Suzuki, H. and Miyajima, H. (2009) Ataxia with vitamin E deficiency with a mutation in a phospholipid transfer protein gene. *J Neurol* **256**, 1180-1181
- 104 Doerflinger, N., Linder, C., Ouahchi, K., Gyapay, G., Weissenbach, J., Le Paslier, D., Rigault, P., Belal, S., Ben Hamida, C., Hentati, F. and et al. (1995) Ataxia with vitamin E deficiency: refinement of genetic localization and analysis of linkage disequilibrium by using new markers in 14 families. *Am J Hum Genet* **56**, 1116-1124
- 105 Ingold, K. U., Webb, A. C., Witter, D., Burton, G. W., Metcalfe, T. A. and Muller, D. P. (1987) Vitamin E remains the major lipid-soluble, chain-breaking antioxidant in human plasma even in individuals suffering severe vitamin E deficiency. *Arch Biochem Biophys* **259**, 224-225

- 106 Schuelke, M., Elsner, A., Finckh, B., Kohlschutter, A., Hubner, C. and Brigelius-Flohe, R. (2000) Urinary alpha-tocopherol metabolites in alpha-tocopherol transfer protein-deficient patients. *J Lipid Res* **41**, 1543-1551
- 107 Marzouki, N., Benomar, A., Yahyaoui, M., Birouk, N., Elouazzani, M., Chkili, T. and Benlemlih, M. (2005) Vitamin E deficiency ataxia with (744 del A) mutation on alpha-TTP gene: genetic and clinical peculiarities in Moroccan patients. *Eur J Med Genet* **48**, 21-28
- 108 Ben Hamida, C., Doerflinger, N., Belal, S., Linder, C., Reutenauer, L., Dib, C., Gyapay, G., Vignal, A., Le Paslier, D., Cohen, D. and et al. (1993) Localization of Friedreich ataxia phenotype with selective vitamin E deficiency to chromosome 8q by homozygosity mapping. *Nat Genet* **5**, 195-200
- 109 Arita, M., Sato, Y., Miyata, A., Tanabe, T., Takahashi, E., Kayden, H. J., Arai, H. and Inoue, K. (1995) Human alpha-tocopherol transfer protein: cDNA cloning, expression and chromosomal localization. *Biochem J* **306** (Pt 2), 437-443
- 110 Burck, U., Goebel, H. H., Kuhlendahl, H. D., Meier, C. and Goebel, K. M. (1981) Neuromyopathy and vitamin E deficiency in man. *Neuropediatrics* **12**, 267-278
- 111 Morley, S., Panagabko, C., Shineman, D., Mani, B., Stocker, A., Atkinson, J. and Manor, D. (2004) Molecular determinants of heritable vitamin E deficiency. *Biochemistry* **43**, 4143-4149
- 112 Shimohata, T., Date, H., Ishiguro, H., Suzuki, T., Takano, H., Tanaka, H., Tsuji, S. and Hirota, K. (1998) Ataxia with isolated vitamin E deficiency and retinitis pigmentosa. *Ann Neurol* **43**, 273
- 113 Qian, J., Atkinson, J. and Manor, D. (2006) Biochemical consequences of heritable mutations in the alpha-tocopherol transfer protein. *Biochemistry* **45**, 8236-8242
- 114 Morley, S., Cecchini, M., Zhang, W., Virgulti, A., Noy, N., Atkinson, J. and Manor, D. (2008) Mechanisms of ligand transfer by the hepatic tocopherol transfer protein. *J Biol Chem* **283**, 17797-17804
- 115 Gohil, K., Oommen, S., Vasu, V. T., Aung, H. H. and Cross, C. E. (2007) Tocopherol transfer protein deficiency modifies nuclear receptor transcriptional networks in lungs: modulation by cigarette smoke in vivo. *Mol Aspects Med* **28**, 453-480
- 116 Gohil, K., Oommen, S., Quach, H. T., Vasu, V. T., Aung, H. H., Schock, B., Cross, C. E. and Vatassery, G. T. (2008) Mice lacking alpha-tocopherol transfer protein gene have severe alpha-tocopherol deficiency in multiple regions of the central nervous system. *Brain Res* **1201**, 167-176

- 117 Jishage, K., Arita, M., Igarashi, K., Iwata, T., Watanabe, M., Ogawa, M., Ueda, O., Kamada, N., Inoue, K., Arai, H. and Suzuki, H. (2001) Alpha-tocopherol transfer protein is important for the normal development of placental labyrinthine trophoblasts in mice. *J Biol Chem* **276**, 1669-1672
- 118 Ren, Y. R., Nishida, Y., Yoshimi, K., Yasuda, T., Jishage, K., Uchihara, T., Yokota, T., Mizuno, Y. and Mochizuki, H. (2006) Genetic vitamin E deficiency does not affect MPTP susceptibility in the mouse brain. *J Neurochem* **98**, 1810-1816
- 119 Bateman, A., Birney, E., Cerruti, L., Durbin, R., Eddy, S. R., Griffiths-Jones, S., Howe, K. L., Marshall, M. and Sonnhammer, E. L. (2002) The Pfam protein families database. *Nucleic Acids Res* **30**, 276-280
- 120 Saito, K., Tautz, L. and Mustelin, T. (2007) The lipid-binding SEC14 domain. *Biochim Biophys Acta* **1771**, 719-726
- 121 Futterman, S. and Saari, J. C. (1977) Occurrence of 11-cis-retinal-binding protein restricted to the retina. *Invest Ophthalmol Vis Sci* **16**, 768-771
- 122 Saari, J. C., Nawrot, M., Stenkamp, R. E., Teller, D. C. and Garwin, G. G. (2009) Release of 11-cis-retinal from cellular retinaldehyde-binding protein by acidic lipids. *Mol Vis* **15**, 844-854
- 123 Ryan, M. M., Temple, B. R., Phillips, S. E. and Bankaitis, V. A. (2007) Conformational dynamics of the major yeast phosphatidylinositol transfer protein sec14p: insight into the mechanisms of phospholipid exchange and diseases of sec14p-like protein deficiencies. *Mol Biol Cell* **18**, 1928-1942
- 124 Singh, D. K., Mokashi, V., Elmore, C. L. and Porter, T. D. (2003) Phosphorylation of supernatant protein factor enhances its ability to stimulate microsomal squalene monooxygenase. *J Biol Chem* **278**, 5646-5651
- 125 Anantharaman, V. and Aravind, L. (2002) The GOLD domain, a novel protein module involved in Golgi function and secretion. *Genome Biol* **3**, research0023
- 126 Hsu, K. T. and Storch, J. (1996) Fatty acid transfer from liver and intestinal fatty acid-binding proteins to membranes occurs by different mechanisms. *J Biol Chem* **271**, 13317-13323
- 127 Storch, J. and McDermott, L. (2009) Structural and functional analysis of fatty acid-binding proteins. *J Lipid Res* **50 Suppl**, S126-131

- 128 Thumser, A. E. and Storch, J. (2000) Liver and intestinal fatty acid-binding proteins obtain fatty acids from phospholipid membranes by different mechanisms. *J Lipid Res* **41**, 647-656
- 129 Wootan, M. G. and Storch, J. (1994) Regulation of fluorescent fatty acid transfer from adipocyte and heart fatty acid binding proteins by acceptor membrane lipid composition and structure. *J Biol Chem* **269**, 10517-10523
- 130 Wootan, M. G., Bernlohr, D. A. and Storch, J. (1993) Mechanism of fluorescent fatty acid transfer from adipocyte fatty acid binding protein to membranes. *Biochemistry* **32**, 8622-8627
- 131 Herr, F. M., Matarese, V., Bernlohr, D. A. and Storch, J. (1995) Surface lysine residues modulate the collisional transfer of fatty acid from adipocyte fatty acid binding protein to membranes. *Biochemistry* **34**, 11840-11845
- 132 Storch, J. and Kleinfeld, A. M. (1986) Transfer of long-chain fluorescent free fatty acids between unilamellar vesicles. *Biochemistry* **25**, 1717-1726
- 133 Kim, H. K. and Storch, J. (1992) Free fatty acid transfer from rat liver fatty acid-binding protein to phospholipid vesicles. Effect of ligand and solution properties. *J Biol Chem* **267**, 77-82
- 134 Cheruku, S. R., Xu, Z., Dutia, R., Lobel, P. and Storch, J. (2006) Mechanism of cholesterol transfer from the Niemann-Pick type C2 protein to model membranes supports a role in lysosomal cholesterol transport. *J Biol Chem* **281**, 31594-31604
- 135 Lund-Katz, S., Hammerschlag, B. and Phillips, M. C. (1982) Kinetics and mechanism of free cholesterol exchange between human serum high- and low-density lipoproteins. *Biochemistry* **21**, 2964-2969
- 136 Lange, Y., Molinaro, A. L., Chauncey, T. R. and Steck, T. L. (1983) On the mechanism of transfer of cholesterol between human erythrocytes and plasma. *J Biol Chem* **258**, 6920-6926
- 137 Thompson, J., Winter, N., Terwey, D., Bratt, J. and Banaszak, L. (1997) The crystal structure of the liver fatty acid-binding protein. A complex with two bound oleates. *J Biol Chem* **272**, 7140-7150
- 138 Storch, J. and Thumser, A. E. (2000) The fatty acid transport function of fatty acid-binding proteins. *Biochim Biophys Acta* **1486**, 28-44
- 139 McMahon, H. T. and Gallop, J. L. (2005) Membrane curvature and mechanisms of dynamic cell membrane remodelling. *Nature* **438**, 590-596

- 140 Taylor, K. M. and Roseman, M. A. (1995) Effect of cholesterol, fatty acyl chain composition, and bilayer curvature on the interaction of cytochrome b5 with liposomes of phosphatidylcholines. *Biochemistry* **34**, 3841-3850
- 141 Chao, H., Martin, G. G., Russell, W. K., Waghela, S. D., Russell, D. H., Schroeder, F. and Kier, A. B. (2002) Membrane charge and curvature determine interaction with acyl-CoA binding protein (ACBP) and fatty acyl-CoA targeting. *Biochemistry* **41**, 10540-10553
- 142 Antonny, B., Bigay, J., Casella, J. F., Drin, G., Mesmin, B. and Gounon, P. (2005) Membrane curvature and the control of GTP hydrolysis in Arf1 during COPI vesicle formation. *Biochem Soc Trans* **33**, 619-622
- 143 Mesmin, B., Drin, G., Levi, S., Rawet, M., Cassel, D., Bigay, J. and Antonny, B. (2007) Two lipid-packing sensor motifs contribute to the sensitivity of ArfGAP1 to membrane curvature. *Biochemistry* **46**, 1779-1790
- 144 Davidson, W. S., Jonas, A., Clayton, D. F. and George, J. M. (1998) Stabilization of alpha-synuclein secondary structure upon binding to synthetic membranes. *J Biol Chem* **273**, 9443-9449
- 145 Nylund, M., Fortelius, C., Palonen, E. K., Molotkovsky, J. G. and Mattjus, P. (2007) Membrane curvature effects on glycolipid transfer protein activity. *Langmuir* **23**, 11726-11733
- 146 Fischer, T., Lu, L., Haigler, H. T. and Langen, R. (2007) Annexin B12 is a sensor of membrane curvature and undergoes major curvature-dependent structural changes. *J Biol Chem* **282**, 9996-10004
- 147 Brewer, J. M., Pollock, K. G., Tetley, L. and Russell, D. G. (2004) Vesicle size influences the trafficking, processing, and presentation of antigens in lipid vesicles. *J Immunol* **173**, 6143-6150
- 148 Matsuzaki, K., Sugishita, K., Ishibe, N., Ueha, M., Nakata, S., Miyajima, K. and Epand, R. M. (1998) Relationship of membrane curvature to the formation of pores by magainin 2. *Biochemistry* **37**, 11856-11863
- 149 Lomize, A. L., Pogozheva, I. D., Lomize, M. A. and Mosberg, H. I. (2006) Positioning of proteins in membranes: a computational approach. *Protein Sci* **15**, 1318-1333
- 150 Lomize, M. A., Lomize, A. L., Pogozheva, I. D. and Mosberg, H. I. (2006) OPM: orientations of proteins in membranes database. *Bioinformatics* **22**, 623-625

- 151 Panagabko, C., Morley, S., Neely, S., Lei, H., Manor, D. and Atkinson, J. (2002) Expression and refolding of recombinant human alpha-tocopherol transfer protein capable of specific alpha-tocopherol binding. *Protein Expr Purif* **24**, 395-403
- 152 Spencer, R. P. and Bow, T. M. (1964) In Vitro Transport of Radiolabeled Vitamins by the Small Intestine. *J Nucl Med* **5**, 251-258
- 153 Kitabchi, A. E. and Wimalasena, J. (1982) Specific binding sites for D-alpha-tocopherol on human erythrocytes. *Biochim Biophys Acta* **684**, 200-206
- 154 Nava, P., Cecchini, M., Chirico, S., Gordon, H., Morley, S., Manor, D. and Atkinson, J. (2006) Preparation of fluorescent tocopherols for use in protein binding and localization with the alpha-tocopherol transfer protein. *Bioorg Med Chem* **14**, 3721-3736
- 155 Huijbregts, R. P., de Kroon, A. I. and de Kruijff, B. (1996) Rapid transmembrane movement of C6-NBD-labeled phospholipids across the inner membrane of *Escherichia coli*. *Biochim Biophys Acta* **1280**, 41-50
- 156 Kol, M. A., van Laak, A. N., Rijkers, D. T., Killian, J. A., de Kroon, A. I. and de Kruijff, B. (2003) Phospholipid flop induced by transmembrane peptides in model membranes is modulated by lipid composition. *Biochemistry* **42**, 231-237
- 157 Lee, J. and Lentz, B. R. (1997) Evolution of lipidic structures during model membrane fusion and the relation of this process to cell membrane fusion. *Biochemistry* **36**, 6251-6259
- 158 McIntyre, J. C. and Sleight, R. G. (1991) Fluorescence assay for phospholipid membrane asymmetry. *Biochemistry* **30**, 11819-11827
- 159 Lehrer, S. S. (1971) Solute perturbation of protein fluorescence. The quenching of the tryptophyl fluorescence of model compounds and of lysozyme by iodide ion. *Biochemistry* **10**, 3254-3263
- 160 Pagano, R. E., Martin, O. C., Schroit, A. J. and Struck, D. K. (1981) Formation of asymmetric phospholipid membranes via spontaneous transfer of fluorescent lipid analogues between vesicle populations. *Biochemistry* **20**, 4920-4927
- 161 Nichols, J. W. and Pagano, R. E. (1982) Use of resonance energy transfer to study the kinetics of amphiphile transfer between vesicles. *Biochemistry* **21**, 1720-1726
- 162 Arvinte, T. and Hildenbrand, K. (1984) N-NBD-L-alpha-dilauroylphosphatidylethanolamine. A new fluorescent probe to study spontaneous lipid transfer. *Biochim Biophys Acta* **775**, 86-94

- 163 Morley, S., Cross, V., Cecchini, M., Nava, P., Atkinson, J. and Manor, D. (2006) Utility of a fluorescent vitamin E analogue as a probe for tocopherol transfer protein activity. *Biochemistry* **45**, 1075-1081
- 164 Huang, C. and Thompson, T. E. (1965) Properties of lipid bilayer membranes separating two aqueous phases: determination of membrane thickness. *J Mol Biol* **13**, 183-193
- 165 Kobayashi, T., Stang, E., Fang, K. S., de Moerloose, P., Parton, R. G. and Gruenberg, J. (1998) A lipid associated with the antiphospholipid syndrome regulates endosome structure and function. *Nature* **392**, 193-197
- 166 Matsuo, H., Chevallier, J., Mayran, N., Le Blanc, I., Ferguson, C., Faure, J., Blanc, N. S., Matile, S., Dubochet, J., Sadoul, R., Parton, R. G., Vilbois, F. and Gruenberg, J. (2004) Role of LBPA and Alix in multivesicular liposome formation and endosome organization. *Science* **303**, 531-534
- 167 Xu, Z., Farver, W., Kodukula, S. and Storch, J. (2008) Regulation of sterol transport between membranes and NPC2. *Biochemistry* **47**, 11134-11143
- 168 Kobayashi, T., Beuchat, M. H., Chevallier, J., Makino, A., Mayran, N., Escola, J. M., Lebrand, C., Cosson, P., Kobayashi, T. and Gruenberg, J. (2002) Separation and characterization of late endosomal membrane domains. *J Biol Chem* **277**, 32157-32164
- 169 LaBrake, C. C. and Fung, L. W. (1998) Sick hemoglobin is more fusogenic than normal hemoglobin at physiological pH and ionic strength conditions. *Biochim Biophys Acta* **1406**, 152-161
- 170 Massey, J. B. (2001) Interfacial properties of phosphatidylcholine bilayers containing vitamin E derivatives. *Chem Phys Lipids* **109**, 157-174
- 171 Basle, A., Rummel, G., Storici, P., Rosenbusch, J. P. and Schirmer, T. (2006) Crystal structure of osmoporin OmpC from *E. coli* at 2.0 Å. *J Mol Biol* **362**, 933-942
- 172 Veeraragavan, K. (1989) Studies on two major contaminating proteins of the cytoplasmic inclusion bodies in *Escherichia coli*. *FEMS Microbiol Lett* **52**, 149-152
- 173 Jeong, K. J. and Lee, S. Y. (2002) Excretion of human beta-endorphin into culture medium by using outer membrane protein F as a fusion partner in recombinant *Escherichia coli*. *Appl Environ Microbiol* **68**, 4979-4985

- 174 Lopez, M. L., Aguilera-Arzo, M., Aguilera, V. M. and Alcaraz, A. (2009) Ion selectivity of a biological channel at high concentration ratio: insights on small ion diffusion and binding. *J Phys Chem B* **113**, 8745-8751
- 175 Yamashita, E., Zhalnina, M. V., Zakharov, S. D., Sharma, O. and Cramer, W. A. (2008) Crystal structures of the OmpF porin: function in a colicin translocon. *Embo J* **27**, 2171-2180
- 176 Jenny, R. J., Mann, K. G. and Lundblad, R. L. (2003) A critical review of the methods for cleavage of fusion proteins with thrombin and factor Xa. *Protein Expr Purif* **31**, 1-11
- 177 Falomir-Lockhart, L. J., Laborde, L., Kahn, P. C., Storch, J. and Corsico, B. (2006) Protein-membrane interaction and fatty acid transfer from intestinal fatty acid-binding protein to membranes. Support for a multistep process. *J Biol Chem* **281**, 13979-13989
- 178 Liou, H. L. and Storch, J. (2001) Role of surface lysine residues of adipocyte fatty acid-binding protein in fatty acid transfer to phospholipid vesicles. *Biochemistry* **40**, 6475-6485
- 179 Smith, E. R. and Storch, J. (1999) The adipocyte fatty acid-binding protein binds to membranes by electrostatic interactions. *J Biol Chem* **274**, 35325-35330
- 180 Herr, F. M., Aronson, J. and Storch, J. (1996) Role of portal region lysine residues in electrostatic interactions between heart fatty acid binding protein and phospholipid membranes. *Biochemistry* **35**, 1296-1303
- 181 Herr, F. M., Li, E., Weinberg, R. B., Cook, V. R. and Storch, J. (1999) Differential mechanisms of retinoid transfer from cellular retinol binding proteins types I and II to phospholipid membranes. *J Biol Chem* **274**, 9556-9563
- 182 Huang, C. (1969) Studies on phosphatidylcholine vesicles. Formation and physical characteristics. *Biochemistry* **8**, 344-352
- 183 Szoka, F., Jr. and Papahadjopoulos, D. (1980) Comparative properties and methods of preparation of lipid vesicles (liposomes). *Annu Rev Biophys Bioeng* **9**, 467-508
- 184 Konigsberg, P. J., Debrick, J. E., Pawlowski, T. J. and Staerz, U. D. (1999) Liposome encapsulated aurothiomalate reduces collagen-induced arthritis in DBA/1J mice. *Biochim Biophys Acta* **1421**, 149-162
- 185 Pencer, J., White, G. F. and Hallett, F. R. (2001) Osmotically induced shape changes of large unilamellar vesicles measured by dynamic light scattering. *Biophys J* **81**, 2716-2728

- 186 Komatsu, H., Guy, P. T. and Rowe, E. S. (1993) Effect of unilamellar vesicle size on ethanol-induced interdigitation in dipalmitoylphosphatidylcholine. *Chem Phys Lipids* **65**, 11-21
- 187 Chiu, S. W., Jakobsson, E., Subramaniam, S. and Scott, H. L. (1999) Combined monte carlo and molecular dynamics simulation of fully hydrated dioleoyl and palmitoyl-oleoyl phosphatidylcholine lipid bilayers. *Biophys J* **77**, 2462-2469
- 188 Swann, M. J., Peel, L. L., Carrington, S. and Freeman, N. J. (2004) Dual-polarization interferometry: an analytical technique to measure changes in protein structure in real time, to determine the stoichiometry of binding events, and to differentiate between specific and nonspecific interactions. *Anal Biochem* **329**, 190-198
- 189 Thompsett, A. R. and Brown, D. R. (2007) Dual polarisation interferometry analysis of copper binding to the prion protein: evidence for two folding states. *Biochim Biophys Acta* **1774**, 920-927
- 190 Qian, J., Wilson, K., Nava, P., Morley, S., Atkinson, J. and Manor, D. (2004) Intracellular localization of alpha-tocopherol transfer protein and alpha-tocopherol. *Ann N Y Acad Sci* **1031**, 330-331
- 191 Kobayashi, T., Beuchat, M. H., Lindsay, M., Frias, S., Palmiter, R. D., Sakuraba, H., Parton, R. G. and Gruenberg, J. (1999) Late endosomal membranes rich in lysobisphosphatidic acid regulate cholesterol transport. *Nat Cell Biol* **1**, 113-118
- 192 Sleight, R. G. and Pagano, R. E. (1984) Transport of a fluorescent phosphatidylcholine analog from the plasma membrane to the Golgi apparatus. *J Cell Biol* **99**, 742-751
- 193 Elvington, S. M. and Nichols, J. W. (2007) Spontaneous, intervesicular transfer rates of fluorescent, acyl chain-labeled phosphatidylcholine analogs. *Biochim Biophys Acta* **1768**, 502-508
- 194 Huster, D., Muller, P., Arnold, K. and Herrmann, A. (2001) Dynamics of membrane penetration of the fluorescent 7-nitrobenz-2-oxa-1,3-diazol-4-yl (NBD) group attached to an acyl chain of phosphatidylcholine. *Biophys J* **80**, 822-831
- 195 Cowan, S. W., Schirmer, T., Rummel, G., Steiert, M., Ghosh, R., Pauptit, R. A., Jansonius, J. N. and Rosenbusch, J. P. (1992) Crystal structures explain functional properties of two E. coli porins. *Nature* **358**, 727-733
- 196 John, K., Kubelt, J., Muller, P., Wustner, D. and Herrmann, A. (2002) Rapid transbilayer movement of the fluorescent sterol dehydroergosterol in lipid membranes. *Biophys J* **83**, 1525-1534

- 197 Lapinski, M. M., Castro-Forero, A., Greiner, A. J., Ofoli, R. Y. and Blanchard, G. J. (2007) Comparison of liposomes formed by sonication and extrusion: rotational and translational diffusion of an embedded chromophore. *Langmuir* **23**, 11677-11683
- 198 Zhang, W. X., Frahm, G., Morley, S., Manor, D. and Atkinson, J. (2009) Effect of bilayer phospholipid composition and curvature on ligand transfer by the alpha-tocopherol transfer protein. *Lipids* **44**, 631-641
- 199 Crouthamel, M., Thiagarajan, M. M., Evanko, D. S. and Wedegaertner, P. B. (2008) N-terminal polybasic motifs are required for plasma membrane localization of Galpha(s) and Galpha(q). *Cell Signal* **20**, 1900-1910
- 200 Heo, W. D., Inoue, T., Park, W. S., Kim, M. L., Park, B. O., Wandless, T. J. and Meyer, T. (2006) PI(3,4,5)P3 and PI(4,5)P2 lipids target proteins with polybasic clusters to the plasma membrane. *Science* **314**, 1458-1461
- 201 Wang, J., Gambhir, A., Hangyas-Mihalyne, G., Murray, D., Golebiewska, U. and McLaughlin, S. (2002) Lateral sequestration of phosphatidylinositol 4,5-bisphosphate by the basic effector domain of myristoylated alanine-rich C kinase substrate is due to nonspecific electrostatic interactions. *J Biol Chem* **277**, 34401-34412
- 202 Kutateladze, T. G. (2007) Mechanistic similarities in docking of the FYVE and PX domains to phosphatidylinositol 3-phosphate containing membranes. *Prog Lipid Res* **46**, 315-327
- 203 Kutateladze, T. G., Capelluto, D. G., Ferguson, C. G., Cheever, M. L., Kutateladze, A. G., Prestwich, G. D. and Overduin, M. (2004) Multivalent mechanism of membrane insertion by the FYVE domain. *J Biol Chem* **279**, 3050-3057
- 204 Dowler, S., Currie, R. A., Campbell, D. G., Deak, M., Kular, G., Downes, C. P. and Alessi, D. R. (2000) Identification of pleckstrin-homology-domain-containing proteins with novel phosphoinositide-binding specificities. *Biochem J* **351**, 19-31
- 205 Cheever, M. L., Kutateladze, T. G. and Overduin, M. (2006) Increased mobility in the membrane targeting PX domain induced by phosphatidylinositol 3-phosphate. *Protein Sci* **15**, 1873-1882
- 206 Davies, J. K., Thumser, A. E. and Wilton, D. C. (1999) Binding of recombinant rat liver fatty acid-binding protein to small anionic phospholipid vesicles results in ligand release: a model for interfacial binding and fatty acid targeting. *Biochemistry* **38**, 16932-16940

- 207 Huang, H., Ball, J. M., Billheimer, J. T. and Schroeder, F. (1999) Interaction of the N-terminus of sterol carrier protein 2 with membranes: role of membrane curvature. *Biochem J* **344 Pt 2**, 593-603
- 208 Rao, C. S., Lin, X., Pike, H. M., Molotkovsky, J. G. and Brown, R. E. (2004) Glycolipid transfer protein mediated transfer of glycosphingolipids between membranes: a model for action based on kinetic and thermodynamic analyses. *Biochemistry* **43**, 13805-13815
- 209 Liou, H. L., Kahn, P. C. and Storch, J. (2002) Role of the helical domain in fatty acid transfer from adipocyte and heart fatty acid-binding proteins to membranes: analysis of chimeric proteins. *J Biol Chem* **277**, 1806-1815
- 210 Corsico, B., Franchini, G. R., Hsu, K. T. and Storch, J. (2005) Fatty acid transfer from intestinal fatty acid binding protein to membranes: electrostatic and hydrophobic interactions. *J Lipid Res* **46**, 1765-1772
- 211 Rand, R. P. and Sengupta, S. (1972) Cardiolipin forms hexagonal structures with divalent cations. *Biochim Biophys Acta* **255**, 484-492
- 212 Ortiz, A., Killian, J. A., Verkleij, A. J. and Wilschut, J. (1999) Membrane fusion and the lamellar-to-inverted-hexagonal phase transition in cardiolipin vesicle systems induced by divalent cations. *Biophys J* **77**, 2003-2014
- 213 Ingebrigtsen, L. and Brandl, M. (2002) Determination of the size distribution of liposomes by SEC fractionation, and PCS analysis and enzymatic assay of lipid content. *AAPS PharmSciTech* **3**, E7
- 214 Brumm, T., Jorgensen, K., Mouritsen, O. G. and Bayerl, T. M. (1996) The effect of increasing membrane curvature on the phase transition and mixing behavior of a dimyristoyl-sn-glycero-3-phosphatidylcholine/ distearoyl-sn-glycero-3-phosphatidylcholine lipid mixture as studied by Fourier transform infrared spectroscopy and differential scanning calorimetry. *Biophys J* **70**, 1373-1379
- 215 Pol, A. and Enrich, C. (1997) Membrane transport in rat liver endocytic pathways: preparation, biochemical properties and functional roles of hepatic endosomes. *Electrophoresis* **18**, 2548-2557
- 216 Frederick, T. E., Chebukati, J. N., Mair, C. E., Goff, P. C. and Fanucci, G. E. (2009) Bis(monoacylglycero)phosphate forms stable small lamellar vesicle structures: insights into vesicular body formation in endosomes. *Biophys J* **96**, 1847-1855
- 217 van der Goot, F. G. and Gruenberg, J. (2006) Intra-endosomal membrane traffic. *Trends Cell Biol* **16**, 514-521

- 218 Shichiri, M., Takanezawa, Y., Rotzoll, D. E., Yoshida, Y., Kokubu, T., Ueda, K., Tamai, H. and Arai, H. (2009) ATP-Binding cassette transporter A1 is involved in hepatic alpha-tocopherol secretion. *J Nutr Biochem*
- 219 Oram, J. F., Vaughan, A. M. and Stocker, R. (2001) ATP-binding cassette transporter A1 mediates cellular secretion of alpha-tocopherol. *J Biol Chem* **276**, 39898-39902
- 220 Neufeld, E. B., Remaley, A. T., Demosky, S. J., Stonik, J. A., Cooney, A. M., Comly, M., Dwyer, N. K., Zhang, M., Blanchette-Mackie, J., Santamarina-Fojo, S. and Brewer, H. B., Jr. (2001) Cellular localization and trafficking of the human ABCA1 transporter. *J Biol Chem* **276**, 27584-27590
- 221 Neufeld, E. B., Stonik, J. A., Demosky, S. J., Jr., Knapper, C. L., Combs, C. A., Cooney, A., Comly, M., Dwyer, N., Blanchette-Mackie, J., Remaley, A. T., Santamarina-Fojo, S. and Brewer, H. B., Jr. (2004) The ABCA1 transporter modulates late endocytic trafficking: insights from the correction of the genetic defect in Tangier disease. *J Biol Chem* **279**, 15571-15578
- 222 Bradford, M. M. (1976) A rapid and sensitive method for the quantitation of microgram quantities of protein utilizing the principle of protein-dye binding. *Anal Biochem* **72**, 248-254
- 223 Commoner, B. and Lipkin, D. (1949) The Application of the Beer-Lambert Law to Optically Anisotropic Systems. *Science* **110**, 41-43
- 224 Laemmli, U. K. (1970) Cleavage of structural proteins during the assembly of the head of bacteriophage T4. *Nature* **227**, 680-685
- 225 Dusa, A., Kaylor, J., Edridge, S., Bodner, N., Hong, D. P. and Fink, A. L. (2006) Characterization of oligomers during alpha-synuclein aggregation using intrinsic tryptophan fluorescence. *Biochemistry* **45**, 2752-2760
- 226 Webster, J. and Oxley, D. *Peptide Mass Fingerprinting*
- 227 Bligh, E. G. and Dyer, W. J. (1959) A rapid method of total lipid extraction and purification. *Can J Biochem Physiol* **37**, 911-917
- 228 Schroeder, F., Barenholz, Y., Gratton, E. and Thompson, T. E. (1987) A fluorescence study of dehydroergosterol in phosphatidylcholine bilayer vesicles. *Biochemistry* **26**, 2441-2448
- 229 Rouser, G., Siakotos, A. N. and Fleischer, S. (1966) Quantitative analysis of phospholipids by thin-layer chromatography and phosphorus analysis of spots. *Lipids* **1**, 85-86

- 230 Massey, J. B., Bick, D. H. and Pownall, H. J. (1997) Spontaneous transfer of monoacyl amphiphiles between lipid and protein surfaces. *Biophys J* **72**, 1732-1743
- 231 Terry, C. J., Popplewell, J. F., Swann, M. J., Freeman, N. J. and Fernig, D. G. (2006) Characterisation of membrane mimetics on a dual polarisation interferometer. *Biosens Bioelectron* **22**, 627-632
- 232 Cross, G. H., Reeves, A. A., Brand, S., Popplewell, J. F., Peel, L. L., Swann, M. J. and Freeman, N. J. (2003) A new quantitative optical biosensor for protein characterisation. *Biosens Bioelectron* **19**, 383-390

7. APPENDIX I

MALDI-TOF Spectrum Analysis Report

Note: Individual ions scores > 48 indicate identity or extensive homology (p<0.05).

1.) Analysis of α -TTP control digest:

Query Peptide	Observed	Mr(expt)	Mr(calc)	Score	Rank
R.EAGVPLAPLPLTDSFLLR.F	1908.9569	1907.9496	1908.0720	65	1

Best match: S54352 Mass: 31844 Score: 72.09 human alpha-tocopherol transfer protein

Matched peptide is underlined in **Bold**

```

1 MAEARSQPSA GPQLNALPDH SPLLPGLAA LRRRAREAGV PLAPLPLTDS FLLRFLRARD
61 FDLDLAWRLK KNYKWRAC PEISADLHPR SIIGLLKAGY HGVLRSDPT GSKVLIYRIA
121 HWDPKVFTAY DVFRVSLITS ELIVQEVETQ RNGIKAIFDL EGWQFSHAFQ ITPSVAKKIA
181 AVLTDSPFLK VRGIHLINP VIFHAVFSMI KPFLTEKIKE RIHMHGNNYK QSLQHFQDI
241 LPLEYGGEF SMEDICQEWTFIMKSEDYL SSISESIQ

```

Peak	Mass	Intensity
1	112.280	4437.933
3	175.328	20055.810
9	258.301	6171.498
11	282.377	12015.834
12	288.369	2021.502
16	329.347	3450.440
19	357.336	4467.962
26	454.342	1832.846
31	539.433	905.425
32	548.471	2536.627
33	567.442	578.208
34	610.337	436.940
37	635.515	19844.868
38	638.449	1391.773
45	750.553	2118.825
49	851.563	748.172
55	1061.708	1480.959
62	1271.951	869.838
64	1343.021	543.055
65	1456.024	228.629
66	1553.068	380.997
68	1709.241	217.056
70	1780.247	480.779
75	1891.583	2288.227
76	1908.948	9052.963

Calculated Masses for the peptide digest: **EAGVPLAPLPLTDSFLLR**

N-Term	Ion	a	b	y	C-Term	Ion
1	E	102.055	130.050	175.119	18	R
2	A	173.092	201.087	288.203	17	L
3	G	230.114	258.108	401.287	16	L
4	V	329.182	357.1777	548.355	15	F
5	P	426.235	454.230	635.388	14	S
6	L	539.319	567.314	750.414	13	D
7	A	610.356	638.351	851.462	12	T
8	P	707.409	735.404	964.546	11	L
9	L	820.493	848.488	1061.599	10	P
10	P	917.545	945.540	1174.683	9	L
11	L	1030.630	1058.624	1271.736	8	P
12	T	1131.677	1159.672	1342.773	7	A
13	D	1246.704	1274.699	1455.857	6	L
14	S	1333.736	1361.731	1552.910	5	P
15	F	1480.805	1508.800	1651.978	4	V
16	L	1593.889	1621.884	1709.000	3	G
17	L	1706.973	1734.968	1780.037	2	A
18	R	1863.074	1891.069	1909.079	1	E

2.) Analysis of 39 kD *E. coli* unknown digest:

Best match: MMECF Mass: 39309 Score: 89

outer membrane porin ompF precursor - Escherichia coli (strain K-12)

Query Peptide	Observed	Mr(expt)	Mr(calc)	Score	Rank
K.YDANNIYLAANYGETR.N	1847.9950	1846.9877	1846.8485	89	1

Matched peptides are underlined in **Bold**

```

1  MMKRNILAVI VPALLVAGTA NAAEIYNKDG NKVDLYGKAV GLHYFSKGNG ENSYGGNGDM
61 TYARLGFKGE TQINSDLTGY GQWEYNFQGN NSEGADAQTG NKTRLAFAGL KYADVGSFDY
121 GRNYGVVYDA LGYTDMLPEF GGDTAYSDDF FVGRVGGVAT YRNSNFFGLV DGLNFAVQYL
181 GKNERDTARR SNGDGVGGSI SYEYEGFGIV GAYGAADRTN LQEESSLGKG KKAEQWATGL
241 KYDANNIYLA ANYGETRNAT PITNKFTNTS GFANKTQDVL LVAQYQFDFG LRPSIAYTKS
301 KAKDVEGIGD VDLVNYFEVG ATYYFNKNMS TYVDYIINQI DSDNKLGVGS DDTVAVGIVY
361 QF

```

Calculated Masses for the peptide digest: **KYDANNIYLAANYGETRN**

N-Term	Ion	a	b	y	C-Term	Ion
1	Y	136.076	164.071	175.119	16	R
2	D	251.103	279.098	276.167	15	T
3	A	322.140	350.135	405.209	14	E
4	N	436.183	464.178	462.231	13	G
5	N	550.226	578.221	625.294	12	Y
6	I	663.310	691.305	739.337	11	N
7	Y	826.373	854.368	810.374	10	A
8	L	939.457	967.452	881.411	9	A
9	A	1010.494	1038.489	994.495	8	L
10	A	1081.531	1109.526	1157.559	7	Y
11	N	1195.574	1223.569	1270.643	6	I
12	Y	1358.638	1386.632	1384.686	5	N
13	G	1415.659	1443.654	1498.728	4	N
14	E	1544.702	1572.695	1569.766	3	A
15	T	1645.749	1673.744	1684.793	2	D
16	R	1801.850	1829.845	1847.856	1	Y

7. APPENDIX II

Nucleotide Sequence of Hydrophobic Mutants

Note: Mutated nucleotides are the underlined bold fonts

	10	20	30	40	50
84-F165A	CCNNN~~~~~	~~~~~	~~~~~NNNNNN	N~~~~~	~~~~~
44-F165D	C~~~~~	~~~~~	~~~~~	~~~~~	~~NNNNNNNN
19-F169D	NNNNN~~~~~	~~~~~	~~~~~NNNNNN	NN~~~~~	~~~~~
86-I202A	N~~~~~	~~~~~	~~~~~	~~~~~	~~~~~NNNN
67-I202D	~~~~~	~~~~~	~~~~~	~~~~~	~~~NNNNNNN
91-V206A	~~~~~	~~~~~	~~~~~	~~~~~	~~NN~NNNNN
92-V206D	C~~~~~	~~~~~	~~~~~	~~~~~	~~~~~NNNNNN
87-M209A	~~~~~	~~~~~	~~~~~	~~~~~	~~~~~CNNNNN
45-F165D/M	C~~~~~	~~~~~	~~~~~	~~~~~	~~~~~NNNNNNN
69-I202D/M	NN~~~~~	~~~~~	~~~~~	~~~~~	~~~~~NNNNNNN
47-M264D	~~~~~	~~~~~	~~~~~	~~~~~	~~~~~CNNNNN
hTTP D4948	gcagcagcgg	cggcgggcat	ggcagaggcg	cgatcccagc	cctcggcggg

	60	70	80	90	100
84-F165A	~~~~~NNNCN	CACGCGCTAC	CGGACCACTC	TCCGTTGCTG	CAGCCGGGCC
44-F165D	NNNNNNNNCN	NNCGCGCTAC	CGGACCACTC	TCCGTTGCTG	CAGCCGGGCC
19-F169D	~~~~~N	NACGCGCTAC	CGGACCACTC	TCCGTTGCTG	CAGCCGGGCC
86-I202A	NNNNNNNNNN	NNCGCGCTAC	CGGACCACTC	TCCGTTGCTG	CAGCCGGGCC
67-I202D	NNNNNNNNCT	NNCGCGCTAC	CGGACCNCTC	TCCGTTGCTG	CAGCCGGGCC
91-V206A	NNNNNCNNCT	CACGCGCTAC	CGGACCACTC	TCCGTTGCTG	CAGCCGGGCC
92-V206D	NNNNNNNNCT	NNCGCGCTAC	CGGACCACTC	TCCGTTGCTG	CAGCCGGGCC
87-M209A	NNNNNCNNCT	CACGCGCTAC	CGGACCACTC	TCCGTTGCTG	CAGCCGGGCC
45-F165D/M	NNNNNCNNCT	CACGCGCTAC	CGGACCACTC	TCCGTTGCTG	CAGCCGGGCC
69-I202D/M	NNNNNNNNNT	NNCGCGCTAC	CGGACCACTC	TCCGTTGCTG	CAGCCGGGCC
47-M264D	NNNNNNNNCT	NNCGCGCTAC	CGGACCACTC	TCCGTTGCTG	CAGCCGGGCC
hTTP D4948	gccgcagctc	aacgcgctac	cggaccactc	tccgttgctg	cagccggggc

	110	120	130	140	150
84-F165A	TGGCGGCGCT	GCGGCgcgg	gcccggGAAG	CTGGCGTCCC	GCTCGCGCCG
44-F165D	TGGCGGCGCT	GCGGCGCCGG	GCCCggGAAG	CTGGCGTCCC	GCTCGCGCCG
19-F169D	TGGcGGCGCT	GCGGCGCCGG	GCCCggGAAG	CTGGCGTCCC	GCTCGCGCCG
86-I202A	TGGCGGCGCT	GCGGCGCCGG	GCCCggGAAG	CTGGCGTCCC	GCTCGCGCCG
67-I202D	TGGCGGCGCT	GCGGCGCCGG	GCCCggGAAG	CTGGCGTCCC	GCTCGCGCCG
91-V206A	TGGCGGCGCT	GCGGCGCCGG	GCCCggGAAG	CTGGCGTCCC	GCTCGCGCCG
92-V206D	TGGCGGCGCT	GCGGCGCCGG	GCCCggGAAG	CTGGCGTCCC	GCTCGCGCCG
87-M209A	TGGCGGCGCT	GCGGCGCCGG	GCCCggGAAG	CTGGCGTCCC	GCTCGCGCCG
45-F165D/M	TGGCGGCGCT	GCGGCGCCGG	GCCCggGAAG	CTGGCGTCCC	GCTCGCGCCG
69-I202D/M	TGGCGGCGCT	GCGGCGCCGG	GCCCggGAAG	CTGGCGTCCC	GCTCGCGCCG
47-M264D	TGGCGGCGCT	GCGGCGCCGG	GCCCggGAAG	CTGGCGTCCC	GCTCGCGCCG
hTTP D4948	tgggcgcgct	gcggcgccgg	gcccgggaag	ctggcgctccc	gctcgcgccg

	160	170	180	190	200
84-F165A	CTGCCGCTCA	cCgACTCCTT	CCTGCTGCGG	TTCTTGCGCG	CCCGGGATTT
44-F165D	CTGCCGCTCA	CCGACTCCTT	CCTGCTGCGG	TTCTTGCGCG	CCCGGGATTT
19-F169D	CTGCCGCTCA	CCGACTCCTT	CCTGCTGCGG	TTCTTGCGCG	CCCGGGATTT
86-I202A	CTGCCGCTCA	CCGACTCCTT	CCTGCTGCGG	TTCTTGCGCG	CCCGGGATTT

67-I202D	CTGCCGCTCA	CCGACTCCTT	CCTGCTGCGG	TTCCTGCGCG	CCCGGGATTT
91-V206A	CTGCCGCTCA	CCGACTCCTT	CCTGCTGCGG	TTCCTGCGCG	CCCGGGATTT
92-V206D	CTGCCGCTCA	CCGACTCCTT	CCTGCTGCGG	TTCCTGCGCG	CCCGGGATTT
87-M209A	CTGCCGCTCA	CCGACTCCTT	CCTGCTGCGG	TTCCTGCGCG	CCCGGGATTT
45-F165D/M	CTGCCGCTCA	CCGACTCCTT	CCTGCTGCGG	TTCCTGCGCG	CCCGGGATTT
69-I202D/M	CTGCCGCTCA	CCGACTCCTT	CCTGCTGCGG	TTCCTGCGCG	CCCGGGATTT
47-M264D	CTGCCGCTCA	CCGACTCCTT	CCTGCTGCGG	TTCCTGCGCG	CCCGGGATTT
hTTP D4948	ctgcccgtca	ccgactcctt	cctgctgcgg	ttcctgcgcg	cccgggattt

.....
210	220	230	240	250

84-F165A	CGATCTGGAC	CTGGCCTGGC	GGTTACTAAA	AAACTATTAT	AAGTGGAGAG
44-F165D	CGATCTGGAC	CTGGCCTGGC	GGTTACTAAA	AAACTATTAT	AAGTGGAGAG
19-F169D	CGATCTGGAC	CTGGCCTGGC	GGTTACTAAA	AAACTATTAT	AAGTGGAGAG
86-I202A	CGATCTGGAC	CTGGCCTGGC	GGTTACTAAA	AAACTATTAT	AAGTGGAGAG
67-I202D	CGATCTGGAC	CTGGCCTGGC	GGTTACTAAA	AAACTATTAT	AAGTGGAGAG
91-V206A	CGATCTGGAC	CTGGCCTGGC	GGTTACTAAA	AAACTATTAT	AAGTGGAGAG
92-V206D	CGATCTGGAC	CTGGCCTGGC	GGTTACTAAA	AAACTATTAT	AAGTGGAGAG
87-M209A	CGATCTGGAC	CTGGCCTGGC	GGTTACTAAA	AAACTATTAT	AAGTGGAGAG
45-F165D/M	CGATCTGGAC	CTGGCCTGGC	GGTTACTAAA	AAACTATTAT	AAGTGGAGAG
69-I202D/M	CGATCTGGAC	CTGGCCTGGC	GGTTACTAAA	AAACTATTAT	AAGTGGAGAG
47-M264D	CGATCTGGAC	CTGGCCTGGC	GGTTACTAAA	AAACTATTAT	AAGTGGAGAG
hTTP D4948	cgatctggac	ctggcctggc	ggttactaaa	aaactattat	aagtggagag

.....
260	270	280	290	300

84-F165A	CAGAATGTCC	AGAAATAAGT	GCAGATCTAC	ACCCTAGAAG	TATTATTGGC
44-F165D	CAGAATGTCC	AGAAATAAGT	GCAGATCTAC	ACCCTAGAAG	TATTATTGGC
19-F169D	CAGAATGTCC	AGAAATAAGT	GCAGATCTAC	ACCCTAGAAG	TATTATTGGC
86-I202A	CAGAATGTCC	AGAAATAAGT	GCAGATCTAC	ACCCTAGAAG	TATTATTGGC
67-I202D	CAGAATGTCC	AGAAATAAGT	GCAGATCTAC	ACCCTAGAAG	TATTATTGGC
91-V206A	CAGAATGTCC	AGAAATAAGT	GCAGATCTAC	ACCCTAGAAG	TATTATTGGC
92-V206D	CAGAATGTCC	AGAAATAAGT	GCAGATCTAC	ACCCTAGAAG	TATTATTGGC
87-M209A	CAGAATGTCC	AGAAATAAGT	GCAGATCTAC	ACCCTAGAAG	TATTATTGGC
45-F165D/M	CAGAATGTCC	AGAAATAAGT	GCAGATCTAC	ACCCTAGAAG	TATTATTGGC
69-I202D/M	CAGAATGTCC	AGAAATAAGT	GCAGATCTAC	ACCCTAGAAG	TATTATTGGC
47-M264D	CAGAATGTCC	AGAAATAAGT	GCAGATCTAC	ACCCTAGAAG	TATTATTGGC
hTTP D4948	cagaatgtcc	agaaataagt	gcagatctac	accctagaag	tattattggc

.....
310	320	330	340	350

84-F165A	CTCCTAAAGG	CTGGCTACCA	TGGAGTCCTG	AGATCCAGGG	ATCCCCTGG
44-F165D	CTCCTAAAGG	CTGGCTACCA	TGGAGTCCTG	AGATCCAGGG	ATCCCCTGG
19-F169D	CTCCTAAAGG	CTGGCTACCA	TGGAGTCCTG	AGATCCAGGG	ATCCCCTGG
86-I202A	CTCCTAAAGG	CTGGCTACCA	TGGAGTCCTG	AGATCCAGGG	ATCCCCTGG
67-I202D	CTCCTAAAGG	CTGGCTACCA	TGGAGTCCTG	AGATCCAGGG	ATCCCCTGG
91-V206A	CTCCTAAAGG	CTGGCTACCA	TGGAGTCCTG	AGATCCAGGG	ATCCCCTGG
92-V206D	CTCCTAAAGG	CTGGCTACCA	TGGAGTCCTG	AGATCCAGGG	ATCCCCTGG
87-M209A	CTCCTAAAGG	CTGGCTACCA	TGGAGTCCTG	AGATCCAGGG	ATCCCCTGG
45-F165D/M	CTCCTAAAGG	CTGGCTACCA	TGGAGTCCTG	AGATCCAGGG	ATCCCCTGG
69-I202D/M	CTCCTAAAGG	CTGGCTACCA	TGGAGTCCTG	AGATCCAGGG	ATCCCCTGG
47-M264D	CTCCTAAAGG	CTGGCTACCA	TGGAGTCCTG	AGATCCAGGG	ATCCCCTGG
hTTP D4948	ctcctaaagg	ctggctacca	tggagtcctg	agatccaggg	atcccactgg

.....
360	370	380	390	400

84-F165A	CAGCAAAGTT	CTTATTTACA	GAATCGCACA	CTGGGACCCC	AAAGTTTTTTA
----------	------------	------------	------------	------------	-------------

44-F165D	CAGCAAAGTT	CTTATTTTACA	GAATCGCACA	CTGGGACCCC	AAAGTTTTTTA
19-F169D	CAGCAAAGTT	CTTATTTTACA	GAATCGCACA	CTGGGACCCC	AAAGTTTTTTA
86-I202A	CAGCAAAGTT	CTTATTTTACA	GAATCGCACA	CTGGGACCCC	AAAGTTTTTTA
67-I202D	CAGCAAAGTT	CTTATTTTACA	GAATCGCACA	CTGGGACCCC	AAAGTTTTTTA
91-V206A	CAGCAAAGTT	CTTATTTTACA	GAATCGCACA	CTGGGACCCC	AAAGTTTTTTA
92-V206D	CAGCAAAGTT	CTTATTTTACA	GAATCGCACA	CTGGGACCCC	AAAGTTTTTTA
87-M209A	CAGCAAAGTT	CTTATTTTACA	GAATCGCACA	CTGGGACCCC	AAAGTTTTTTA
45-F165D/M	CAGCAAAGTT	CTTATTTTACA	GAATCGCACA	CTGGGACCCC	AAAGTTTTTTA
69-I202D/M	CAGCAAAGTT	CTTATTTTACA	GAATCGCACA	CTGGGACCCC	AAAGTTTTTTA
47-M264D	CAGCAAAGTT	CTTATTTTACA	GAATCGCACA	CTGGGACCCC	AAAGTTTTTTA
hTTP D4948	cagcaaagtt	cttatattaca	gaatcgcaca	ctgggacccc	aaagtttttta

....
	410	420	430	440	450

84-F165A	CAGCTTATGA	CGTATTTTCGA	GTAAGTCTAA	TCACATCCGA	GCTTATTGTA
44-F165D	CAGCTTATGA	CGTATTTTCGA	GTAAGTCTAA	TCACATCCGA	GCTTATTGTA
19-F169D	CAGCTTATGA	CGTATTTTCGA	GTAAGTCTAA	TCACATCCGA	GCTTATTGTA
86-I202A	CAGCTTATGA	CGTATTTTCGA	GTAAGTCTAA	TCACATCCGA	GCTTATTGTA
67-I202D	CAGCTTATGA	CGTATTTTCGA	GTAAGTCTAA	TCACATCCGA	GCTTATTGTA
91-V206A	CAGCTTATGA	CGTATTTTCGA	GTAAGTCTAA	TCACATCCGA	GCTTATTGTA
92-V206D	CAGCTTATGA	CGTATTTTCGA	GTAAGTCTAA	TCACATCCGA	GCTTATTGTA
87-M209A	CAGCTTATGA	CGTATTTTCGA	GTAAGTCTAA	TCACATCCGA	GCTTATTGTA
45-F165D/M	CAGCTTATGA	CGTATTTTCGA	GTAAGTCTAA	TCACATCCGA	GCTTATTGTA
69-I202D/M	CAGCTTATGA	CGTATTTTCGA	GTAAGTCTAA	TCACATCCGA	GCTTATTGTA
47-M264D	CAGCTTATGA	CGTATTTTCGA	GTAAGTCTAA	TCACATCCGA	GCTTATTGTA
hTTP D4948	cagcttatga	cgtattttcga	gtaagtctaa	tcacatccga	gcttattgta

....
	460	470	480	490	500

84-F165A	CAGGAGGTAG	AAACTCAGCG	GAATGGAATC	AAGGCTATCT	TTGATCTGGA
44-F165D	CAGGAGGTAG	AAACTCAGCG	GAATGGAATC	AAGGCTATCT	TTGATCTGGA
19-F169D	CAGGAGGTAG	AAACTCAGCG	GAATGGAATC	AAGGCTATCT	TTGATCTGGA
86-I202A	CAGGAGGTAG	AAACTCAGCG	GAATGGAATC	AAGGCTATCT	TTGATCTGGA
67-I202D	CAGGAGGTAG	AAACTCAGCG	GAATGGAATC	AAGGCTATCT	TTGATCTGGA
91-V206A	CAGGAGGTAG	AAACTCAGCG	GAATGGAATC	AAGGCTATCT	TTGATCTGGA
92-V206D	CAGGAGGTAG	AAACTCAGCG	GAATGGAATC	AAGGCTATCT	TTGATCTGGA
87-M209A	CAGGAGGTAG	AAACTCAGCG	GAATGGAATC	AAGGCTATCT	TTGATCTGGA
45-F165D/M	CAGGAGGTAG	AAACTCAGCG	GAATGGAATC	AAGGCTATCT	TTGATCTGGA
69-I202D/M	CAGGAGGTAG	AAACTCAGCG	GAATGGAATC	AAGGCTATCT	TTGATCTGGA
47-M264D	CAGGAGGTAG	AAACTCAGCG	GAATGGAATC	AAGGCTATCT	TTGATCTGGA
hTTP D4948	caggaggtag	aaactcagcg	gaatggaatc	aaggctatct	ttgatctgga

....
	510	520	530	540	550

84-F165A	AGGTTGGCAG	<u>GCT</u> TCTCATG	CTTTTCAAAT	CACTCCATCC	GTAGCCAAGA
44-F165D	AGGTTGGCAG	<u>GAT</u> TCTCATG	CTTTTCAAAT	CACTCCATCC	GTAGCCAAGA
19-F169D	AGGTTGGCAG	TTTTCTCATG	CT <u>GAT</u> CAAAT	CACTCCATCC	GTAGCCAAGA
86-I202A	AGGTTGGCAG	TTTTCTCATG	CTTTTCAAAT	CACTCCATCC	GTAGCCAAGA
67-I202D	AGGTTGGCAG	TTTTCTCATG	CTTTTCAAAT	CACTCCATCC	GTAGCCAAGA
91-V206A	AGGTTGGCAG	TTTTCTCATG	CTTTTCAAAT	CACTCCATCC	GTAGCCAAGA
92-V206D	AGGTTGGCAG	TTTTCTCATG	CTTTTCAAAT	CACTCCATCC	GTAGCCAAGA
87-M209A	AGGTTGGCAG	TTTTCTCATG	CTTTTCAAAT	CACTCCATCC	GTAGCCAAGA
45-F165D/M	AGGTTGGCAG	<u>GAT</u> TCTCATG	CTTTTCAAAT	CACTCCATCC	GTAGCCAAGA
69-I202D/M	AGGTTGGCAG	TTTTCTCATG	CTTTTCAAAT	CACTCCATCC	GTAGCCAAGA
47-M264D	AGGTTGGCAG	TTTTCTCATG	CTTTTCAAAT	CACTCCATCC	GTAGCCAAGA
hTTP D4948	aggttggcag	ttttctcatg	cttttcaaat	cactccatcc	gtagccaaga

	560 570 580 590 600
84-F165A	AGATTGCTGC TGTACTTACG GATTCATTTT CATTGAAAGT TCGTGGCATC
44-F165D	AGATTGCTGC TGTACTTACG GATTCATTTT CATTGAAAGT TCGTGGCATC
19-F169D	AGATTGCTGC TGTACTTACG GATTCATTTT CATTGAAAGT TCGTGGCATC
86-I202A	AGATTGCTGC TGTACTTACG GATTCATTTT CATTGAAAGT TCGTGGCATC
67-I202D	AGATTGCTGC TGTACTTACG GATTCATTTT CATTGAAAGT TCGTGGCATC
91-V206A	AGATTGCTGC TGTACTTACG GATTCATTTT CATTGAAAGT TCGTGGCATC
92-V206D	AGATTGCTGC TGTACTTACG GATTCATTTT CATTGAAAGT TCGTGGCATC
87-M209A	AGATTGCTGC TGTACTTACG GATTCATTTT CATTGAAAGT TCGTGGCATC
45-F165D/M	AGATTGCTGC TGTACTTACG GATTCATTTT CATTGAAAGT TCGTGGCATC
69-I202D/M	AGATTGCTGC TGTACTTACG GATTCATTTT CATTGAAAGT TCGTGGCATC
47-M264D	AGATTGCTGC TGTACTTACG GATTCATTTT CATTGAAAGT TCGTGGCATC
hTTP D4948	agattgctgc tgtacttacg gattcatttc cattgaaagt tcgtggcatc

	610 620 630 640 650
84-F165A	CATTTGATAA ATGAACCAGT AATTTTCCAT GCTGTCTTTT CCATGATCAA
44-F165D	CATTTGATAA ATGAACCAGT AATTTTCCAT GCTGTCTTTT CCATGATCAA
19-F169D	CATTTGATAA ATGAACCAGT AATTTTCCAT GCTGTCTTTT CCATGATCAA
86-I202A	CATTTGATAA ATGAACCAGT <u>AGCT</u> TTTCCAT GCTGTCTTTT CCATGATCAA
67-I202D	CATTTGATAA ATGAACCAGT <u>AGAT</u> TTTCCAT GCTGTCTTTT CCATGATCAA
91-V206A	CATTTGATAA ATGAACCAGT AATTTTCCAT GCT <u>GCC</u> TTTT CCATGATCAA
92-V206D	CATTTGATAA ATGAACCAGT AATTTTCCAT GCT <u>GAC</u> TTTT CCATGATCAA
87-M209A	CATTTGATAA ATGAACCAGT AATTTTCCAT GCTGTCTTTT <u>CCGCG</u> ATCAA
45-F165D/M	CATTTGATAA ATGAACCAGT AATTTTCCAT GCTGTCTTTT <u>CCGAT</u> ATCAA
69-I202D/M	CATTTGATAA ATGAACCAGT <u>AGAT</u> TTTCCAT GCTGTCTTTT <u>CCGAT</u> ATCAA
47-M264D	CATTTGATAA ATGAACCAGT AATTTTCCAT GCTGTCTTTT CCATGATCAA
hTTP D4948	catttgataa atgaaccagt aattttccat gctgtctttt ccatgatcaa

	660 670 680 690 700
84-F165A	ACCATTCCTG ACTGAAAAAA TTAAGGAACG GATTCACATG CATGGGAACA
44-F165D	ACCATTCCTG ACTGAAAAAA TTAAGGAACG GATTCACATG CATGGGAACA
19-F169D	ACCATTCCTG ACTGAAAAAA TTAAGGAACG GATTCACATG CATGGGAACA
86-I202A	ACCATTCCTG ACTGAAAAAA TTAAGGAACG GATTCACATG CATGGGAACA
67-I202D	ACCATTCCTG ACTGAAAAAA TTAAGGAACG GATTCACATG CATGGGAACA
91-V206A	ACCATTCCTG ACTGAAAAAA TTAAGGAACG GATTCACATG CATGGGAACA
92-V206D	ACCATTCCTG ACTGAAAAAA TTAAGGAACG GATTCACATG CATGGGAACA
87-M209A	ACCATTCCTG ACTGAAAAAA TTAAGGAACG GATTCACATG CATGGGAACA
45-F165D/M	ACCATTCCTG ACTGAAAAAA TTAAGGAACG GATTCACATG CATGGGAACA
69-I202D/M	ACCATTCCTG ACTGAAAAAA TTAAGGAACG GATTCACATG CATGGGAACA
47-M264D	ACCATTCCTG ACTGAAAAAA TTAAGGAACG GATTCACATG CATGGGAACA
hTTP D4948	accattcctg actgaaaaaa ttaaggaacg gattcacatg catgggaaca

	710 720 730 740 750
84-F165A	ACTACAAACA AAGCTTGCTT CAGCATTTCC CAGACATTCT TCCTCTGGAA
44-F165D	ACTACAAACA AAGCTTGCTT CAGCATTTCC CAGACATTCT TCCTCTGGAA
19-F169D	ACTACAAACA AAGCTTGCTT CAGCATTTCC CAGACATTCT TCCTCTGGAA
86-I202A	ACTACAAACA AAGCTTGCTT CAGCATTTCC CAGACATTCT TCCTCTGGAA
67-I202D	ACTACAAACA AAGCTTGCTT CAGCATTTCC CAGACATTCT TCCTCTGGAA
91-V206A	ACTACAAACA AAGCTTGCTT CAGCATTTCC CAGACATTCT TCCTCTGGAA

92-V206D	ACTACAAACA	AAGCTTGCTT	CAGCATTTCC	CAGACATTCT	TCCTCTGGAA
87-M209A	ACTACAAACA	AAGCTTGCTT	CAGCATTTCC	CAGACATTCT	TCCTCTGGAA
45-F165D/M	ACTACAAACA	AAGCTTGCTT	CAGCATTTCC	CAGACATTCT	TCCTCTGGAA
69-I202D/M	ACTACAAACA	AAGCTTGCTT	CAGCATTTCC	CAGACATTCT	TCCTCTGGAA
47-M264D	ACTACAAACA	AAGCTTGCTT	CAGCATTTCC	CAGACATTCT	TCCTCTGGAA
hTTP D4948	actacaaaca	aagcttgctt	cagcatttcc	cagacattct	tcctctggaa

	760	770	780	790	800
84-F165A	TATGGTGGTG	AAGAATTCTC	CATGGAGGAC	ATTTGTCAGG	AATGGACAAA
44-F165D	TATGGTGGTG	AAGAATTCTC	CATGGAGGAC	ATTTGTCAGG	AATGGACAAA
19-F169D	TATGGTGGTG	AAGAATTCTC	CATGGAGGAC	ATTTGTCAGG	AATGGACAAA
86-I202A	TATGGTGGTG	AAGAATTCTC	CATGGAGGAC	ATTTGTCAGG	AATGGACAAA
67-I202D	TATGGTGGTG	AAGAATTCTC	CATGGAGGAC	ATTTGTCAGG	AATGGACAAA
91-V206A	TATGGTGGTG	AAGAATTCTC	CATGGAGGAC	ATTTGTCAGG	AATGGACAAA
92-V206D	TATGGTGGTG	AAGAATTCTC	CATGGAGGAC	ATTTGTCAGG	AATGGACAAA
87-M209A	TATGGTGGTG	AAGAATTCTC	CATGGAGGAC	ATTTGTCAGG	AATGGACAAA
45-F165D/M	TATGGTGGTG	AAGAATTCTC	CATGGAGGAC	ATTTGTCAGG	AATGGACAAA
69-I202D/M	TATGGTGGTG	AAGAATTCTC	CATGGAGGAC	ATTTGTCAGG	AATGGACAAA
47-M264D	TATGGTGGTG	AAGAATTCTC	CATGGAGGAC	ATTTGTCAGG	AATGGACAAA
hTTP D4948	tatggtggtg	aagaattctc	catggaggac	atttgtcagg	aatggacaaa

	810	820	830	840	850
84-F165A	TTTTATAATG	AAGTCTGAAG	ATTATCTCAG	CAGCATTTCT	GAGAGCATTC
44-F165D	TTTTATAATG	AAGTCTGAAG	ATTATCTCAG	CAGCATTTCT	GAGAGCATTC
19-F169D	TTTTATAATG	AAGTCTGAAG	ATTATCTCAG	CAGCATTTCT	GAGAGCATTC
86-I202A	TTTTATAATG	AAGTCTGAAG	ATTATCTCAG	CAGCATTTCT	GAGAGCATTC
67-I202D	TTTTATAATG	AAGTCTGAAG	ATTATCTCAG	CAGCATTTCT	GAGAGCATTC
91-V206A	TTTTATAATG	AAGTCTGAAG	ATTATCTCAG	CAGCATTTCT	GAGAGCATTC
92-V206D	TTTTATAATG	AAGTCTGAAG	ATTATCTCAG	CAGCATTTCT	GAGAGCATTC
87-M209A	TTTTATAATG	AAGTCTGAAG	ATTATCTCAG	CAGCATTTCT	GAGAGCATTC
45-F165D/M	TTTTATAATG	AAGTCTGAAG	ATTATCTCAG	CAGCATTTCT	GAGAGCATTC
69-I202D/M	TTTTATAATG	AAGTCTGAAG	ATTATCTCAG	CAGCATTTCT	GAGAGCATTC
47-M264D	TTTTATAGAT	AAGTCTGAAG	ATTATCTCAG	CAGCATTTCT	GAGAGCATTC
hTTP D4948	ttttataatg	aagtctgaag	attatctcag	cagcatttct	gagagcattc

	860	870	880	890	900
84-F165A	AATGATAGGC	GGCCGCATCG	TGACTGACTG	ACGATCTGCC	TCGCGCGTTT
44-F165D	AATGATAGGC	GGCCGCATCG	TGACTGACTG	ACGATCTGCC	TCGCGCGTTT
19-F169D	AATGATAGGC	GGCCGCATCG	TGACTGACTG	ACGATCTGCC	TCGCGCGTTT
86-I202A	AATGATAGGC	GGCCGCATCG	TGACTGACTG	ACGATCTGCC	TCGCGCGTTT
67-I202D	AATGATAGGC	GGCCGCATCG	TGACTGACTG	ACGATCTGCC	TCGCGCGTTT
91-V206A	AATGATAGGC	GGCCGCATCG	TGACTGACTG	ACGATCTGCC	TCGCGCGTTT
92-V206D	AATGATAGGC	GGCCGCATCG	TGACTGACTG	ACGATCTGCC	TCGCGCGTTT
87-M209A	AATGATAGGC	GGCCGCATCG	TGACTGACTG	ACGATCTGCC	TCGCGCGTTT
45-F165D/M	AATGATAGGC	GGCCGCATCG	TGACTGACTG	ACGATCTGCC	TCGCGCGTTT
69-I202D/M	AATGATAGGC	GGCCGCATCG	TGACTGACTG	ACGATCTGCC	TCGCGCGTTT
47-M264D	AATGATAGGC	GGCCGCATCG	TGACTGACTG	ACGATCTGCC	TCGCGCGTTT
hTTP D4948	aatgagaagt	tatgtcatgt	gaatggcttc	ctaactaaaa	atacatgagt

....|....||....||....||....||....|

	910	920	930	940	950
84-F165A	CGGTGATGAC	GGTGAAAACC	TCTGACACAT	GCAGCTCCCG	GANACGGTCA
44-F165D	CGGTGATGAC	GGTGAAAACC	TCTGACACAT	GCAGCTCCCG	GANANGGTCA
19-F169D	CGGTGATGAC	GGTGAAAACC	TCTGACACNT	GCAGCTCCCG	GAGACGGTCA
86-I202A	CGGTGATGAC	GGTGAAAACC	TCTGACNCNT	GCN.....
67-I202D	CGGTGATGAC	GGTGAAAACC	TCTGACACAT	GCAGCTCCCG	GANANGGTCA
91-V206A	CGGTGATGAC	GGTGAAAACC	TCTGACACAT	GCAGCTCCCG	GAGACGGTCA
92-V206D	CGGTGATGAC	GGTGAAAACC	TCTGACACAT	GCAGCTCCCG	GANANGGTCA
87-M209A	CGGTGANGAC	GGTGAAAACC	TCTGANACAT	GCAGCTCCCG	GANACGGTCA
45-F165D/M	CGGTGATGAC	GGTGAAAACC	TCTGACACAT	GCAGCTCNCG	GANANNGTCA
69-I202D/M	CGGTGATGAC	GGTGAAAACC	TCTGACACAT	GCAGCTCCCG	GAGANGGTCA
47-M264D	CGGTGATGAC	NGTGAAAACC	TCTGACNCAT	GCAGCTCNCG	GANACGGTCA
hTTP D49488	gatatccaac	ctgggttaa	gaatgaaaga	aaaggagcaa	atctttttaa

Translation of hTTP D49488 Nucleotide Sequence

1	gca gca gcg gcg gcg ggc atg gca gag gcg cga tcc cag ccc tcg	45
1	A A A A A G M A E A R S Q P S	15
46	gcg ggg ccg cag ctc aac gcg cta ccg gac cac tct ccg ttg ctg	90
16	A G P Q L N A L P D H S P L L	30
91	cag ccg ggc ctg gcg gcg ctg cgg cgc cgg gcc cgg gaa gct ggc	135
31	Q P G L A A L R R R A R E A G	45
136	gtc ccg ctc gcg ccg ctg ccg ctc acc gac tcc ttc ctg ctg cgg	180
46	V P L A P L P L T D S F L L R	60
181	ttc ctg cgc gcc cgg gat ttc gat ctg gac ctg gcc tgg cgg tta	225
61	F L R A R D F D L D L A W R L	75
226	cta aaa aac tat tat aag tgg aga gca gaa tgt cca gaa ata agt	270
76	L K N Y Y K W R A E C P E I S	90
271	gca gat cta cac cct aga agt att att ggc ctc cta aag gct ggc	315
91	A D L H P R S I I G L L K A G	105
316	tac cat gga gtc ctg aga tcc agg gat ccc act ggc agc aaa gtt	360
106	Y H G V L R S R D P T G S K V	120
361	ctt att tac aga atc gca cac tgg gac ccc aaa gtt ttt aca gct	405
121	L I Y R I A H W D P K V F T A	135
406	tat gac gta ttt cga gta agt cta atc aca tcc gag ctt att gta	450
136	Y D V F R V S L I T S E L I V	150
451	cag gag gta gaa act cag cgg aat gga atc aag gct atc ttt gat	495
151	Q E V E T Q R N G I K A I F D	165
496	ctg gaa ggt tgg cag ttt tct cat gct ttt caa atc act cca tcc	540
166	L E G W Q F S H A F Q I T P S	180
541	gta gcc aag aag att gct gct gta ctt acg gat tca ttt cca ttg	585
181	V A K K I A A V L T D S F P L	195
586	aaa gtt cgt ggc atc cat ttg ata aat gaa cca gta att ttc cat	630
196	K V R G I H L I N E P V I F H	210
631	gct gtc ttt tcc atg atc aaa cca ttc ctg act gaa aaa att aag	675
211	A V F S M I K P F L T E K I K	225
676	gaa cgg att cac atg cat ggg aac aac tac aaa caa agc ttg ctt	720
226	E R I H M H G N N Y K Q S L L	240
721	cag cat ttc cca gac att ctt cct ctg gaa tat ggt ggt gaa gaa	765
241	Q H F P D I L P L E Y G G E E	255
766	ttc tcc atg gag gac att tgt cag gaa tgg aca aat ttt ata atg	810
256	F S M E D I C Q E W T N F I M	270
811	aag tct gaa gat tat ctc agc agc att tct gag agc att caa tga	855
271	K S E D Y L S S I S E S I Q *	285

7. APPENDIX III
Efficiency of Glutathion Agarose Affinity Purification

	Invitrogen G2879		Sigma G4510	
	Protein Yield (mg protein/g cells)	# of trials	Protein Yield (mg protein/g cells)	# of purifications
WT	0.43 ± 0.16	> 4	1.59 ± 0.19	> 4
F165A	n/a		3.16	2
F165D	0.49	2	2.17 ± 0.66	3
F169D	n/a		1.66 ± 0.53	3
I202A	n/a		0.06	2
I202D	0.62	1	1.85	1
V206A	n/a		2.69	1
V206D	n/a		0.08	2
M209A	n/a		2.27	1
M209D	0.43	1	0.67	1
F165D_M209D	0.25	2	1.86	2
I202D_M209D	0.48	1	1.81	2
M264D	n/a		2.15	1
R192H	n/a		2.55	2
K211A	n/a		1.25	2
K217A	n/a		1.36	3